João Carlos Ferreira de Almeida Casaleiro

Licenciado

Analysis and Design of Sinusoidal Quadrature RC-Oscillators

Dissertação para obtenção do Grau de Doutor em

Engenharia Electrotécnica e de Computadores

Orientador: Luís Augusto Bica Gomes de Oliveira, Professor Auxiliar, Universidade Nova de Lisboa

Júri

Presidente:	Prof. Dr. Paulo da Costa Luís da Fonseca Pinto
Arguentes:	Prof. Dr. João Manuel Torres Caldinhas Simões Vaz
	Prof. Dr. Vítor Manuel Grade Tavares
Vogais:	Prof. Dr. Igor Filanovsky
	Prof. Dr. Jorge Manuel dos Santos Ribeiro Fernandes
	Prof. Dr. Luís Humberto Viseu Melo
	Prof. Dr. João Carlos da Palma Goes

FACULDADE DE CIÊNCIAS E TECNOLOGIA
UNIVERSIDADE NOVA DE LISBOA

Setembro, 2015

Analysis and Design of Sinusoidal Quadrature RC-Oscillators

ACKNOWLEDGEMENTS

I would like to express my sincere thanks to my supervisor Prof. Dr. Luís Augusto Bica Gomes de Oliveira for the continuous support, for his patience and motivation. His supervision helped me focus on the research and writing of this thesis. Besides my supervisor, I would like to thank Prof. Dr. Igor M. Filanovsky for his long lessons on differential equations and on Van der Pol oscillators, which were essential for the research, and for his suggestions to clarify the text.

Further, I would like to thank the other members of my thesis committee: Prof. Dr. João Goes and Prof. Dr. Manuel Medeiros Silva for their suggestions to focus the research. I wish to present my special thanks to Prof. Dr. Manuel Medeiros Silva for the contribution to the thesis's quality, for the helpful discussions about the capacitive coupling theory, and his illuminating suggestions to clarify the text. In addition, I thank my fellow lab mates in UNINOVA for the support with the simulations and the stimulating discussions. Also, I thank my friends in CEDET for the overall support and encouragement.

I acknowledge the support given by the following institutions:

- Instituto Superior de Engenharia de Lisboa – ISEL, for the 6-month sabbatical leave for the writing of this thesis.
- Portuguese Foundation for Science and Technology (FCT/MCTES) (CTS multi-annual funding) through PIDDAC program funds and under projects DISRUPTIVE (EXCL/EEI-ELC/0261/2012) and PEST (PEST-OEEEI/UI0066/2014), for the financial support.
- CTS-UNINOVA and INESC-ID Lisboa for providing access to their laboratory facilities, for the circuit prototypes simulations and measurements.

ABSTRACT

Modern telecommunication equipment requires components that operate in many different frequency bands and support multiple communication standards, to cope with the growing demand for higher data rate. Also, a growing number of standards are adopting the use of spectrum efficient digital modulations, such as quadrature amplitude modulation (QAM) and orthogonal frequency division multiplexing (OFDM). These modulation schemes require accurate quadrature oscillators, which makes the quadrature oscillator a key block in modern radio frequency (RF) transceivers. The wide tuning range characteristics of inductorless quadrature oscillators make them natural candidates, despite their higher phase noise, in comparison with *LC*-oscillators. This thesis presents a detailed study of inductorless sinusoidal quadrature oscillators. Three quadrature oscillators are investigated: the active coupling *RC*-oscillator, the novel capacitive coupling *RC*-oscillator, and the two-integrator oscillator. The thesis includes a detailed analysis of the Van der Pol oscillator (VDPO). This is used as a base model oscillator for the analysis of the coupled oscillators. Hence, the three oscillators are approximated by the VDPO. From the nonlinear Van der Pol equations, the oscillators' key parameters are obtained. It is analysed first the case without component mismatches and then the case with mismatches. The research is focused on determining the impact of the components' mismatches on the oscillator key parameters: frequency, amplitude-, and quadrature-errors. Furthermore, the minimization of the errors by adjusting the circuit parameters is addressed. A novel quadrature *RC*-oscillator using capacitive coupling is proposed. The advantages of using the capacitive coupling are that it is noiseless, requires a small area, and has low power dissipation. The equations of the oscillation amplitude, frequency, quadrature-error, and amplitude mismatch are derived. The theoretical results are confirmed by simulation and by measurement of two prototypes fabricated in 130 nm standard complementary metal-oxide-semiconductor (CMOS) technology. The measurements reveal that the power increase due to the coupling is marginal, leading to a figure-of-merit of -154.8 dBc/Hz. These results are consistent with the noiseless feature of this coupling and are comparable to those of the best state-of-the-art *RC*-oscillators, in the GHz range, but with the lowest power consumption (about 9 mW). The results for the three oscillators show that the amplitude- and the quadrature-errors are proportional to the component mismatches and inversely proportional to the coupling strength. Thus, increasing the coupling strength decreases both the amplitude- and quadrature-errors. With proper coupling strength, a quadrature error below 1° and amplitude imbalance below 1% are

obtained. Furthermore, the simulations show that increasing the coupling strength reduces the phase noise. Hence, there is no trade-off between phase noise and quadrature error. In the two-integrator oscillator study, it was found that the quadrature error can be eliminated by adjusting the transconductances to compensate the capacitance mismatch. However, to obtain outputs in perfect quadrature one must allow some amplitude error.

Keywords: Quadrature oscillators, coupled oscillators, capacitive coupling, quadrature error, amplitude error, Van der Pol oscillator, sinusoidal oscillators.

RESUMO

Os equipamentos modernos de telecomunicações, para acompanharem a crescente procura por ritmos de transmissão mais elevados, necessitam de componentes que funcionem numa vasta gama de frequências e que suportem vários protocolos de comunicação. Além disso, tem vindo a aumentar o número de protocolos que utilizam modulações digitais espectralmente mais eficientes, como a modulação de amplitude em quadratura (QAM) e a multiplexagem por divisão ortogonal de frequência (OFDM). Estas modulações necessitam de osciladores em quadratura de grande precisão, o que torna o oscilador em quadratura num bloco fundamental nos transmissores modernos de RF. A elevada gama de sintonia dos osciladores sem bobina torna-os candidatos privilegiados para esta aplicação, apesar de terem um ruído de fase pior do que os osciladores LC. Esta tese apresenta um estudo detalhado sobre osciladores sinusoidais, sem bobina, com saídas em quadratura. São investigados três osciladores: o oscilador *RC* com acoplamento activo, o novo oscilador *RC* com acoplamento capacitivo e o oscilador com dois integradores. A tese inclui também uma análise detalhada do oscilador de Van der Pol (VDPO) que é utilizado como modelo para a análise dos osciladores acoplados. Assim, os três osciladores são aproximados por VDPOs. Sendo os seus parâmetros fundamentais obtidos a partir das equações, não lineares, de Van der Pol. São efetuadas duas análises aos osciladores, considerando ou não a existência de assimetrias entre os componentes. A investigação incide particularmente sobre a influência das assimetrias dos componentes nos erros de amplitude e de quadratura, e sobre as formas de minimização desses erros. É proposto um novo oscilador *RC* em quadratura com acoplamento capacitivo. O acoplamento capacitivo tem como vantagens não adicionar ruído, ocupar uma área reduzida e de ter um baixo consumo. São deduzidas as equações da amplitude e frequência de oscilação, bem como, as equações dos erros de quadratura e amplitude. Os resultados teóricos são confirmados por simulação e por medidas, tendo sido fabricados, para o efeito, dois protótipos numa tecnologia CMOS de 130 nm. Os resultados de medida mostraram um aumento marginal do consumo devido ao acoplamento, tendo permitido obter um fator de mérito de -154 dBc/Hz. Estes resultados estão de acordo com as características de baixo ruído deste tipo de acoplamento e são comparáveis aos melhores resultados obtidos com osciladores *RC*, na gama de frequências dos GHz, mas apresentando um menor consumo (cerca de 9 mW). Os resultados dos três osciladores mostram que os erros de amplitude e de quadratura são proporcionais às assimetrias dos componentes e inversamente proporcionais ao fator de acoplamento. Por isso, o aumento do fator de acoplamento

faz diminuir, tanto o erro de amplitude, como o erro de quadratura. Com um fator de acoplamento adequado obtêm se erros de quadratura inferiores a 1° e erros de amplitude inferiores a 1%. As simulações mostraram que o ruído de fase diminui com o aumento do fator de acoplamento. Assim sendo, não existe compromisso entre o erro de quadratura e o ruído de fase do oscilador. A teoria do oscilador com dois integradores revelou que o erro de quadratura pode ser eliminado, ajustando as transcondutâncias de forma a compensarem a assimetria das capacidades. No entanto, para obter saídas em perfeita quadratura tem de existir alguma diferença nas amplitudes.

Palavras-chave: Osciladores em quadratura, osciladores acoplados, acoplamento capacitivo, erro de quadratura, erro de amplitude, oscilador de Van der Pol, osciladores sinusoidais.

CONTENTS

LIST OF FIGURES

LIST OF TABLES

ACRONYMS

AAC	Automatic amplitude control
CMOS	Complementary metal-oxide-semiconductor
FoM	Figure-of-merit
ILFD	Injection-locked frequency divider
IoT	Internet-of-things
IRR	Image rejection ratio
ISM	Industrial, scientific and medical
KCL	Kirchhoff's current law
KVL	Kirchhoff's voltage law
MIMO	Multi-input multi-output
MOSFET	Metal-oxide-semiconductor field effect transistor
OFDM	Orthogonal frequency division multiplexing
QAM	Quadrature amplitude modulation
QO	Quadrature oscillator
QPSK	Quadrature phase-shift keying
QVCO	Quadrature voltage-controlled oscillator
RF	Radio frequency
SNR	Signal-to-noise ratio
THD	Total harmonic distortion
VDP	Van der Pol
VDPO	Van der Pol oscillator
WMTS	Wireless medical telemetry services
WSN	Wireless sensor network

CHAPTER 1

INTRODUCTION

Contents

1.1 Background and motivation

The objective of an oscillator circuit is to generate a periodic signal. Radio frequency circuits require sinusoidal oscillators (or second-order oscillators) with a stable amplitude, frequency and phase. Digital circuits and analog-to-digital converters require square-wave signals, known as clock signal. These signals are generated by relaxation oscillators (also called first-order oscillators), a topic that is outside the scope of this thesis and will not be further discussed. In this thesis, the investigation is focused on sinusoidal oscillators.

Modern radio frequency (RF) receiver architectures, like the Low–IF receiver shown in Fig. 1.1, require sinusoidal oscillators with low phase-noise and accurate quadrature signals to reject the image band [1, 2]. The sensitivity of the receiver is limited by the image rejection ratio (IRR), which is in turn limited by the circuit mismatches and quadrature error. This makes the quadrature oscillator (QO) a key block for receivers. In recent years, significant research efforts have been invested in the study of oscillators with accurate quadrature outputs, with less than 1° of error. The demand for low–power QOs that generate accurate quadrature signals has been growing with the widespread adoption of digital communications, systems and standards that use quadrature amplitude modulation (QAM) and quadrature phase-shift keying (QPSK). Examples of such standards are ZigBee (IEEE 802.15.4) and Bluetooth (IEEE 802.15.1), used in a multitude

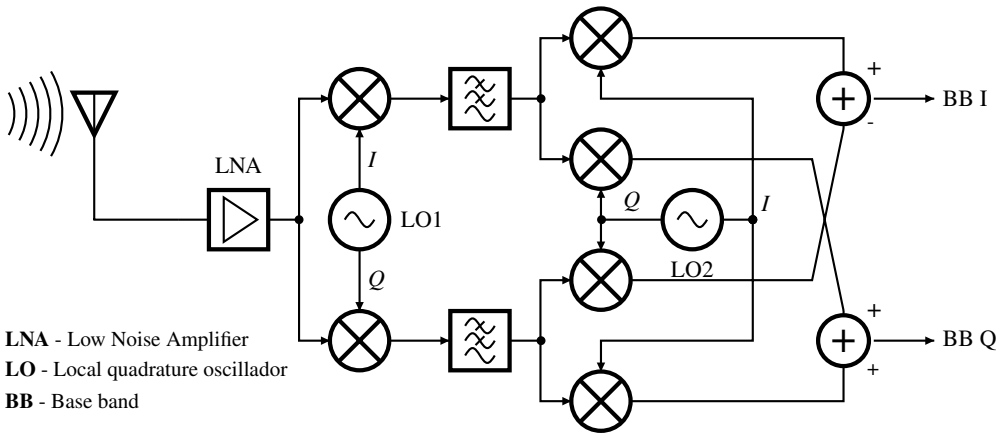

Figure 1.1: Low-IF receiver front-end block diagram.

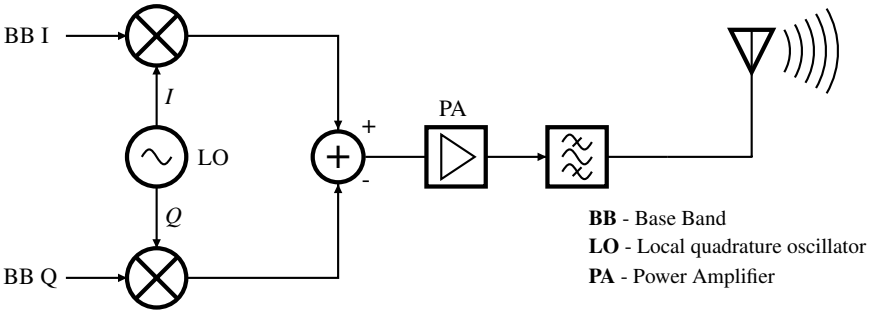

Figure 1.2: Direct upconversion transmitter block diagram.

of applications, such as wireless sensor network (WSN), home automation, healthcare, smart energy, and many others. Moreover, in modern receivers the cost and size reduction are important requirements. The minimization of external components reduces the equipment cost. Full integration poses several challenges. For instance, the Low-IF receiver requires image cancellation. If quadrature signals are available, the image-rejection filters requiring a large die area can be avoided [1, 3].

Modern RF transmitters, like the direct upconversion shown in Fig. 1.2, using spectrum efficient modulations, such as orthogonal frequency division multiplexing (OFDM) also require QO with accurate quadrature signals. The quadrature error can limit the achievable signal-to-noise ratio (SNR) at the receiver and the size of supported constellation and data rates. Currently, signal processing techniques in the digital domain are used to compensate the quadrature error [4].

1.1.1 Quadrature signal generation

Several methods to generate quadrature signals are found in the literature. In this section, we review the open–loop approaches. We review first the $RC-CR$ networks and polyphase filters. Both are passive networks that need large die area and power (to overcome the attenuation imposed by the filtering) to achieve acceptable quadrature inaccuracies (below 1°) [1, 3]. Afterwards, the frequency division method is reviewed.

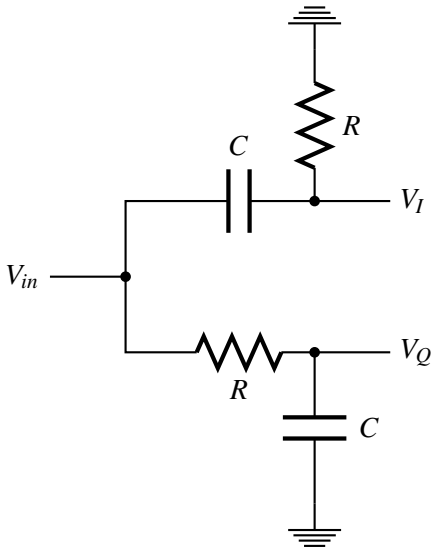

Figure 1.3: *RC-CR* network circuit

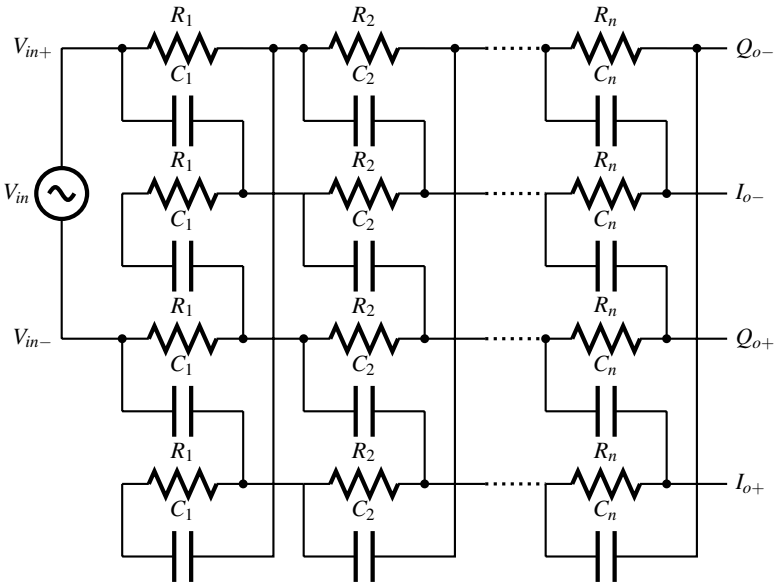

Figure 1.4: Passive *RC* polyphase filter with n stages.

1.1.1.1 *RC-CR* network

This method splits the input signal V_{in} in two, passing it in the *RC* and *CR* branches, as shown Fig. 1.3. The *CR* branch is a high-pass filter that shifts the signal by -45 ° and the *RC* branch is a low-pass filter that shifts the signal by +45 °, at the pole frequency $\omega_p \approx 1/(RC)$. Although, the phase shift of each branch varies with the frequency, the phase difference between the two branches is always 90°. However, the branches attenuations are only equal at the pole frequency [2, 3]. In theory, this is not a problem because one can design the network so that the pole frequency is equal to the oscillator frequency. In practice, however, due to the temperature and process variations, one cannot guarantee nor the absolute value of the network components and neither a perfect match

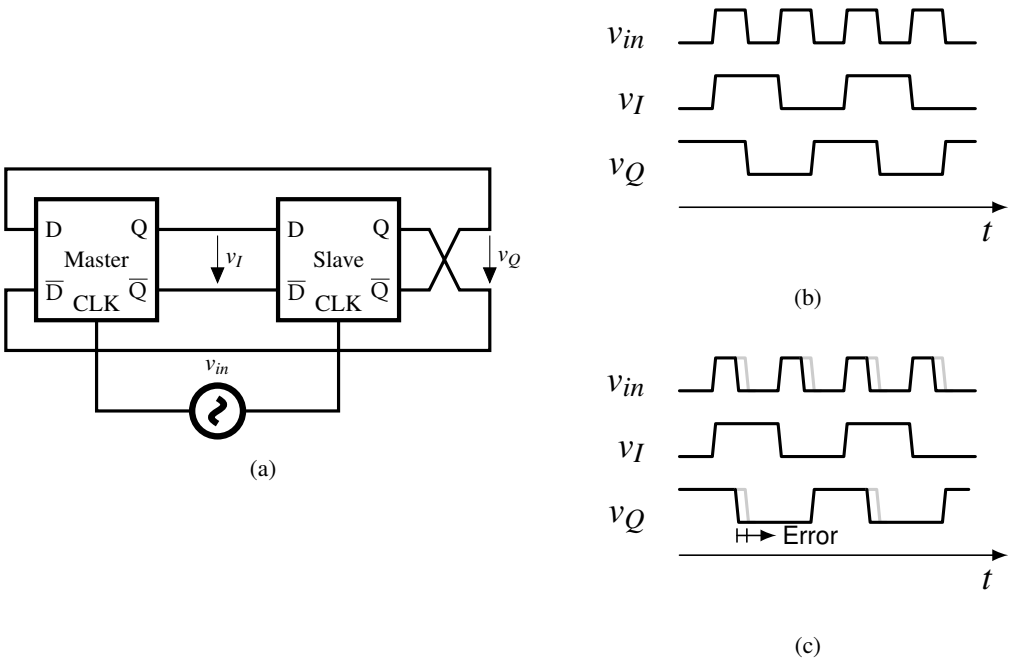

Figure 1.5: Digital divider-by-two (a) circuit, (b) waveforms, and (c) waveforms with phase error.

between them. Hence, in practical circuit there are amplitude- and quadrature-errors. To minimise the errors more stages can be added to the network, as shown in Fig. 1.4. A multi-stage $RC-CR$ network is known as a polyphase filter. With more stages, the errors decrease and the operating bandwidth increases, but the signal loss increases considerably.

1.1.1.2 Frequency division

Frequency dividers are wideband quadrature generators. However, the divider-by-two method uses twice the nominal frequency which increases the power requirements, especially at high frequencies [2]. The divider consists of two latches connected in a master/slave configuration, as shown in Fig. 1.5(a). A square-wave input signal with 50% duty-cycle is required to generate two quadrature signals, as shown in Fig. 1.5(b). If the input signal does not have a 50% duty-cycle, then the output signals have a quadrature error, as shown in Fig. 1.5(c). This problem can be solved by using a divider-by-four, but in this case the frequency of the input signal must be four times the desired operating frequency.

The divider-by-two based on latches is inadequate for quadrature sinusoidal signals because the outputs are square-waves. Hence, it requires additional filtering that needs a large chip area to cope with the components mismatches. For sinusoidal outputs dynamic frequency dividers, such as the injection-locked frequency divider (ILFD) [5, 6] or the regenerative divider [7, 8], are more adequate.

In general, these open-loop methods have worse performance than the close-loop ones, investigated in this thesis. In addition, open–loop methods do not allow the compensation of the mismatches.

1.1.1.3 Coupled oscillators

The closed-loop approaches, include coupled oscillators and ring oscillators. The best are the QOs based on two coupled $LC-$oscillators: they have the lowest phase-noise and phase error [9]. Recently it was also shown that they can achieve perfect quadrature [10]. However, coupled $LC-$oscillators require two inductors, which, depending on the frequency, can occupy a large die area. Moreover, inductors do not scale down with the technology, and designing inductors with acceptable quality factor (Q>5) requires the use of thick top metal layers, increasing the chip cost [11]. Inductorless oscillators, like the two-integrator oscillator or the coupled *RC*-oscillators, are viable alternatives to avoid the use of inductors. Although, in comparison with the coupled $LC-$oscillators both have poor phase-noise performance [9], for industrial, scientific and medical (ISM) band, the phase-noise of inductorless oscillators may satisfy the requirements. For instance, the phase-noise specification for 2.4-GHz ISM band at the offset of 1 MHz from the carrier is -110 dBc/Hz for Bluetooth and -88 dBc/Hz for Zigbee; these values are within the performance capability of inductorless oscillators [12].

The analysis of sinusoidal oscillators using the linear positive feedback model usually is sufficient for deriving the oscillation frequency. However, due to the circuit linearization, as will be shown below, the amplitude limiter mechanism is lost, since it is dependent of the circuit nonlinearities. A large-signal analysis can overcome this limitation, but leads to long and complicated equations that do not help the designer. In this thesis an analysis, based on the weak nonlinearity of the transistors' transconductances, is presented. This approach allows to avoid a large-signal analysis.

Coupled oscillators consist of two identical oscillators connected by either an active or a passive network. Several active coupling methods were proposed; they can be grouped into parallel or series topologies. The parallel topology was first proposed in [13] for $LC-$oscillators, with the coupling amplifier transistors in parallel with the oscillators' core. In the series topology, proposed in [14], the transistors are in series with the oscillators' core. A comprehensive comparison between these two topologies for $LC-$ oscillators can be found in [15]. The disadvantage of the parallel topologies is the use of two extra gain blocks, which increases the power dissipation [2]. The series topology reuses the current of the oscillator, but the output swing is limited. Since the trend in future complementary metal-oxide-semiconductor (CMOS) technologies is to lower the supply voltages towards 0.5-0.7V [16], this topology is not useful for future designs.

In passive coupling, the amplifiers are substituted by passive elements (usually inductors or capacitors). The coupling based on inductors [17] and transformers [18, 19], requires a higher area than active coupling. Capacitive coupling of $LC-$oscillators has shown interesting results [20]; as opposed to traditional active coupling, it does not increase the power consumption. However, the area minimization is still limited by the inductors and the oscillation frequency is lower [21].

In this work, three quadrature oscillators working in the sinusoidal regime are investigated: $RC-$oscillator with active coupling, the $RC-$oscillator with capacitive coupling, and the two-integrator oscillator. Of special interest is the research of quadrature $RC-$oscillator with capacitive coupling [22]. The capacitive coupling is noiseless and requires a small area. Since the coupling

capacitors do not add noise, we expect a 3 dB phase-noise improvement (due to the coupling), and with a marginal increase of the power, a figure-of-merit (FoM) comparable to that of the best state-of-the-art $RC-$oscillators is achieved. Contrarily to what might be expected, with the increase of the coupling capacitances (higher coupling strength) the oscillation frequency increases [22]. We present the theory to explain this behaviour, and we derive the equations for the frequency, phase-error and amplitude mismatch, which are validated by simulation. The theory shows that the phase-error is proportional to the amplitude mismatch, indicating that an automatic phase-error minimization based on the amplitude mismatch is possible. We also study bimodal oscillations and phase ambiguity, for this coupling topology, comparing it with other circuits [23]. To validate the theory, a 2.4-GHz quadrature voltage-controlled oscillator (QVCO) based on two $RC-$oscillators with capacitive coupling was fabricated, in standard 130nm CMOS process.

1.2 Organization of the thesis

This thesis is organised into seven chapters. In the second chapter, an overview of sinusoidal oscillators models is presented: we describe the positive-feedback and the negative-resistance models. Afterwards, a survey of the automatic amplitude control methods is presented. We focus mainly on the method that uses the intrinsic nonlinearities of the oscillator to limit the amplitude. The Van der Pol oscillator (VDPO) is used as an example and is analysed using both models. To conclude the single sinusoidal oscillator modelling we describe the frequency selectivity and introduce the concept of the oscillator's quality factor.

In Chapter 3 we analyse driven oscillators. The oscillator is driven by an external periodic signal (locking signal) by injecting a current. Both the parallel and series topologies are studied, and their locking range is derived. The VDPO is used for the analysis. We use the VDPO as a base oscillator for the analysis because its nonlinearities are similar to the nonlinearities of the inductorless oscillators studied in the next chapters.

In Chapter 4 we present the analysis of the actively cross-coupled $RC-$oscillator, which is a QO that consists of two $RC-$oscillators coupled by transconductance amplifiers. First, we derive the single $RC-$oscillator equations which show that a single $RC-$oscillator can be modelled by the series VDPO. Afterwards, we analyse the quadrature oscillator, deriving the frequency, amplitude-, and phase-error equations. A stability analysis of the equilibrium points is presented. The theoretical results are validated by simulation.

In Chapter 5 we study the capacitive coupling $RC-$oscillator regarding oscillation frequency, amplitude- and phase-error. We focus the investigation on the relation between the coupling and the quadrature generation, on the impact of the coupling strength on the frequency, amplitude- and phase-error, and the impact of the mismatches on the amplitude- and phase-errors. We derive the equations for the frequency, amplitude- and phase-error as a function of the circuits mismatches. The theoretical results are validated by simulation.

In Chapter 6 we study the two-integrator oscillator working in the near sinusoidal regime. We focus the investigation on the impact of the circuits mismatches on the frequency, amplitude-

and phase-error. We derive the equation for these key parameters as a function of the circuits mismatches. The theoretical results are validated by simulation.

Finally, in Chapter 7 we present the conclusions.

1.3 Main contributions

Several papers in international conferences and journals were published. To the best of the author's knowledge, the main original contributions of this work are:

- A study (in Chapter 4) of the quadrature generation in active coupling $RC-$oscillators working in the sinusoidal regime. The research is focused on the impact of the mismatches and of the coupling strength on the frequency, amplitude- and phase-errors. The analysis in this chapter differs from other research works because weak coupling strengths are assumed. Other research works analysed this oscillator assuming a strong coupling (coupling amplifiers work as hard limiters) making the coupling signal a square wave. The theoretical results were validated by simulation.

- A study (in Chapter 5) of the quadrature generation in capacitive coupling $RC-$oscillators. The research is focused on the impact of the coupling strength on the frequency, amplitude- and phase-errors [24]. A prototype at 2.4 GHz was designed to confirm the theoretical results.

- A study (in Chapter 6), using the Van der Pol (VDP) approximation, of the two-integrator oscillator in the linear regime. The research is focused on the impact of the coupling strength on the frequency, amplitude- and phase-errors [25]. The theoretical results are validated by simulation.

A minor contribution is the improvement of the model of the single $RC-$oscillator (in Chapter 4). We show the relation between the circuit elements and the VDP parameters. There is a special focus on the metal-oxide-semiconductor field effect transistor (MOSFET) transconductance with weak nonlinearities. We analyse these nonlinearities for the strong, moderate and weak inversion (in Appendix A).

The study of $RC-$oscillators and VDPO has led to further results on relaxation oscillators and the VDP approximation. This includes the proposal of CMOS coupled multivibrators for wireless medical telemetry services (WMTS) applications [26, 27]. A relaxation oscillator with improved FoM [28] was also obtained. Modelling the Wien bridge oscillators by a VDP approximation [29] was also presented. However, these results, although related with, are outside the scope of this thesis.

CHAPTER 2

SINUSOIDAL OSCILLATORS

Contents

2.1 Introduction

In this chapter we review two basic models of the sinusoidal oscillator. We first describe the linear positive-feedback model and the associated Barkhausen criterion. Next, we focus on the model of negative-resistance oscillator. For both models, the parallel and series topologies are described. We review the amplitude control techniques with the main focus on the amplitude limiting by nonlinearities using the VDPO as an example. The stability of the single VDPO is studied. Two implementations of a negative-resistance circuit are presented and, at the end of the chapter, we briefly discuss the frequency control.

2.2 Sinusoidal oscillator models

Sinusoidal oscillators are usually analysed as linear positive-feedback systems [3], like the one shown in Fig. 2.1. We will refer to this as the feedback model. The feedback model is suitable for oscillators topologies with a feedback loop, such as the ring and phase-shift oscillators. However, with few exceptions, it can be used in the analysis of most topologies. The model assumes a system

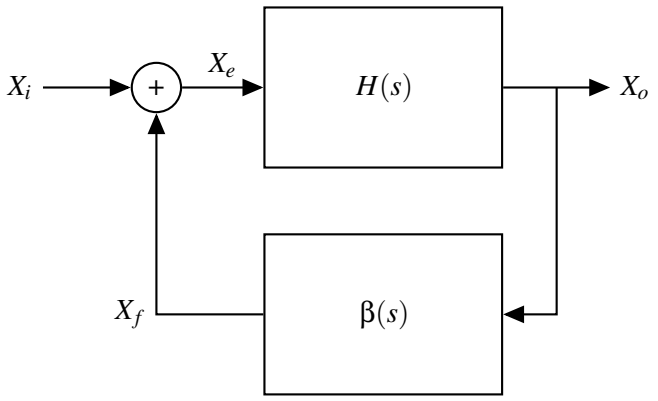

Figure 2.1: Oscillator feedback model.

composed of a forward network, $H(s)$, a feedback network, $\beta(s)$, and an adder that sums the input, X_i, and feedback, X_f, signals. The function of the feedback network is to sense the output, X_o, and convert it to a feedback signal,

$$X_f = \beta(s)X_o,$$

The adder output signal is

$$X_e = X_i + \beta(s)X_o,$$

which is applied to the forward network resulting in

$$X_o\,[1-\beta(s)H(s)] = H(s)X_i. \tag{2.1}$$

An important aspect to note from (2.1) is that for a zero input, i.e. $X_i = 0$, the output can be a nonzero signal, if the left-hand side is zero, i.e. $1 - H(s)\beta(s) = 0$. For oscillators, this particular case ($X_i = 0$) is known as the free-running mode, and the model of Fig. 2.1 is reduced to a closed-loop including the forward and feedback networks. In the next chapter, we will discuss a more general case, known as driven mode, where $X_i \neq 0$ and the input is used to couple or synchronize with other oscillators.

From (2.1) we can derive the network function

$$A_f(s) = \frac{X_o(s)}{X_i(s)} = \frac{H(s)}{1-H(s)\beta(s)}. \tag{2.2}$$

For a steady-state oscillation to be maintained, the system poles[1] must be purely imaginary, i.e. $1 - H(s)\beta(s) = 0$ with $s = \pm j\omega_0$, leading to the condition that the loop gain is $H(s)\beta(s) = 1$. This condition, known as the Barkhausen criterion, can be split into two conditions, that must be met simultaneously. These two conditions concern the magnitude of the loop gain

$$|H(s)\beta(s)| = 1,$$

[1]Poles of a network function are the values of s-variable for which the denominator becomes zero

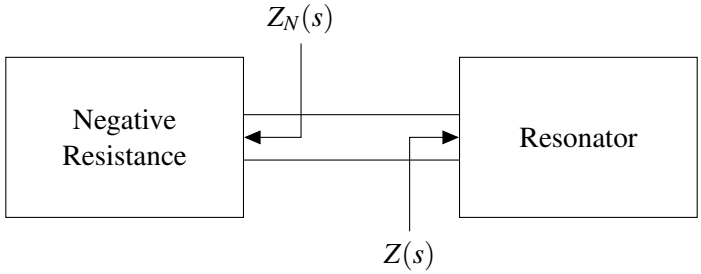

Figure 2.2: Oscillator negative-resistance model.

and the phase

$$arg\,[H(s)\beta(s)] = 0.$$

To stabilize the oscillation frequency the networks $H(s)$, $\beta(s)$ or both, are frequency-selective networks (resonators) that force the Barkhausen criteria to be met at a specific frequency, ω_0, as we will show in Section 2.4.

An important aspect of the Barkhausen criterion is that it is a necessary, but not sufficient, condition for the oscillation to occur [3]. For instance, if we have a system with $\beta = 1$ and $|H(s)| > 1$, for any value of s, there is an exponential increase of the output, but no oscillation occurs since there are no complex-conjugate poles [3]. Another example is at start-up, where the magnitude of the loop gain must be above unity $|H(s)\beta(s)| > 1$ [2]. For this reason, the oscillator loop gain is always designed slightly higher than one: the difference is known as excess loop gain. However, a loop gain higher than one will force the amplitude to grow, which is desirable at start-up, but should be reduced to unity at steady-state. This gain control mechanism, in the majority of oscillators, is due to non-linearities, making the feedback model unsuited to analyze this mechanism because it is based on the linearization of the system.

An alternative model, described by Kurokawa in [30] and Strauss in [31], is the negative-resistance model, shown in Fig. 2.2, which models the circuit as two one-port networks. The resonator is a frequency-selective network and defines the oscillation frequency. It can be made of passive or active elements. Usually, in $LC-$oscillators the resonator is a passive network, and in $RC-$oscillators the resonator has active elements. In either case, the resonator is not lossless, with an impedance $Z(\omega) = R + jX(\omega)$, which causes a fraction of the energy to be dissipated on the lumped parasitic resistance, R. The equivalent impedance of the negative resistance network is assumed to be $Z_N(A,\omega) = R(A,\omega) + jX(A,\omega)$. The impedance Z_N is dependent of the oscillation amplitude, A, due to the circuit nonlinearities. To maintain the oscillation, the negative resistance circuit must compensate the loss in R, leading to the steady-state oscillating condition $Z(\omega) = -Z_N(A,\omega)$. For the oscillation to start, the negative resistance should supply more energy then the loss in R. A negative resistance behaviour can be obtained by using a nonlinear device, such as tunnel diode, a Gunn diode or IMPATT (IMPact ionization Avalanche Transit-Time) diode. It can also be based on an active circuit, as will be detailed along this document.

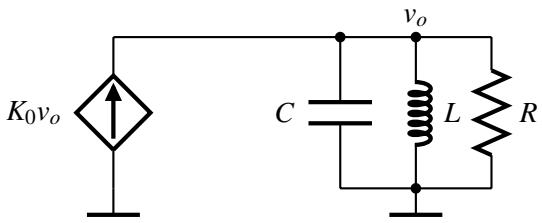

Figure 2.3: Parallel $LC-$oscillator.

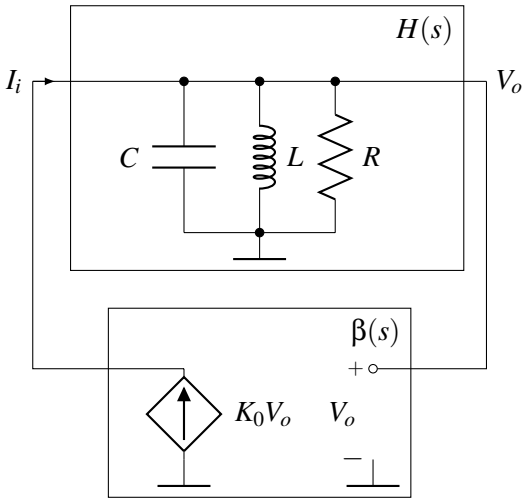

Figure 2.4: Parallel $LC-$oscillator rearranged in a feedback model.

As an example, the $LC-$oscillator of Fig. 2.3 will be analysed using both models. Rearranging the circuit as shown in Fig. 2.4 it becomes clear that the feedback transconductance, $\beta(s)$, is

$$\beta(s) = \frac{I_i}{V_o} = K_0, \tag{2.3}$$

and the transimpedance is

$$H(s) = \frac{V_o}{I_i} = \frac{s\frac{1}{C}}{s^2 + s\frac{1}{RC} + \frac{1}{LC}}. \tag{2.4}$$

Substituting (2.3) and (2.4) into (2.1), one obtains the characteristic equation

$$s^2 + s\frac{1}{RC}(1 - K_0 R) + \frac{1}{LC} = 0, \tag{2.5}$$

from which it is possible to obtain the oscillation condition for the loop gain

$$K_0 R \geq 1, \tag{2.6}$$

and the oscillation frequency

$$\omega_0 = \frac{1}{\sqrt{LC}}.$$

For simplicity, in (2.5) we suppress the explicit dependence on V_o in the notation.

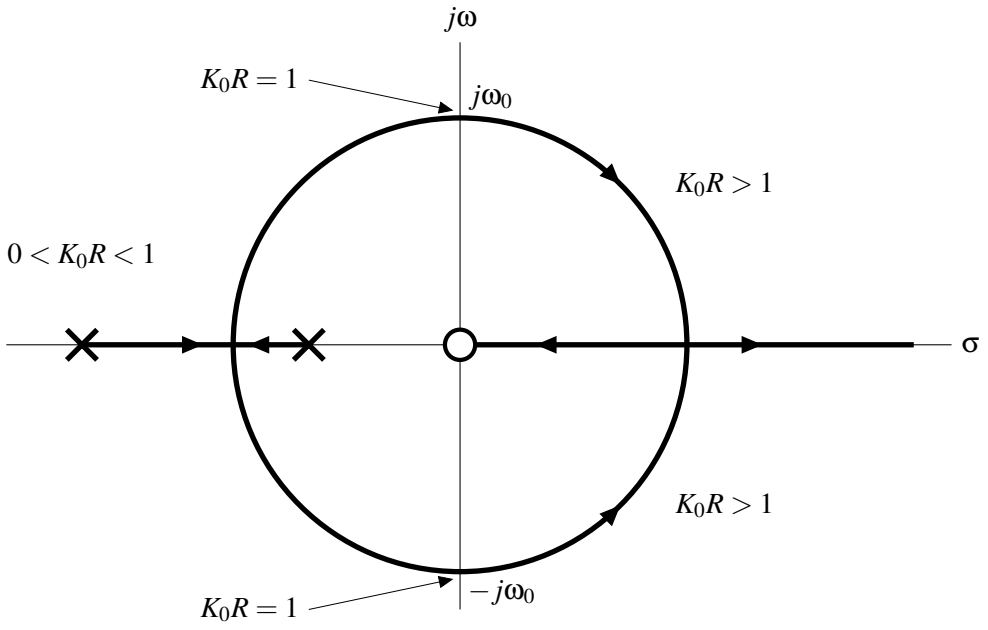

Figure 2.5: Root locus.

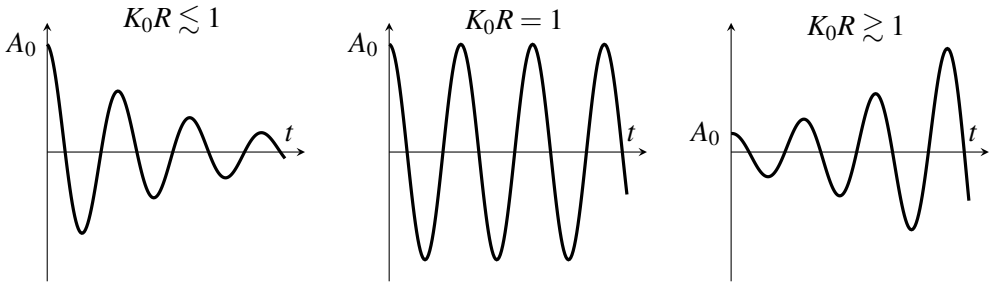

(a) (b) (c)

Figure 2.6: Time solutions for amplitude (a) decay, (b) steady, and (c) growth.

Using (2.2) and K_0 as a system parameter, we can plot the root locus and draw the same conclusion of (2.6), as shown in Fig. 2.5.

The time-domain solution of (2.5), for a loop gain near one, $K_0R \approx 1$, is

$$v_o(t) \approx A_0 e^{-\frac{(1-K_0R)}{RC}t} \cos(\omega_0 t), \tag{2.7}$$

where A_0 is the initial amplitude. From (2.7), or Fig. 2.5, three possible particular solution can be obtained, as shown in Fig. 2.6. For a loop gain slightly below unity, $K_0R \lesssim 1$, the oscillation can start, but cannot be maintained because the amplitude will decay exponentially until the oscillation stops. For a loop gain equal to unity, $K_0R = 1$, the loss in R is compensated, and the oscillation amplitude will be steady. For a loop gain with an excess, $K_0R \gtrsim 1$, the oscillation amplitude will grow exponentially.

We will now analyze the same circuit (Fig. 2.3), using the negative-resistance model.

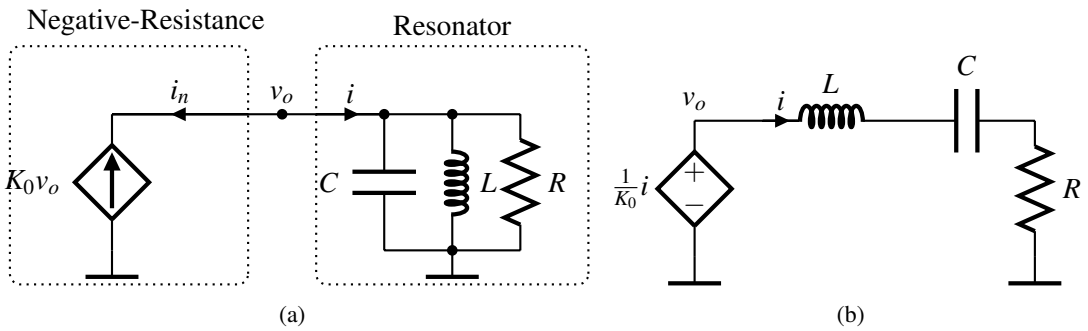

Figure 2.7: Negative-resistance model of (a) parallel, (b) series $LC-$oscillator.

Rearranging the circuit as shown in Fig. 2.7(a), it is clear that the resonator impedance is given by

$$Z(s) = \frac{V_o}{I} = \frac{s\frac{1}{C}}{s^2 + s\frac{1}{RC} + \frac{1}{LC}},$$

and the negative impedance is

$$Z_N = \frac{V_o}{I_n} = -\frac{1}{K_0}.$$

Applying Kurokawa's method, $Z(s) = -Z_N(s)$, yields the same characteristic equation

$$s^2 + s\frac{1}{RC}(1 - K_0 R) + \frac{1}{LC} = 0.$$

Therefore, we can conclude that, for linear systems, both methods give the same result.

The dual circuit (Fig. 2.7(b)) yields a similar result for the current, i. For clarity, we will refer to the first as parallel $LC-$oscillator and to the second the series $LC-$oscillator.

In the series $LC-$oscillator, the impedance of the resonator is

$$Z(s) = \frac{V_o}{I} = sL + \frac{1}{sC} + R,$$

and the impedance of the negative-resistance block is

$$Z_N(s) = \frac{V_o}{I_N} = -\frac{1}{K_0}.$$

Applying again the Kurokawa's method one obtains the characteristic equation

$$s^2 + s\frac{R}{L}\left(1 - \frac{1}{K_0 R}\right) + \frac{1}{LC} = 0,$$

which yields the time-domain solution

$$i(t) \approx A_0 e^{-\frac{R}{L}\left(1 - \frac{1}{K_0 R}\right)t} \cos(\omega_0 t). \tag{2.8}$$

From the time-domain solutions, (2.7) and (2.8), it is clear that the oscillation starts when the system has an excess loop gain $K_0 R > 1$. However, to reach steady-state amplitude it is necessary

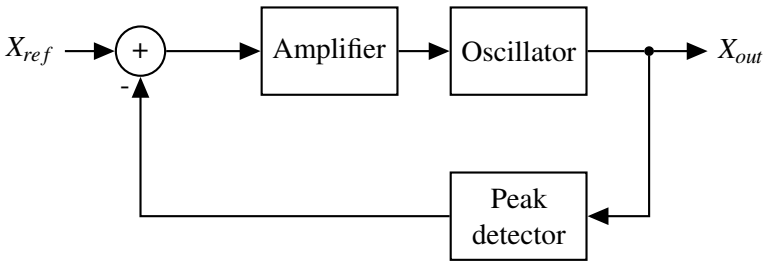

Figure 2.8: Conceptually automatic amplitude control.

an amplitude control technique to reduce the loop gain to one, $K_0R = 1$ and to keep it at this value. In the next section such techniques are discussed in detail.

2.3 Amplitude control

Sinusoidal oscillators require an excess loop gain to ensure startup, leading to an exponential growth of the oscillation amplitude. The amplitude must be regulated, or controlled, to avoid unwanted harmonics and distortion due to the clipping. In Fig. 2.8, a conceptual diagram of an automatic amplitude control (AAC) based on a negative feedback of the amplitude is shown. This type of AAC circuit works as follows: the output amplitude is measured, using a peak detector, and compares it with a reference, X_{ref}. If the amplitude is larger than X_{ref} the oscillator's gain is proportionally reduced and if the amplitude is lower the gain is increased, until the amplitude stabilizes at the reference level, i.e. $X_{out} \approx X_{ref}$.

Using an AAC circuit, as the one of Fig. 2.8, has several advantages: it ensures a correct startup; allows to set the optimum gain to reduce the total harmonic distortion and minimize the phase noise [32]; it maintains a constant output power regardless of the resonator quality factor, temperature and process variations [32]. The phase noise flattening, as reported in [33, 34, 35], is also an advantage. However, an AAC circuit increases the oscillator complexity, requiring more power and die area, and can become unstable [36, 37]. Another important aspect, often neglected, is to ensure an independent amplitude and frequency control. Otherwise a multi-input multi-output (MIMO), or multivariable, controller is required which increases the controller complexity. The $LC-$oscillator is an example in which the variable independence is guaranteed, since the frequency is determined only by the resonant tank and the amplitude can be controlled by the negative-resistance (usually controlled by the bias current). However, this is not the case for the majority of $RC-$oscillators, which leads to a more complex controller, therefore limiting the use of this technique for this type of oscillator.

Another common method to control the amplitude, usually for lower frequencies, is to use clamping elements (with a nonlinear characteristics), e.g. rectifier diodes. In comparison with the above method, this solution leads to higher harmonic distortion [38].

A third method is the use of the oscillator's intrinsic nonlinearities. In this case, the circuit parameters can be adjusted to obtain the desired output amplitude. For that, an accurate characterization of the oscillator is necessary, specially of its nonlinearities. A classic example is

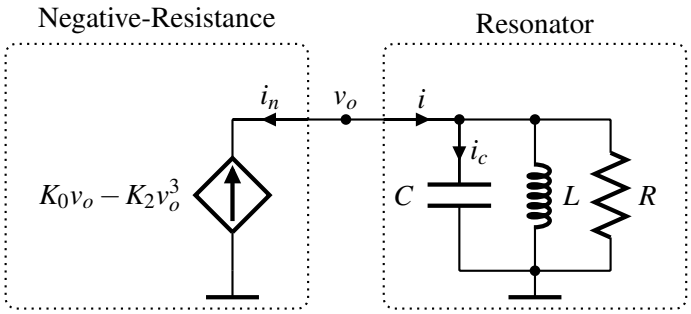

Figure 2.9: Parallel Van der Pol oscillator.

the VDPO in which the negative-resistance block has a linear term, $K_0 v_o$, and a nonlinear term, $K_2 v_o^3$, as shown in Fig. 2.9. The first generates the negative-resistance and the later regulates the amplitude growth.

We present the VDPO because many modern oscillators have similar behaviour presenting an equivalent characteristic equation as shown in [26, 39, 40]. For this reason, in the next chapter, we will use the VDPO to study several types of coupling.

Next we study the stability of this amplitude control mechanism and derive the oscillator solutions.

2.3.1 Equilibrium points and stability

Although Kurokawa has presented in [30] the conditions for stability, we will use a more general method to study the stability of the VDPO in detail. Since the circuit has a nonlinearity, it is simpler to derive the system dynamics in the time domain, rather than working in the frequency domain. Applying the Kirchhoff's current law at node v_o we obtain

$$C\frac{\mathrm{d}v_o}{\mathrm{d}t} + \frac{1}{L}\int v_o \mathrm{d}t + \frac{v_o}{R} = K_0 v_o - K_2 v_o^3, \tag{2.9}$$

that can be simplified to a nonlinear second-order differential equation by differentiating and dividing both sides by the capacitance C

$$\frac{\mathrm{d}^2 v_o}{\mathrm{d}t^2} + \frac{1}{RC}\left[(1 - K_0 R) + 3K_2 R v_o^2\right]\frac{\mathrm{d}v_o}{\mathrm{d}t} + \frac{1}{LC}v_o = 0. \tag{2.10}$$

Equation (2.10) can be reduced to the general form of the VDPO

$$\frac{\mathrm{d}^2 v_o}{\mathrm{d}t^2} - 2\left(\delta_0 - \delta_2 v_o^2\right)\frac{\mathrm{d}v_o}{\mathrm{d}t} + \omega_0^2 v_o = 0, \tag{2.11}$$

where $\delta_0 = (K_0 R - 1)/(2RC)$ and $\delta_2 = 3K_2 R/(2RC)$ represent the negative-resistance and the amplitude limiter, respectively, ω_0 is the oscillator free-running frequency.

To assess the stability of the system, we do a qualitative analysis. First, we take the second-order differential equation (2.11) and convert it into an equivalent system of two first-order differential equations

$$\begin{cases} \dfrac{\mathrm{d}v_o}{\mathrm{d}t} = \dfrac{1}{C} i_c & (2.12a) \\ \dfrac{\mathrm{d}i_c}{\mathrm{d}t} = 2\left(\delta_0 - \delta_2 v_o^2\right) i_c + \omega_0^2 v_o & (2.12b) \end{cases}$$

where the relation between the output voltage, v_o, and the current of the capacitance, i_c.

From (2.12) we can determine the equilibrium points, also known as critical points, by making the left-hand side of both equations zero. In this case, there is a single equilibrium point at $i_c = 0$ and $v_o = 0$. An equilibrium point is where the system stays in equilibrium (assuming a noiseless system). From the mathematical point of view, this means that an amplitude zero is a solution for (2.11). Physically it means that if the oscillator start with the capacitance and inductance discharged (voltage and current zero) it will remains in that state permanently.

We start by studying the local stability near the equilibrium point based on the linearised system. We find the linear version of the system, for any point in the phase space, calculating its Jacobian matrix

$$J = \begin{bmatrix} \frac{\partial f}{\partial v_o} & \frac{\partial f}{\partial i_c} \\ \frac{\partial g}{\partial v_o} & \frac{\partial g}{\partial i_c} \end{bmatrix} \Rightarrow \begin{bmatrix} 0 & \frac{1}{C} \\ -4\delta_2 i_c v_o - \omega_0^2 & 2\left(\delta_0 - \delta_2 v_o^2\right) \end{bmatrix}, \tag{2.13}$$

where f is a function representing the derivative of the output voltage, $f = \mathrm{d}v_o/\mathrm{d}t$, and g is a function representing the derivative of the capacitance current, $g = \mathrm{d}i_c/\mathrm{d}t$.

From the eigenvalues of the linearised system (eigenvalues of the Jacobian matrix) we can determine its stability. The eigenvalues are the roots of the characteristic polynomial that is obtain from

$$|J - \lambda I| = 0 \Rightarrow \begin{vmatrix} 0 - \lambda & \frac{1}{C} \\ -4\delta_2 i_c v_o - \omega_0^2 & 2\left(\delta_0 - \delta_2 v_o^2\right) - \lambda \end{vmatrix} = 0, \tag{2.14}$$

where J is the Jacobian matrix (2.13), λ is the eigenvalue and I is the identity matrix. From (2.14) we obtain the characteristic polynomial

$$\lambda^2 - T\lambda + D = 0, \tag{2.15}$$

where T is the trace of J and D is the determinant of J. For the VDPO the trace is

$$T = 2\left(\delta_0 - \delta_2 v_o^2\right), \tag{2.16}$$

and determinant is

$$D = \frac{1}{C}\left(4\delta_2 i_c v_o + \omega_0^2\right). \tag{2.17}$$

The stability conditions are: $T < 0$ and $D > 0$ for a stable point. For the equilibrium point at the origin we have

$$D(v_o = 0, i_c = 0) = \frac{\omega_0^2}{C} > 0, \tag{2.18}$$

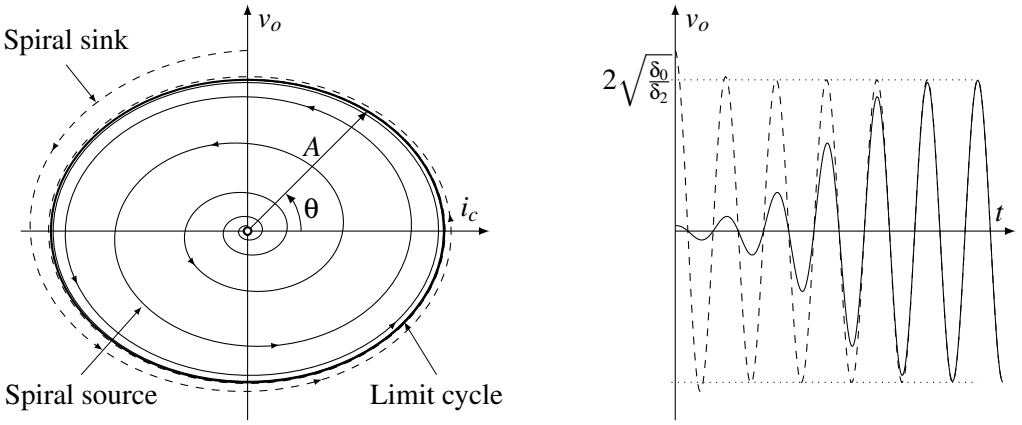

Figure 2.10: Van der Pol oscillator (a) phase diagram, (b) time-domain solution.

and

$$T(v_o = 0, i_c = 0) = 2\delta_0 > 0, \tag{2.19}$$

meaning that the equilibrium point is unstable if the trace of the Jacobian matrix is positive. Since $\delta_0 \sim (K_0 R - 1)$ we can safely say that the oscillation starts if $K_0 R > 1$, i.e. the equilibrium point must be unstable. Furthermore, we can say that near the equilibrium point we have a spiral source, as shown in the phase diagram of Fig. 2.10(a), because $T^2 < 4D$, resulting in two complex-conjugate eigenvalues. We can check this condition by solving (2.15) for λ resulting

$$\lambda = \frac{T}{2} \pm \frac{1}{2}\sqrt{T^2 - 4D}, \tag{2.20}$$

which shows the eigenvalues expressed in terms of the trace, T, and determinate, D.

Since the system is an oscillator, we expect the existence of a stable limit cycle[2]. The existence of a stable limit cycle indicates that at some point, far from the equilibrium point, a spiral sink must exist beyond the limit cycle. A complex-conjugate eigenvalues with $T < 0$ is a necessary condition for the existence of a spiral sink. From (2.16) it is clear that if, and only if, the output voltage is above $v_o > \sqrt{\delta_0/\delta_2}$ then $T < 0$ and, therefore, a spiral sink and a limit cycle exists.

Based on the qualitative analysis of the VDPO, without explicitly determined the solution, we can conclude that the system has an unstable equilibrium point at the origin and a stable limit cycle that limits the oscillation amplitude, see Fig. 2.10(a). Since a stable limit cycle exists, the solution is a sinusoidal signal as shown in Fig. 2.10(b).

We can make a simpler qualitative analysis, assuming that the output signal, v_o is sinusoidal

$$v_o(t) = A(t)\cos(\omega_0 t + \phi). \tag{2.21}$$

Using the harmonic balance method presented in [41], consisting of substituting (2.21) into (2.11) that is rewritten here for clarity,

[2]A limite cicle is a close trajectory in phase diagram that represents a periodic time-solution

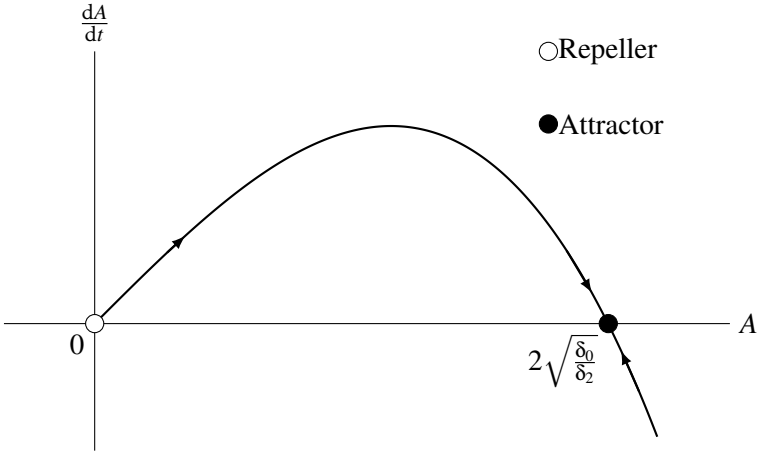

Figure 2.11: Amplitude curve of the Van der Pol oscillator.

$$\frac{d^2 v_o}{dt^2} - 2\left(\delta_0 - \delta_2 v_o^2\right)\frac{dv_o}{dt} + \omega_0^2 v_o = 0,$$

the amplitude and phase derivatives are obtained, see Appendix B. Assuming a slow variation of the amplitude we obtain

$$\begin{cases} \dfrac{dA}{dt} = \delta_0 A - \dfrac{1}{4}\delta_2 A^3 & \text{(2.22a)} \\ \dfrac{d\phi}{dt} = 0, & \text{(2.22b)} \end{cases}$$

For the phase, ϕ, since its derivative is zero means that any constant phase is valid. The absolute phase value will depend on the initial conditions of the circuit and will be maintained indefinitely in steady-state.

For the amplitude, three equilibrium points: $A = 0$, $A = 2\sqrt{\delta_0/\delta_2}$ and $A = -2\sqrt{\delta_0/\delta_2}$ can be determined from Section 2.3.1. However, we will consider only positive values for the amplitude since the negative values can be represented by a phase $\phi = \pi$. The plot of (2.22a) is shown in Fig. 2.11. A qualitative analysis of (2.22a) and Fig. 2.11, shows that the equilibrium point $A = 0$ is unstable, because $dA/dt > 0$ for $A > 0$, meaning that the oscillator can start with a zero amplitude, but any deviation from the equilibrium point and the amplitude will increase, and it never goes back. The second equilibrium point $A = 2\sqrt{\delta_0/\delta_2}$ is an attractor because for an amplitude below the equilibrium point $dA/dt > 0$ and for amplitudes above the equilibrium point $dA/dt > 0$. We also know that this attractor is stable because it is related to the stable limit cycle determined before, see Fig. 2.10(a).

The (2.22) can also be used to obtain the analytical solution for the amplitude since it is a separable first-order equation [41]. The general solution is given by

$$\int \frac{1}{\delta_0 A - \frac{1}{4}\delta_2 A^3} dA = \int dt - T_0,$$

where T_0 is an arbitrary constant. Solving the integrals gives

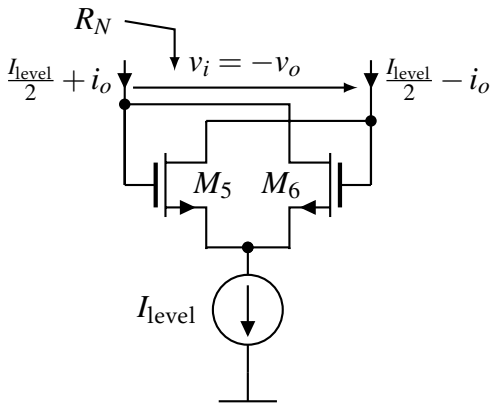

Figure 2.12: Negative resistance circuit.

$$\frac{1}{2\delta_0} ln\left(\frac{4A^2}{4\delta_0 - \delta_2 A^2}\right) = t - T_0,$$

from which results the transient amplitude response

$$A(t) = 2\sqrt{\frac{\delta_0}{\delta_2 + A_0 e^{-2\delta_0 t}}}, \tag{2.23}$$

where $A_0 = 4\delta_0^{-1} e^{2\delta_0 T_0}$ is a parameter that defines the initial amplitude of the circuit, i.e. for $t = 0$.

For steady-state, i.e. $t \to \infty$, the oscillation amplitude given by (2.23) is reduced to

$$A = 2\sqrt{\frac{\delta_0}{\delta_2}}. \tag{2.24}$$

The solution for the parallel topology of VDPO with $K_0 R > 1$ is obtained by substituting (2.23) into (2.21) resulting

$$v_o(t) = 2\sqrt{\frac{\delta_0}{\delta_2 + A_0 e^{-2\delta_0 t}}} \cos(\omega_0 t + \phi).$$

A similar solution for the series topology is obtained. Notice however that the result is expressed in terms of the current and not the voltage.

2.3.2 Negative-resistance circuits

In modern oscillators the negative-resistance is often implemented by a cross-coupled differential pair, as shown in Fig. 2.12. Here, we discard the capacitances, C_{gs} and C_{gd}, of transistors M_1 and M_2, since they can be lumped with the oscillator capacitance, C, resulting the simplified signal model of Fig. 2.13. From Fig. 2.13 we obtain

$$\begin{cases} i_o = -G_1 v_{gs1} & \text{(2.25a)} \\ i_o = G_2 v_{gs2} & \text{(2.25b)} \\ v_i = v_{gs1} - v_{gs2}. & \text{(2.25c)} \end{cases}$$

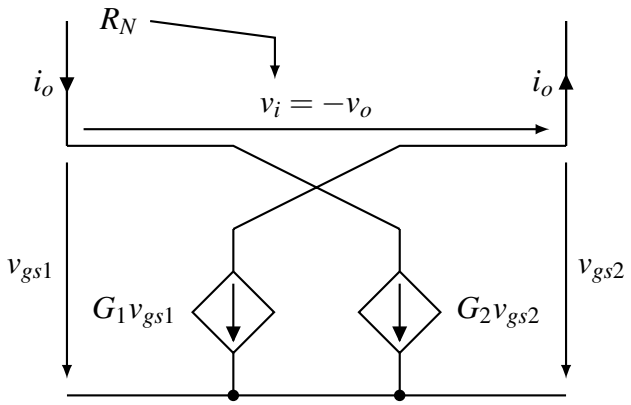

Figure 2.13: Negative resistance small-signal equivalent circuit.

Substituting (2.25a) and (2.25b) into (2.25c) we obtain the equivalent circuit resistance

$$R_N = \frac{v}{i} = -\frac{G_1 + G_2}{G_1 G_2}. \tag{2.26}$$

where G_i is the signal dependent transconductance of the $i-$th transistor, modelled by

$$G_i = g_{m0} + 2Kv_{gsi}, \tag{2.27}$$

where K is a parameter dependent on the transistors dimensions and technology, g_{m0} is the transistors' transconductance assuming no mismatch and v_{gsi} is the gate to source voltage of the $i-$th transistor, see Appendix A. In differential mode we get

$$\begin{cases} v_{gs1} = \dfrac{v_i}{2} & \text{(2.28a)} \\ v_{gs2} = -\dfrac{v_i}{2}. & \text{(2.28b)} \end{cases}$$

Substituting (2.28) into (2.27) and (2.26) results the, approximated, resistance of the circuit of Fig. 2.12

$$R_N \approx \frac{2}{-g_{m0} + \frac{K^2}{g_{m0}} v_i^2}, \tag{2.29}$$

where it is clear that R_{Neg} is a negative resistance in parallel with a nonlinear resistance that depends on the incremental voltage, v_i^2.

Another negative-resistance circuit often used is shown in Fig. 2.14(a). From its small-signal equivalent circuit (Fig. 2.14(b)) we obtain

$$\begin{cases} i = -G_1 v_{gs1} & \text{(2.30a)} \\ i = G_2 v_{gs2} & \text{(2.30b)} \\ v_o = v_o^+ - v_o^- = -2Ri & \text{(2.30c)} \\ v_o = (v_{gs1} - v_{gs2}) + v. & \text{(2.30d)} \end{cases}$$

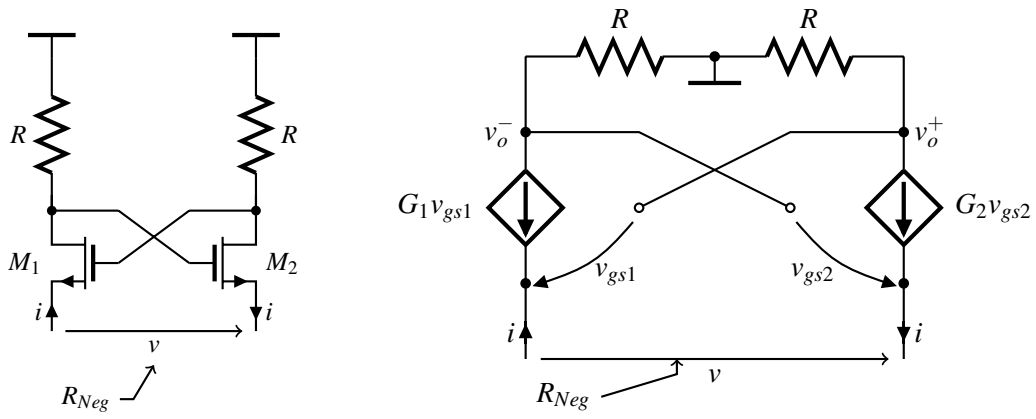

Figure 2.14: Negative resistance circuit (a) and the small-signal equivalent (b).

Substituting (2.30a), (2.30b) and (2.30c) into (2.30d) and rearranging the equation results the equivalent resistance of the circuit

$$R_{Neg} = \frac{v}{i} = \left(\frac{G_1 + G_2}{G_1 G_2}\right) - 2R = 2\left(\frac{1}{g_{m0} - \frac{K^2}{g_{m0}} v^2} - R\right), \tag{2.31}$$

From (2.31) we conclude that the equivalent resistance of the circuit (Fig. 2.14(a)) is a negative resistance in series with a nonlinear positive resistance. Because of this, instead of the parallel, the series VDPO approximation is used.

2.4 Frequency selectivity

The oscillation frequency of a sinusoidal oscillator is forced by the resonator. From the feedback model perspective, the resonator makes the required phase-shift so that the loop gain phase be 2π at the oscillation frequency. For the negative-resistance model, the resonator is a band-pass filter that attenuates unwanted frequencies passing only the frequency of its resonance, ω_0. This usually forces a free-running oscillator, like those we study so far, to have an oscillation frequency equal to the resonant frequency, or close to it if we consider the circuit's parasitic elements. However, that is not the case for coupled oscillators, as we will show in the following chapters.

The opposition of an oscillator to any deviation from its natural oscillation frequency is quantitatively defined by the $Q-$factor. Hence, an oscillator with an high Q will have a more stable oscillation frequency since it strongly opposes to any deviation from its oscillation frequency. Therefore, an oscillator with a low Q will have a less stable oscillation frequency. Usually an oscillator deviates from its natural frequency due to the circuit noise. Several noise sources in the circuit contribute to the overall noise, called the phase noise. The active elements contribute mainly with flicker, shot and thermal noise; resistors with thermal noise and the inductor and capacitor do not generate noise. The noise does not generate a uniformly distributed random walk near the resonant frequency, instead creates a specific spectrum shape. The Phase

noise spectrum shape is modelled by the equation proposed by Leeson in [42]. The phase noise along with Q are the common figures of merit for oscillators. Here, we will not discuss the phase noise topic; a comprehensive description can be found in [2, 3, 9, 11, 43]. We will focus on the definitions of Q and their equivalences.

In literature [2, 3], the general definition of the Q is

$$Q = 2\pi \frac{\text{Maximum Energy stored}}{\text{Energy dissipated per cycle}}, \tag{2.32}$$

which physically means the number of oscillations that a resonator does with the maximum energy stored in one cycle. From the general definition, we can derive the Q of a resonator network. For the parallel *RLC* resonator the voltage is the same for all elements. Hence, the maximum energy stored per cycle is related to the maximum voltage, A, on the capacitor, so that

$$E_C = \frac{1}{2} C A^2, \tag{2.33}$$

where A is the oscillation amplitude (maximum voltage).

The energy dissipated per cycle in the resistor is

$$E_R = \int_0^T P(t)\mathrm{d}t = \int_0^T \frac{v^2(t)}{R}\mathrm{d}t,$$

where $v(t) = A\cos(\omega_0 t)$, T is the oscillation period and R is the resistance value. Using the trigonometric identity $\cos^2 \omega_0 t = \frac{1}{2}(1 + \cos 2\omega_0 t)$ we get

$$E_R = \frac{1}{2}\frac{1}{R} A^2 T. \tag{2.34}$$

Substituting (2.33) and (2.34) into (2.32) results the well-known quality factor of the parallel *RLC* circuit

$$Q = 2\pi \frac{\frac{1}{2} C A^2}{\frac{1}{2}\frac{1}{R} A^2 T} = \omega_0 RC = R\sqrt{\frac{C}{L}}. \tag{2.35}$$

For the series *RLC* resonator it is the current that is common to all elements. Hence, the maximum energy stored per cycle is related to the maximum current in the inductor

$$E_L = \frac{1}{2} L A^2, \tag{2.36}$$

where A is the amplitude of the current. Reusing the energy dissipation equation so that

$$E_R = \int_0^T R i^2(t)\mathrm{d}t = \frac{1}{2} R A^2 T. \tag{2.37}$$

Substituting (2.36) and (2.37) into (2.32) results

$$Q = 2\pi \frac{\frac{1}{2} L A^2}{\frac{1}{2} R A^2 T} = \omega_0 \frac{L}{R} = \frac{1}{R}\sqrt{\frac{L}{C}}. \tag{2.38}$$

To use equations (2.35) and (2.38) the exact circuit parameters: R, L and C must be known. In practice, however, this is not always possible since parasitic elements are dispersed and cannot be

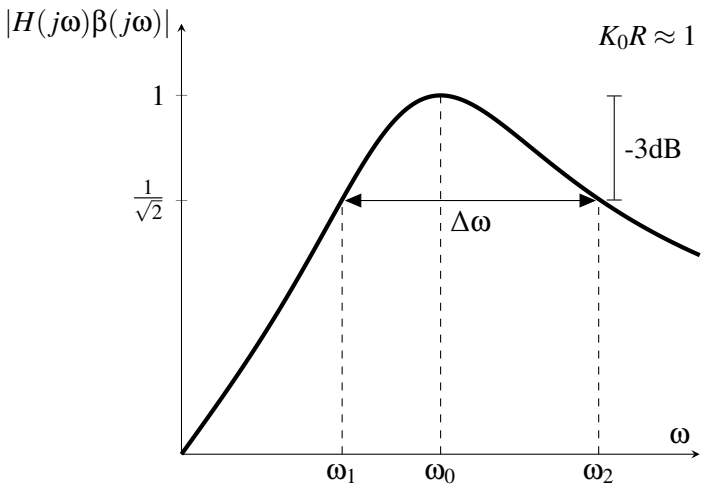

Figure 2.15: Loop gain frequency response.

easily grouped e.g. microwave circuits. However, if the exact Q cannot be determined, it should be measurable. In 1966 Leeson presented in [42] another definition for Q that solves this problem. The Leeson's definition relates the resonant frequency and the -3dB bandwidth of the resonator

$$Q = \frac{\omega_0}{\Delta\omega}, \tag{2.39}$$

where ω_0 is the resonant frequency and $\Delta\omega$ is the -3dB bandwidth. This definition allows to measure the Q from the resonator's frequency response. No formal proof was presented in [42]. The proof that both definitions are equivalent was derived in [44]. Take the loop gain of the $LC-$oscillator of Section 2.2, that we rewrite here for clarity, and assume $K_0R \approx 1$

$$H(s)\beta(s) = \frac{s\frac{1}{RC}}{s^2 + s\frac{1}{RC} + \frac{1}{LC}},$$

make the square of its magnitude equal to $\frac{1}{2}$

$$|H(j\omega)\beta(j\omega)|^2 = \frac{\omega^2\left(\frac{1}{RC}\right)^2}{\left(\omega_0^2 - \omega^2\right)^2 + \omega^2\left(\frac{1}{RC}\right)^2} = \frac{1}{2},$$

which is equivalent to a -3dB attenuation of the loop gain, as shown in Fig. 2.15. Solving for ω we obtain the polynomial

$$\omega^2 \pm \omega\frac{1}{RC} - \omega_0^2 = 0,$$

with the positive roots:

$$\omega_1 = -\tfrac{1}{2RC} + \sqrt{\left(\tfrac{1}{RC}\right)^2 + 4\omega_0^2}, \quad \omega_2 = \tfrac{1}{2RC} + \sqrt{\left(\tfrac{1}{RC}\right)^2 + 4\omega_0^2},$$

Subtracting the roots we obtain the -3dB bandwidth

$$\Delta\omega = \omega_2 - \omega_1 = \frac{1}{RC}. \tag{2.40}$$

Substituting (2.40) into (2.39) for $\omega = \omega_0$ results

$$Q = \frac{\omega_0}{\frac{1}{RC}} = R\sqrt{\frac{C}{L}}, \tag{2.41}$$

which is equal to (2.35). Hence, we can conclude that both definitions yield the same result for second order resonators [2]. A similar conclusion can be drawn for the series *RLC* resonator. However, for oscillators with distributed elements, which cannot be reduced to a second-order *RLC* circuit, the Leeson definition for Q is not accurate, as explained in [11, 45].

A third definition in Clarke-Hess [44] and in Rhea [46], based on the feedback model, defined Q as the phase slope at the resonance frequency

$$Q = -\frac{1}{2}\omega_0\frac{\partial\theta}{\partial\omega},$$

latter it was showed that this definition only can be applied to oscillators with resonators since it only considers the phase for the frequency stability. The definition fails for resonatorless oscillators like the two-integrator and the phase-shift oscillator [11].

A fourth definition proposed by Razavi in [11], called the open-loop Q, is based on the open-loop gain derivatives of the magnitude and phase,

$$Q = \frac{\omega_0}{2}\sqrt{\left(\frac{\mathrm{d}A}{\mathrm{d}\omega}\right)^2 + \left(\frac{\mathrm{d}\theta}{\mathrm{d}\omega}\right)^2}, \tag{2.42}$$

where A is the magnitude and θ is the phase of the loop gain. This definition is especially useful for analysis using the feedback model. A similar definition based on the Rhea definition, was proposed by Randall and Hock in [47], using the phase slope or group delay to determine the quality factor. They use the S-parameters to describe the open loop gain and from it the Q.

More recently, the definition proposed by Razavi was extended by Ohira in [48] and generalized to one- and two-port passive networks and in [49] to active networks as well. Ohira defines the Q factor as "the logarithmic derivative of port impedance"

$$Q = \frac{\omega_0}{2}\left|\frac{\mathrm{d}}{\mathrm{d}\omega}\ln\left(Z(j\omega)\right)\right| = \frac{\omega_0}{2}\frac{1}{|Z|}\left|\frac{\mathrm{d}Z}{\mathrm{d}\omega}\right|, \tag{2.43}$$

where Z is the resonator impedance. Using the resonators impedance presented in Section 2.2 we can verify the equivalence between the Ohira's definition and the other four definitions. Starting with the series *RLC* resonator, we know that the impedance is

$$Z(s) = sL + \frac{1}{sC} + R,$$

using $s = j\omega$ the magnitude of the impedance is

$$|Z(j\omega)| = \sqrt{\left(\omega L - \frac{1}{\omega C}\right)^2 + R^2}, \tag{2.44}$$

and the derivative is

$$\left|\frac{\mathrm{d}Z(j\omega)}{\mathrm{d}\omega}\right| = \left(L+\frac{1}{\omega^2 C}\right) = \left(\frac{\omega^2 LC+1}{\omega^2 C}\right). \tag{2.45}$$

Substituting (2.44) and (2.45) into (2.43) with $\omega = \omega_0$ results the expected Q of a series *RLC* circuit

$$Q = \frac{\omega_0}{2}\frac{1}{R}\frac{2}{\omega_0^2 C} = \frac{1}{R}\sqrt{\frac{L}{C}}.$$

For the parallel *RLC*, the impedance is

$$Z(s) = \frac{s\frac{1}{C}}{s^2 + s\frac{1}{RC} + \omega_0^2},$$

using $s = j\omega$ the magnitude of the impedance is

$$|Z(j\omega)| = \frac{\omega\frac{1}{C}}{\sqrt{\left(\omega_0^2-\omega^2\right)^2 + \omega^2\left(\frac{1}{RC}\right)^2}}, \tag{2.46}$$

and the derivative is

$$\left|\frac{\mathrm{d}Z(j\omega)}{\mathrm{d}\omega}\right| = 2R^2C. \tag{2.47}$$

Substituting (2.46) and (2.47) into (2.43) with $\omega = \omega_0$ results the expected Q of a parallel *RLC* circuit

$$Q = \frac{\omega_0}{2}\frac{1}{R}2R^2C = R\sqrt{\frac{C}{L}}.$$

The fifth method yield the same result for second order resonators, therefore, we can conclude that they are equivalent. Since we will use the VDPO as a basic oscillator to study the coupled oscillators it is pertinent to write the Van der Pol equation in terms of Q. Writing the VDPO in terms of Q yields an advantage since the series and parallel topologies can be described by a single equation. The VDPO coefficients δ_0 and δ_2 are described in terms of Q as:

$$\delta_0 = \frac{\omega_0}{2Q}\left(K_0R-1\right), \delta_2 = \frac{\omega_0}{2Q}\left(3K_2R\right),$$

from which the characteristic equation is

$$s^2 + \frac{\omega_0}{Q}\left[\left(K_0R-1\right)+3K_2RA^2\right]s + \omega_0^2 = 0,$$

and the differential equations is

$$\frac{\mathrm{d}^2x_o}{\mathrm{d}t^2} + \frac{\omega_0}{Q}\left[\left(K_0R-1\right)+3K_2Rx_o^2\right]\frac{\mathrm{d}x_o}{\mathrm{d}t} + \omega_0^2x_o = 0,$$

where x can be the output voltage or current for parallel or series topology, respectively.

CHAPTER 3

INJECTION LOCKING

Contents

3.1 Introduction

In Chapter 2 we studied the series and parallel topology of sinusoidal oscillators in free-running mode, in which the oscillator input is zero. In this chapter we study a more general case, known as driven mode, in which the oscillator input is connected to an external periodic signal generator (a nonzero input). We use the VDPO to study the coupling and derive the equations for the oscillation frequency, amplitude, and phase. We consider both the series and parallel topologies of the VDPO since we want to apply the results to the study of the coupled $RC-$oscillator (which is modelled by the series VDPO) and the Two-Integrator (modelled by the parallel VDPO). We start by describing the synchronization of a single oscillator with an external sinusoidal source, then in the following chapters we substitute the external source by a second oscillator and study its influence on the quadrature oscillator key parameters.

Before studying coupled oscillators, we present here a description of the injection-locking mechanism. This mechanism was extensively studied by Adler [5], Kurokawa [50], and others [51, 52]. The injection-locking principle is commonly found in frequency dividers and coupled oscillators [52]. It is also used for phase-noise improvement. The ILFD forces an oscillator to

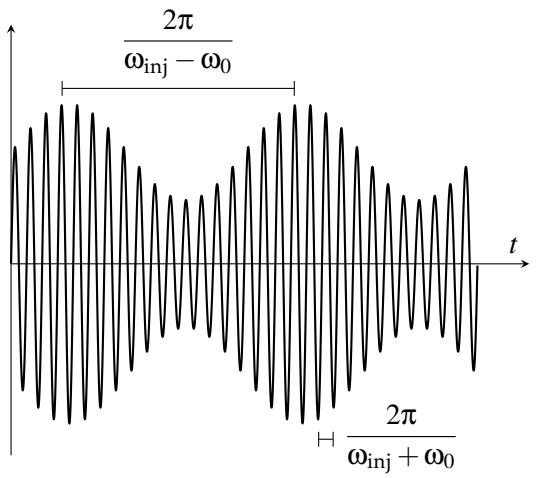

Figure 3.1: Beat.

be locked with a sub-harmonic of its free-running frequency, thus implementing a divide-by-two or divide-by-three circuit, as explained in [53]. Another useful application is the improvement of an oscillator phase-noise by direct injection the signal of a reference oscillator (with low phase-noise); the advantage of this method is the reduction of the phase-noise without requiring additional circuits and power. A comprehensive study of the above applications can be found in [52]. In this chapter we focus on using the injection-locking theory to study coupled oscillators.

Injection-locking occurs when an oscillator is driven by an external periodic signal (locking signal) and the injected current, or voltage, forces the oscillator to change its frequency, synchronizing it with the locking signal. However, this synchronization only occurs if the locking frequency is within a band (dependent of the oscillator parameters), commonly known as locking range. Otherwise, if the frequency is either below or above the locking range, the output will be a high frequency sinusoid (with the sum of the external and free-running frequencies) modulated in amplitude by a low frequency sinusoid (the difference between the two frequencies), as shown in Fig. 3.1. This phenomenon is called Beat.

The locking range is an important parameter also for coupled oscillators because practical oscillators have mismatches and their oscillation frequencies may diverge. The mismatches and the parasitic elements should not separate the oscillation frequencies beyond the locking range, otherwise the locking between the two oscillators does not occur, leading to an undesired output signal, as shown in Fig. 3.1.

As will be derived next, the steady-state amplitude of the oscillator in the locked condition will depend on the phase and amplitude of the locking signal. The phase difference, between the locking signal and the oscillator output signal, depends on the frequencies and on the amplitudes of the free-running and external signals.

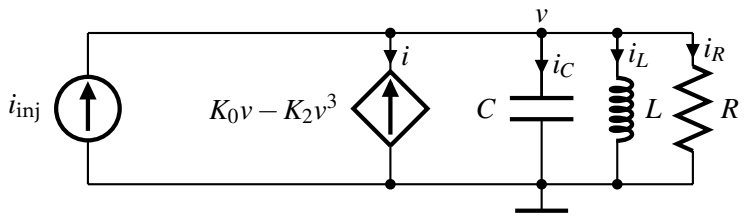

Figure 3.2: Injection-lock parallel VDPO

3.2 Parallel VDPO

In this section we study the injection-lock in the parallel VDPO. The results obtained here will be relevant to the study of the two-integrator oscillator, in Chapter 6, which consists of two integration stages coupled by transconductance amplifiers. The two-integrator oscillator can be modelled by two injection-locked stages, in which the output of a stage will drive the injection current on the other.

Let us analyse the parallel VDPO with an external sinusoidal current source (locking signal) in parallel, as shown in Fig. 3.2. Applying the Kirchhoff's current law (KCL) we obtain

$$i_C + i_R + i + i_L = i_{\text{inj}},$$

substituting the currents by their equations we get

$$C\frac{\mathrm{d}v}{\mathrm{d}t} + \frac{1}{R}v - K_0 v + K_2 v^3 + \frac{1}{L}\int v\mathrm{d}t = i_{\text{inj}},$$

Dividing both sides of the equation by C and differentiating one obtains

$$\frac{\mathrm{d}^2 v}{\mathrm{d}t^2} - 2\left(\delta_0 - \delta_2 v^2\right)\frac{\mathrm{d}v}{\mathrm{d}t} + \omega_0^2 v = \frac{\omega_0 R}{Q}\frac{\mathrm{d}i_{\text{inj}}}{\mathrm{d}t}, \tag{3.1}$$

where

$$\delta_0 = \frac{\omega_0}{2Q}\left(K_0 R - 1\right), \qquad \delta_2 = \frac{\omega_0}{2Q} 3K_2 R,$$

and Q is the quality factor of the parallel *RLC* circuit. We call (3.1) the driven VDPO equation because the right-hand side is non zero. In mathematical terminology, this is a non-homogeneous differential equation.

From differential equations theory, we know that the general solution of a linear differential equation is the solution of the homogeneous equations, v_H, plus the particular solution of the non-homogeneous, v_P

$$v(t) = v_H(t) + v_P(t). \tag{3.2}$$

Although the left-hand side of (3.1) is not linear, it can be approximated by a linear expression if the coefficient of $\mathrm{d}v/\mathrm{d}t$ is very small and can be approximated by a constant [41], which is true

near the steady-state. Hence, assuming that the system is near steady-state and knowing that the solution is sinusoidal, (3.2) can be written as

$$v(t) = V\sin(\omega t - \phi) = (V_H + V_P)\sin[\omega t - (\phi_H + \phi_P)], \tag{3.3}$$

where V_H and ϕ_H are the amplitude and phase of the homogeneous solution, V_P and ϕ_P are the amplitude and phase of the particular solution. The amplitude and phase derivatives of the homogeneous solution were already derived in (2.22) and the result is

$$\begin{cases} \dfrac{dV_H}{dt} = \delta_0 V_H - \dfrac{1}{4}\delta_2 V_H^3 & \text{(3.4a)} \\ \dfrac{d\phi_H}{dt} = 0. & \text{(3.4b)} \end{cases}$$

To obtain the particular solution we first have to match the left- and right-hand sides of (3.1), writing the latter in terms of $\sin\omega t$ and $\cos\omega t$. To do this, we assume a locking signal of the form

$$i_{\text{inj}} = I_{\text{inj}}\sin\left(\omega_{\text{inj}} t - \phi_{\text{inj}}\right). \tag{3.5}$$

Using the trigonometric relationship $\cos(\alpha+\beta) = \cos\alpha\cos\beta - \sin\alpha\sin\beta$ in the derivative of (3.5), result in

$$\frac{di_{\text{inj}}}{dt} = I_{\text{inj}}\omega_{\text{inj}}\left[\cos\left(\Omega t - \phi_{\text{inj}}\right)\cos\omega t - \sin\left(\Omega t - \phi_{\text{inj}}\right)\sin\omega t\right], \tag{3.6}$$

where $\Omega = \left(\omega_{\text{inj}} - \omega\right)$ is the frequencies difference (it is zero when there is locking). Substituting (3.6) into (3.1) and, using the harmonic balance method, and neglecting the second term of (3.1) (see Appendix C for details) we obtain the amplitude and phase derivatives of the particular solution:

$$\begin{cases} \dfrac{dV_P}{dt} = \dfrac{\omega_0}{Q}\cdot\dfrac{\omega_{\text{inj}}}{2\omega}\cdot RI_{\text{inj}}\cos\left[\left(\omega_{\text{inj}} - \omega\right)t + \phi\right] & \text{(3.7a)} \\ \dfrac{d\phi_P}{dt} = \dfrac{\omega^2 - \omega_0^2}{2\omega} - \dfrac{\omega_0}{Q}\cdot\dfrac{\omega_{\text{inj}}}{2\omega}\cdot\dfrac{RI_{\text{inj}}}{V}\sin\left[\left(\omega_{\text{inj}} - \omega\right)t + \phi\right], & \text{(3.7b)} \end{cases}$$

where ϕ is the phase difference between the oscillator output and the locking signal. From (3.4) and (3.7) we obtain the amplitude and phase derivatives of the general solution

$$\begin{cases} \dfrac{dV}{dt} = \left(\delta_0 V - \dfrac{1}{4}\delta_2 V^3\right) + \dfrac{\omega_0\omega_{\text{inj}}}{2Q\omega}RI_{\text{inj}}\cos\left[\left(\omega_{\text{inj}} - \omega\right)t + \phi\right] & \text{(3.8a)} \\ \dfrac{d\phi}{dt} = \dfrac{\omega^2 - \omega_0^2}{2\omega} - \dfrac{\omega_0\omega_{\text{inj}}RI_{\text{inj}}}{2Q\omega V}\sin\left[\left(\omega_{\text{inj}} - \omega\right)t + \phi\right]. & \text{(3.8b)} \end{cases}$$

Note that the pair of equations (3.8) are non-autonomous since they explicitly depend on t. The differential equation (3.8) must be autonomous to have a steady-state with constant amplitude and phase. This is possible only if the oscillator is locked to the external signal (i.e. $\omega = \omega_{\text{inj}}$). Otherwise, the amplitude and phase vary with t, generating beats.

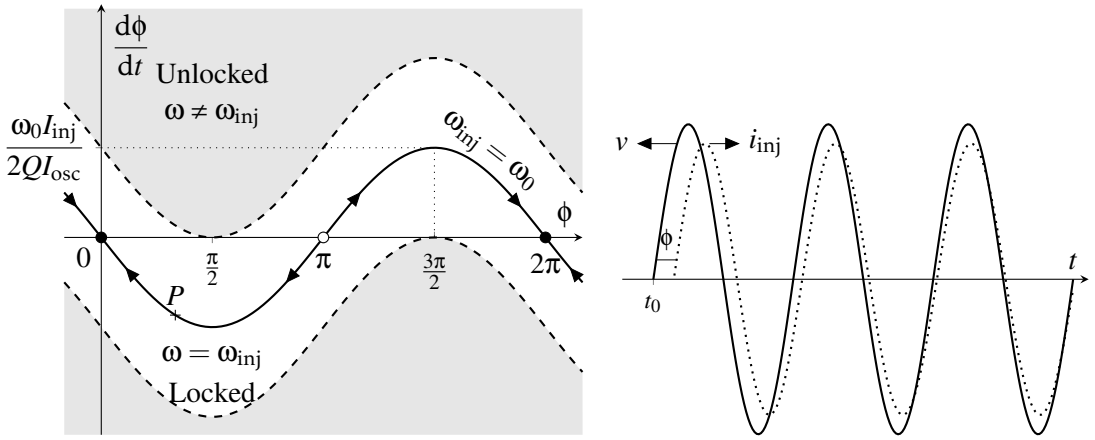

(a) (b)

Figure 3.3: Phase curve of the injection-lock parallel VDPO (a) and the time solution of path path P (b).

Assuming that the oscillator is locked $\omega = \omega_{inj}$, (3.8) becomes

$$\begin{cases} \dfrac{dV}{dt} = \left(\delta_0 V - \dfrac{1}{4}\delta_2 V^3\right) + \dfrac{\omega_0}{2Q} R I_{inj} \cos(\phi) & \text{(3.9a)} \\ \dfrac{d\phi}{dt} = \dfrac{\omega_{inj}^2 - \omega_0^2}{2\omega_{inj}} - \dfrac{\omega_0}{2Q} \cdot \dfrac{I_{inj}}{I} \sin(\phi). & \text{(3.9b)} \end{cases}$$

where I is the oscillator's bias current (Figure 3.2).

We analyse first the phase derivative given by (3.8) and illustrated in Fig. 3.3(a). In Fig. 3.3(a) the locking region (in which the oscillator frequency equals the locking frequency) is represented in white and the unlocking regions (where $\omega \neq \omega_{inj}$) are shaded. The dashed curves represent the boundary between the unlocking and locking regions. To better understand the circuit behaviour, consider the particular case of a locking signal with the same frequency of the free-running oscillator, $\omega_{inj} = \omega_0$, (represented in the figure by the solid curve). From (3.9) we find two equilibrium points: a stable equilibrium point at $\phi = 0$ and an unstable at $\phi = \pi$. Hence, in steady-state, the locking signal and the oscillator output will be in-phase.

Let us consider the signals of Fig. 3.3(b) with a phase difference $\phi = \pi/3$, which corresponds to point P in the phase curve of Fig. 3.3(a). At this point, the phase derivative is negative meaning that the oscillator phase will be forced to decrease until both signals are in-phase. Hence, as time passes the phase difference is reduced, as shown in Fig. 3.3(b). If we consider a phase difference higher than π the derivative is positive meaning that the phase will increase until it reaches a $\phi = 2\pi$.

From (3.9) we can see that the other curves (that will be within the white region) are offset versions of this particular case. For $\omega_{inj} > \omega_0$ the curve is shifted upwards and the stable equilibrium point shifts to the right (increasing the phase difference). For $\omega_{inj} < \omega_0$ the curve is shifted downwards and the stable equilibrium point shifts to the left (decreasing the phase difference). Let us consider a frequency sweep of the locking signal. We start with a frequency equal to ω_0 having a zero phase difference, as the frequency increases so does the phase difference

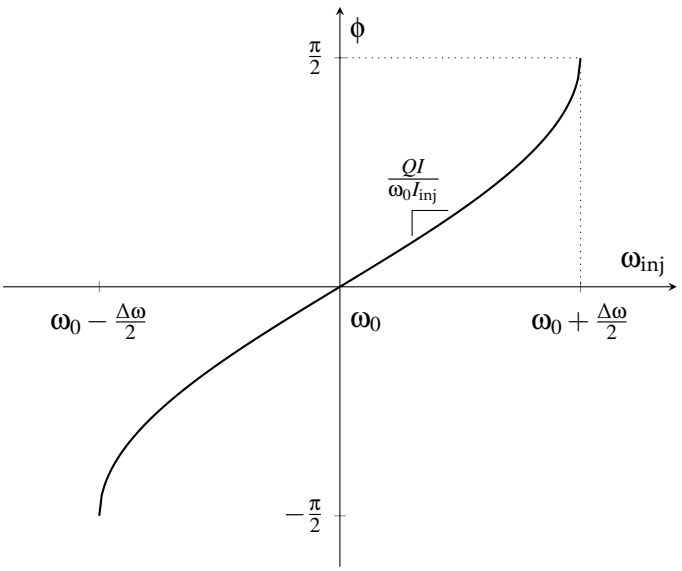

Figure 3.4: Injection Lock phase curve.

until the high boundary is reached (higher dashed curve). At this point a single equilibrium point exists (at $\phi = \pi/2$), but it is unstable, meaning that the oscillator cannot follow further the locking signal and enters the unlocking region. This frequency is the upper limit of the locking range, $\Delta\omega$. On the opposite direction, if we decrease the frequency until the bottom limit is reached, the same happens (the only difference is that the unstable equilibrium point is at $\phi = 3\pi/2 = -\pi/2$). From (3.9), we can analytically determine the locking range by equating the left-hand side to zero and solving to ω_{inj} for the two boundary cases. Hence, for $\omega_{inj} < \omega_0$ and $\phi = -\pi/2$,

$$\omega_{inj.min}^2 + \frac{\omega_0}{Q} \cdot \frac{I_{inj}}{I} \omega_{inj.min} - \omega_0^2 = 0, \tag{3.10}$$

so that the positive root is

$$\omega_{inj.min} = -\frac{\omega_0}{2Q}\frac{I_{inj}}{I} + \frac{1}{2}\sqrt{\left(\frac{1}{2Q}\frac{I_{inj}}{I}\right)^2 \omega_0^2 + 4\omega_0^2}. \tag{3.11}$$

For $\omega_{inj} > \omega_0$ and $\phi = \pi/2$,

$$\omega_{inj.max}^2 - \frac{\omega_0}{Q} \cdot \frac{I_{inj}}{I} \omega_{inj.max} - \omega_0^2 = 0, \tag{3.12}$$

so that the positive root is

$$\omega_{inj.max} = \frac{\omega_0}{2Q}\frac{I_{inj}}{I} + \frac{1}{2}\sqrt{\left(\frac{1}{2Q}\frac{I_{inj}}{I}\right)^2 \omega_0^2 + 4\omega_0^2}. \tag{3.13}$$

The difference between the maximum (3.13) and minimum (3.12) frequencies gives the locking range

$$\Delta\omega = \omega_{inj.max} - \omega_{inj.min} = \frac{\omega_0}{Q}\frac{I_{inj}}{I}. \tag{3.14}$$

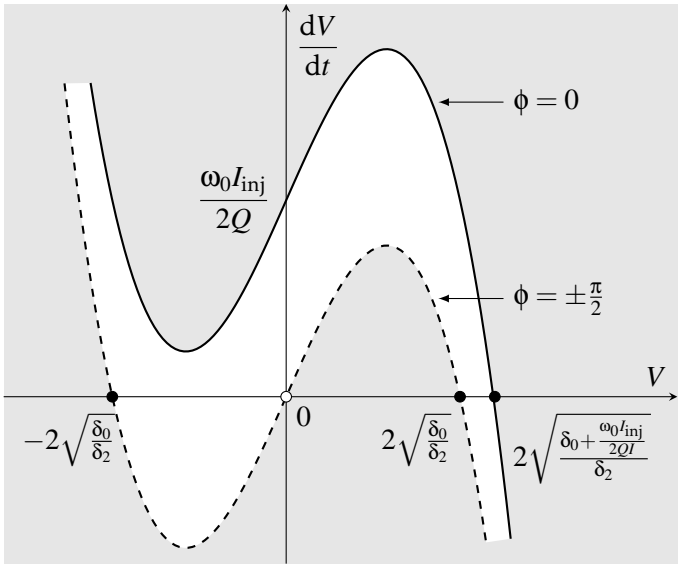

Figure 3.5: Amplitude phase curve of the injection locking

which is consistent with the locking range equation in [52].

By taking again (3.9), equating the left-hand side to zero, and solving the equation for ϕ we get

$$\phi = \arcsin\left(\frac{Q}{\omega_0}\frac{I}{I_{inj}}\frac{\omega_{inj}^2 - \omega_0^2}{\omega_{inj}}\right), \tag{3.15}$$

which relates the phase difference with the frequency of the locking signal, as shown in Fig. 3.4. From Fig. 3.4 we can see that the phase difference decreases with the increase of the locking frequency. Near the free-running frequency, ω_0, the characteristic is almost linear with slope $\frac{QI}{\omega_0 I_{inj}}$. Note that the graph in Fig. 3.4 is not defined for frequencies outside the locking range, since the oscillator is not locked and the phase is not constant.

Let us analyse now the amplitude derivative given by (3.8) and illustrated in Fig. 3.5 where the shaded areas correspond to states where the oscillator is unlocked. The white area corresponds to states where the oscillator is locked (3.9). We rewrite it here for convenience

$$\frac{dV}{dt} = \left(\delta_0 V - \frac{1}{4}\delta_2 V^3\right) + \frac{\omega_0}{2Q} R I_{inj}\cos(\phi). \tag{3.16}$$

The dashed curve represents the boundary between the locking and unlocking areas. Notice that at the boundary the oscillator is unlocked, although it seems to be a steady-state solution, since it has stable equilibrium points. The reason for that is the phase dynamics. This boundary occurs for a phase difference of $\phi = \pi/2$, or $\phi = -\pi/2$, which both are unstable in the phase curve, as shown in Fig. 3.3(a). From (3.16) we can see that the other cases, within the white area, are offset versions of the boundary. The upper limit occurs when the locking and the free-running frequencies are equal forcing the oscillator to be in-phase with the locking signal. Note that the stable equilibrium points are shifted to the right as the offset increases, which is equivalent to an increase of the amplitude.

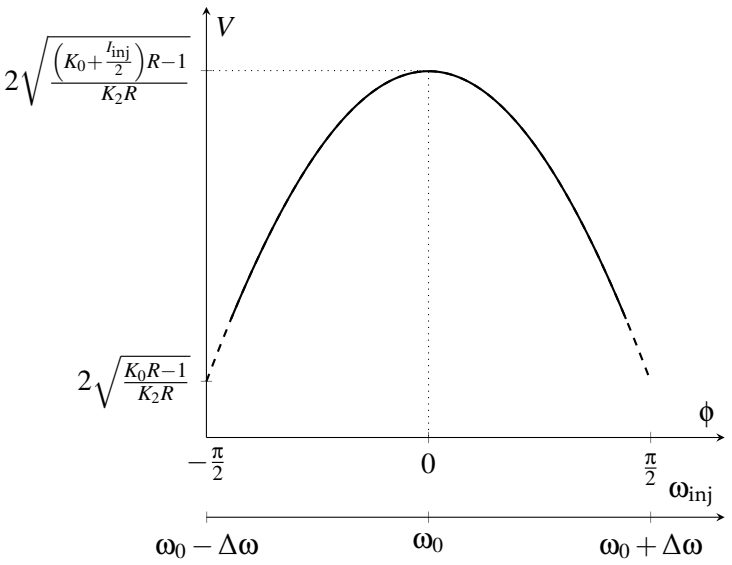

Figure 3.6: Amplitude as a function of the oscillation frequency.

Solving (3.16) for steady-state (i.e. $dV/dt = 0$) and substituting δ_0 and δ_2 by the equations in terms of circuit parameters, results in

$$V \approx 2\sqrt{\frac{\left(K_0 + \frac{I_{inj}}{2}\cos\phi\right)R - 1}{3K_2R}}, \qquad \text{for } V > 0, \tag{3.17}$$

which relates the amplitude with the phase difference, as shown in Fig. 3.6. The curve in Fig. 3.6 is an approximate representation, since the relationship between the phase and the frequency is not linear especially near the boundary, as can be seen from Fig. 3.4.

We can conclude that, if the frequency of the external signal is within the locking range the oscillator locks in frequency. Although the frequency locks, the phase and amplitude depend on the locking frequency. From (3.15), we conclude that for frequencies near ω_0, the phase is proportional to Q and to the ratio between the oscillator current, I, and the injected current, I_{inj}, such as

$$\phi \propto \left(\frac{Q}{\omega_0}\cdot\frac{I}{I_{inj}}\right)\left(\omega_{inj}-\omega_0\right).$$

From (3.17), we conclude that the amplitude depends on the phase (which in turn depends on the locking frequency) and on the injection signal amplitude, I_{inj}.

3.3 Series VDPO

In this section we analyse the injection-locking of a series VDPO, which is relevant because $RC-$oscillators are best modelled by a series VDPO. The results obtained here will be useful for the analysis of the active and passive coupling of $RC-$oscillators in Chapter 4 and Chapter 5. We first analyse the injection-locking with a single external source (similar to the last section), which is suitable for the active coupling. Afterwards, we analyse the double injection, best suited for the

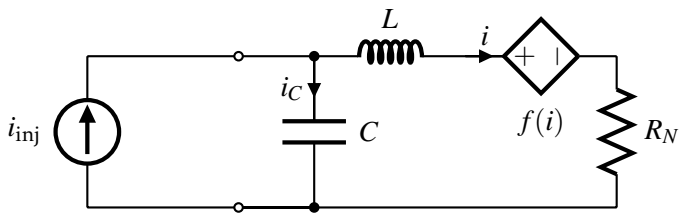

Figure 3.7: Driven series Van der Pol oscillator.

passive coupling. Note that the analysis of the passive coupling is more cumbersome because the current injected into an oscillator is outputted by another oscillator, meaning that each oscillator will have two injection currents, one coming in and the other going out.

3.3.1 Single external source

Let us analyse the series VDPO with a single external current source (locking signal) in parallel, as shown in Fig. 3.7, where $f(i) = K_0 i - K_2 i^3$ represent the VDP non-linearity and R_N is a negative resistance. Although, the series VDPO is dual of the parallel, with a locking signal in parallel the result is not exactly the same. Applying the KCL and Kirchhoff's voltage law (KVL) we obtain

$$\begin{cases} i_C + i = i_{\text{inj}} \\ v_L + f(i) + v_{R_N} - v_C = 0 \end{cases}$$

substituting the currents and voltages by the elements equations we get

$$L\frac{\mathrm{d}i}{\mathrm{d}t} + R_N i + K_0 i - K_2 i^3 + \frac{1}{C}\int i\mathrm{d}t = \frac{1}{C}\int i_{\text{inj}}\mathrm{d}t.$$

Dividing by L and differentiating both sides this equation is reduced to

$$\frac{\mathrm{d}^2 i}{\mathrm{d}t^2} - 2\left(\delta_0 - \delta_2 i^2\right)\frac{\mathrm{d}i}{\mathrm{d}t} + \omega_0^2 i = \omega_0^2 i_{\text{inj}}, \tag{3.19}$$

where

$$\delta_0 = -\frac{R_N + K_0}{2L}; \qquad \delta_2 = -3\frac{K_2}{2L}.$$

Comparing (3.1) with (3.19) shows that the two systems are not fully dual of each other, since the right-hand side of (3.19) depends directly on the locking signal and not on its derivative. From (3.19) assuming a locking signal of the form (3.5) and that the oscillator is locked ($\omega = \omega_{\text{inj}}$) we obtain the amplitude and phase derivatives

$$\begin{cases} \dfrac{\mathrm{d}I}{\mathrm{d}t} = \left(\delta_0 I - \dfrac{1}{4}\delta_2 I^3\right) + \dfrac{\omega_0^2}{2\omega_{\text{inj}}} I_{\text{inj}} \sin(\phi) & \text{(3.20a)} \\ \dfrac{\mathrm{d}\phi}{\mathrm{d}t} = \dfrac{\omega_{\text{inj}}^2 - \omega_0^2}{2\omega_{\text{inj}}} + \dfrac{\omega_0^2}{2\omega_{\text{inj}}} \cdot \dfrac{I_{\text{inj}}}{I}\cos(\phi). & \text{(3.20b)} \end{cases}$$

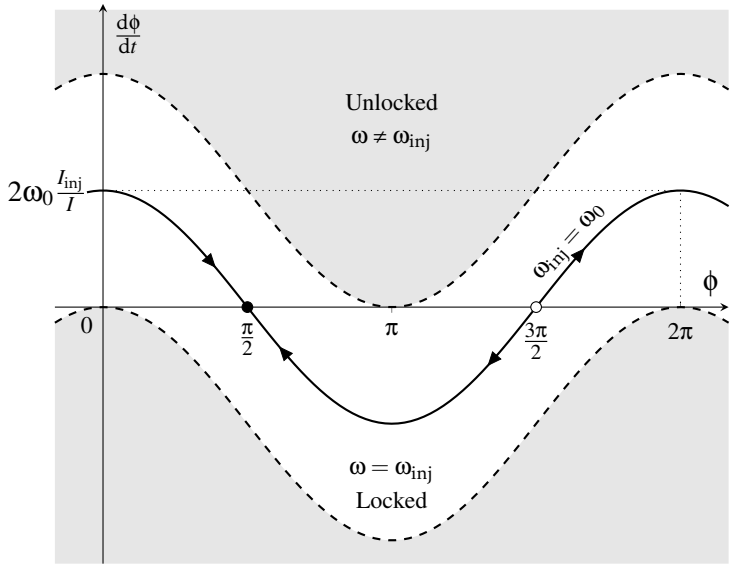

Figure 3.8: Phase curve of the series VDPO.

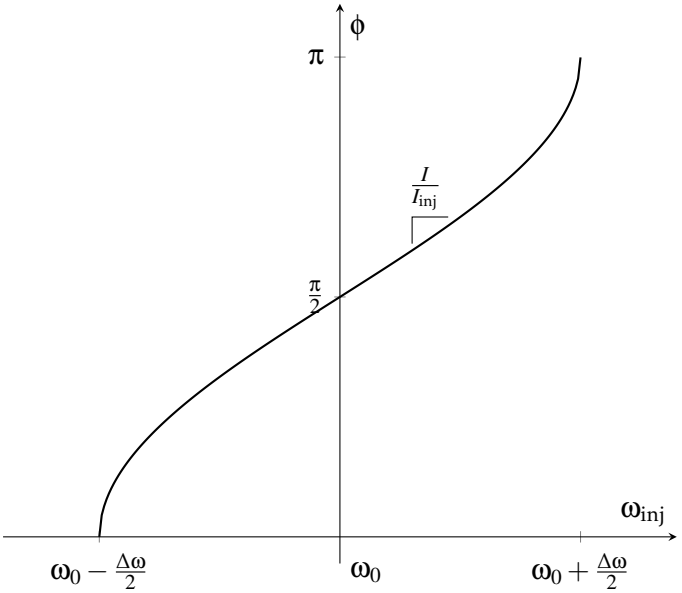

Figure 3.9: Phase as a function of the frequency of the external signal.

We can conclude from (3.20) that the stable equilibrium point for the phase difference is shifted by $\pi/2$, in comparison with the driven parallel VDPO, as shown in Fig. 3.8. Hence, a locking signal with a frequency near the free-running frequency of the oscillator, ω_0, forces a phase difference of $\pi/2$ between the signals, as shown by the injection-lock phase curve in Fig. 3.9.

Moreover, the locking range is given by

$$\Delta\omega \approx 2\omega_0 \frac{I_{inj}}{I}.$$

which is higher in comparison with the driven parallel VDPO.

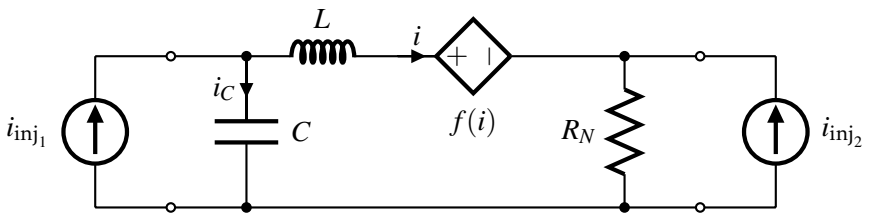

Figure 3.10: Driven series Van der Pol oscillator with double injection.

3.3.2 Double external source

Let us now analyse the series VDPO with a double external current sources (locking signals) in parallel, as shown in Fig. 3.10. This type of injection locking and the study presented here is important to understand the coupling with passive networks, which will be particularly useful in Chapter 5. Usually, passive coupling networks are reciprocal which means that the output current of an oscillator is injected into a second oscillator and the other way around. This behaviour is well modelled by the double injection-locking, which is the main reason for presenting this study. Thus, consider the circuit of Fig. 3.10. Applying the KCL and KVL) to the circuit (Fig. 3.10) we obtain

$$\begin{cases} i_C + i = i_{\text{inj}_1} \\ i_{R_N} = i + i_{\text{inj}_2} \\ v_L + f(i) + v_{R_N} - v_C = 0 \end{cases}$$

substituting the currents and voltages by the elements equations we get

$$L\frac{\mathrm{d}i}{\mathrm{d}t} + R_N i + K_0 i - K_2 i^3 + \frac{1}{C}\int i\mathrm{d}t = \frac{1}{C}\int i_{\text{inj}_1}\mathrm{d}t + R_N i_{\text{inj}_2}.$$

Dividing by L and differentiating both sides this equation is reduced to

$$\frac{\mathrm{d}^2 i}{\mathrm{d}t^2} - 2\left(\delta_0 - \delta_2 i^2\right)\frac{\mathrm{d}i}{\mathrm{d}t} + \omega_0^2 i = \omega_0^2 i_{\text{inj}_1} + \frac{R_N}{L}\frac{\mathrm{d}i_{\text{inj}_2}}{\mathrm{d}t}, \tag{3.22}$$

where the VDP parameters are given by

$$\delta_0 = -\frac{R_N + K_0}{2L}; \qquad \delta_2 = -3\frac{K_2}{2L}.$$

From (3.22) it is clear that the solution depends on both locking signals, i_{inj_1} and i_{inj_2}, as expected. However, due to the many possibilities, we have to simplify the problem by assuming that both signals have the same frequency and the oscillator is locked to both signals (i.e. $\omega_{\text{inj}_1} = \omega_{\text{inj}_2} = \omega$). With locking signals of the form (3.5) and with a locked oscillator we obtain the amplitude and phase derivatives

$$\begin{cases} \dfrac{\mathrm{d}I}{\mathrm{d}t} = \left(\delta_0 I - \dfrac{1}{4}\delta_2 I^3\right) + \dfrac{\omega_0^2}{2\omega} I_{\text{inj}_1}\sin\phi + \omega\dfrac{R_N}{L} I_{\text{inj}_2}\cos\phi & \text{(3.23a)} \\ \dfrac{\mathrm{d}\phi}{\mathrm{d}t} = \dfrac{\omega^2 - \omega_0^2}{2\omega} + \dfrac{\omega_0^2}{2\omega}\cdot\dfrac{I_{\text{inj}_1}}{I}\cos\phi - \dfrac{R_N}{2\omega L}\cdot\dfrac{I_{\text{inj}_2}}{I}\sin\phi. & \text{(3.23b)} \end{cases}$$

From the system of equations (3.23) we can see that, both for the amplitude and phase, the effect of the injected signals can be gathered into a single injection signal. However, the result and conclusions that we can obtain here are too abstract. Thus, we will not derive or conclude further. We draw the conclusion relating the double injection when we study the passive coupling, using more realistic injected signals (the output signals of each oscillator).

3.4 Conclusion

From the analysis of the three injection locking topologies, we can conclude that the driven VDPO locks to the frequency of the locking signal within a limited band (locking range). The phase and amplitude are adjusted accordingly with attenuation and phase imposed by the oscillator's resonant tank at the locked frequency. For instance, the parallel topology imposes a relative phase between the oscillator and the locking signal in the range of $-\pi/2$ to $\pi/2$. The series topology relative phase is within the range of 0 to π. The oscillation amplitude has its peak at the resonant frequency of the tank, ω_0, but away from the resonant frequency the amplitude drops slightly. Moreover, the series topology has a higher locking range than the parallel and the relationship between the phase and frequency has a higher slope.

It worth mentioning that although we analysed the injection locking assuming sinusoidal sources other signals can be used. The only requirement is that the locking signal has to be periodic. Knowing, from the Fourier series, that any periodic signal can be represented by a sum of sines and cosines, the injection locking analysis can be generalized to any periodic signal if we use the Fourier series of the locking signal in the right-hand side of (3.1). Moreover, if the resonator has enough selectivity we can assume that the high-order harmonics are strongly attenuated and reduces the locking signal to its fundamental frequency (first harmonic only). Meaning that for a high-selective resonator, the theory presented in this section can be used, we only need to calculate one coefficient of the Fourier series and substitute in I_{inj}. However, for a low-selective resonator, like the $RC-$oscillators that we present in the next chapters, the high-order harmonics are attenuated slightly, therefore, we cannot neglect these harmonics. For this reason, in the next chapter we will assume small coupling-factors to maintain the oscillators in the near sinusoidal regime.

CHAPTER 4

ACTIVE COUPLING *RC*−OSCILLATOR

Contents

4.1 Introduction

In this chapter, we study the actively cross-coupled *RC*−oscillator, which consists of two *RC*−oscillators coupled by transconductance amplifiers. The single and cross-coupled relaxation oscillators were extensively studied in [2], where a comprehensive analysis of the cross-coupled *RC*−oscillator in relaxation regime can be found. Here, we study the cross-coupled *RC*−oscillator in near sinusoidal regime with low coupling strength. For a strong coupling, amplifiers are approximated by hard limiters injecting a square wave current into the other oscillator [54]. In oscillators with high quality factor resonant tanks (such as the *LC*−oscillators), the high-order harmonics are filtered out and the injected signal is reduced to the first harmonic of the Fourier

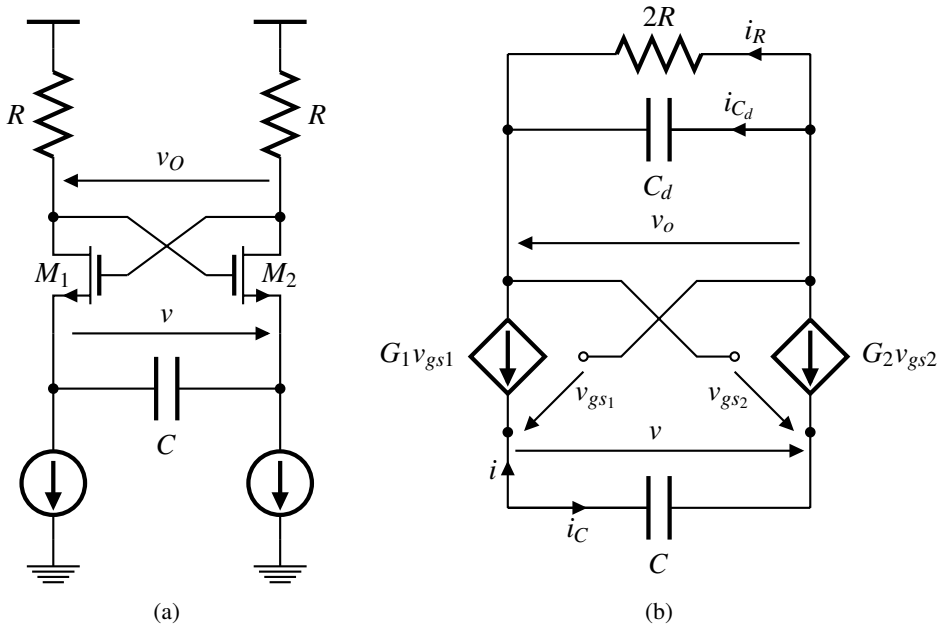

Figure 4.1: Single *RC*−oscillator (a) circuit and (b) small-signal equivalent circuit.

series. However, to maintain low quality-factor oscillators (like the *RC*−oscillator) in the sinusoidal regime, low coupling strength is necessary since the high-order harmonics are only slightly attenuated. The assumption of low coupling strength makes the analysis more cumbersome.

We first review the single *RC*−oscillator using the approximation proposed in [55], in which the *RC*−oscillator working in the near sinusoidal regime can be modelled by an *RLC* circuit. We approximate it to the VDPO as in [39], to account for the amplitude control mechanism. Next, we substitute each *RC*−oscillator by a VDPO and the transconductance amplifiers by voltage controlled current sources, reducing each oscillator to the series injected locking circuit of Chapter 3. Afterwards, we derive the quadrature oscillator key parameters: amplitude, frequency, and quadrature error. The parameters are obtained for steady-state assuming no mismatches. This derivation is followed by a stability analysis of the steady-state solution. Then, assuming mismatches and steady-state, we derive the amplitude and phase error equations. In the last section we draw the conclusions.

4.2 Single *RC*−oscillator

In this section the single *RC*−oscillator, as shown in Fig. 4.1(a), is analysed assuming ideal current sources and mismatches only in the transistors transconductances. The circuit in analysed in the nearly sinusoidal regime and it is shown that it can be approximated by the series VDPO. The small-signal equivalent circuit of the single oscillator is shown in Fig. 4.1(b). Here, capacitance C_d is the capacitance of the transistors, and C_p (which is not shown in the circuit) represents other parasitic capacitances lumped together. We approximate C_d as

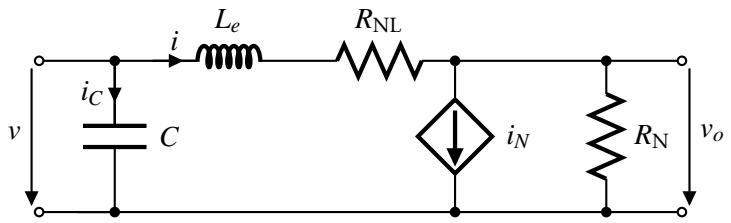

Figure 4.2: Equivalent circuit of a single $RC-$oscillator.

$$C_d \approx 2C_{gd} + \frac{1}{2}C_{gs} + C_p. \tag{4.1}$$

It should be noted that, although the capacitance C_d does not appear directly in Fig. 4.1, it is in the equations of L_e and R_N.

The parameters G_1 and G_2 represent the signal dependent transconductances of M_1 and M_2, respectively. It should be noted that G_1 and G_2 are nonlinear. Their approximation for the following time-domain analysis can be found in Appendix A.

Applying the KVL and KCL to the small-signal circuit (Fig. 4.1(b)) we obtain

$$\begin{cases} i = -G_1 v_{gs1} & \text{(4.2a)} \\ i = G_2 v_{gs2} & \text{(4.2b)} \\ i = -i_{c_d} - i_r = -C_d \dfrac{\mathrm{d}v_o}{\mathrm{d}t} - \dfrac{v_o}{2R} & \text{(4.2c)} \\ v_o = v_{gs1} - v_{gs2} + v & \text{(4.2d)} \\ i = -i_c = -C\dfrac{\mathrm{d}v}{\mathrm{d}t} & \text{(4.2e)} \end{cases}$$

Substituting (4.2a) and (4.2b) into (4.2d) we obtain

$$v_o = -\frac{i}{G_1} - \frac{i}{G_2} + v \tag{4.3}$$

which substituted into (4.2c) and solving with respect to v results in

$$v \approx \left(\frac{G_1+G_2}{G_1 \cdot G_2}\right) i - 2R\left(1 - \frac{C_d}{C}\right) i + 2RC_d \left(\frac{G_1+G_2}{G_1 \cdot G_2}\right) \frac{\mathrm{d}i}{\mathrm{d}t}, \tag{4.4}$$

The first term on the right-hand side represents a nonlinear resistance, the second term a negative resistance (that compensates the loss in the nonlinear resistance) and the last term represents a nonlinear inductance. It should be noted that the last term on the right-hand side of (4.4) is an approximation [39, 55]. If the incremental current, i, is small, the nonlinear terms of the signal dependent transconductances, G_1 and G_2, are small in comparison with the linear term. With this assumption we can assume that

$$\frac{\mathrm{d}}{\mathrm{d}t}\left[\frac{G_1+G_2}{G_1 \cdot G_2} i\right] \approx \left(\frac{G_1+G_2}{G_1 \cdot G_2}\right) \frac{\mathrm{d}i}{\mathrm{d}t}.$$

Thus, the single $RC-$oscillator can be substituted by the equivalent circuit shown in Fig. 4.2 [39, 55]. In this circuit the equivalent inductance is given by

$$L_e \approx 4RC_d g_{m0}^{-1}, \tag{4.5}$$

where g_{m0} is the transconductance of $M_{1,2}$. The positive resistance, generated by the cross-coupled pair $M_{1,2}$, is given by

$$R_{\mathrm{NL}} = 2g_{m0}^{-1}. \tag{4.6}$$

The negative resistance by

$$R_{\mathrm{N}} = -2R\left(1 - \frac{C_d}{C}\right), \tag{4.7}$$

and the dependent current source, related to the nonlinear resistance, by

$$i_N = K^2 i^3, \tag{4.8}$$

where K is a parameter that depends on the transistor working region, as shown in Appendix A.

Substituting (4.4) into (4.2e) and rearranging the terms we obtain the differential equation of the circuit in Fig. 4.2 as

$$\frac{\mathrm{d}^2 i}{\mathrm{d}t^2} + \left(\frac{R_{\mathrm{NL}} + R_{\mathrm{N}}}{L_e}\right)\frac{\mathrm{d}i}{\mathrm{d}t} - \left(\frac{R_{\mathrm{N}}}{L_e}\right)\frac{\mathrm{d}i_N}{\mathrm{d}t} + \frac{1}{L_e C} i \approx 0. \tag{4.9}$$

Substituting (4.5), (4.6), (4.7) and (4.8) into (4.9) we obtain

$$\frac{\mathrm{d}^2 i}{\mathrm{d}t^2} + 2\frac{1 - Rg_{m0}\left(1 - \frac{C_d}{C}\right) + 3Rg_{m0}\left(1 - \frac{C_d}{C}\right)K^2 i^2}{4RC_d}\frac{\mathrm{d}i}{\mathrm{d}t} + \frac{g_{m0}}{4RC_d C} i = 0. \tag{4.10}$$

The differential equation (4.10) can be written in the form

$$\frac{\mathrm{d}^2 i}{\mathrm{d}t^2} - 2\left(\delta_0 - \delta_2 i^2\right)\frac{\mathrm{d}i}{\mathrm{d}t} + \omega_0^2 i = 0. \tag{4.11}$$

This is the equation of the VDPO with parameters

$$\delta_0 = \frac{Rg_{m0}\left(1 - \frac{C_d}{C}\right) - 1}{4RC_d}; \qquad \delta_2 = \frac{3Rg_{m0}\left(1 - \frac{C_d}{C}\right)K^2}{4RC_d}. \tag{4.12}$$

From the study of the VDPO in Chapter 2, (2.23), we know that the amplitude general solution is given by

$$I_{\mathrm{osc}}(t) = 2\sqrt{\frac{\delta_0}{\delta_2 + Be^{-2\delta_0 t}}}, \tag{4.13}$$

where $B = -\delta_2 + 4\delta_0/I_0^2$ is a constant that depends on the initial conditions and I_0 is the initial amplitude (i.e. for $t = 0$).

For steady-state (i.e. $t \to \infty$) the oscillation amplitude given by (4.13) is

$$I_{\mathrm{osc}} = 2\sqrt{\frac{\delta_0}{\delta_2}}. \tag{4.14}$$

Substituting the VDP parameters (4.12) into (4.14) we obtain the steady-state amplitude as a function of the circuit parameters:

$$I_{\text{osc}} \approx 2\sqrt{\frac{Rg_{m0}\left(1-\frac{C_d}{C}\right)-1}{3Rg_{m0}\left(1-\frac{C_d}{C}\right)K^2}} = \frac{2}{K}\sqrt{\frac{Rg_{m0}-\left(\frac{C}{C-C_d}\right)}{3Rg_{m0}}}, \tag{4.15}$$

The parameter K depends on the transistor working region. If the transistor is in strong inversion, i.e. $V_{GS}-V_T$ is higher than 100 mV [56], K is given by

$$K = \frac{1}{4I}. \tag{4.16}$$

If the transistor is in weak inversion, i.e. $V_{GS}-V_T$ is lower than 100 mV [56], K is given by

$$K \approx \frac{1}{I}. \tag{4.17}$$

If the transistor is working in a region between the strong and weak inversions, i.e. in moderate inversion, for which a model was proposed recently [57], one can use the strong inversion model considering, K, as a fitting parameter.

To obtain the amplitude of the output voltage (which is easier to compare with measurement results) we multiply (4.15) by the output resistance ($2R$), resulting in

$$V_{\text{osc}} \approx \frac{16R\left(1-\frac{C_d}{C}\right)I}{\sqrt{3}}\sqrt{\frac{Rg_{m0}-\left(\frac{C}{C-C_d}\right)}{Rg_{m0}}}. \tag{4.18}$$

The oscillation frequency is obtained from the third term on the left-hand side of (4.11) as

$$\omega_0 \approx \sqrt{\frac{g_{m0}}{4RC_dC}} \tag{4.19}$$

The derived equations give approximate values for the amplitude and oscillation frequency at steady-state. Next, we discuss the conditions necessary for the oscillation to start and the limit condition to avoiding clipping and maintain the oscillator in the near-sinusoidal regime.

4.2.1 Start-up conditions

An important aspect for the designer is the condition for the oscillation to start. The oscillation starts if the negative resistance exceeds the loss resistance in modulus (that is generated by the oscillator's core transistors, R_{NL}) leading to the condition

$$|R_{\text{N}}| > R_{\text{NL}}. \tag{4.20}$$

At start-up ($i \approx 0$) the nonlinear resistance, R_{NL}, depends on the transconductances, g_{m0}, the average transconductance of M_1 and M_2 . The negative resistance, R_{N}, depends on the oscillator capacitance, C, as can be seen in (4.7), and condition $(C > C_d)$ is necessary to have R_{N} negative. Thus, the criteria for the oscillation to start are [55]:

$$\begin{cases} R \cdot \left(1 - \dfrac{C_d}{C}\right) > \dfrac{1}{g_{m0}} & \text{(4.21a)} \\ C > C_d. & \text{(4.21b)} \end{cases}$$

From (4.21) it is clear that the oscillator capacitance, C, must be higher than the parasitic capacitances, C_d, and the negative resistance should be higher than the inverse of the average tranconductance, g_{m0}. If the above criteria are met the amplitude of oscillation grows exponentially and the nonlinear resistance also grows until it matches the negative resistance, at steady-state. However, to ensure that the oscillator works in the near sinusoidal regime an upper limit (for Rg_{m0}) must be set, otherwise the amplitude will not be limited by the circuit nonlinearities but rather by the supply voltage V_{dd} (generating a square-wave). The upper limit is obtained by equating (4.15) to the maximum amplitude and solve with respect to Rg_{m0}. Thus, equating (4.15) to I, which is the maximum amplitude, using $K = 1/(4I)$, and solve with respect to Rg_{m0} we obtain

$$R \cdot \left(1 - \frac{C_d}{C}\right) < \frac{1{,}049}{g_{m0}}. \tag{4.22}$$

The criteria in (4.21) define the minimum values for the oscillation to start and (4.22) gives the maximum value without signal distortion (clipping).

4.2.2 Quality factor

The Q of the circuit (Fig. 4.2) is given by

$$Q = \frac{1}{R_{\mathrm{NL}}}\sqrt{\frac{L_e}{C}} = g_{m0}\sqrt{\frac{RC_d}{C}\frac{1}{g_{m0}}}. \tag{4.23}$$

Substituting (4.5) and (4.6) into (4.23), and considering that in steady-state $R\,(1 - C_d/C) \approx g_{m0}^{-1}$ we finally obtain

$$Q = \frac{Rg_{m0}}{C}\sqrt{C_d\,(C - C_d)}, \tag{4.24}$$

The maximum quality factor, $Q_{\max}$, is obtained by differentiating (4.24) with respect to C_d and equating the result to zeros as

$$\frac{\mathrm{d}Q}{\mathrm{d}C_d} = \frac{Rg_{m0}}{C}\frac{C - 2C_d}{2\sqrt{C_d\,(C - C_d)}} = 0. \tag{4.25}$$

From (4.25) one finds that

$$Q_{\max} = \frac{Rg_{m0}}{2} \approx 1. \tag{4.26}$$

which is reached at $C = 2C_d$, which is in accordance with [3].

Thus, as a rule of thumb, the designer should enforce a floating capacitance, C, as two times the parasitics capacitance, C_d, (i.e. $C = 2C_d$) to guarantee a $Q \approx 1$. Hence, contrary to the

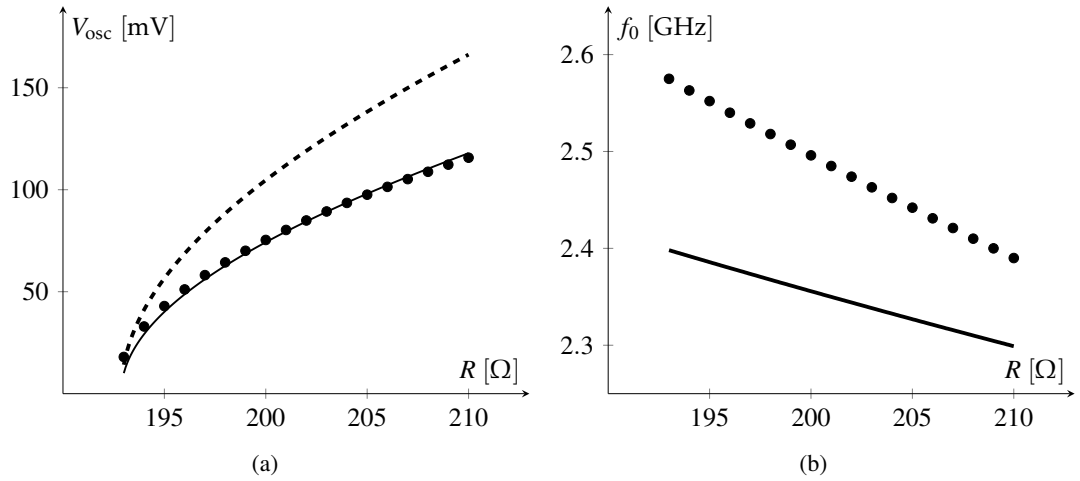

Figure 4.3: Oscillation (a) amplitude and (b) frequency.

$LC-$oscillator, the Q of an $RC-$oscillator is limited to one and, therefore, Q cannot be used to reduce the phase-noise.

The circuit parameters optimum values guarantee the minimization of the phase-noise [3]. With $Q \approx 1$, (4.21a) reduces to $R > 2/g_{m0}$. Thus, for the oscillation to start, one has to ensure that R compensates the loss in the transconductance, g_{m0}. Moreover, to maximize the amplitude, the designer should use the maximum value for Rg_{m0} that is obtained from (4.22) with ($C = 2C_d$) resulting in

$$Rg_{m0} \approx 2.1$$

Although, the above rule maximizes the amplitude for near sinusoidal regime, for some applications the total harmonic distortion (THD) is too high. In these cases, the designer should use the THD as a figure-of-merit to set the Rg_{m0} value. Moreover, a trade-off exists between the maximum amplitude and power consumption, since to maintain the desired frequency the ratio between R and g_{m0} must be constant. This trade-off can also be used to set the limit to Rg_{m0}. Next we present the design and simulation of an $RC-$oscillator (Fig. 4.1(a)), in which the design rules and a comparison between theory and simulation are discussed.

4.2.3 Design and simulation result

To confirm the theoretical analysis, we designed a 2.4 GHz $RC-$oscillator using a 130 nm standard CMOS technology considering ideal resistances, capacitances and current sources (circuit of Fig. 4.1(a)). To minimize the power requirements, we select the NMOS transistors with the largest W/L ratio available in the technology library ($W/L = 115.2\ \mu m/120\ nm$). From simulation, we obtain an approximated value for the lumped parasitics capacitance of about $C_d = 172$ fF. It follows that the floating capacitance must be $C = 2C_d = 344$ fF. Substituting the frequency and capacitances values into (4.19) and using the criteria (4.21), we obtain the minimum values for the resistances and transconductances: $R > 191.6\ \Omega$ and $g_{m0} > 10.4$ mS.

From the transconductance value, we obtain the required bias current, I, based on the transistors dimension and technology parameters, to be $I \approx 600$ μA. With this low current the transistors work in moderate inversion, and, hence, K is used as a fitting parameter.

It should be noted that the theoretical analysis is neglecting the gate currents. This can be done for low frequencies (or for high bias currents). At high-frequency and low bias current the gate current cannot be neglected and has a significant impact on I_{osc}. For the designed oscillator, the gate current can be about 20% of the oscillator current, I_{osc}. Moreover, the transistors output impedance and their impact on I_{osc} was neglected. However, as we show next, these approximations can be compensated by choosing the proper value of K.

The RC-oscillator with the above parameters was simulated to confirm the amplitude trend predicted by the theoretical analysis. The value of R was varied from 193 Ω to 210 Ω maintaining the other parameters constant. Simulation results show the amplitude (Fig. 4.3(a)) and frequency change (Fig. 4.3(b)) with respect to R. For the amplitude, a comparison between the simulation results and the theoretical analysis is shown in Fig. 4.3(a), where the simulation results are represented by black dots. The dashed curve represents the values predicted by (4.18), using the strong inversion K, and the solid curve the values predicted by (4.18) with $K = 1.41/(4I)$.It can be seen from Fig. 4.3(a) that the oscillation amplitude increases with R as predicted by the theoretical analysis. Although, the approximation using the strong inversion K is poor, due to the oscillator being in moderate inversion. Hence, an increase of K by 41% gives a better agreement between simulation and theory, as shown in Fig. 4.3(a) (solid curve).

Figure 4.3(b) shows the frequency: the simulation results are represented by the black dots, and the solid curve represents the values predicted by (4.19). Although, the frequency trend is in agreement with the theoretical analysis, the value has a significant difference. Investigating further, we conclude that neglecting the channel-length-modulation explains this difference.

The simulation results show that the $RC-$oscillator in the nearly sinusoidal regime can be approximated by the series VDPO (Fig. 4.2). Moreover, if we consider the transconductances nonlinearities of the core transistors a large-signal analysis can be avoided.

4.3 Quadrature $RC-$oscillator

In this section, we analyse an oscillator with quadrature outputs using two $RC-$oscillators. Two transconductance amplifiers are used to couple the oscillators, as shown in Fig. 4.4. The coupling forces the oscillators to synchronize and oscillate at the same frequency, as shown in Chapter 3, where the locking of an oscillator to an external signal is studied. The synchronization process of coupled oscillators is equivalent to the synchronization of injection locked oscillators: in coupled oscillators the locking signal is the output of the other oscillator. Thus, coupling ensures frequency synchronization, but the oscillators can lock either in-phase or in quadrature. To obtain quadrature outputs it is necessary to cross-couple the oscillators (Fig. 4.4); direct coupling synchronizes both oscillators, but generates in-phase outputs. Here, we focus on cross-coupling, since we are interested in quadrature signal generators.

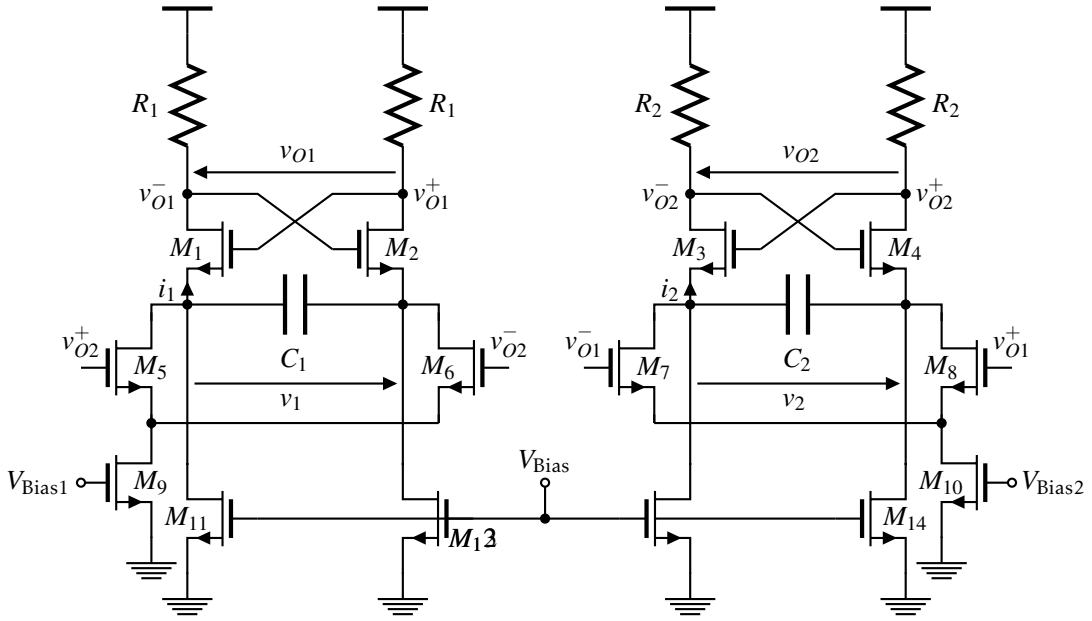

Figure 4.4: Quadrature oscillator with active coupling.

The circuit implementation of a quadrature oscillator is shown in Fig. 4.4. Resistances R_1 and R_2, and the current mirrors implemented by transistors M_{11} to M_{14} set the oscillator bias point. The differential transconductance amplifiers are implemented by the differential pairs composed of transistors M_5, M_6 and M_7, M_8, and their current sources respectively M_9 and M_{10}.

The circuit analysis is done as follows. First, the small-signal equivalent circuit is obtained. From it, the differential equations that govern the system are derived. These differential equations are used to obtain both the transient and steady-state performance of the circuit. Then, assuming that there are no mismatches between the oscillators, the key parameters, frequency, amplitude, and phase, of the quadrature oscillator are derived for steady-state. Afterwards, using the steady-state results (equilibrium points), a stability analysis of each equilibrium point is presented. In the last subsection, considering mismatches between the oscillators, the amplitude- and phase-error equations are derived.

4.3.1 Incremental model

The small-signal equivalent circuit is obtained by substituting each $RC-$oscillator by its equivalent circuit (Fig. 4.2) and the transconductance amplifiers by current sources controlled by the output voltage of each oscillator, as shown in Fig. 4.5.

The circuit (Fig. 4.5) consists of two series VDPO driven by a current source. For both oscillators, the driven series VDPO differential equation (3.19), derived in Section 3.3, we obtain

$$\begin{cases} \dfrac{\mathrm{d}^2 i_1}{\mathrm{d}t^2} - 2\left(\delta_0 - \delta_2 i_1^2\right)\dfrac{\mathrm{d}i_1}{\mathrm{d}t} + \omega_1^2 i = 2R_2\left(1 - \dfrac{C_{d2}}{C_2}\right)\omega_1^2\alpha_2 i_2 & \text{(4.27a)} \\ \dfrac{\mathrm{d}^2 i_2}{\mathrm{d}t^2} - 2\left(\gamma_0 - \gamma_2 i_2^2\right)\dfrac{\mathrm{d}i_2}{\mathrm{d}t} + \omega_2^2 i = -2R_1\left(1 - \dfrac{C_{d1}}{C_1}\right)\omega_2^2\alpha_1 i_1 & \text{(4.27b)} \end{cases}$$

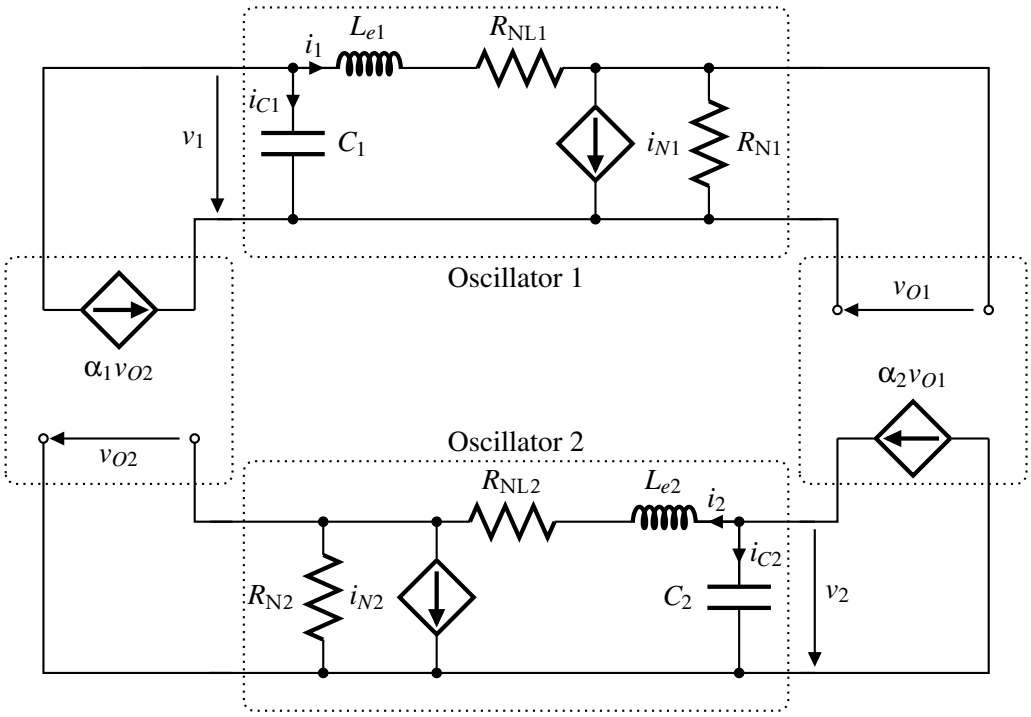

Figure 4.5: Active coupling small-signal equivalent circuit.

where ω_i is the free-running frequency, and α_i is the coupling factor of the $i-$th oscillator. The parameters of the first VDPO are given by

$$\delta_0 = \frac{R_1 g_{m1}\left(1-\frac{C_{d1}}{C_1}\right)-1}{4R_1C_{d1}}, \quad \delta_2 = \frac{3R_1 g_{m1}\left(1-\frac{C_{d1}}{C_1}\right)K^2}{4R_1C_{d1}}. \tag{4.28}$$

and the parameters of the second oscillator are given by

$$\gamma_0 = \frac{R_2 g_{m2}\left(1-\frac{C_{d2}}{C_2}\right)-1}{4R_2C_{d2}}, \quad \gamma_2 = \frac{3R_1 g_{m1}\left(1-\frac{C_{d1}}{C_1}\right)K^2}{4R_1C_{d1}}. \tag{4.29}$$

To solve the differential equations (4.27), we use the harmonic balance method [41], with the assumptions of slowly varying amplitude and phase, and neglecting the high-order terms. Thus, the solutions have the form

$$\begin{cases} i_1(t) = I_{\mathrm{o1}}(t)\sin(\omega t - \phi_1) & \text{(4.30a)} \\ i_2(t) = I_{\mathrm{o2}}(t)\sin(\omega t - \phi_2). & \text{(4.30b)} \end{cases}$$

where I_{oi} is the current amplitude, ϕ_i is the phase of the $i-$th oscillator, and ω is the angular frequency of oscillation. Note that we are assuming that both oscillators are working at the same frequency but with different phases. Using the harmonic balance, results in a system of four first order differential equations:

$$\begin{cases} \dfrac{dI_1}{dt} = \delta_0 I_1 - \dfrac{1}{4}\delta_2 I_1^3 - \dfrac{\alpha_{K1}}{2\omega} I_2 \sin\Delta\phi & (4.31a) \\ \dfrac{dI_2}{dt} = \gamma_0 I_2 - \dfrac{1}{4}\gamma_2 I_2^3 - \dfrac{\alpha_{K2}}{2\omega} I_1 \sin\Delta\phi & (4.31b) \\ \dfrac{d\phi_1}{dt} = \dfrac{\omega^2 - \omega_1^2}{2\omega} + \dfrac{\alpha_{K1}}{2\omega}\dfrac{I_2}{I_1}\cos\Delta\phi & (4.31c) \\ \dfrac{d\phi_2}{dt} = \dfrac{\omega^2 - \omega_2^2}{2\omega} - \dfrac{\alpha_{K2}}{2\omega}\dfrac{I_1}{I_2}\cos\Delta\phi & (4.31d) \end{cases}$$

where $\Delta\phi = \phi_2 - \phi_1$ is the phase difference and ω_i is the free-running frequency of the $i-$th oscillator. The coupling strength parameters are given by

$$\alpha_{K1} = 2R_2\left(1 - \frac{C_{d2}}{C_2}\right)\omega_1^2\alpha_1, \qquad \alpha_{K2} = 2R_1\left(1 - \frac{C_{d1}}{C_1}\right)\omega_2^2\alpha_2. \tag{4.32}$$

From (4.31) we can analyse both the steady-state and the transient performance.

4.3.2 Quadrature oscillator without mismatches

To determine the oscillators' phase, amplitude, and frequency, we consider that there are no mismatches between the oscillators, i.e. $R_1 = R_2 = R$, $C_1 = C_2 = C$, $L_{e1} = L_{e1} = L_e$, and $\alpha_1 = \alpha_2 = \alpha$. The free-running frequencies are $\omega_1 = \omega_2 = \omega_0$, and the VDP parameters are $\delta_0 = \gamma_0$ and $\delta_2 = \gamma_2$, and the coupling strengths $\alpha_{K1} = \alpha_{K2} = \alpha_K$. At steady-state, for which $dI_1/dt = dI_2/dt = d\phi_1/dt = d\phi_2/dt = 0$, (4.31) is reduced to

$$\begin{cases} \delta_0 I_1 - \dfrac{1}{4}\delta_2 I_1^3 - \dfrac{\alpha_K}{2\omega} I_2 \sin\Delta\phi = 0 & (4.33a) \\ \delta_0 I_2 - \dfrac{1}{4}\delta_2 I_2^3 - \dfrac{\alpha_K}{2\omega} I_1 \sin\Delta\phi = 0 & (4.33b) \\ \dfrac{\omega^2 - \omega_0^2}{2\omega} + \dfrac{\alpha_K}{2\omega}\dfrac{I_1}{I_2}\cos\Delta\phi = 0 & (4.33c) \\ \dfrac{\omega^2 - \omega_0^2}{2\omega} - \dfrac{\alpha_K}{2\omega}\dfrac{I_2}{I_1}\cos\Delta\phi = 0 & (4.33d) \end{cases}$$

Three solutions are possible. A zero amplitude for both oscillators, i.e. $I_{o1} = I_{o2} = 0$, satisfies the equations. Note that to avoid the indeterminate form $0/0$ one can multiply I_1 by (4.33c) and I_2 by (4.33d). A second and third solutions with equal amplitudes $I_1 = I_2 = I_{osc}$ and with quadrature outputs $\Delta\phi = \pi/2$ and $\Delta\phi = -\pi/2$, respectively, satisfies the equations. The second and third solutions are obtained by dividing the terms of (4.33a) by I_1, (4.33b) by I_2 and subtracting (4.33a) from (4.33b), resulting in

$$-\frac{1}{4}\delta_2\left(I_2^2 - I_1^2\right) - \frac{\alpha_K}{2\omega}\left(\frac{I_1}{I_2} - \frac{I_2}{I_1}\right)\sin\Delta\phi = 0. \tag{4.34}$$

It is clear from (4.34) that the case of equal amplitudes, i.e. $|I_1| = |I_2|$, satisfies the equation. Hence, for equal amplitudes, subtraction of (4.33c) from (4.33d) results in

$$-\alpha_K \cos\Delta\phi = 0. \tag{4.35}$$

Thus, only the phase differences $\Delta\phi = \pi/2$ and $\Delta\phi = -\pi/2$ satisfy (4.35).

Solving (4.33a), or (4.33b), with respect to I_{osc}, considering equal amplitudes $I_1 = I_2 = I_{\text{osc}}$, we obtain

$$I_{\text{osc}} = 2\sqrt{\frac{\delta_0 \pm \frac{\alpha_K}{2\omega}}{\delta_2}}, \tag{4.36}$$

and by subtracting (4.33c) from (4.33d) and solving with respect to $\Delta\phi$ we obtain

$$\Delta\phi = \pm\frac{\pi}{2}. \tag{4.37}$$

Moreover, combining (4.33c) and (4.33d) results in

$$\omega = \omega_0. \tag{4.38}$$

These results lead us to the conclusion that, with no mismatches between the oscillators, at steady-state, the outputs are in perfect quadrature. The oscillation frequency is equal to the free-running frequency. The oscillation amplitude is different from that of a single *RC*−oscillator. Moreover, the amplitude has two modes, described by (4.36). The mechanism by which a particular mode is selected is discussed in the next section.

4.3.3 Stability of the equilibrium points

To analyse the stability of the steady-state solutions, we determine the stability of each equilibrium point. This is done by analysing the characteristic equation and its eigenvalues. Further, to understand how the circuit reaches the steady-state, the paths in the vicinity of each equilibrium point are drawn.

Simplifying the system (4.31) by combining (4.31c) and (4.31d), we obtain

$$\begin{cases} \dfrac{dI_1}{dt} = \delta_0 I_1 - \dfrac{1}{4}\delta_2 I_1^3 - \dfrac{\alpha_K}{2\omega} I_2 \sin\Delta\phi & \text{(4.39a)} \\ \dfrac{dI_2}{dt} = \delta_0 I_2 - \dfrac{1}{4}\delta_2 I_2^3 - \dfrac{\alpha_K}{2\omega} I_1 \sin\Delta\phi & \text{(4.39b)} \\ \dfrac{d\Delta\phi}{dt} = -\dfrac{\alpha_K}{2\omega}\left(\dfrac{I_1}{I_2} - \dfrac{I_2}{I_1}\right)\cos\Delta\phi & \text{(4.39c)} \end{cases}$$

From (4.39c) one finds that $d\Delta\phi/dt = 0$ when quadrature is reached. Thus, if we assume that the system is in quadrature $\Delta\phi = \pi/2$, equations (4.39) can be reduced to

$$\begin{cases} \dfrac{dI_1}{dt} = \delta_0 I_1 - \dfrac{1}{4}\delta_2 I_1^3 - \dfrac{\alpha_K}{2\omega} I_2 & \text{(4.40a)} \\ \dfrac{dI_2}{dt} = \delta_0 I_2 - \dfrac{1}{4}\delta_2 I_2^3 - \dfrac{\alpha_K}{2\omega} I_1 & \text{(4.40b)} \end{cases}$$

Note that the differential equations are nonlinear, which leads to a cumbersome analysis. For convenience, we analyse the transient in the vicinity of the equilibrium point, where the system can be linearized. To linearize (4.40), for any point in the phase plane, we calculate its Jacobian matrix:

$$J = \begin{bmatrix} \delta_0 - \frac{3}{4}\delta_2 I_{\text{osc}}^2 & -\frac{\alpha_K}{2\omega} \\ -\frac{\alpha_K}{2\omega} & \delta_0 - \frac{3}{4}\delta_2 I_{\text{osc}}^2 \end{bmatrix}, \tag{4.41}$$

where I_{osc} is the steady-state amplitude at the equilibrium points. To conclude about the stability of an equilibrium point and determine the geometric figures of the paths near it, we must determine the characteristic equation,

$$\lambda^2 - T\lambda + D = 0, \tag{4.42}$$

where T is the trace (sum of the main diagonal elements) and D is the determinant of the Jacobian matrix. The conditions for stability are $T < 0$ and $D > 0$ [41]. For $T > 0$ or $D < 0$ the equilibrium point is unstable [41].

From the steady-state analysis in the last subsection. Three equilibrium points were determined: one is at the origin $E_0 = (0,0)$, the other two are $E_1 = (I_{\text{osc}}, I_{\text{osc}})$, and $E_2 = (-I_{\text{osc}}, -I_{\text{osc}})$, in the first and third quadrants respectively. At the equilibrium point E_0, the amplitudes are equal ($I_1 = I_2 = 0$) and, therefore, the Jacobian matrix is

$$J_{E_0} = \begin{bmatrix} \delta_0 & -\frac{\alpha_K}{2\omega} \\ -\frac{\alpha_K}{2\omega} & \delta_0 \end{bmatrix}, \tag{4.43}$$

From (4.43) we obtain the characteristic equation

$$\lambda^2 - 2\delta_0\lambda + \left(\delta_0^2 - \frac{\alpha_K^2}{4\omega^2}\right) = 0,$$

where the trace $T = 2\delta_0 > 0$ since δ_0 is positive, which means that the equilibrium point E_0 is unstable. If we consider that $|\delta_0| < |\alpha_K|$, the determinant of (4.43) is negative meaning that we have a saddle at E_0. If $|\delta_0| > |\alpha_K|$ we have an unstable node.

At the equilibrium point E_1, the amplitudes are equal $I_1 = I_2 = I_{\text{osc}}$. Substituting (4.36) into (4.41), the Jacobian for E_1 is obtained:

$$J_{E_1} = \begin{bmatrix} -2\delta_0 & -\frac{\alpha_K}{2\omega} \\ -\frac{\alpha_K}{2\omega} & -2\delta_0 \end{bmatrix}. \tag{4.44}$$

The characteristic equation of (4.44) is

$$\lambda^2 + 4\delta_0\lambda + \left(4\delta_0^2 - \frac{\alpha_K^2}{4\omega^2}\right) = 0,$$

where $T < 0$ and $D > 0$ since δ_0 is positive, which means that the equilibrium point E_1 is stable. The eigenvalues are the roots of the characteristic equation given by

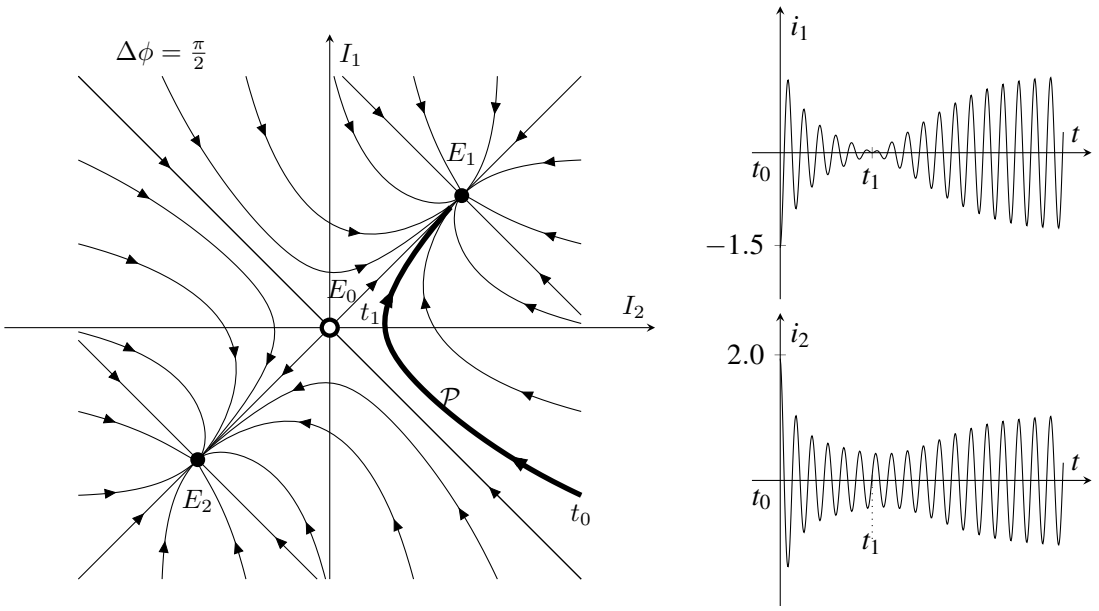

(a) Phase portrait

(b) Time solution

Figure 4.6: Series active coupling.

$$\lambda = -\frac{T}{2} \pm \frac{1}{2}\sqrt{T^2 - 4D} = -\frac{T}{2} \pm \frac{1}{2}\sqrt{\Delta}.$$

If $\Delta > 0$ the eigenvalues are real. For E_1, substituting T and D of J_{E_1} into Δ, results in

$$\Delta = \frac{\alpha_K^2}{\omega^2}.$$

Since $\alpha_K^2/\omega^2 > 0$ we can conclude that at E_1 we have a stable node. The same conclusion can be drawn for E_2 since its Jacobian matrix is equal to J_{E_1}, as shown by the phase portrait in Fig. 4.6(a). The stable and unstable equilibrium points are represented, in Fig. 4.6(a), as black and white circles, respectively.

The phase portrait (Fig. 4.6(a)) is a graphic representation of the amplitudes evolution. Consider, for instance, the path $\mathcal{P}$ that corresponds to the initial conditions: $i_1(t_0) = -1.5\text{mA}$, $i_2(t_0) = 2\text{mA}$, and $\Delta\phi = -\pi/2$. The phase portrait shows that, from this initial point, the amplitude I_2 decreases until it reaches its minimum value, at $t = t_1$. For $t > t_1$ the amplitude I_2 increases until it reaches the equilibrium point. The amplitude I_1 increases until it reaches the steady-state at E_1 passing from negative to positive values at $t = t_1$. This behaviour can be seen in the time-domain representations in Fig. 4.6(b).

4.3.4 Quadrature oscillator with mismatches

In this subsection, we analyse the impact of the components mismatches on the amplitude- and phase-error. We consider that there are components mismatches between the *RC*−oscillators. Moreover, we assume that the oscillators core transistors are identical, and, therefore, their transconductances and capacitances are equal.

In the following derivation, we also consider that the oscillators reach steady-state and that the mismatches are small, i.e. $\Delta R/R < 1\%$ and $\Delta C/C < 1\%$. To simplify the derivation, we neglect the terms with a multiplication of relative mismatches, e.g. $\Delta R\Delta C/(RC) \approx 0$. The error equations are derived as functions of the mismatches of R and C.

For $\omega_1 \neq \omega_2$, $\gamma_0 \neq \delta_0$, $\gamma_2 \neq \delta_2$, and $\alpha_{K1} \neq \alpha_{K2}$ at steady-state (4.31) is reduced to

$$\begin{cases} \delta_0 - \dfrac{1}{4}\delta_2 I_1^2 - \dfrac{\alpha_{K1}}{2\omega}\dfrac{I_2}{I_1}\sin\Delta\phi = 0 & \text{(4.45a)} \\ \gamma_0 - \dfrac{1}{4}\gamma_2 I_2^2 - \dfrac{\alpha_{K2}}{2\omega}\dfrac{I_1}{I_2}\sin\Delta\phi = 0 & \text{(4.45b)} \\ \dfrac{\omega^2-\omega_1^2}{2\omega} + \dfrac{\alpha_{K1}}{2\omega}\dfrac{I_2}{I_1}\cos\Delta\phi = 0, & \text{(4.45c)} \\ \dfrac{\omega^2-\omega_2^2}{2\omega} - \dfrac{\alpha_{K2}}{2\omega}\dfrac{I_1}{I_2}\cos\Delta\phi = 0, & \text{(4.45d)} \end{cases}$$

The oscillation frequency is obtained by adding (4.45c) and (4.45d), resulting in

$$2\omega^2 = \left(\omega_1^2+\omega_2^2\right) - \left(\alpha_{K1}\frac{I_2}{I_1} - \alpha_{K2}\frac{I_1}{I_2}\right)\cos\Delta\phi, \tag{4.46}$$

If we assume small mismatches and small coupling strength then (4.46) is reduced to

$$\omega \approx \sqrt{\frac{\omega_1^2+\omega_2^2}{2}}. \tag{4.47}$$

The equation (4.47) shows that the oscillation frequency of the quadrature oscillator is the quadratic mean of the free-running frequencies of the $RC-$oscillators.

To obtain the phase error equation, one should subtract (4.45c) from (4.45d). This results in

$$\left(\alpha_{K2}\frac{I_1}{I_2} + \alpha_{K1}\frac{I_2}{I_1}\right)\cos\Delta\phi = \omega_1^2 - \omega_2^2, \tag{4.48}$$

Note that the phase difference $\Delta\phi$ can be written as $\Delta\phi = \pi/2 + \varepsilon_\phi$, where ε_ϕ is the phase error. Using the trigonometrical relation $\cos(\Delta\phi) = -\sin(\varepsilon_\phi)$ and assuming small phase-error $-\sin(\varepsilon_\phi) \approx -\varepsilon_\phi$ in (4.48) and solve it with respect to the phase error, result in

$$\varepsilon_\phi \approx -\frac{\omega_1^2-\omega_2^2}{\alpha_{K2}\frac{I_1}{I_2} + \alpha_{K1}\frac{I_2}{I_1}}, \tag{4.49}$$

By definition, the amplitudes are given by

$$I_1 = I_{\text{osc}}\left(1-\frac{\varepsilon_A}{2}\right), \qquad I_2 = I_{\text{osc}}\left(1+\frac{\varepsilon_A}{2}\right). \tag{4.50}$$

where ε_A is the amplitude error. Using (4.50) in (4.49) we obtain

$$\varepsilon_\phi \approx -\frac{\omega_1^2-\omega_2^2}{(\alpha_{K1}+\alpha_{K2}) + (\alpha_{K1}-\alpha_{K2})\,\varepsilon_A}, \tag{4.51}$$

Considering that $C_{d1} = C_{d2} = C_d$, $g_{m1} = g_{m2} = g_m$, and using $R_1 = R(1-\Delta R/(2R))$, $R_2 = R(1+\Delta R/(2R))$, $C_1 = C(1-\Delta C/(2C))$ and $C_2 = C(1-\Delta C/(2C))$. The difference between the free-running frequencies of each $RC-$oscillator is given by

$$\omega_1^2 - \omega_2^2 = \omega_0^2 \left(\frac{\Delta R}{R} + \frac{\Delta C}{C} \right). \tag{4.52}$$

Using the same assumptions, the term $\alpha_{K1} - \alpha_{K2}$ is given by

$$\alpha_{K1} - \alpha_{K2} \approx -2R\omega_0^2 \left[\left(1 - \frac{C_d}{C} \right) \frac{\Delta\alpha}{\alpha} + \left(\alpha \frac{C_d}{C} \right) \frac{\Delta R}{R} \right] \tag{4.53}$$

and the term $\alpha_{K1} + \alpha_{K2}$ is given by

$$\alpha_{K1} + \alpha_{K2} \approx 4R\omega_0^2 \alpha \left(1 - \frac{C_d}{C} \right) \tag{4.54}$$

Substituting (4.52), (4.53), and (4.54) into (4.51) results in

$$\varepsilon_\phi \approx -\frac{\frac{\Delta R}{R} + \frac{\Delta C}{C}}{4R\left(1-\frac{C_d}{C}\right)\alpha - 2R\left(1-\frac{C_d}{C}\right)\frac{\Delta\alpha}{\alpha}\varepsilon_A - 2R\frac{C_d}{C}\alpha\frac{\Delta R}{R}\varepsilon_A} \tag{4.55}$$

Assuming that for small mismatches $\Delta\alpha/\alpha \ll \alpha$ and $\Delta R/R\varepsilon_A \ll 1$ (4.55) is reduced to

$$\varepsilon_\phi \approx -\frac{1}{4R\left(1-\frac{C_d}{C}\right)\alpha}\left(\frac{\Delta R}{R} + \frac{\Delta C}{C} \right) \tag{4.56}$$

The equation (4.56) gives the phase error in radians. To obtain the phase error in degrees one has to multiply (4.56) by $180/\pi$,

$$\varepsilon_\phi \approx -\frac{180}{\pi}\frac{1}{4R\left(1-\frac{C_d}{C}\right)\alpha}\left(\frac{\Delta R}{R} + \frac{\Delta C}{C} \right) \tag{4.57}$$

Hence, it is clear that the phase error is directly proportional to the mismatches and inversely proportional to the coupling strength.

4.4 Simulation results

We simulate the circuit (Fig. 4.4) using standard 130 nm CMOS technology parameters. The circuit parameters are: $C_1 = C_2 = C = 77$ fF, $R_1 = R_2 = R = 600\ \Omega$, $(W/L) = 115.2$ µm/120 nm for transistors M_1,M_2,M_3,M_4,M_9, and M_{10}, $(W/L) = 14.4$ µm/120 nm for M_5,M_6,M_7 and M_8, $I = 0.6$ mA, $I_{cp} = 100$ µA, and the supply voltage is 1.2 V. The voltage and current sources are assumed to be ideal.

Simulating the circuit with component mismatches from -2% to +2%, we obtain the results of the amplitude- and phase-error shown in Fig. 4.7 and Fig. 4.8, respectively. In these figures, the errors due to the resistance mismatches are marked with black dots and the errors due to the capacitance mismatch with square marks. In Fig. 4.8, the solid line is the plot of the theoretical

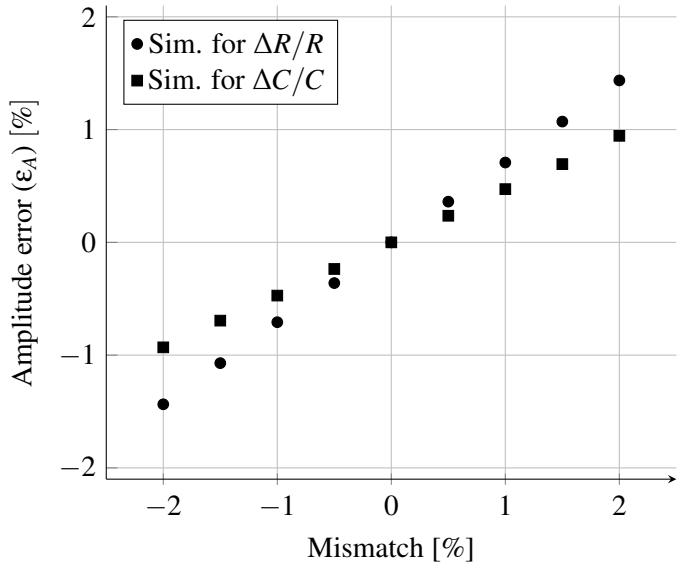

Figure 4.7: Impact of the resistance and capacitances mismatches on the amplitude error, using the circuit parameters: $R = 210\ \Omega$, $I = 600\ \mu$A, and $I_{cp} = 100\ \mu$A ($\alpha = g_{m0} \approx 0.758$ mS).

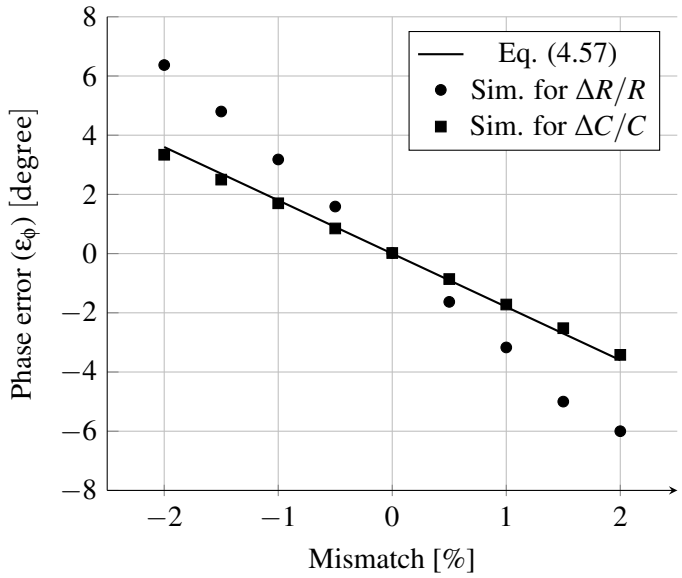

Figure 4.8: Impact of the resistance and capacitances mismatches on the phase error, using the circuit parameters: $R = 210\ \Omega$, $I = 600\ \mu$A, and $I_{cp} = 100\ \mu$A ($\alpha = g_{m0} \approx 0.758$ mS).

phase error given by (4.57). Note that this line represents the phase error with respect to one of the mismatches considering the other zero.

The simulation results show that the phase error with respect to the capacitances mismatches agrees well with the theory, as shown in Fig. 4.8. However, for the resistance mismatch, the simulation results diverge slightly (higher slope) from the theory. The deviation between simulation and analytical results are explained by the neglect of the drain-to-source dynamic resistance of the transistors. To determine the impact of the coupling strength on the phase error, we simulate the

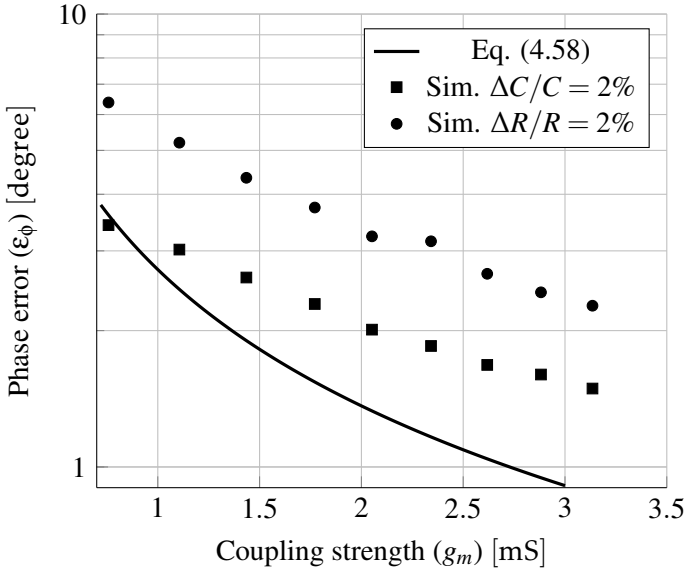

Figure 4.9: Phase error as a function of the coupling strength, using the circuit parameters: $R = 210\ \Omega$, $I = 600\ \mu$A.

circuit with a constant mismatch of 2% and sweep the coupling strength. Results show that the phase error is inversely proportional to the coupling strength, as shown in Fig. 4.9. These results show a significant deviation from the theory that is explained by the drain to source dynamic resistance of the transistors, and also by the change in the parasitic capacitances. Due to the Miller effect, the input capacitances of the transconductance amplifiers, used in coupling increase with the increase of the coupling strength. Thus, the input capacitances of the transconductance amplifiers load the circuit, meaning that the capacitance C_d increases and opposes the phase error reduction. Another consequence of the increase of C_d is the decrease of the oscillation frequency.

4.5 Conclusions

In this chapter we presented the study of the active coupling quadrature *RC*−oscillator. It was shown that for the sinusoidal regime, this quadrature oscillator can be modelled as two VDPOs coupled by two transconductances. First, it was shown that the single *RC*−oscillator can be modelled by the VDPO. The relationships between the circuit parameters and the VDPO parameters were derived and confirmed by simulation. Next, the incremental circuit of the quadrature oscillator was obtained by substituting each single *RC*−oscillator by a VDPO. Then, the transient and steady-state performance of the quadrature oscillator was studied and the equations of the oscillator key parameters, oscillation frequency, and phase error were derived and validated by simulation.

We found that the oscillation frequency is insensitive to the mismatches and is given by the quadratic mean between the free-running frequencies of the coupled oscillators. However, contrary to what the theory predicted, simulations reveal that the oscillation frequency depends on the

coupling strength. The increase of the coupling strength decreases the oscillation frequency. This is explained by the input capacitances of the transconductance amplifiers, which are proportional to the coupling strength. Due to the Miller effect, the input capacitances of the transconductance amplifiers depends on this bias current. Since the input capacitances are in parallel with the oscillator capacitance, they influence the oscillation frequency.

CHAPTER 5

CAPACITIVE COUPLING *RC*−OSCILLATOR

Contents

5.1 Introduction

In the previous chapter the active coupling method was analyzed. The active coupling uses transconductance amplifiers to couple two oscillators. The disadvantages of this method are the increase of the noise and power dissipation. In this chapter we analyze the passive coupling that is an alternative method that minimizes these disadvantages. In passive coupling the amplifiers are substituted by passive elements (usually inductors or capacitors). The coupling based on inductors [17] and transformers [18, 19], has a higher area penalty than active coupling. Capacitive coupling of *LC*−oscillators has shown interesting results [20]. However, the area minimization is still limited by the inductors and it has the disadvantage of lowering the oscillation frequency [21].

Here, the quadrature *RC*−oscillator with capacitive coupling is investigated [22]. The capacitive coupling is noiseless and requires a small area. Since the coupling capacitors do not

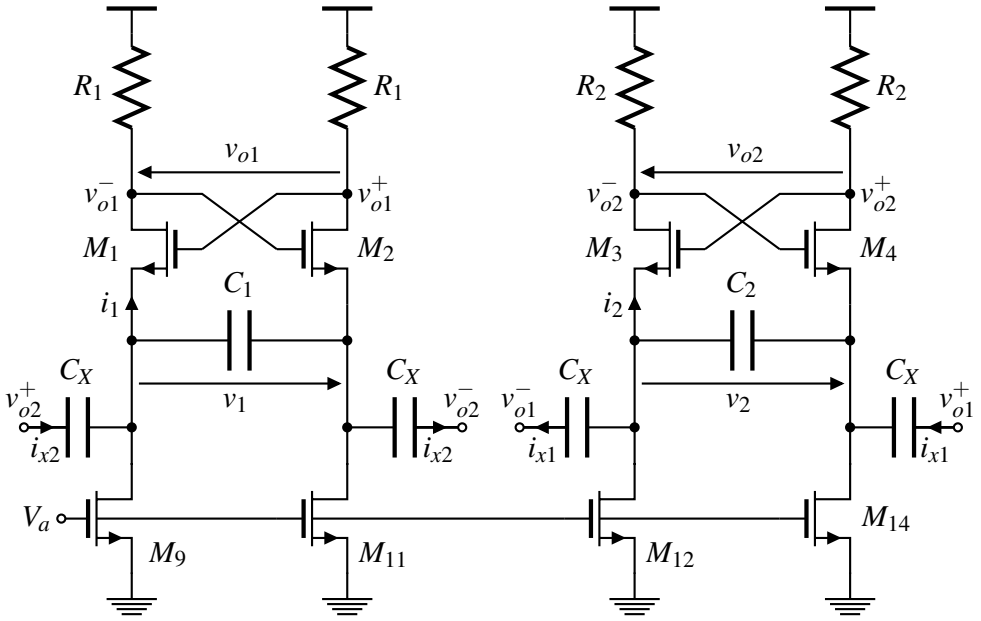

Figure 5.1: Quadrature oscillator with capacitive coupling circuit.

add noise, we expect a 3 dB phase-noise improvement (due to the coupling), with a marginal increase of the power, and a figure-of-merit (FoM) comparable to the best state-of-the-art *RC*−oscillators. Contrary to what may be expected, with the increase of the coupling capacitances (higher coupling strength) the oscillation frequency increases [22]. We present the theory to explain this behavior and we derive the equations for the frequency, phase-error and amplitude mismatch, which are validated by simulation. The theory shows that phase- and amplitude-error are reduced with the increase of the coupling strength. Moreover, the phase-error is proportional to the amplitude mismatch, indicating that an automatic phase-error minimization based on the amplitude mismatches is possible. The theory also shows that the phase-noise has a low sensitivity to the coupling strength. We also study bimodal oscillations and phase ambiguity, for this coupling topology, comparing it with other works [23]. To validate the theory, a 2.4 GHz quadrature voltage-controlled oscillator (QVCO) based on two *RC*−oscillators with capacitive coupling was fabricated, in UMC 130 nm CMOS process.

The chapter is organized as follows. We first present the circuit implementation and its incremental circuits based on the VDP approximation. Afterwards, we present the analysis of the capacitive coupling and, derive the equations for the oscillation frequency, phase, and amplitude. A stability analysis is included; extending the analysis presented in [24]. Equations of the phase-error and amplitude mismatch are derived, relating them with the circuit parameters, extending the results presented in [22]. Following the theoretical analysis, simulation results are presented and a comparison with the theory is done. In the end of the chapter, the experimental results followed by the conclusions are presented. The experimental results are compared with the state-of-the-art of nearly sinusoidal *RC*−oscillators with the same circuit topology. The conclusions highlight the inverse proportionality between the errors and the coupling strength and the insensitivity of the phase noise with respect to the coupling strength.

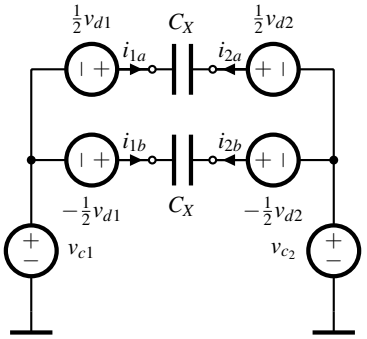

Figure 5.2: Capacitive network currents.

5.2 Quadrature oscillator

In a quadrature $RC-$oscillator with capacitive coupling the two $RC-$oscillators are coupled by four coupling capacitances, C_X, as shown in Fig. 5.1. It is worth mentioning that quadrature outputs are obtained with cross-coupling (Fig. 5.1). The transistors M_{1-4} are the oscillators' core transistors. The oscillators' current sources are implemented by multiple output current mirror. The other elements, capacitances C_1, C_2, and resistance R_1, R_2, set the amplitude and oscillation frequency.

The incremental circuit of the quadrature oscillator is obtained by substituting each oscillator by the series VDPO and substituting the capacitive coupling network by two-port networks. The former was shown in Chapter 4 to be a valid approximation. The latter will be seen in the following analysis as a valid approximation too.

At the end of this section, and to validate the theoretical analysis, we present the design steps of a 2.4GHz oscillator and the respective simulation results.

5.2.1 Two-port modelling of capacitive coupling networks

Modelling the capacitive coupling as a two-port network simplifies the analysis of the quadrature oscillator, since the oscillator can be reduced to two driven VDPOs (similar to the one shown in Section 3.3.2). However, it is worth noting that, a passive network cannot guarantee the port condition (i.e. the currents flowing into the two terminals of the port are anti-symmetric [58]). In passive networks, the current flowing into each terminal is dependent on the external circuits connected to the network (in this case, two $RC-$oscillators). The port condition requires that these circuits cannot inject common-mode currents, which is only possible for ideal current sources without circuit mismatches. To better understand this requirementt, consider the circuit of Fig. 5.2 where each port of the capacitive network is connected to a differential and common mode voltage sources. From the circuit (Fig. 5.2) we can easily obtain the equations of the currents that flow into each terminal:

$$\begin{cases} I_{1_a} = -I_{2_a} = sC_X\left(V_{c_1} - V_{c_2}\right) + s\dfrac{C_X}{2}\left(V_{d_1} - V_{d_2}\right) & \text{(5.1a)} \\ I_{1_b} = -I_{2_b} = sC_X\left(V_{c_1} - V_{c_2}\right) - s\dfrac{C_X}{2}\left(V_{d_1} - V_{d_2}\right). & \text{(5.1b)} \end{cases}$$

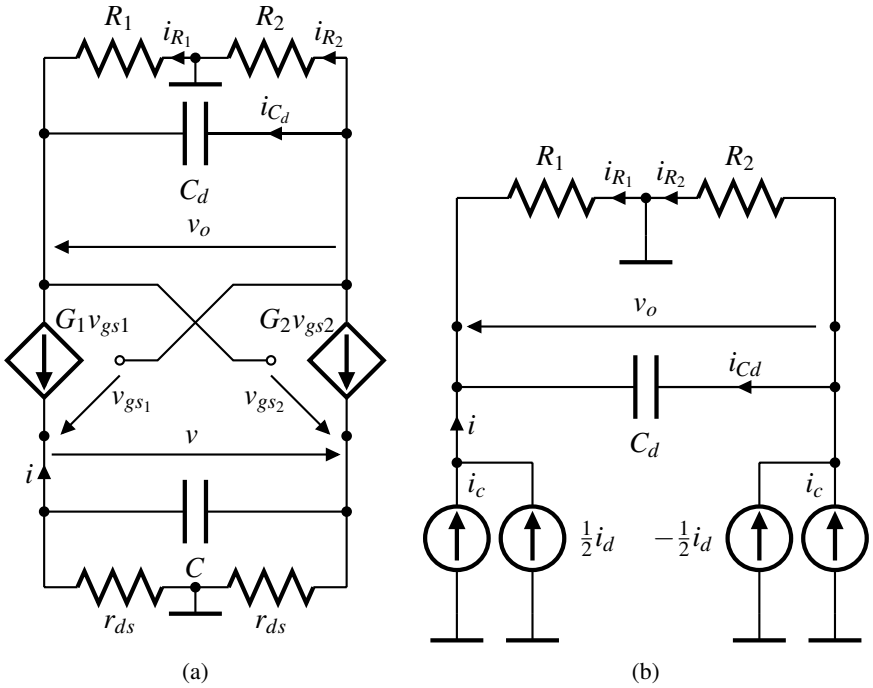

Figure 5.3: Incremental circuit of a single $RC-$oscillator (a) and simplified circuit (b).

Adding the two equations in (5.1), eliminates the term dependent on the differential voltages (second term on the right hand-side of both equations) and doubles the term dependent on the common-mode voltages, resulting in

$$I_{1_a} + I_{1_b} = -\left(I_{2_a} + I_{2_b}\right) = s2C_X\left(V_{c_1} - V_{c_2}\right). \tag{5.2}$$

If the common mode voltages V_{c_1} and V_{c_2} are equal, the port condition is met, i.e. the sum of the currents that flow into each pair of terminals is zero (i.e. $I_{1_a} + I_{1_b} = -I_{2_a} - I_{2_b} = 0$). Thus, for this condition, the capacitive coupling network can be modelled by a two-port network.,

Since mismatches exists in practical circuits and the dynamic resistances of the current sources are not infinite, the two-port modeling is an approximation. Moreover, even without mismatch different common-mode voltages should be expected, since the coupling network is connected to different nodes in each oscillator. If we assume current sources with high dynamic resistances and assume small mismatches (i.e. below 1%) the approximation is valid.

To analyse the output voltage, v_o, with respect to the common- and differential-mode currents, we simplify the single $RC-$oscillator (Fig. 5.3(a)) into Fig. 5.3(b). Applying the KCL and KVL to the circuit (Fig. 5.3(b)) we obtain the following system of equations:

$$\begin{cases} \dfrac{1}{2}I_d + I_c + I_{C_d} + I_{R_1} = 0 & \text{(5.3a)} \\ I_{C_d} = sC_dV_o & \text{(5.3b)} \\ V_o = R_2I_{R_2} + R_1I_{R_1}. & \text{(5.3c)} \end{cases}$$

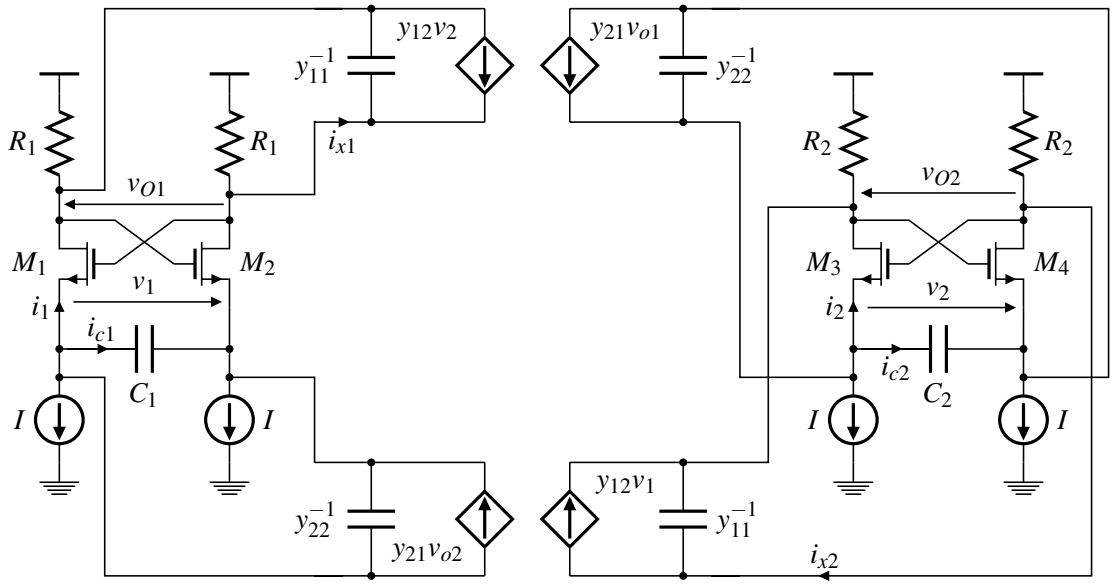

Figure 5.4: Coupling with two-port networks.

Substituting (5.3a) and (5.3b) into (5.3c) we obtain the voltage V_o with respect to both the differential- and common-mode currents:

$$V_o = \frac{R_2 - R_1}{1 + s(R_1 + R_2)C_d} I_c - \frac{1}{2} \frac{R_2 + R_1}{1 + s(R_1 + R_2)C_d} I_d, \tag{5.4}$$

from which we can conclude that the voltage V_o depends on the common-mode current, I_c. If there is no mismatch between R_1 and R_2 (i.e. $R_1 = R_2 = R$) the common-mode term can be omitted. A similar conclusion can be drawn for the voltage V with respect to the dynamic resistances, r_{ds}. If there are no mismatches in the oscillators, which eliminates the common-mode voltages, the capacitive coupling network can be modelled by a two-port network . However, since the common-mode terms are proportional to the mismatch, as can be seen in the first term of the right-hand side of (5.4), we will assume small mismatches (about 1%) and neglect the common-mode terms to use the two-port model for the mismatch case.

With the above assumptions, the coupling networks can be substituted by the two-port equivalent circuit, as shown in Fig. 5.4. To model the capacitive coupling network we use the admittance-parameters (y-parameters) equations, where the terminals currents are dependent variables controlled by the ports' voltages. The parameters of the network are given by

$$\begin{bmatrix} y_{11} & y_{12} \\ y_{21} & y_{22} \end{bmatrix} = \begin{bmatrix} s\frac{C_X}{2} & -s\frac{C_X}{2} \\ -s\frac{C_X}{2} & s\frac{C_X}{2} \end{bmatrix}. \tag{5.5}$$

Note that the current sources at the bottom in comparison to those at the top (Fig. 5.4) are antisymmetric to model the cross-coupling. The input and output impedances, y_{11}^{-1} and y_{22}^{-1}, are added to C_d and C, respectively, increasing both by $C_X/2$. Thus, $C'_{di} = C_d + C_X/2$ and $C'_i = C_i + C_X/2$, are the new capacitances of the $i-$th oscillator.

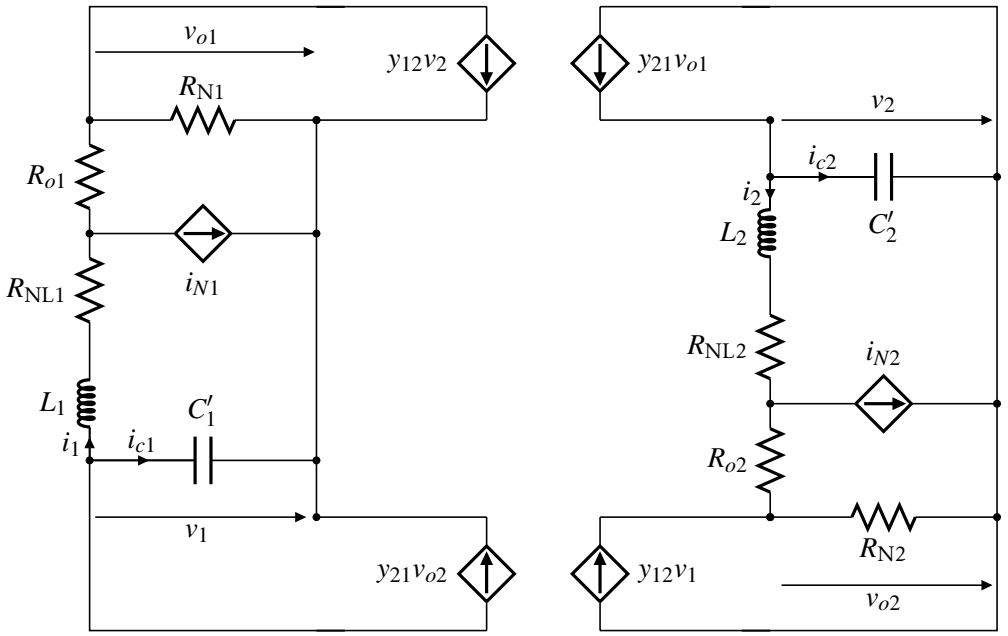

Figure 5.5: Coupled VDPOs.

5.2.2 Incremental model

Substituting each oscillator by the equivalent VDPO result in the circuit of Fig. 5.5. The incremental circuit is a two double injection locked VDPOs, each of them is equivalent to the circuit studied in Section 3.3.2.

Each oscillator is driven by two coupling currents, as shown in Fig. 5.5. Applying the KVL to the circuit on the left side of Fig. 5.5 we obtain

$$L_1\frac{\mathrm{d}i_1}{\mathrm{d}t}+R_{\mathrm{NL1}}i_1+R_{\mathrm{o1}}\left(i_1-i_{N1}\right)+R_{\mathrm{N1}}\left(i_1-i_{N1}\right)+R_{\mathrm{N1}}\frac{C_X}{2}\frac{\mathrm{d}v_2}{\mathrm{d}t}-\frac{1}{C_1'}\int i_1\mathrm{dt} - \frac{1}{C_1'}\int\left[\frac{C_X}{2}\frac{\mathrm{d}v_{o2}}{\mathrm{d}t}\right]\mathrm{dt}=0, \quad (5.6)$$

where i_{N1} is a nonlinear current given by

$$i_{N1}=K^2i_1^3. \quad (5.7)$$

The current, i_{N1}, models the nonlinearities of the oscillators' core transistors. Rearranging the terms in (5.6) leads to

$$\frac{\mathrm{d}i_1}{\mathrm{d}t}+\frac{R_{\mathrm{NL1}}+R_{\mathrm{o1}}+R_{\mathrm{N1}}}{L_1}i_1-\frac{R_{\mathrm{o1}}+R_{\mathrm{N1}}}{L_1}i_{N1}+\frac{1}{L_1C_1'}\int i_1\mathrm{dt}=-R_{\mathrm{N1}}\frac{C_X}{2}\frac{\mathrm{d}v_2}{\mathrm{d}t}+\frac{C_X}{2C_1'}v_{o2}. \quad (5.8)$$

To simplify the equation, the terms on the right-hand side of (5.8) are written as a function of the second oscillator's current, i_2. To this end, the input voltages derivative and the output voltages equations, of both oscillators, are obtained from the incremental circuit of Fig. 5.5:

$$\begin{cases} \dfrac{\mathrm{d}v_1}{\mathrm{d}t} = -\dfrac{i_1}{C_1'} + \dfrac{C_X}{2}\dfrac{\mathrm{d}v_{o2}}{\mathrm{d}t}, & (5.9a) \\ \dfrac{\mathrm{d}v_2}{\mathrm{d}t} = -\dfrac{i_2}{C_2'} - \dfrac{C_X}{2}\dfrac{\mathrm{d}v_{o1}}{\mathrm{d}t}, & (5.9b) \\ v_{o1} = R_{\mathrm{N1}}\left(i_1 - i_{N1}\right) + R_{\mathrm{N1}}\dfrac{C_X}{2}\dfrac{\mathrm{d}v_2}{\mathrm{d}t}, & (5.9c) \\ v_{o2} = R_{\mathrm{N2}}\left(i_2 - i_{N2}\right) - R_{\mathrm{N2}}\dfrac{C_X}{2}\dfrac{\mathrm{d}v_1}{\mathrm{d}t}. & (5.9d) \end{cases}$$

The output voltages, are obtain by substituting (5.9b) into (5.9c) and (5.9a) into (5.9d) resulting in

$$\begin{cases} v_{o1} = R_{\mathrm{N1}}\left(i_1 - i_{N1}\right) - R_{\mathrm{N1}}\dfrac{C_X}{2C_2'}i_2 - R_{\mathrm{N1}}\dfrac{C_X^2}{4}\dfrac{\mathrm{d}v_{o1}}{\mathrm{d}t}, & (5.10a) \\ v_{o2} = R_{\mathrm{N2}}\left(i_2 - i_{N2}\right) - R_{\mathrm{N2}}\dfrac{C_X}{2C_1'}i_1 - R_{\mathrm{N2}}\dfrac{C_X^2}{4}\dfrac{\mathrm{d}v_{o2}}{\mathrm{d}t}. & (5.10b) \end{cases}$$

Note that the third term on the right-hand side of both equations, (5.10a) and (5.10b), is small in comparison with the other terms and, therefore, it is neglected. Moreover, the currents i_{Ni} are small in comparison with the oscillator current (i.e. $i_{Ni} \ll i_i$). Neglecting these terms, one reduces equations (5.10) to

$$\begin{cases} v_{o1} \approx R_{\mathrm{N1}} i_1 - R_{\mathrm{N1}}\alpha_2 i_2, & (5.11a) \\ v_{o2} \approx R_{\mathrm{N2}} i_2 + R_{\mathrm{N2}}\alpha_1 i_1, & (5.11b) \end{cases}$$

where α_i is the coupling strength:

$$\alpha_i = \frac{C_X}{2C_i + C_X} \qquad i = 1, 2.$$

The derivatives of the input voltages, are obtained substituting (5.11a) and (5.11b) into (5.9a) and (5.9b), respectively, resulting in both input and output voltages as functions of the oscillators' currents:

$$\begin{cases} \dfrac{\mathrm{d}v_1}{\mathrm{d}t} = -\dfrac{i_1}{C_1'} + R_{\mathrm{N2}}\dfrac{C_X}{2}\dfrac{\mathrm{d}i_2}{\mathrm{d}t} + R_{\mathrm{N2}}\alpha_1\dfrac{C_X}{2}\dfrac{\mathrm{d}i_1}{\mathrm{d}t}, & (5.12a) \\ \dfrac{\mathrm{d}v_2}{\mathrm{d}t} = -\dfrac{i_2}{C_2'} - R_{\mathrm{N1}}\dfrac{C_X}{2}\dfrac{\mathrm{d}i_1}{\mathrm{d}t} + R_{\mathrm{N1}}\alpha_2\dfrac{C_X}{2}\dfrac{\mathrm{d}i_2}{\mathrm{d}t}, & (5.12b) \end{cases}$$

Substituting (5.11b) and (5.12b) into (5.8) result in

$$L_1\frac{\mathrm{d}i_1}{\mathrm{d}t} + \left(R_{\mathrm{NL1}} + R_{\mathrm{o1}} + R_{\mathrm{N1}}\right)i_1 - \left(R_{\mathrm{o1}} + R_{\mathrm{N1}}\right)i_{N1} + \frac{1}{C_1'}\int i_1 \mathrm{dt} = R_{\mathrm{N1}}\alpha_2 i_2 + R_{\mathrm{N1}}^2\frac{C_X^2}{4}\frac{\mathrm{d}i_1}{\mathrm{d}t} - R_{\mathrm{N1}}^2\frac{C_X^2}{4}\alpha_2\frac{\mathrm{d}i_2}{\mathrm{d}t} + \alpha_1 R_{\mathrm{N2}} i_2 + R_{\mathrm{N2}}\alpha_1^2 i_1. \quad (5.13)$$

The terms with C_X^2 and α_1^2 parameters on the right-hand side of (5.13) can be neglected because, in comparison with the other terms, they are significantly smaller. The coupling capacitances, C_X, are tens of femto farads and the coupling strength,α_1, is much lower than one. Thus, neglecting the smaller terms, dividing both sides of (5.13) by L_1, and differentiating we obtain

$$\frac{\mathrm{d}^2 i_1}{\mathrm{d}t^2} + \frac{R_{\mathrm{NL1}} + R_{\mathrm{o1}} + R_{\mathrm{N1}}}{L_1}\frac{\mathrm{d}i_1}{\mathrm{d}t} - \frac{3K^2\left(R_{\mathrm{o1}} + R_{\mathrm{N1}}\right) i_1^2}{L_1}\frac{\mathrm{d}i_1}{\mathrm{d}t} + \omega_{01}^2\left(1-\alpha_1\right) i_1 \approx \frac{R_{\mathrm{N1}}\alpha_2 + R_{\mathrm{N2}}\alpha_1}{L_1}\frac{\mathrm{d}i_2}{\mathrm{d}t}. \quad (5.14)$$

It is interesting to analyze (5.14), where the right-hand side is the sum of the coupling currents injected by the second oscillator into the first. Equation (5.14) is the driven VDPO. Writing (5.14) in the Van der Pol's form result in

$$\frac{\mathrm{d}^2 i_1}{\mathrm{d}t^2} - 2\left(\delta_0 - \delta_2 i_1^2\right)\frac{\mathrm{d}i_1}{\mathrm{d}t} + \omega_{01}^2\left(1-\alpha_1\right) i_1 \approx -\left(\alpha_1 R_2 + \alpha_2 R_1\right)\frac{\omega_{01}}{Q_1 R_1}\frac{\mathrm{d}i_2}{\mathrm{d}t}, \quad (5.15)$$

where the VDP parameters are given by

$$\delta_0 = \frac{R_{\mathrm{NL1}} + R_{\mathrm{o1}} + R_{\mathrm{N1}}}{L_1} = \frac{R_1\left(1 - \frac{C_d}{C}\right) - g_{m0}^{-1}}{L_1}, \quad (5.16)$$

and

$$\delta_2 = -\frac{3K^2\left(R_{\mathrm{o1}} + R_{\mathrm{N1}}\right)}{L_1} = \frac{3K^2 R_1\left(1 - \frac{C_d}{C}\right)}{L_1}. \quad (5.17)$$

For the second oscillator the result is similar:

$$\frac{\mathrm{d}^2 i_2}{\mathrm{d}t^2} - 2\left(\gamma_0 - \gamma_2 i_1^2\right)\frac{\mathrm{d}i_2}{\mathrm{d}t} + \omega_{02}^2\left(1-\alpha_2\right) i_2 \approx \left(\alpha_2 R_1 + \alpha_1 R_2\right)\frac{\omega_{02}}{Q_2 R_2}\frac{\mathrm{d}i_1}{\mathrm{d}t}, \quad (5.18)$$

where the VDP parameters are given by

$$\gamma_0 = \frac{R_{\mathrm{NL2}} + R_{\mathrm{o2}} + R_{\mathrm{N2}}}{L_1} = \frac{R_2\left(1 - \frac{C_d}{C}\right) - g_{m0}^{-1}}{L_2}, \quad (5.19)$$

$$\gamma_2 = -\frac{3K^2\left(R_{\mathrm{o2}} + R_{\mathrm{N2}}\right)}{L_1} = \frac{3K^2 R_2\left(1 - \frac{C_d}{C}\right)}{L_2}. \quad (5.20)$$

From (5.15) and (5.18) we see that the frequency should decrease when the coupling strength, α, increases. This looks consistent with the intuitive idea that increasing the capacitance lowers the frequency. However, as we show next, the forcing term (the right-hand side of (5.15) and (5.18)) opposes to this tendency and forces the oscillation frequency to increase.

To solve the differential equations, (5.15) and (5.18), we use the harmonic balance method [41], with the assumptions of a slow varying amplitude and phase, and neglecting the high-order terms. Thus, the solutions have the form:

$$\begin{cases} i_1(t) = I_{o1}(t)\sin(\omega t - \phi_1), \\ i_2(t) = I_{o2}(t)\sin(\omega t - \phi_2). \end{cases}$$

where I_{oi} is the current amplitude, ϕ_i the phase and ω is the angular frequency of oscillation. Note that we are assuming that both oscillators are working at the same frequency, but with different phases. The harmonic balance method simplifies the problem, describing it by the amplitudes' envelopes and phases. Two nonlinear second-order differential equations are reduced to the following system of four differential equations of the first order:

$$\begin{cases} \dfrac{dI_{o1}}{dt} = \left(\delta_0 I_{o1} - \dfrac{1}{4}\delta_2 I_{o1}^3\right) + \dfrac{\alpha_{K1}}{2} I_{o2}\cos(\Delta\phi) & \text{(5.22a)} \\ \dfrac{dI_{o2}}{dt} = \left(\gamma_0 I_{o2} - \dfrac{1}{4}\gamma_2 I_{o2}^3\right) + \dfrac{\alpha_{K2}}{2} I_{o1}\cos(\Delta\phi) & \text{(5.22b)} \\ \dfrac{d\phi_1}{dt} = \dfrac{\omega^2 - \omega_{01}^2(1-\alpha_1)}{2\omega} + \dfrac{\alpha_{K1}}{2}\dfrac{I_{o2}}{I_{o1}}\sin(\Delta\phi) & \text{(5.22c)} \\ \dfrac{d\phi_2}{dt} = \dfrac{\omega^2 - \omega_{02}^2(1-\alpha_2)}{2\omega} - \dfrac{\alpha_{K2}}{2}\dfrac{I_{o1}}{I_{o2}}\sin(\Delta\phi), & \text{(5.22d)} \end{cases}$$

where α_{K1} and α_{K2} are given by

$$\alpha_{K1} = -(\alpha_1 R_2 + \alpha_2 R_1)\frac{\omega_{01}}{Q_1 R_1}; \quad \alpha_{K2} = (\alpha_2 R_1 + \alpha_1 R_2)\frac{\omega_{02}}{Q_2},$$

and $\Delta\phi = \phi_2 - \phi_1$ is the phase difference of the currents, i_1 and i_2. From the system (5.22) we can derive the steady-state equations for the amplitudes, frequency and phase. In the next subsection, we analyze first the oscillator without mismatches and afterwards the mismatched case.

5.2.3 Oscillators without mismatches

In this section we analyze the coupled oscillator considering that there are no mismatches, i.e. $R_1 = R_2 = R$, $C_1 = C_2 = C$, $L_1 = L_2 = L$, and $\alpha_1 = \alpha_2 = \alpha$. The free-running frequencies are $\omega_{01} = \omega_{02} = \omega_0$, and the VDP parameters are $\delta_0 = \gamma_0$ and $\delta_2 = \gamma_2$, and the quality factors are $Q_1 = Q_2 = Q$. The coupling strengths are symmetrical $\alpha_{K2} = -\alpha_{K1} = \alpha_K$.

With the above assumptions we simplify the system of differential equation (5.22) and derive the steady-state solutions (equilibrium points). This analysis shows that without mismatches, the amplitudes are equal, the oscillators are in perfect quadrature and the oscillation frequency increases with the coupling strength. Next, to understand how the circuit reaches the steady-state, a transient analysis is done, by linearizing the system near the equilibrium points. The transient analysis shows that the stable equilibrium points are the nonzero amplitudes.

Before we proceed, it is important to define the equilibrium points notation and their coordinates. Although the system (5.22) has four equations, the last two (5.22c) and (5.22d) can be merged. If we use the phase difference, $\Delta\phi$, instead of the absolute phase of each oscillator. Hence, a three dimensions coordinate system (that we refer to as phase-space) can be used. We

refer to an equilibrium point by a letter E with a subscript. The position of each equilibrium point is uniquely determined by three coordinates (in the phase-space), identified by a triplet, where the first and second coordinates represent, respectively, the amplitude I_{o1} and I_{o2}, and the third coordinate the phase difference, $\Delta\phi$.

The equilibrium points, of the system of differential equations (5.22), are obtained with all derivative terms equal to zero (i.e. $\frac{dI_{o1}}{dt} = \frac{dI_{o1}}{dt} = 0$ and $\frac{d\phi_1}{dt} = \frac{d\phi_2}{dt} = 0$). To avoid the indeterminate form $\frac{0}{0}$, we multiply (5.22c) by I_{o1} and (5.22d) by I_{o2} reducing (5.22) to

$$\begin{cases} \left(\delta_0 I_{o1} - \frac{1}{4}\delta_2 I_{o1}^3\right) + \frac{\alpha_K}{2} I_{o2}\cos(\Delta\phi) = 0 & \text{(5.23a)} \\ \left(\delta_0 I_{o2} - \frac{1}{4}\delta_2 I_{o2}^3\right) + \frac{\alpha_K}{2} I_{o1}\cos(\Delta\phi) = 0 & \text{(5.23b)} \\ \frac{\omega^2 - \omega_0^2(1-\alpha)}{2\omega} I_{o1} + \frac{\alpha_K}{2} I_{o2}\sin(\Delta\phi) = 0 & \text{(5.23c)} \\ \frac{\omega^2 - \omega_0^2(1-\alpha)}{2\omega} I_{o2} - \frac{\alpha_K}{2} I_{o1}\sin(\Delta\phi) = 0. & \text{(5.23d)} \end{cases}$$

From (5.23) we find equilibrium points where the current amplitudes are zero (i.e. $I_{o1} = I_{o2} = 0$, meaning that the oscillators do not start). Thus, along the phase-space $\Delta\phi$ axis we have an infinite number of equilibrium points that we identify generically by $E_0 = (0, 0, \Delta\phi)$. Luckily, these equilibrium points are not stable and, therefore, the circuit thermal noise guarantees that the oscillators start. In real circuits these solutions are transient.

Four more equilibrium points exists in the system (5.23), if we consider negative amplitudes and quadrature outputs $\Delta\phi = \frac{\pi}{2}$ and $\Delta\phi = -\frac{\pi}{2}$. Since physically these four solutions are the same. We consider only the equilibrium point of the first quadrant, which have positive amplitudes and positive phase-difference. Thus, at equal amplitudes $I_{o1} = I_{o2} = I_{osc}$ and in quadrature, $\Delta\phi = \frac{\pi}{2}$, we find the equilibrium point $E_1 = (I_{osc}, I_{osc}, \frac{\pi}{2})$. Where the current amplitude, I_{osc}, is obtained by solving (5.23a) or (5.23b) with respect to I_{osc}, and with a $\Delta\phi = \frac{\pi}{2}$, resulting in

$$I_{osc} = 2\sqrt{\frac{\delta_0}{\delta_2}} = 8I\sqrt{\frac{Rg_{m0} - \left(\frac{C}{C-C_d}\right)}{3Rg_{m0}}}. \tag{5.24}$$

To obtain the output voltage, which is easier to compare with measurement results. we multiply (5.24) by the output resistance $2R$,

$$V_{osc} = 16RI\sqrt{\frac{Rg_{m0} - \left(\frac{C}{C-C_d}\right)}{3Rg_{m0}}}. \tag{5.25}$$

The oscillation frequency, ω, is derived by combining (5.23c) and (5.23d) (note that for equal amplitudes $I_{o1} = I_{o2} = I_{osc}$ both equations are equal) resulting in

$$\omega^2 - \omega\alpha_K \sin(\Delta\phi) - \omega_0^2(1-\alpha) = 0. \tag{5.26}$$

Equation (5.26) can be split in two: one for $\Delta\phi = \pi/2$ and other for $\Delta\phi = -\pi/2$. Each equation has two solutions making a total of four solutions. However, the negative frequency solutions can be ruled out remaining two possible solutions. Thus, the positive frequency solutions of (5.26) for the two phases are:

$$\begin{cases} \omega = \dfrac{2\alpha\omega_0}{2Q} + \dfrac{1}{2}\sqrt{\dfrac{4\alpha^2\omega_0^2}{Q^2} + 4\omega_0^2(1-\alpha)}, & \text{if } \Delta\phi = \frac{\pi}{2} \quad (5.27a) \\ \omega = -\dfrac{2\alpha\omega_0}{2Q} + \dfrac{1}{2}\sqrt{\dfrac{4\alpha^2\omega_0^2}{Q^2} + 4\omega_0^2(1-\alpha)}, & \text{if } \Delta\phi = -\frac{\pi}{2}. \quad (5.27b) \end{cases}$$

Using the mathematical approximation $\sqrt{1 \pm x} \approx (1 \pm x/2)$ for $|x| \ll 1$, one can simplify the system of equations (5.27) to

$$\begin{cases} \omega \approx \omega_0 \left(1 + \dfrac{2 - Q + 2\alpha/Q}{2Q}\alpha\right), & \text{if } \Delta\phi = \frac{\pi}{2} \quad (5.28a) \\ \omega \approx \omega_0 \left(1 - \dfrac{2 + Q - 2\alpha/Q}{2Q}\alpha\right). & \text{if } \Delta\phi = -\frac{\pi}{2}. \quad (5.28b) \end{cases}$$

The system (5.28) shows that the oscillator can operate in one of two modes. If $Q \approx 0.5$ then the mode frequencies are:

$$\begin{cases} \omega \sim \omega_0 (1 + 1.5\alpha), & \text{if } \Delta\phi = \frac{\pi}{2} \quad (5.29a) \\ \omega \sim \omega_0 (1 - 2.5\alpha), & \text{if } \Delta\phi = -\frac{\pi}{2}. \quad (5.29b) \end{cases}$$

The results in (5.29) are interesting. For the second mode $\Delta\phi = -\frac{\pi}{2}$, they show that when the coupling strength, α, increases the oscillation frequency decreases. This result makes physical sense since the circuit capacitance increase. The coupling reinforces the natural trend, decreasing further the frequency with the increase of the coupling strength; this also explains the asymmetry between the two modes. However, in the first mode, $\Delta\phi = \pi/2$, this trend is counteracted by the coupling mechanism, such that, the frequency increases rather than decrease, as shown in (5.29a). Moreover, as we will show at the end of this chapter, both modes are stable, mutually exclusive and both are possible in practice. This situation, called bimodal oscillation, has been already identified in coupled $LC-$oscillators. Although, both modes are stable, in practice, with proper initial conditions, the prevailing mode can be selected [23]. The analysis of the second mode has little novelty. Thus, we focus the research in the first mode with, $\Delta\phi = \pi/2$.

5.2.4 Stability of the equilibrium points

To understand how the circuit reaches the steady-state, we do a transient analysis by deriving the phase-space paths. Simplifying the system (5.22) for symmetrical coupling factors, $\alpha_{K1} = -\alpha_{K2} = \alpha_K$, and combining (5.22c) and (5.22d), we obtain

$$\begin{cases} \dfrac{\mathrm{d}I_{\mathrm{o}1}}{\mathrm{d}t} = \delta_0 I_{\mathrm{o}1} - \dfrac{1}{4}\delta_2 I_{\mathrm{o}1}^3 - \dfrac{\alpha_K}{2} I_{\mathrm{o}2}\cos\Delta\phi & \text{(5.30a)} \\ \dfrac{\mathrm{d}I_{\mathrm{o}2}}{\mathrm{d}t} = \delta_0 I_{\mathrm{o}2} - \dfrac{1}{4}\delta_2 I_{\mathrm{o}2}^3 + \dfrac{\alpha_K}{2} I_{\mathrm{o}1}\cos\Delta\phi. & \text{(5.30b)} \\ \dfrac{\mathrm{d}\Delta\phi}{\mathrm{d}t} = -\dfrac{\alpha_K}{2}\left(\dfrac{I_{\mathrm{o}1}}{I_{\mathrm{o}2}} - \dfrac{I_{\mathrm{o}2}}{I_{\mathrm{o}1}}\right)\sin\Delta\phi. & \text{(5.30c)} \end{cases}$$

Although these are first-order differential equations, they are nonlinear, which leads to a cumbersome analysis. For convenience we analyze the transient in the vicinity of the equilibrium point, where the system can be linearized. Thus, linearizing the system (5.30) with respect to $I_{\mathrm{o}1}$, $I_{\mathrm{o}2}$ and $\Delta\phi$ we obtain

$$\begin{cases} \dfrac{\mathrm{d}I_{\mathrm{o}1}}{\mathrm{d}t} \approx \left(\delta_0 - \dfrac{3}{4}\delta_2 I_E^2\right)(I_{\mathrm{o}1} - I_E) - \dfrac{\alpha_K}{2}\cos\Delta\phi_E\,(I_{\mathrm{o}2} - I_E) + \dfrac{\alpha_K}{2} I_E\,(\Delta\phi - \Delta\phi_E) & \text{(5.31a)} \\ \dfrac{\mathrm{d}I_{\mathrm{o}2}}{\mathrm{d}t} \approx \left(\delta_0 - \dfrac{3}{4}\delta_2 I_E^2\right)(I_{\mathrm{o}2} - I_E) + \dfrac{\alpha_K}{2}\cos\Delta\phi_E\,(I_{\mathrm{o}1} - I_E) - \dfrac{\alpha_K}{2} I_E\,(\Delta\phi - \Delta\phi_E), & \text{(5.31b)} \\ \dfrac{\mathrm{d}\Delta\phi}{\mathrm{d}t} \approx \dfrac{\alpha_K}{I_E}\,(I_{\mathrm{o}2} - I_{\mathrm{o}1}). & \text{(5.31c)} \end{cases}$$

where I_E and $\Delta\phi_E$ are, respectively, the steady-state current and the phase-difference at the equilibrium points.

At the equilibrium point E_0, the current amplitudes are equal and, therefore, (5.31c) is equal to zero and the system (5.31) is reduced to two equations that can be written in matrix form as

$$\begin{bmatrix} \frac{\mathrm{d}I_{\mathrm{o}1}}{\mathrm{d}t} \\ \frac{\mathrm{d}I_{\mathrm{o}2}}{\mathrm{d}t} \end{bmatrix} = J \cdot \begin{bmatrix} I_{\mathrm{o}1} \\ I_{\mathrm{o}2} \end{bmatrix},$$

where J is the Jacobian matrix. The Jacobian matrix at E_0 is given by

$$J_{E_0} = \begin{bmatrix} \frac{\partial}{\partial I_{\mathrm{o}1}}\left(\frac{\mathrm{d}I_{\mathrm{o}1}}{\mathrm{d}t}\right) & \frac{\partial}{\partial I_{\mathrm{o}1}}\left(\frac{\mathrm{d}I_{\mathrm{o}2}}{\mathrm{d}t}\right) \\ \frac{\partial}{\partial I_{\mathrm{o}2}}\left(\frac{\mathrm{d}I_{\mathrm{o}1}}{\mathrm{d}t}\right) & \frac{\partial}{\partial I_{\mathrm{o}2}}\left(\frac{\mathrm{d}I_{\mathrm{o}2}}{\mathrm{d}t}\right) \end{bmatrix} = \begin{bmatrix} \delta_0 & \frac{\alpha_K}{2}\cos\Delta\phi_E \\ -\frac{\alpha_K}{2}\cos\Delta\phi_E & \delta_0 \end{bmatrix}.$$

To conclude about the stability of an equilibrium point and determine the geometric figures near it, we must determine the characteristic equation,

$$\lambda^2 - T\lambda + D = 0, \tag{5.32}$$

where T is the trace of J (sum of the main diagonal elements) and D is the determinant of J. The conditions for stability are $T < 0$ and $D > 0$ [41]. For $T > 0$ or $D < 0$ the equilibrium point is unstable [41]. From the Jacobian matrix at the equilibrium point E_0, J_{E_0}, we obtain the characteristic equation

$$\lambda^2 - 2\delta_0\lambda + \left(\delta_0^2 + \frac{\alpha_K^2}{4}\cos\Delta\phi^2\right) = 0. \tag{5.33}$$

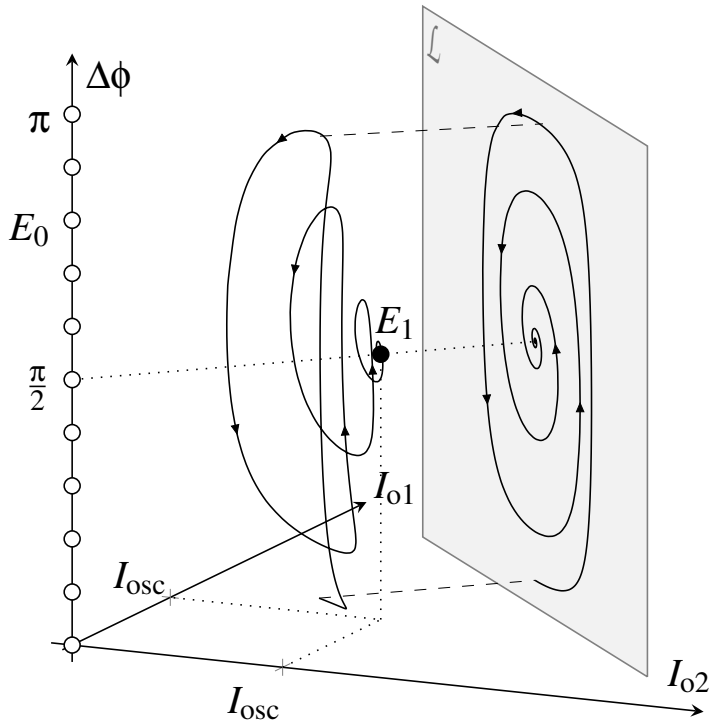

Figure 5.6: Phase space of the capacitive coupling oscillator.

From (5.33), if $\delta_0 > 0$ we conclude that all the equilibrium points on the $\Delta\phi$ axis are unstable, because both the trace and the determinant are positive. However, we have two distinct cases. At $\Delta\phi = \pi/2$ the eigenvalues are real meaning that near that point we have an unstable node. For $\Delta\phi \neq \pi/2$ the eigenvalues are complex with a negative real part which means that at those points we have spiral sources. For $\Delta\phi > \pi/2$, the spiral direction is counterclockwise, and for $\Delta\phi < \pi/2$ it is clockwise. The relevant conclusion is that the points near the origin or along the $\Delta\phi$-axis are unstable, which means that the oscillator will start.

Another equilibrium point exists at $E_1 = (I_{osc}, I_{osc}, \pi/2)$. However, it should be noted that on the right-hand side of (5.30) $\sin\Delta\phi \neq 0$ making the problem three-dimensional, as shown in Fig. 5.6.

The system (5.31) at E_1 result in

$$\begin{cases} \dfrac{dI_{o1}}{dt} \approx -2\delta_0 (I_{o1} - I_E) + \dfrac{\alpha_K}{2} I_E \left(\Delta\phi - \dfrac{\pi}{2}\right) & \text{(5.34a)} \\ \dfrac{dI_{o2}}{dt} \approx -2\delta_0 (I_{o2} - I_E) - \dfrac{\alpha_K}{2} I_E \left(\Delta\phi - \dfrac{\pi}{2}\right) & \text{(5.34b)} \\ \dfrac{d\Delta\phi}{dt} \approx \dfrac{\alpha_K}{I_E} (I_{o2} - I_{o1}) . & \text{(5.34c)} \end{cases}$$

Near E_1 we can reduce the system to two-dimensions by projecting the paths onto the plane $\mathcal{L}$, as illustrated by Fig. 5.6. It should be noted that the plane $\mathcal{L}$ can be any plane perpendicular to the

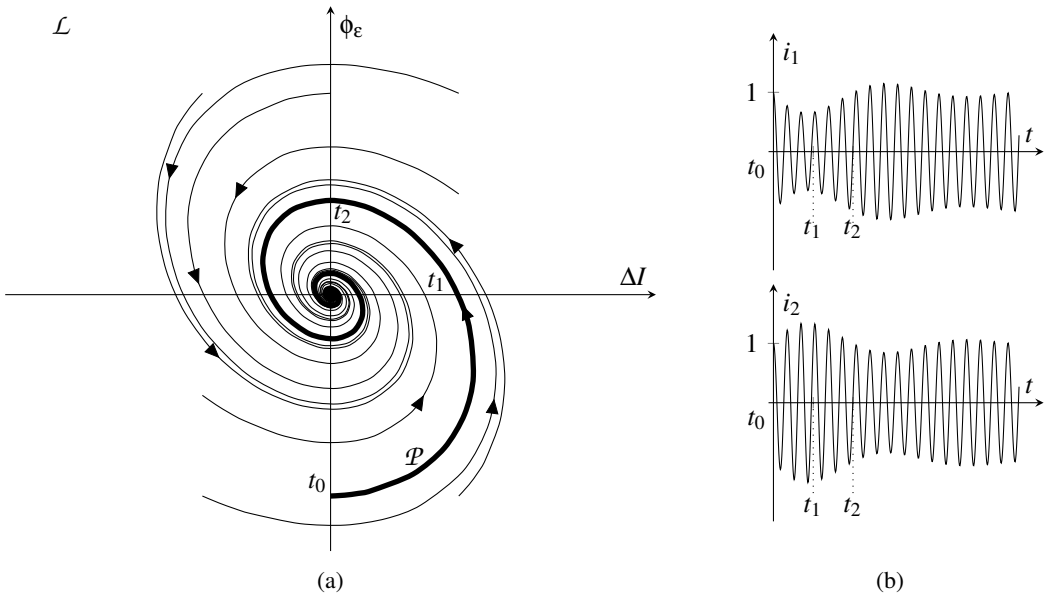

Figure 5.7: Capacitive coupling (a) phase-portrait and (b) transient for path $\mathcal{P}$.

straight line containing the points $(0,0,\pi/2)$ and E_1. If a plane perpendicular to this line is chosen we can make the simple transformations

$$\begin{cases} \Delta I = I_{o2} - I_{o1} \\ \phi_\varepsilon = \Delta\phi - \dfrac{\pi}{2}, \end{cases}$$

where ΔI is the amplitude error and ϕ_ε is the phase error, and subtracting (5.34a) from (5.34b), the system can be reduced to

$$\begin{cases} \dfrac{d\Delta I}{dt} \approx -2\delta_0(\Delta I) + \alpha_K I_{osc}\phi_\varepsilon & (5.36a) \\ \dfrac{d\phi_\varepsilon}{dt} \approx \dfrac{\alpha_K}{I_{osc}}\Delta I & (5.36b) \end{cases}$$

The equilibrium point E_1 on the new coordinates is at the origin $\widehat{E}_1 = (\Delta I = 0, \phi_\varepsilon = 0)$. Hence, the Jacobian matrix is given by

$$J_{\widehat{E}_1} = \begin{bmatrix} -2\delta_0 & -\alpha_K I_{osc} \\ \frac{\alpha_K}{I_{osc}} & 0 \end{bmatrix}, \tag{5.37}$$

and the characteristic equation is

$$\lambda^2 + 2\delta_0\lambda + 4\alpha_K^2 = 0. \tag{5.38}$$

From (5.38) we can conclude that the equilibrium point $\widehat{E}_1$ is stable, since the trace is negative and the determinant is positive. if $\delta_0 > |\alpha_K|/2$ the geometric figure near the $\widehat{E}_1$ is a node, and if

$\delta_0 < |\alpha_K|/2$ is a spiral sink. For the former case the system behaves as an over damped system and for the latter case as an under damped system. The phase portrait (in plane $\mathcal{L}$) for the second case (which occurs for low coupling factors) is shown in Fig. 5.7(a). The highlighted path $\mathcal{P}$ in the phase portrait of Fig. 5.7(a) represents the transients for the case where both oscillators start with the same amplitude and phase. Three instants are marked along the path for easier matching with the time solution shown in Fig. 5.7(b) on the right. From path $\mathcal{L}$ and the top and middle plots on the right-hand side, we see that at instant $t = t_0$ the two oscillators are in-phase with an amplitude of 1V. Following the path direction (indicated by the arrow) we expect an increase of the amplitude error ΔI, meaning that the amplitude of the second oscillator, I_{o2}, increases and I_{o1} decreases, reaching a peak at the instant $t = t_1$. For $t > t_1$ an inversion of the trend occurs and I_{o2} starts decreasing and I_{o1} increasing until another inversion occurs. The cycle repeats until the equilibrium point is reached. Although, the phase, amplitude and frequency becomes closer to steady-state values in each cycle, as shown in the bottom plot of Fig. 5.7(b).

Solving (5.37) we obtain

$$\lambda = -\delta_0 \pm \sqrt{\delta_0^2 - 4\alpha_K^2}. \tag{5.39}$$

If $\delta_0 > |\alpha_K|/2$, there are two negative real eigenvalues (indicating the behaviour of an over damped system). If $\delta_0 < |\alpha_K|/2$ there are two complex conjugate eigenvalues, which indicates an under damped second-order system as shown in the phase portrait and time solution in Fig. 5.7. The amplitude envelope of the latter will have a damping factor,ζ, natural frequency,ω_n, and damped natural frequency,ω_m, respectively, given by

$$\zeta = \frac{1}{2}(K_0 R - 1); \qquad \omega_n = \frac{1}{RC}; \qquad \omega_m = \omega_n \sqrt{4|\alpha_K|^2 R^2 - (K_0 R - 1)^2}. \tag{5.40}$$

For the condition $\delta_0 < |\alpha_K|/2$ the solution is given by

$$\begin{cases} I_{o1} = I_{osc} + K_{I_{o1}} e^{-\delta_0 t} \sin(\omega_n t + \theta_v) \\ I_{o2} = I_{osc} + K_{I_{o2}} e^{-\delta_0 t} \sin(\omega_n t + \theta_v) \\ \Delta\phi = \pm\dfrac{\pi}{2} + K_\phi e^{-\delta_0 t} \cos\left(\omega_n t + \theta_\phi\right) \end{cases},$$

where the K_v, K_ϕ, θ_v and θ_ϕ are arbitrary constants dependent of the initial conditions.

During the transient the oscillators outputs are not in quadrature and the amplitudes are not steady. The settling time, t_s, is an important indicator to estimate the transient interval. It is defined as

$$t_s = -\frac{\ln\left(\frac{\Delta I_o}{I_o}\right)}{\zeta\omega_n} = \frac{\ln\frac{I_o}{\Delta I_o}}{\delta_0},$$

where $\frac{\Delta I_o}{I_o}$ is the relative variation of the amplitude to consider the oscillator in steady-state. Hence, the settling time for $\frac{\Delta I_o}{I_o} = 1\%$ is given by

$$t_s > \frac{2RC\ln 100}{(K_0 R - 1)} \approx \frac{9.21RC}{(K_0 R - 1)}.$$

5.2.5 Mode selection

By definition, the frequency is the derivative of the phase. Hence, from (5.21) the instantaneous frequency of the oscillator is given by

$$\omega_i(t) = \omega_i(0) - \frac{\mathrm{d}\phi_i}{\mathrm{d}t}, \qquad i = 1,2 \tag{5.42}$$

where $\omega_i(0)$ is the frequency at start-up ($t \approx 0$).

Let us consider that the oscillators at start-up are almost in-phase ($\phi_2 > \phi_1 \gtrsim 0$), have low amplitudes ($I_{o1} = I_{o2} \gtrsim 0$), and their oscillation frequency starts from the free-running value, ω_0, since the coupling has negligible influence. With these conditions, (5.22c) and (5.22d) can be approximated as

$$\begin{cases} \dfrac{\mathrm{d}\phi_1}{\mathrm{d}t} \approx \alpha_{K_1} \cdot \Delta\phi & \text{(5.43a)} \\ \dfrac{\mathrm{d}\phi_2}{\mathrm{d}t} \approx -\alpha_{K_2} \cdot \Delta\phi, & \text{(5.43b)} \end{cases}$$

and it becomes clear that the product of the coupling factors and the phase difference determines the sign of the phase derivative and the frequency at steady-state. Hence, on the one hand, if $\alpha_{K1} < 0$, $\alpha_{K2} > 0$ and $\phi_2 > \phi_1 \gtrsim 0$ it can be seen from (5.22c) and (5.22d) that the derivatives of the phases are negative. This, in accordance with (5.42), leads to an increase of the oscillation frequency. On the other hand, if $\phi_1 > \phi_2 \gtrsim 0$, the derivatives are positive and the frequency decreases. However, note that the opposite conclusion can be drawn if we consider $\alpha_{K1} > 0$ and $\alpha_{K2} < 0$, since the derivatives will have the same sign of the phase difference.

Note that when the frequency starts to change in one direction it never goes back and it continues until the derivatives of the phase are zero ($\mathrm{d}\phi_1/\mathrm{d}t = \mathrm{d}\phi_2/\mathrm{d}t = 0$).

Applying the above theory to the circuit of Fig. 5.1, one concludes that if the oscillator 1 (at the left-hand side in Fig. 5.1) start, first, the high frequency mode is selected. Conversely, if the oscillator 2 (at the right-hand side in Fig. 5.1) start, first, the low frequency mode is selected.

5.2.6 Capacitive coupling oscillator with mismatches

In this section we derive the amplitude- and phase errors for the mode $\Delta\phi \approx \pi/2$, considering that there are components mismatches. This analysis is important to understand the impact of the element mismatches on the quadrature error and also on the amplitude-error. The complete derivation is cumbersome, and therefore, in this section, we present only the important steps to the final equations. More details of the derivation are found in Appendix D. In the following derivation we assume that the oscillators core transistors are identical, therefore, their transconductances and capacitances are equal. We consider also that the oscillators reach steady-state making all derivative terms in (5.22) equal to zero.

We assume small mismatches (i.e. $\frac{\Delta R}{R} < 1\%$ and $\frac{\Delta C}{C} < 1\%$) and, to simplify the derivation, we neglect the terms with a multiplication of relative mismatches (e.g. $\frac{\Delta R}{R}\frac{\Delta C}{C} \approx 0$). The error equations

are derived as functions of the mismatches of R and C. Considering the resistances mismatch, $\frac{\Delta R}{R}$, as

$$R_1 = R\left(1-\frac{\Delta R}{2R}\right); \qquad R_2 = R\left(1+\frac{\Delta R}{2R}\right), \tag{5.44}$$

and the capacitance mismatch, $\frac{\Delta C}{C}$, as

$$C_1 = C\left(1-\frac{\Delta C}{2C}\right); \qquad C_2 = C\left(1+\frac{\Delta C}{2C}\right). \tag{5.45}$$

The mismatches of the inductances, L_{e1} and L_{e2}, are related to the mismatches of the resistances as

$$L_{e1} = L_e\left(1-\frac{\Delta R}{2R}\right); \qquad L_{e2} = L_e\left(1+\frac{\Delta R}{2R}\right), \tag{5.46}$$

where L_e is the inductance with no mismatch given by

$$L_e = 4Rg_{m0}^{-1}\left(C_d + C_X\right).$$

Moreover, by definition the amplitudes as functions of the amplitude-error are given by

$$I_{\mathrm{o}1} \stackrel{\mathrm{def}}{=} I_{\mathrm{osc}}\left(1-\frac{\varepsilon_A}{2}\right); \qquad I_{\mathrm{o}2} \stackrel{\mathrm{def}}{=} I_{\mathrm{osc}}\left(1+\frac{\varepsilon_A}{2}\right),$$

where ε_A is the amplitude error.

Before we derive the amplitude-error equation we need to derive first the oscillation frequency, ω. The amplitude-error is derived from (5.22c) and (5.22d) that depend on the oscillation frequency.

The oscillation frequency is obtained by combining (5.22c) and (5.22d). Rearranging the terms with respect to ω, substituting the resistances R_1 and R_2 by the respective mismatches equations (5.44) and grouping α_1 and α_2 parameters we obtain

$$\frac{2\omega^2 - \left[\omega_{01}^2\left(1-\alpha_1\right) + \omega_{02}^2\left(1-\alpha_2\right)\right]}{2\omega} - \left(R_1\alpha_2 + R_2\alpha_1\right)\left(\frac{1}{L_1'}\frac{I_{\mathrm{o}2}}{I_{\mathrm{o}1}} + \frac{1}{L_2'}\frac{I_{\mathrm{o}1}}{I_{\mathrm{o}2}}\right)\sin\left(\Delta\phi\right) = 0. \tag{5.47}$$

Rearranging the terms of the above equation with respect to ω, substituting the resistances R_1 and R_2 by the respective mismatches equations, (5.44), and grouping α_1 and α_2 parameters in the second term on the left-hand side of (5.47) we obtain

$$\omega^2 - R\omega\left[\left(\alpha_1+\alpha_2\right) + \left(\frac{\Delta R}{2R}\right)\left(\alpha_1-\alpha_2\right)\right]\left(\frac{1}{L_1'}\frac{I_{\mathrm{o}2}}{I_{\mathrm{o}1}} + \frac{1}{L_2'}\frac{I_{\mathrm{o}1}}{I_{\mathrm{o}2}}\right)\sin\left(\Delta\phi\right) - \frac{1}{2}\left[\frac{1}{L_1'C_1'} + \frac{1}{L_2'C_2'}\right] = 0.$$

Using the approximations $\left(\alpha_1+\alpha_2 \approx 2\alpha\right)$ and $\alpha_1-\alpha_2 \approx \alpha\left(1-\alpha\right)\frac{\Delta C}{C}$ in the above equation one obtains

$$\omega^2 - R\omega\left[2\alpha + \left(\frac{\Delta R}{2R}\right)\left(\frac{\Delta C}{C}\right)\alpha\left(1-\alpha\right)\right]\left(\frac{1}{L_1'}\frac{I_{\mathrm{o}2}}{I_{\mathrm{o}1}} + \frac{1}{L_2'}\frac{I_{\mathrm{o}1}}{I_{\mathrm{o}2}}\right)\sin\left(\Delta\phi\right) - \frac{1}{2}\frac{1}{LC}2\left(1-\alpha\right) \approx 0.$$

Assuming small mismatches (i.e. $\left(\frac{\Delta R}{R}\right) \leq 1\%$ and $\left(\frac{\Delta C}{C}\right) \leq 1\%$), so that $\left(\frac{\Delta R}{2R}\right)\left(\frac{\Delta C}{C}\right)(1-\alpha) \ll 2$ one obtains

$$\omega^2 - 2R\alpha\omega\left(\frac{1}{L_1'}\frac{I_{o2}}{I_{o1}} + \frac{1}{L_2'}\frac{I_{o1}}{I_{o2}}\right)\sin(\Delta\phi) - \omega_0^2(1-\alpha) \approx 0. \tag{5.48}$$

Using $I_{o1}^2 \approx I_{osc}^2(1-\varepsilon_A)$, $I_{o2}^2 \approx I_{osc}^2(1+\varepsilon_A)$ and $I_{o1}I_{o2} \approx I_{osc}^2\left(1-\frac{\varepsilon_A^2}{4}\right) \approx I_{osc}$, the above equation can be written as

$$\omega^2 - 2R\alpha\omega\left[\frac{L_2'-L_1'}{L_1'L_2'}\varepsilon_A + \frac{L_1'+L_2'}{L_1'L_2'}\right]\sin(\Delta\phi) - \omega_0^2(1-\alpha) \approx 0.$$

Substituting L_{e1} and L_{e2} by their mismatch equations (5.46), the above equation can be written as

$$\omega^2 - \frac{2R\alpha}{L}\omega\left[\left(1+\frac{\Delta R}{2R}-1+\frac{\Delta R}{2R}\right)\varepsilon_A + \left(1+\frac{\Delta R}{2R}+1-\frac{\Delta R}{2R}\right)\right]\sin(\Delta\phi) - \omega_0^2(1-\alpha) \approx 0,$$

which can be reduced to

$$\omega^2 - \frac{4R\alpha}{L}\omega\sin(\Delta\phi) - \omega_0^2(1-\alpha) \approx 0. \tag{5.49}$$

Note that $\frac{R}{L_e} = \frac{\omega_0}{Q}$, where ω_0 is the free-running frequency. Assuming that the oscillators are synchronized and in quadrature, equation (5.49) can be split into two equations: one for $\Delta\phi \approx \frac{\pi}{2}$ and the other for $\Delta\phi \approx -\frac{\pi}{2}$. Thus, we can substitute $\sin(\Delta\phi) \approx \pm 1$, resulting in

$$\begin{cases} \omega^2 - \dfrac{2\omega_0}{Q}\alpha\omega - \omega_0^2(1-\alpha) \approx 0, & \text{if } \Delta\phi \approx \frac{\pi}{2} \quad (5.50a) \\ \omega^2 + \dfrac{2\omega_0}{Q}\alpha\omega - \omega_0^2(1-\alpha) \approx 0. & \text{if } \Delta\phi \approx -\frac{\pi}{2} \quad (5.50b) \end{cases}$$

Four solutions can be derived from (5.50). However, if we rule out the solution with negative frequencies, two solutions remain. Considering $\frac{4\alpha^2}{Q^2} \ll 1$ and $\sqrt{1-x} \approx \left(1-\frac{x}{2}\right)$ for $|x| \ll 1$ yields

$$\begin{cases} \omega \approx \omega_0\left(1 - \dfrac{\alpha}{2} + \dfrac{\alpha}{Q} + \dfrac{\alpha^2}{2Q^2}\right) & (5.51a) \\ \omega \approx \omega_0\left(1 - \dfrac{\alpha}{2} - \dfrac{\alpha}{Q} - \dfrac{\alpha^2}{2Q^2}\right), & (5.51b) \end{cases}$$

Assuming $Q \approx 1$, to ensure the minimum phase noise, this result can be further simplified to

$$\begin{cases} \omega \approx \omega_0\left(1 + \dfrac{2-Q}{2Q}\alpha\right) & (5.52a) \\ \omega \approx \omega_0\left(1 - \dfrac{2+Q}{2Q}\alpha\right). & (5.52b) \end{cases}$$

It can be seen from (5.52) that the impact of the mismatches on the oscillation frequency is negligible. Moreover, equations (5.52) are identical to those in the matched case (in Section 5.2.3).

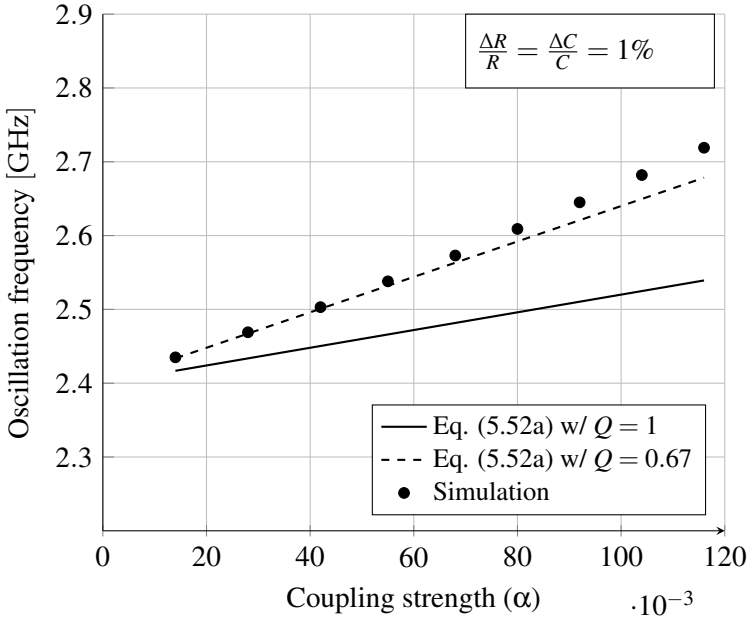

Figure 5.8: Oscillation frequency of the capacitive coupling.

The simulated oscillation frequency is shown in Fig. 5.8, together with the results of (5.52a) for two values of Q. Note that a small deviation from (5.52a) is expected because the Q changes with the coupling.

5.2.6.1 Amplitude error

Knowing the oscillation frequency, we are now able to derive the amplitude error. Subtracting (5.22c) from (5.22d), we obtain

$$\frac{\mathrm{d}\phi_2}{\mathrm{d}t} - \frac{\mathrm{d}\phi_1}{\mathrm{d}t} = \frac{\omega^2 - \omega_{02}^2(1-\alpha_2) - \omega^2 + \omega_{01}^2(1-\alpha_1)}{2\omega} - \frac{1}{2}\left(\alpha_{K2}\frac{I_{o1}}{I_{o2}} + \alpha_{K1}\frac{I_{o2}}{I_{o1}}\right)\sin(\Delta\phi). \quad (5.53)$$

At steady-state the derivatives are zero. If one assumes that the oscillations are nearly in quadrature $(\sin\Delta\phi \approx 1)$, equation (5.53) is reduced to

$$-\Delta\omega - \frac{1}{2}\left(\alpha_{K2}\frac{I_{o1}}{I_{o2}} + \alpha_{K1}\frac{I_{o2}}{I_{o1}}\right) \approx 0. \quad (5.54)$$

where $\Delta\omega$ is the free-running frequencies mismatch given by

$$\Delta\omega = \frac{\omega_{02}^2(1-\alpha_2) - \omega_{01}^2(1-\alpha_1)}{2\omega}. \quad (5.55)$$

The left-hand side of (5.54) has two terms. To obtain the amplitude error we will derive each term with respect to the mismatches and the amplitude-error. Now using $\omega_{0i}^2(1-\alpha_i) = 1/(L_iC_i)$ and substituting this result into (5.55), the free-running frequency mismatch can be approximated by

$$\Delta\omega = \frac{1}{2\omega}\left(\frac{1}{L_2'C_2'} - \frac{1}{L_1'C_1'}\right). \tag{5.56}$$

Substituting the inductances and capacitances into (5.56) results

$$\Delta\omega \approx -\frac{\omega_0^2(1-\alpha)}{2\omega}\left[\left(\frac{\Delta C}{C}\right)(1-\alpha) + \left(\frac{\Delta R}{R}\right)\right], \tag{5.57}$$

Equation (5.57) shows that the frequency mismatch (difference between the free-running frequencies) is dependent on the capacitances and resistances mismatch.

Let us now simplify the second term on the left-hand side of (5.54). For $\alpha_{K1} = -2(R_2\alpha_1 + R_1\alpha_2)/L_{e1}'$ and $\alpha_{K2} = 2(R_2\alpha_1 + R_1\alpha_2)/L_{e2}'$, assuming small mismatches and using the approximations $(\alpha_1 + \alpha_2 \approx 2\alpha)$ and $(\alpha_1 - \alpha_2 \approx \frac{\Delta C}{C}(1-\alpha)\alpha)$, one can obtain

$$-\frac{1}{2}\left(\alpha_{K2}\frac{I_{o1}}{I_{o2}} + \alpha_{K1}\frac{I_{o2}}{I_{o1}}\right)\sin\Delta\phi, \tag{5.58}$$

where $\alpha_{K1} = -2(R_2\alpha_1 + R_1\alpha_2)\frac{2}{L_{e1}}$ and $\alpha_{K2} = 2(R_2\alpha_1 + R_1\alpha_2)\frac{2}{L_{e2}}$. Expanding α_{K1} and α_{K2}, gives

$$\alpha_{K1} = -\frac{4R}{L_{e1}}\left[(\alpha_1 + \alpha_2) + \left(\frac{\Delta R}{2R}\right)(\alpha_1 - \alpha_2)\right],$$

which can be simplified if we use the approximations $\alpha_1 + \alpha_2 \approx 2\alpha$ and $\alpha_1 - \alpha_2 \approx \frac{\Delta C}{C}(1-\alpha)\alpha$,

$$\alpha_{K1} \approx -\frac{4R}{L_{e1}}\left[2\alpha + \left(\frac{\Delta R}{2R}\right)\left(\frac{\Delta C}{C}\right)\alpha(1-\alpha)\right]. \tag{5.59}$$

For small mismatches the second term on the right-hand side of (5.59) can be neglected, which result in

$$\alpha_{K1} \approx -\frac{4R}{L_{e1}}\alpha. \tag{5.60}$$

Similarly,

$$\alpha_{K2} \approx \frac{4R}{L_{e2}}\alpha. \tag{5.61}$$

Substituting (5.60) and (5.61) into the second term on the left-hand side of (5.58), one obtains

$$-\frac{1}{2}\left(\alpha_{K2}\frac{I_{o1}}{I_{o2}} + \alpha_{K1}\frac{I_{o2}}{I_{o1}}\right)\sin\Delta\phi \approx -2R\alpha\left(\frac{L_1'I_{o1}^2 - L_2'I_{o2}^2}{L_1'L_2'I_{o1}I_{o2}}\right). \tag{5.62}$$

Using $I_{o1}^2 \approx I_{osc}^2(1-\varepsilon_A)$, $I_{o2}^2 \approx I_{osc}^2(1+\varepsilon_A)$ and $I_{o1}I_{o2} \approx I_{osc}^2\left(1 - \frac{\varepsilon_A^2}{4}\right) \approx I_{osc}$, the above equation is reduced to

$$-\frac{1}{2}\left(\alpha_{K2}\frac{I_{o1}}{I_{o2}} + \alpha_{K1}\frac{I_{o2}}{I_{o1}}\right)\sin\Delta\phi \approx -2R\alpha\left[\frac{L_1' - L_2'}{L_1'L_2'} - \frac{L_1' + L_2'}{L_1'L_2'}\varepsilon_A\right]. \tag{5.63}$$

Substituting the inductance equations (5.46) in (5.63) gives

$$-\frac{1}{2}\left(\alpha_{K2}\frac{I_{o1}}{I_{o2}} + \alpha_{K1}\frac{I_{o2}}{I_{o1}}\right)\sin\Delta\phi \approx \frac{2R}{L}\alpha\left[\left(\frac{\Delta R}{R}\right) + 2\varepsilon_A\right]. \tag{5.64}$$

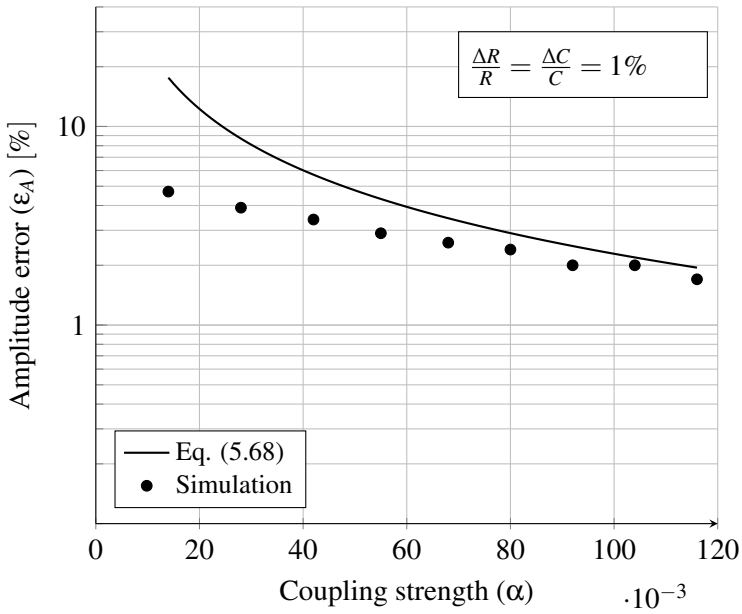

Figure 5.9: Simulation results for the amplitude error of the capacitive coupling.

Finally, with both terms simplified, substituting (5.57) and (5.64) into (5.54) gives

$$\frac{\omega_0^2(1-\alpha)}{2\omega}\left[\left(\frac{\Delta R}{R}\right)+\left(\frac{\Delta C}{C}\right)(1-\alpha)\right] \approx -\frac{2R\alpha}{L}\left[\frac{\Delta R}{R}+2\varepsilon_A\right]. \tag{5.65}$$

Using $\frac{2R}{L} = \frac{\omega_0}{Q}$ and $\omega \approx \omega_0\left(1+\frac{2-Q}{2Q}\alpha\right)$ for $\Delta\phi \approx \frac{\pi}{2}$, the above equation becomes

$$(1-\alpha)\left[\left(\frac{\Delta R}{R}\right)+\left(\frac{\Delta C}{C}\right)(1-\alpha)\right] \approx \mp\frac{2\left(1+\frac{2-Q}{2Q}\alpha\right)\alpha}{Q}\left(\frac{\Delta R}{R}\right) \mp \frac{4\left(1+\frac{2-Q}{2Q}\alpha\right)\alpha}{Q}\varepsilon_A, \tag{5.66}$$

If (5.66) is solved with respect to the amplitude-error, ε_A, the result will be

$$\varepsilon_A \approx -\frac{1}{4}\left[1+\frac{(1-\alpha)}{(2+\alpha)\alpha}\right]\left(\frac{\Delta R}{R}\right) - \frac{1}{4}\left[\frac{(1-\alpha)^2}{(2+\alpha)\alpha}\right]\left(\frac{\Delta C}{C}\right). \tag{5.67}$$

Equation (5.67) shows that the amplitude-error increases with both resistance and capacitance mismatches. The error reduces substantially with the increase of the coupling strength. The resistance mismatch has a slightly higher impact on the amplitude-error. An interesting aspect is that the resistance mismatch defines the lower limit of the amplitude-error: even for very large values of the coupling strength the amplitude-error cannot be less than a quarter of the resistance mismatch.

In comparison with the simulations results, (5.67) gives a more conservative result (approximately doubles the amplitude error), as shown in Fig. 5.9. Despite the higher values given by (5.67), the trend follows the simulation results diverging strongly only for low coupling strengths.

5.2.6.2 Phase error

We obtain the phase error by subtracting (5.22b) from (5.22a). This gives

$$(\gamma_0-\delta_0)-\frac{1}{4}\left(\gamma_2 I_{o2}^2-\delta_2 I_{o1}^2\right)+\frac{1}{2}\left(\alpha_{K2}\frac{I_{o1}}{I_{o2}}-\alpha_{K1}\frac{I_{o2}}{I_{o1}}\right)\cos(\Delta\phi)=0. \tag{5.68}$$

Writing the first term on the left-hand side of (5.68) as a function of the resistance and capacitance mismatches, $\Delta R/R$ and $\Delta C/C$, respectively, result in

$$(\gamma_0-\delta_0)=\frac{R\left(1+\frac{\Delta R}{2R}\right)\left(1-\frac{C_d}{C_2'}\right)-g_{m0}^{-1}}{L\left(1+\frac{\Delta R}{2R}\right)}-\frac{R\left(1-\frac{\Delta R}{2R}\right)\left(1-\frac{C_d}{C_1'}\right)-g_{m0}^{-1}}{L\left(1-\frac{\Delta R}{2R}\right)} \tag{5.69}$$

Assuming small mismatches $\left(\frac{\Delta R}{2R}\right)^2 \ll 1$, and reducing both terms, on the right-hand side, to a common denominator yields

$$(\gamma_0-\delta_0)\approx\frac{RC_d\left(\frac{1}{C_1'}-\frac{1}{C_2'}\right)+g_{m0}^{-1}\left(\frac{\Delta R}{R}\right)}{L}. \tag{5.70}$$

With $\frac{1}{C_1'}-\frac{1}{C_2'}\approx\frac{1}{C}\left(\frac{\Delta C}{C}\right)(1-\alpha)^2$, equation (5.70) is simplified to

$$\begin{aligned}(\gamma_0-\delta_0)&\approx\frac{RC_d\left(\frac{\Delta C}{C}\right)(1-\alpha)^2+g_{m0}^{-1}C\left(\frac{\Delta R}{R}\right)}{LC}\\&\approx\omega_0^2(1-\alpha)\left[RC_d\left(\frac{\Delta C}{C}\right)(1-\alpha)+g_{m0}^{-1}C\left(\frac{\Delta R}{R}\right)\right].\end{aligned} \tag{5.71}$$

For the second term on the left-hand side of (5.68), using $I_{o1}=I_{osc}\left(1-\frac{\varepsilon_A}{2}\right)$ and $I_{o2}=I_{osc}\left(1+\frac{\varepsilon_A}{2}\right)$, one obtains

$$\begin{aligned}\frac{1}{4}\left(\gamma_2 I_{o2}^2-\delta_2 I_{o1}^2\right)&=\frac{I_{osc}^2}{4}\left[\left(1+\varepsilon_A+\frac{\varepsilon_A^2}{4}\right)\gamma_2-\left(1-\varepsilon_A+\frac{\varepsilon_A^2}{4}\right)\delta_2\right]\\&\approx\frac{I_{osc}^2}{4}\left[(\gamma_2-\delta_2)+(\gamma_2+\delta_2)\varepsilon_A\right]\end{aligned} \tag{5.72}$$

Then substituting parameters δ_2 and γ_2 by their equations as a function of the circuit elements, result in

$$\begin{aligned}\frac{1}{4}\left(\gamma_2 I_{o2}^2-\delta_2 I_{o1}^2\right)\approx\frac{3K^2I_{osc}^2}{4}\Bigg[&\left(\frac{R_2\left(1-\frac{C_d}{C_2'}\right)}{L_2'}-\frac{R_1\left(1-\frac{C_d}{C_1'}\right)}{L_1'}\right)\\&+\left(\frac{R_2\left(1-\frac{C_d}{C_2'}\right)}{L_2'}+\frac{R_1\left(1-\frac{C_d}{C_1'}\right)}{L_1'}\right)\varepsilon_A\Bigg]\end{aligned} \tag{5.73}$$

Since $K=\frac{1}{4I}$, $R_1=R\left(1-\frac{\Delta R}{2R}\right)$, $R_2=\left(1+\frac{\Delta R}{2R}\right)$, $L_1'=L\left(1-\frac{\Delta R}{2R}\right)$ and $L_2'=L\left(1+\frac{\Delta R}{2R}\right)$, the second term of (5.68) is reduced to

$$\frac{1}{4}\left(\gamma_2 I_{o2}^2 - \delta_2 I_{o1}^2\right) \approx \frac{3I_{osc}^2 R}{4^3 I^2 LC}\left[C_d\left(\frac{\Delta C}{C}\right)(1-\alpha)^2 + 2\left(C - C_d(1-\alpha)\right)\varepsilon_A\right]. \tag{5.74}$$

Note that $I_{osc} \approx 8I\sqrt{\frac{Rg_{m0}-\frac{C}{C-C_d}}{3Rg_{m0}}}$, when substituted into (5.74), yields

$$\frac{1}{4}\left(\gamma_2 I_{o2}^2 - \delta_2 I_{o1}^2\right) \approx \frac{Rg_{m0}-\frac{C}{C-C_d}}{Rg_{m0}}\omega_0^2 R\left[C_d\left(\frac{\Delta C}{C}\right)(1-\alpha)^2 + 2\left(C - C_d(1-\alpha)\right)\varepsilon_A\right]. \tag{5.75}$$

A similar procedure should be done for the third term on the left-hand side of (5.68). Substituting α_{K1} and α_{K2} by (5.60) and (5.61) into (5.75), results in

$$\frac{1}{2}\left(\alpha_{K2}\frac{I_{o1}}{I_{o2}} - \alpha_{K1}\frac{I_{o2}}{I_{o1}}\right)\cos(\Delta\phi) = (R_2\alpha_1 + R_1\alpha_2)\left(\frac{1}{L_2'}\frac{I_{o1}}{I_{o2}} + \frac{1}{L_1'}\frac{I_{o2}}{I_{o1}}\right)\cos(\Delta\phi) = 0 \tag{5.76}$$

Multiplying both sides of (5.76) by I_{o1} and I_{o2}, result in $I_{o1}I_{o2}$ as common denominator:

$$\frac{1}{2}\left(\alpha_{K2}\frac{I_{o1}}{I_{o2}} - \alpha_{K1}\frac{I_{o2}}{I_{o1}}\right)\cos(\Delta\phi) = (R_2\alpha_1 + R_1\alpha_2)\left(\frac{1}{L_2'}\frac{I_{o1}^2}{I_{o2}I_{o1}} + \frac{1}{L_1'}\frac{I_{o2}^2}{I_{o1}I_{o2}}\right)\cos(\Delta\phi) = 0 \tag{5.77}$$

Now using (5.44) and (5.46) in (5.77) one obtains

$$\frac{1}{2}\left(\alpha_{K2}\frac{I_{o1}}{I_{o2}} - \alpha_{K1}\frac{I_{o2}}{I_{o1}}\right)\cos(\Delta\phi) \approx \frac{R}{L}\left[(\alpha_1+\alpha_2) + \frac{\Delta R}{2R}(\alpha_1-\alpha_2)\right]\left(\frac{\left(I_{o1}^2 + I_{o2}^2\right) + \frac{\Delta R}{2R}\left(I_{o2}^2 - I_{o1}^2\right)}{I_{o2}I_{o1}}\right)\cos(\Delta\phi) \tag{5.78}$$

Further, using $I_{o1}^2 \approx I_{osc}^2(1-\varepsilon_A)$, $I_{o2}^2 \approx I_{osc}^2(1+\varepsilon_A)$ and $I_{o1}I_{o2} \approx I_{osc}^2$, after extensive calculations one simplifies the third term of (5.78) to

$$\frac{1}{2}\left(\alpha_{K2}\frac{I_{o1}}{I_{o2}} - \alpha_{K1}\frac{I_{o2}}{I_{o1}}\right)\cos(\Delta\phi) \approx \frac{R}{L}\left[(\alpha_1+\alpha_2) + \frac{\Delta R}{2R}(\alpha_1-\alpha_2)\right]\left(2 + \frac{\Delta R}{2R}\varepsilon_A\right)\cos(\Delta\phi) \tag{5.79}$$

Note that if we assume small mismatches, the terms: $\frac{\Delta R}{2R}\varepsilon_A \ll 2$, $\frac{\Delta R}{2R}\frac{\Delta C}{2C}(1-\alpha) \ll 2$, $\alpha_1+\alpha_2 \approx 2\alpha$ and $\alpha_1 - \alpha_2 \approx \alpha(1-\alpha)\left(\frac{\Delta C}{C}\right)$. Thus, (5.79) is reduced to

$$\frac{1}{2}\left(\alpha_{K2}\frac{I_{o1}}{I_{o2}} - \alpha_{K1}\frac{I_{o2}}{I_{o1}}\right)\cos(\Delta\phi) \approx 4RC\alpha\omega_0^2\cos(\Delta\phi) \tag{5.80}$$

Finally, substituting (5.70), (5.75) and (5.80) into (5.68) and solving the result with respect to $\cos\Delta\phi$ we obtain

$$4RC\alpha\cos(\Delta\phi) = (1-\alpha)\left[RC_d\left(\frac{\Delta C}{C}\right)(1-\alpha) + g_{m0}^{-1}C\left(\frac{\Delta R}{R}\right)\right] + -\frac{Rg_{m0}-\frac{C}{C-C_d}}{Rg_{m0}}\left[RC_d\left(\frac{\Delta C}{C}\right)(1-\alpha)^2 + 2R\left(C - C_d(1-\alpha)\right)\varepsilon_A\right] \tag{5.81}$$

Rearranging the terms in (5.81), gathering the $\Delta R/R$, $\Delta C/C$, and ε_A terms, result in

$$\cos(\Delta\phi) = \frac{(1-\alpha)^2}{\alpha}\frac{1}{4Rg_{m0}}\left[\frac{C_d}{(C-C_d)}\left(\frac{\Delta C}{C}\right)+\frac{1}{(1-\alpha)}\left(\frac{\Delta R}{R}\right)\right.$$
$$\left.-2\left(Rg_{m0}-\frac{C}{C-C_d}\right)\left(\frac{1}{(1-\alpha)^2}-\frac{C_d}{C}\frac{1}{(1-\alpha)}\right)\varepsilon_A\right] \quad (5.82)$$

The phase difference is given by

$$\Delta\phi = \frac{\pi}{2}+\varepsilon_\phi, \quad (5.83)$$

where ε_ϕ is the phase error.

The cosine of the phase difference is equal to the sine of the phase error, i.e. $\cos\Delta\phi = \sin\varepsilon_\phi$. Moreover, assuming that the phase error is small, $\cos\Delta\phi$ is approximately equal to the phase error:

$$\varepsilon_\phi \approx \frac{(1-\alpha)^2}{\alpha}\frac{1}{4Rg_{m0}}\left[\frac{C_d}{C-C_d}\left(\frac{\Delta C}{C}\right)+\frac{1}{(1-\alpha)}\left(\frac{\Delta R}{R}\right)\right.$$
$$\left.-2\frac{Rg_{m0}-\frac{C}{C-C_d}}{(1-\alpha)^2}\left(1-\frac{C_d}{C}(1-\alpha)\right)\varepsilon_A\right] \quad (5.84)$$

For the specific case of $C = 2C_d$, the phase error is reduced to

$$\varepsilon_\phi \approx \frac{(1-\alpha)^2}{\alpha}\frac{1}{4Rg_{m0}}\left[\left(\frac{\Delta C}{C}\right)+\frac{1}{(1-\alpha)}\left(\frac{\Delta R}{R}\right)-\frac{Rg_{m0}-2}{(1-\alpha)^2}(1+\alpha)\varepsilon_A\right]. \quad (5.85)$$

Note that (5.85) is in radians. To obtain the phase-error in degrees we multiply (5.85) by $\frac{180}{\pi}$:

$$\varepsilon_\phi \approx \frac{(1-\alpha)^2}{\alpha}\frac{45}{\pi Rg_{m0}}\left[\left(\frac{\Delta C}{C}\right)+\frac{1}{(1-\alpha)}\left(\frac{\Delta R}{R}\right)-\frac{Rg_{m0}-2}{(1-\alpha)^2}(1+\alpha)\varepsilon_A\right]. \quad (5.86)$$

Equation (5.86) shows that the phase-error increases with both resistance and capacitance mismatches. A dependence on the amplitude-error seems to decrease the phase-error, however, the amplitude-error is usually negative. The error reduces substantially with the increase of the coupling strength. The simulations results are in agreement with the theory (5.86) , as shown in Fig. 5.10. The small difference between the simulation and theoretical results is explained by the used approximations.

Contrary to the $LC-$oscillator [54], the cross-coupled $RC-$oscillator has a low sensitivity of the phase-noise to the coupling strength. This means that, although the phase-error reduces substantially with the increase of the coupling strength, the phase-noise has a negligible variation (about 1 dB), as shown in Figure 5.11. Thus, the designer can focus on the reduction of the phase-error because the penalty in the phase-noise is negligible.

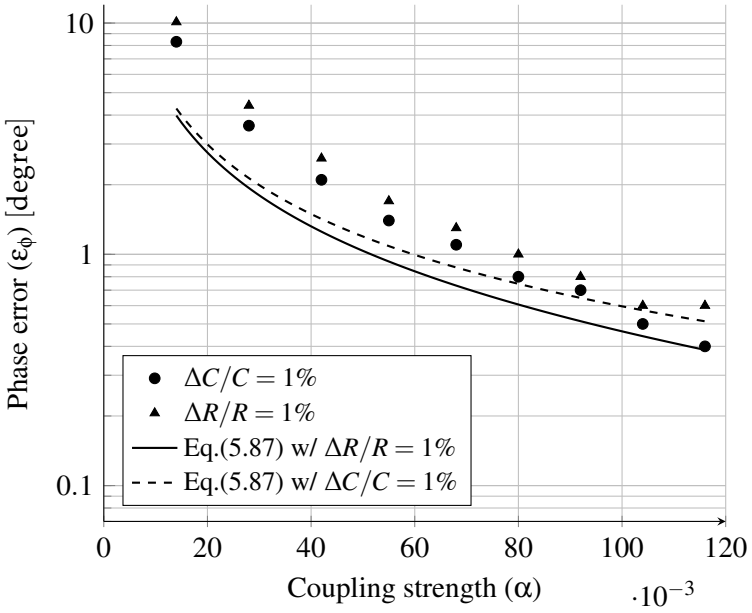

Figure 5.10: Simulated phase error.

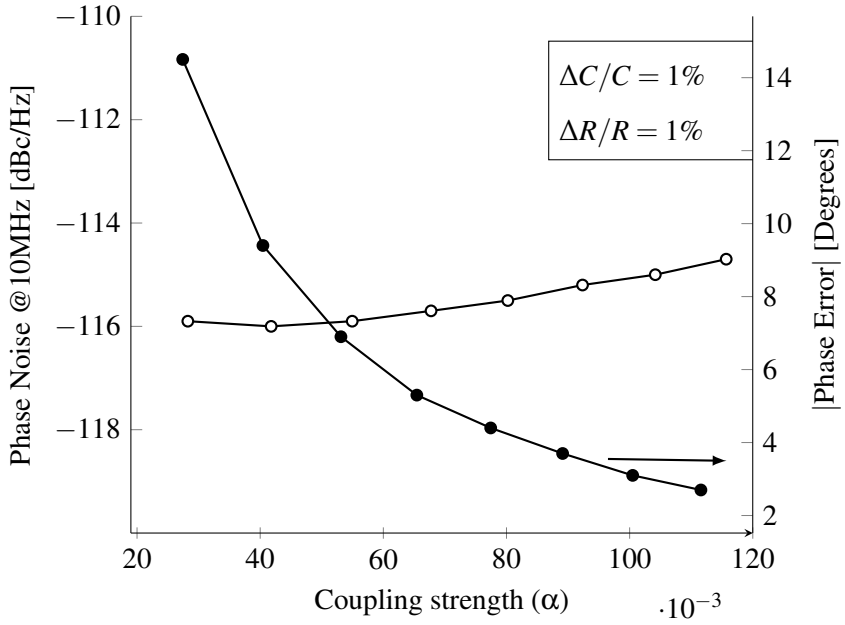

Figure 5.11: Phase noise and phase error.

5.3 Experimental results

To validate the theory, a 2.4 GHz capacitive coupled QVCO with variable coupling capacitances was fabricated in UMC 0.13 μm CMOS process. The circuit schematic is shown in Fig. 5.12. The coupling capacitances are 3-bit binary weighted capacitors arrays, as shown in Fig. 5.13(a). Each capacitor array has a step of 20 fF with 3-bits allowing a capacitance variation range from approximately 0 fF (not coupled) up to 140 fF coupling. The prototype die microphotograph is

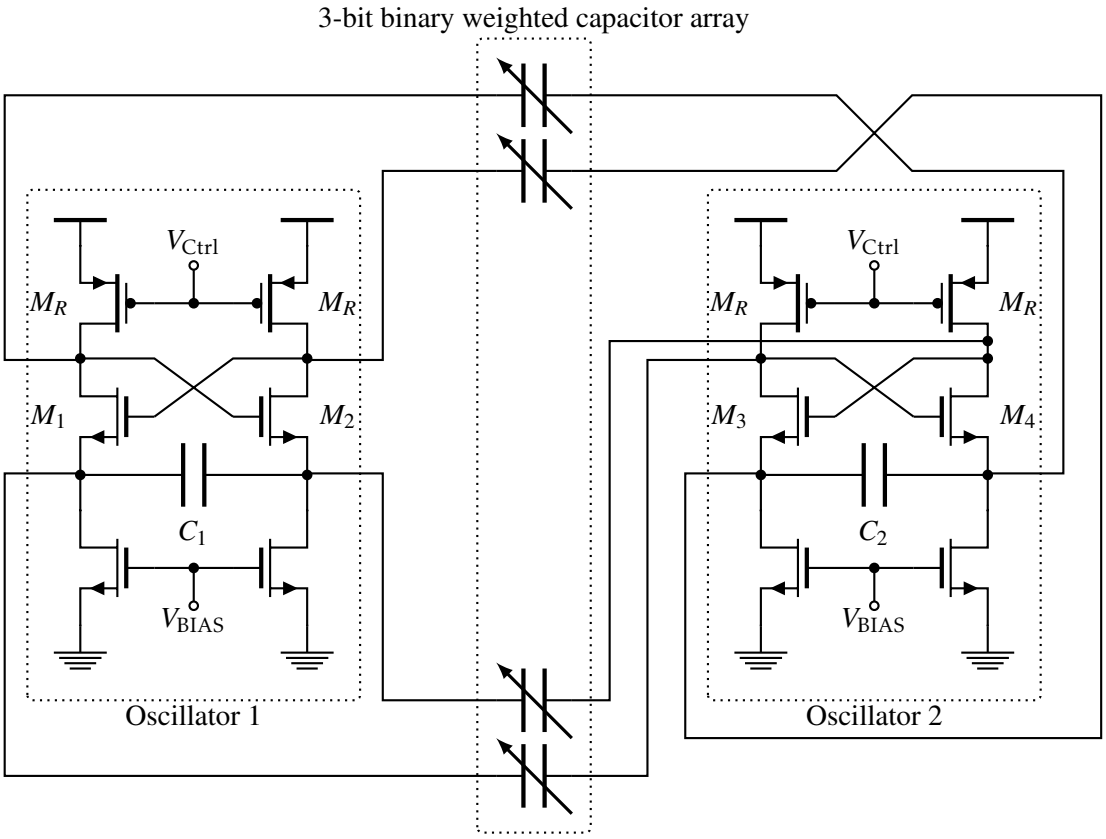

Figure 5.12: Prototype circuit of the capacitive coupling oscillator.

shown in Fig. 5.13(c). A second prototype was made with a single capacitance value to minimize the area. The die microphotograph of the second prototype is shown in Fig. 5.13(d). This prototype has a switch to turn the coupling on and off. Each prototype die was bondwired to a printed circuit board (PCB) making the RF signals accessible through four SMA connectors, as shown in the photograph of Fig. 5.13(b). We refer to this PCB as the daughterboard, since a second PCB (the motherboard) is required to provide the power supplies and control signals.

The dimensions of the oscillators core transistors (M_1, M_2, M_3 and M_4) are $W = 7.2$ µm, and $L = 120$ nm. The dimensions of the current source transistors (M_9, M_{11}, M_{12} and M_{14}) are $W = 7.2$ µm, and $L = 360$ nm. The resistors were implemented with PMOS transistors, operating in the triode region, with $W = 5.4$ µm, $L = 120$ nm. The timing capacitors are of MiM type, with an area of 20 µm $\times$ 20 µm, resulting in the capacitance of 431.7 fF. The supply voltage is 1.2 V, and the bias current is 1.8 mA, which results in 8.64 mW power dissipation. The layout of the circuit occupies an area of 430 µm $\times$ 180 µm (without pads).

Figure 5.14 shows the measured oscillation frequencies when the oscillators are free-running, i.e. $C_X \approx 0$ fF, represented in the figure by the triangles, and coupled with $C_X = 20$ fF (dots). The gap between the two results clearly indicates that the oscillation frequency increases when the oscillators are coupled, which is consistent with the theory.

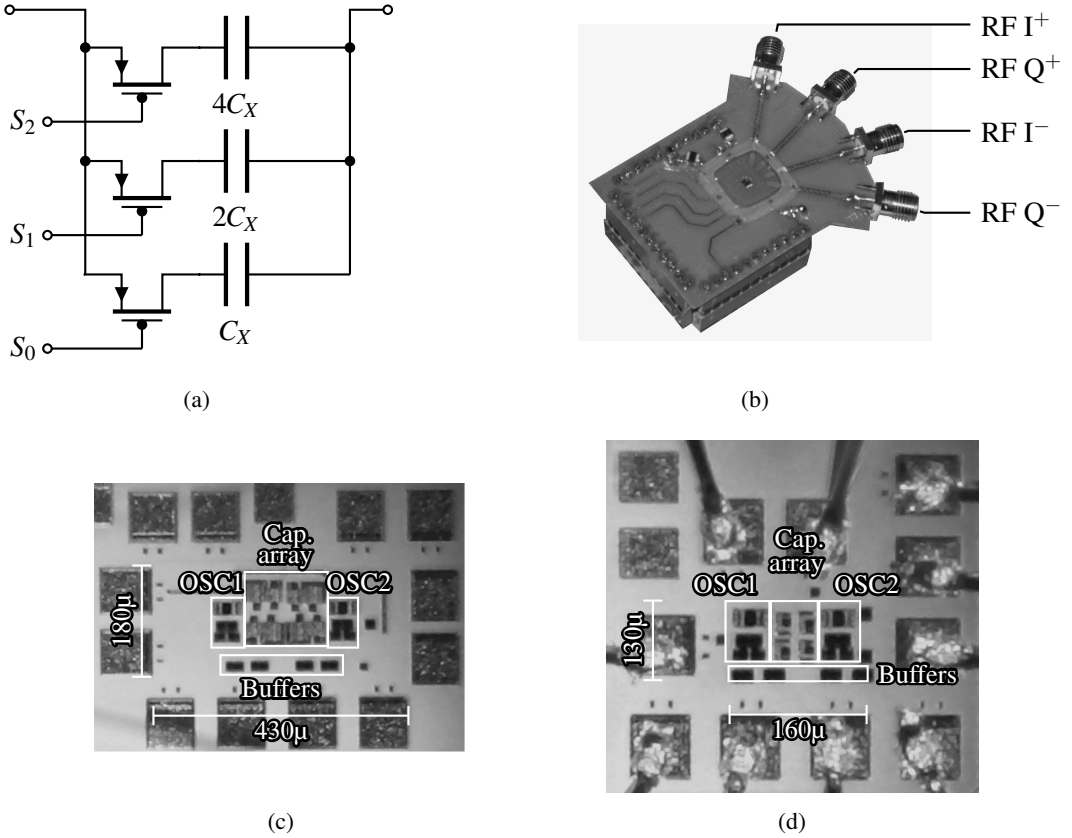

Figure 5.13: 3-bit binary weighted capacitor array (a), photo of the daughterboard (b), the microphotos of the capacitive coupling QVCOs with capacitor array (c), and without capacitor array (d).

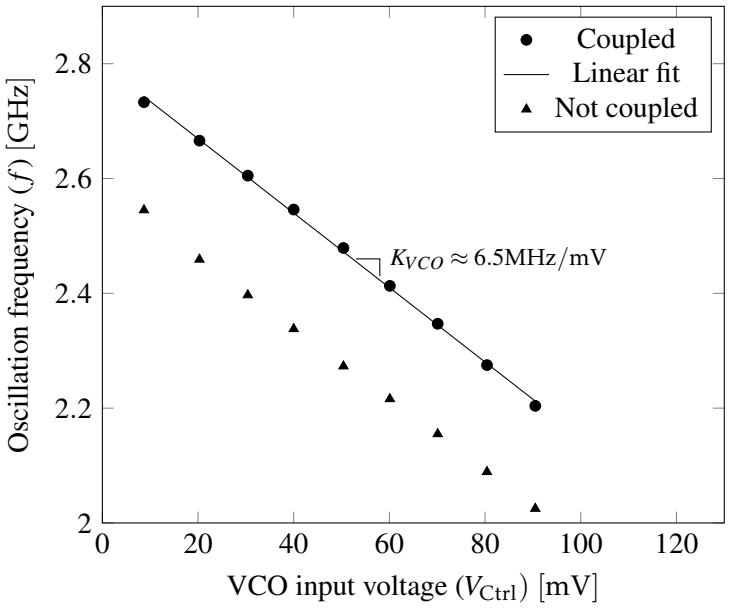

Figure 5.14: Frequency of oscillation with the oscillators uncoupled and coupled ($C_X = 20$fF).

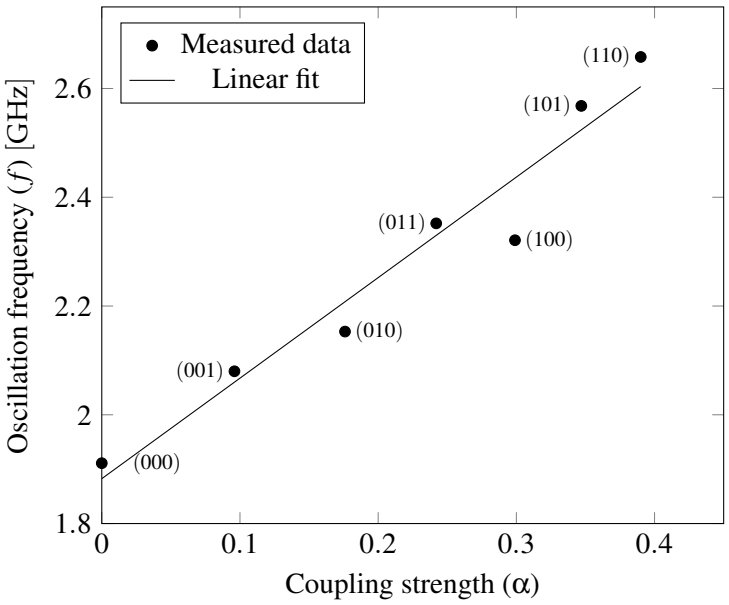

Figure 5.15: Relation between the oscillation frequency and the coupling strength.

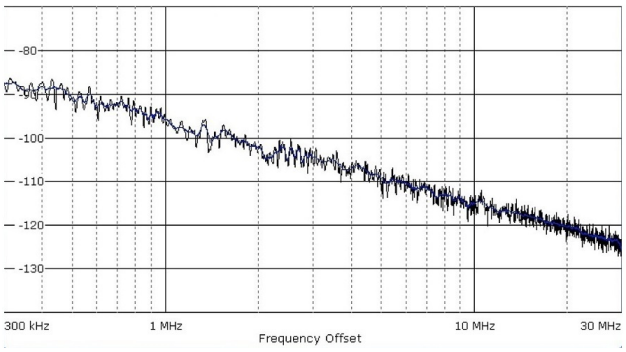

Figure 5.16: Measured phase noise.

The relation between the oscillation frequency and the coupling strength is shown in Fig. 5.15, where the dots are the measurement results and the 3-digit code, beside each dot, are the corresponding logic states of the switches (S_2, S_1, S_0). As expected, the oscillation frequency increases almost linearly with the coupling capacitance C_X and the amplitude of the output voltage decreases. However, note that the frequency increase is higher than expected due to the parasitic capacitances and low quality factor (below 1). Extracting the coupling capacitance value from the trend line (solid line) yields $C_X \approx 92$ fF. This indicates that the parasitics have a strong influence on the coupling capacitances.

The measured phase noise is -115.1 dBc/Hz @ 10 MHz, as shown in Fig. 5.16. To guarantee a nearly sinusoidal output, all the measurements were made with the power of the third harmonic 25 dB below that of the fundamental.

To compare this oscillator with others, with similar topology, we use the conventional FoM [59]:

Table 5.1: Comparison of state-of-the-art nearly sinusoidal $RC-$Oscillators with the same circuit topology.

Reference	Frequency [MHz]	PN@Δf [dBc/Hz]	Power dissipation [mW]	FoM [dBc/Hz]	IQ	Area [µm × µm]
[11]	920	-102@1MHz	9.9	-151.3	No	N/A
[9]	5000	-97.1@1MHz	54	-153.8	Yes	350×700
[60]	2290	-105@1MHz	54.72	-154.8	Yes	300×350
This work	2850	-115.1@10MHz	8.64	-154.8	Yes	160×130

$$\mathrm{FoM} = \mathrm{PN} + 10\log\left(\left(\frac{\Delta f}{f}\right)^2 \frac{P_{\mathrm{DC}}}{P_{\mathrm{ref}}}\right), \tag{5.87}$$

where PN is the phase noise, P_{DC} is the dissipated power in (mW), P_{ref} is the reference power (typically 1 mW), f is the oscillation frequency and Δf is the frequency offset.

Table 5.1 gives a comparison among the state-of-the-art quadrature $RC-$oscillators. A figure-of-merit (FoM) of -154.8 dBc/Hz is obtained for a power of 8.64 mW, which is the best performance for a QVCO with nearly sinusoidal output.

5.4 Conclusion

The capacitive cross-coupling of $RC-$oscillators was analyzed theoretically. Simulation and measurement results confirm that this coupling scheme is a viable solution to generate quadrature outputs. In comparison with active coupling schemes, it reduces the noise and power dissipation.

Several simulations using real MOS transistor models have been performed to validate the theory. Simulations, using SpectreRF, confirmed the inverse proportionality of the phase-error and amplitude mismatch to the coupling strength. A phase-error below 1% and an amplitude mismatch lower than 1% are obtained with the coupling capacitance about 20% of the oscillator's capacitance value.

Simulations also showed that, contrarily to the $LC-$oscillator, the crossed-coupled $RC-$oscillator has a low sensitivity of the phase-noise to the coupling strength. This means that, although the phase-error reduces substantially with the increase of the coupling strength, the phase-noise has a negligible variation (about 1 dB). Thus, the designer can focus on the reduction of the phase-error, because the penalty in the phase-noise is negligible.

A circuit prototype was designed, which has a phase-noise of -115.1 dBc/Hz @10 MHz (about 3 dB improvement in comparison with a single $RC-$oscillator). The increase of power is only marginal, leading to a FoM of -154.8 dBc/Hz. These results are consistent with the noiseless feature of the capacitive coupling and are comparable to the best state-of-the-art $RC-$oscillators in the GHz range, but with the lowest power consumption (about 9mW).

The proportionality between the oscillation frequency and the coupling strength was measured in a prototype with a variable capacitor array used in the coupling of two $RC-$oscillators. Although, in practice an increase of the oscillation frequency was observed, in theory there are two operation

modes; the second operation mode (in which the frequency decreases with the increase of the coupling strength) was not observed.

Finally, the theory presented led to the interesting result that the amplitude mismatch is related to the phase-error. This relation indicates that an automatic phase-error minimization circuit can be implemented, consisting of a feedback loop that measures the amplitude mismatch (using two peak detectors) and adjusts the oscillators' current sources until the amplitudes are matched. This will ensure a reduction of the phase-error.

CHAPTER 6

TWO-INTEGRATOR OSCILLATOR

Contents

6.1 Introduction

In previous chapters coupled $RC-$oscillators were analyzed. First the active coupling using transconductance amplifiers, in Chapter 4, and second the passive coupling using capacitors, in Chapter 5. The results show that these coupled oscillators are a viable solution to generate quadrature outputs with a phase error below 1°. However, the poor phase noise and bimodal oscillations are the main disadvantages. The oscillator presented in this chapter minimizes these disadvantages, while maintaining the advantages of the coupled oscillators.

In this chapter we analyze the two-integrator oscillator, which has a working principle fundamentally different from that of coupled oscillators. Although being an $RC-$oscillator (inductorless), it is a single-loop oscillator with inherent quadrature outputs. In comparison with $LC-$oscillators the phase noise of a two-integrator oscillator is worse. Yet it has better noise

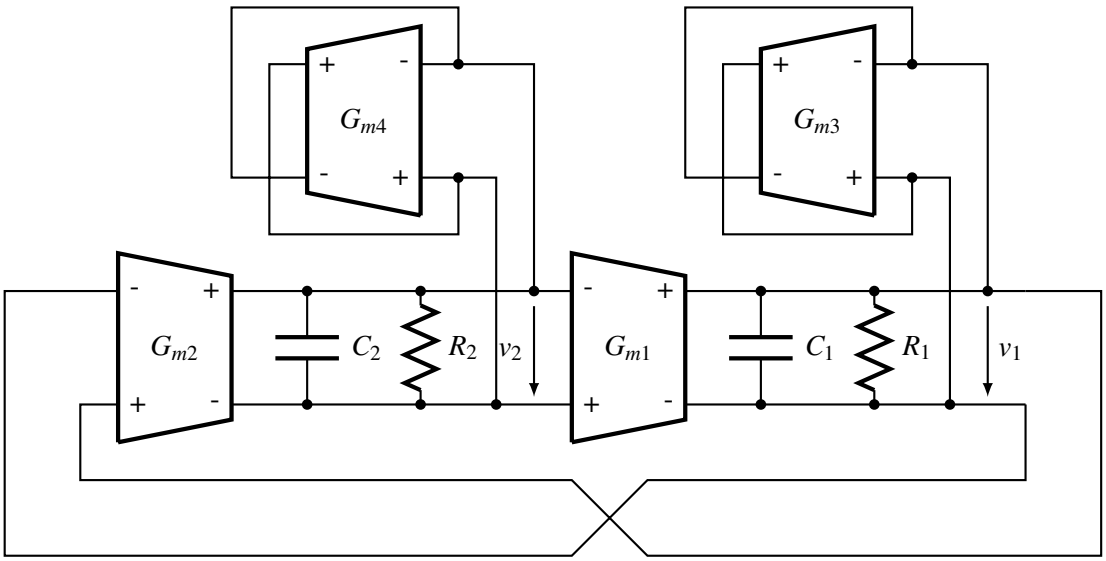

Figure 6.1: Conceptual model of the two integrator oscillator.

performance than the differential cross-coupled $RC-$oscillator [2]. Moreover, an important feature of this oscillator is its wide tuning range. This is important, because a wide tuning range quasi-sinusoidal quadrature voltage-controlled oscillator QVCO is a key block for fully integrated multiband and multistandard RF CMOS receivers. In comparison with using many narrow band receivers, a wideband receiver reduces the cost and increases the flexibility. With the widespread use of internet-of-things (IoT) the demand for receivers and, therefore, QVCOs for the ISMs radio bands, has been growing. To cope with this demand, a considerable research effort has been made towards the design of suitable QVCOs. Typically, a quadrature-error below 1° and a tuning range of one decade are required. Generating such accurate quadrature signals for this wide range of frequencies is challenging [1, 2, 3].

The two-integrator oscillator consists of a cascade of two integrators with the signal inversion in a feedback structure. Ideal integrators add a 90 degrees phase-shift each, generating the quadrature signals. However, real integrators are not ideal and this results in phase- and amplitude-errors. Although, the oscillator can work in both quasi-linear (outputs nearly sinusoidal) and strongly nonlinear (triangular waveform) regimes [2, 61]. We focus the study on the quasi-linear regime because sinusoidal oscillators are the aim of this research. The motivation and the main focus of the research are to determine the impact of the components mismatches on the frequency, and amplitude- and phase-errors. In [62] these errors were investigated without relating the results with the components mismatches. Here we go further, expanding the approach first presented in [63].

The chapter is organized as follows. In section 1, the oscillator conceptual model and a typical implementation of two-integrator oscillator are presented. The derivation of the incremental model follows. This model is derived using the VDPO approximation. The two integrator oscillator is reduced to two coupled parallel VDPOs. From the incremental model we derive the equations of the key parameters: frequency, amplitude and phase using the negative resistance model for the analysis. A brief explanation of the approach can be found in [2]. In section 2, the relation

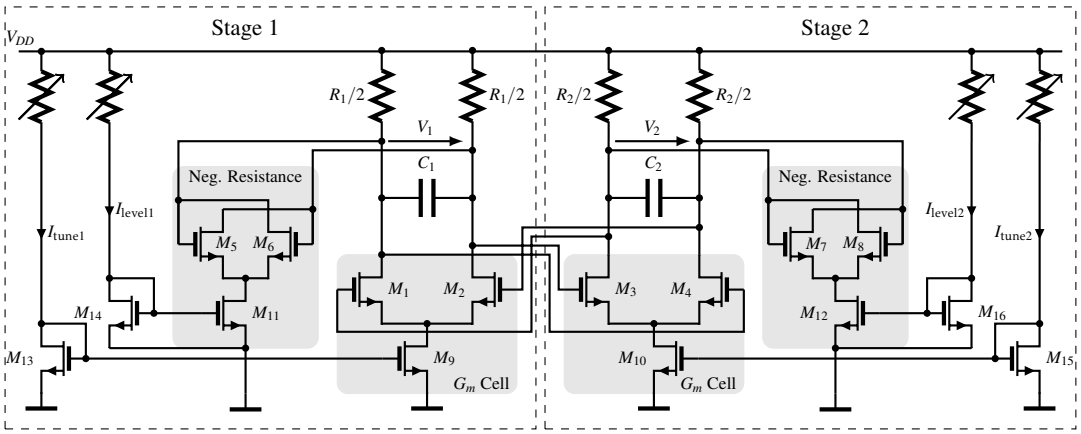

Figure 6.2: Two integrator oscillator.

between the Van der Pol parameters and the circuit implementation is derived. Section 3 presents the simulation results. Section 4 provides conclusions and a discussion on how to improve key parameters of the oscillator.

6.2 Quadrature oscillator

The conceptual model of two-integrator oscillator is shown in Fig. 6.1. It consists of two cascaded integrators with a signal inversion in the feedback path. Each integrator is implemented by a transconductance amplifier, G_{mi}, and a capacitance, C_i, $(i = 1, 2)$. The resistance R_i represent the losses which are compensated by the negative resistance circuits, implemented by transconductance amplifiers, G_{m3} and G_{m4}.

The circuit implementation of a two-integrator oscillator is shown in Fig. 6.2. The loop transconductance amplifiers are implemented by source-coupled differential pairs, $M_{1,2}$ and $M_{3,4}$. The negative resistance circuits are implemented by cross-coupled differential pairs, $M_{5,6}$ and $M_{7,8}$, connected in parallel with the capacitances C_1 and C_2, respectively. The resistances $R_1/2$ and the current mirror implemented by M_9 and M_{13} set the bias point of the first stage, and $R_2/2$, M_{10} and M_{15} set the bias point of the second stage.

A complete analysis of the circuit requires the inclusion of nonlinearities; they provide the amplitude limitation. The VDPO uses the nonlinearities for this purpose. Many modern oscillators including the one considered here may be represented by this equivalent model [27, 39]. The VDPO stability was extensively studied, which is another advantage in approximating the two-integrator oscillator by VDPO.

We consider that the transistors are the only elements in the circuit (Fig. 6.2) that have nonlinearities. We use for this purpose a Taylor expansion for the drain current equation.

6.2.1 Transconductance amplifier

A differential transconductance amplifier is implemented by a differential pair, as shown in Fig. 6.3(a). We assume that both transistors are in strong inversion and that the tail current source

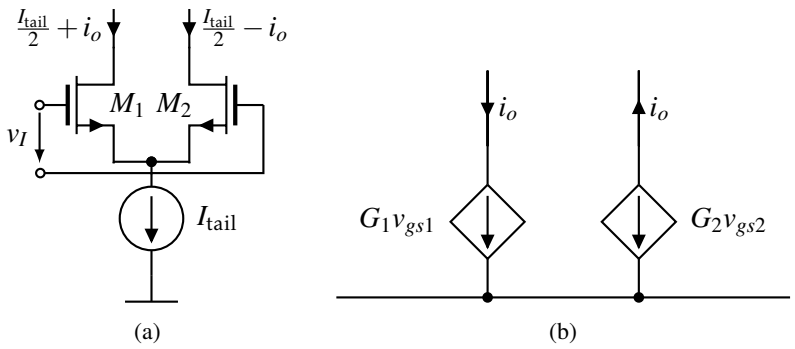

Figure 6.3: Fully differential transconductance amplifier circuit (a) and incremental model (b).

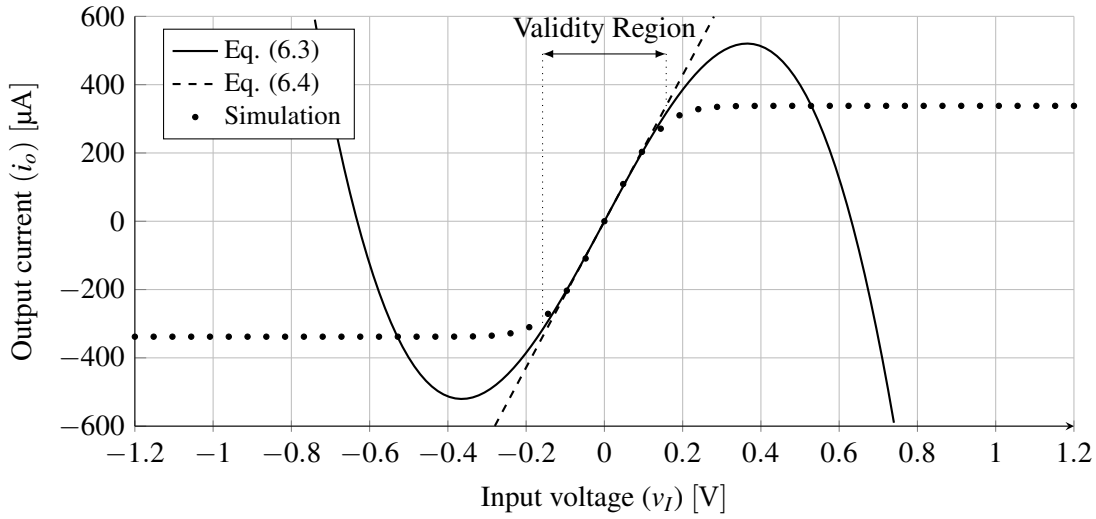

Figure 6.4: Output current of the transconductance amplifier as a function of the differential input voltage. Transistor dimensions of $W = 14.4$ µm, $L = 120$ nm, $I_{tail} = 676$ µA and $g_{m0} = 4.28$ mS.

is ideal.

For an ideal current source, only the differential-mode analysis is relevant. The incremental model of the differential pair is shown in Fig. 6.3(b). Here G_1 and G_2 are signal dependent transconductances (see Appendix A), that, for convenience, we refer from now on by large-signal tranconductances, of M_1 and M_2 respectively. Assuming, at this stage, that there is no mismatch and that the signal is antisymmetric, i.e. $v_{gs1} = -v_{gs2} = v_i/2$, we have antisymmetric signal dependent transconductances

$$\begin{cases} G_1 = g_{m0} + K\dfrac{v_i}{2} & \text{(6.1a)} \\ G_2 = g_{m0} - K\dfrac{v_i}{2} & \text{(6.1b)} \end{cases}$$

Applying the KCL to the circuit we obtain

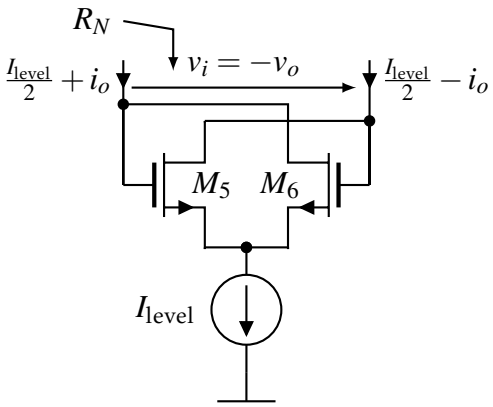

Figure 6.5: Negative resistance circuit.

$$\begin{cases} i_o = G_1 v_{gs1} & \text{(6.2a)} \\ i_o = -G_2 v_{gs2} & \text{(6.2b)} \\ v_i = v_{gs1} - v_{gs2} \quad . & \text{(6.2c)} \end{cases}$$

Substituting (6.2a) and (6.2b) into (6.2c), using the large-signal transconductances, given by (6.1a) and (6.1b), and solving the obtained equation with respect to the output current, i_o, we obtain the output current as a function of the input voltage:

$$i_o = \frac{G_1 G_2}{G_2 + G_1} v_i = \frac{g_{m0}}{2} v_i - \frac{K^2}{8 g_{m0}} v_i^3. \tag{6.3}$$

The second term on the right-hand side of (6.3) indicates a significant distortion for high amplitude input signals. However, for small amplitudes this term can be neglected, resulting in

$$i_o \approx \frac{g_{m0}}{2} v_i. \tag{6.4}$$

Thus, for small amplitude the response is almost linear, as shown in Fig. 6.4. The figure shows a comparison between the theory and simulation using transistors models of a standard CMOS technology. Note that, if $i_o = I_{\text{tail}}/2$ then transistor M_1 is in strong inversion but M_2 is in cutoff. Conversely, if $i_o = -I_{\text{tail}}/2$ then transistor M_2 is in strong inversion but M_1 is in cutoff. Equations (6.3) and (6.4) are valid for $|v_i| < I_{\text{tail}}/g_{m0}$. This validity region is indicated at the top of Fig. 6.4.

6.2.2 Negative resistance circuit

A transconductance amplifier with the output cross-connected to the input (Fig. 6.5), behaves as a negative resistance. As in Section 6.2.1, only the differential-mode analysis is relevant.

The equivalent resistance looking into the drains of M_5 and M_6, is given by the ratio between the output voltage, v_o, and the output current, i. The output current is the negative of that given by (6.3), therefore, the resistance R_{N} is given by

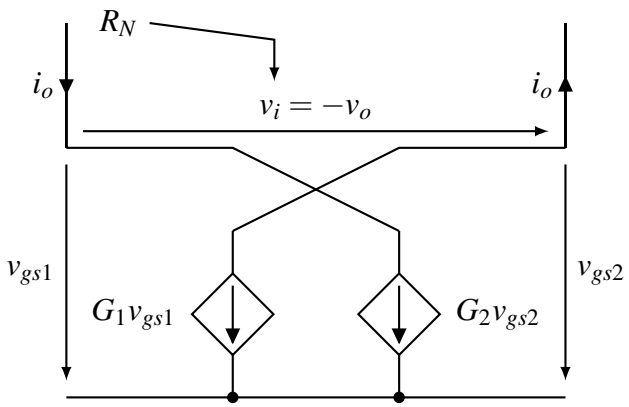

Figure 6.6: Negative resistance equivalent circuit.

$$R_N = \frac{v_o}{i_o} = -\frac{1}{\frac{g_{m0}}{2} - \frac{K^2}{8g_{m0}} v_o^2}. \tag{6.5}$$

Equation (6.5) shows that the circuit of Fig. 6.5 is equivalent to a negative resistance in parallel with a positive nonlinear resistance. The latter, as we will see, is responsible for the amplitude limitation.

6.2.3 Incremental model

If the transconductance amplifiers, G_{m1} and G_{m2}, operate in the linear region, the two-integrator oscillator works linearly. However, the transconductance amplifiers of the negative resistance circuits, G_{m3} and G_{m4}, should work in a nonlinear region to limit the amplitude. Hence, for large-signal operation each stage of the circuit in Fig. 6.2 should be modelled by a parallel $RC-$circuit in parallel with a nonlinear resistance, to limit the amplitude, a negative resistance to compensate the losses, and a dependent current source to represents the transconductance amplifier. The overall oscillator circuit is modelled by two coupled parallel $RC-$circuits (Fig. 6.7). The signal inversion is indicated by a negative transconductance in the second stage.

By applying KCL to the circuit of Fig. 6.7, we obtain, for the circuit dynamics, the system of equations:

$$\begin{cases} C_1 \dfrac{\mathrm{d}v_1}{\mathrm{d}t} + \dfrac{1}{R_1} v_1 + \dfrac{1}{R_{\mathrm{N1}}} v_1 + \dfrac{g_{m1}}{2} v_2 = 0 & \text{(6.6a)} \\ C_2 \dfrac{\mathrm{d}v_2}{\mathrm{d}t} + \dfrac{1}{R_2} v_2 + \dfrac{1}{R_{\mathrm{N2}}} v_2 - \dfrac{g_{m2}}{2} v_1 = 0. & \text{(6.6b)} \end{cases}$$

Dividing these equations by the capacitances, C_1 and C_2, and differentiating both sides we obtain

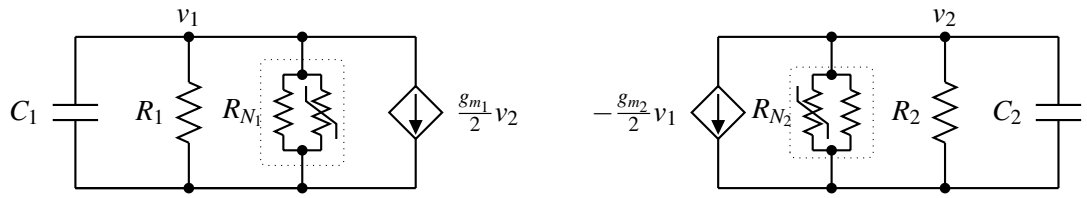

Figure 6.7: Two integrator small-signal equivalent circuit model.

$$\begin{cases} \dfrac{\mathrm{d}^2 v_1}{\mathrm{d}t^2} + \dfrac{1}{C_1}\left[\left(R_1^{-1} - \dfrac{g_{m0}}{2}\right) + \dfrac{3K^2}{8g_{m0}}v_1^2\right]\dfrac{\mathrm{d}v_1}{\mathrm{d}t} + \dfrac{g_{m1}}{2C_1}\dfrac{\mathrm{d}v_2}{\mathrm{d}t} = 0, & \text{(6.7a)} \\ \dfrac{\mathrm{d}^2 v_2}{\mathrm{d}t^2} + \dfrac{1}{C_2}\left[\left(R_2^{-1} - \dfrac{g_{m0}}{2}\right) + \dfrac{3K^2}{8g_{m0}}v_2^2\right]\dfrac{\mathrm{d}v_2}{\mathrm{d}t} - \dfrac{g_{m2}}{2C_2}\dfrac{\mathrm{d}v_1}{\mathrm{d}t} = 0. & \text{(6.7b)} \end{cases}$$

Notice that the damping terms in (6.7a) and (6.7b) are similar to the damping term of the VDPO. Although each stage cannot oscillate by itself, equations (6.7a) and (6.7b) are a system of Van der Pol equations, and the resulting oscillator is able to oscillate.

6.2.4 Oscillator without mismatches

Now we derive the equations of the key parameters: frequency, amplitude, and phase. They are derived for the steady-state assuming no mismatches between the stages. Moreover, to understand how the circuit reaches the steady-state we do a stability analysis by deriving the phase-space paths. Rewriting (6.7) in the Van der Pol form yields

$$\begin{cases} \dfrac{\mathrm{d}^2 v_1}{\mathrm{d}t^2} + \omega_0^2 v_1 = \omega_0^2 v_1 + 2\left(\delta_0 - \delta_2 v_1^2\right)\dfrac{\mathrm{d}v_1}{\mathrm{d}t} - \alpha_1\dfrac{\mathrm{d}v_2}{\mathrm{d}t} & \text{(6.8a)} \\ \dfrac{\mathrm{d}^2 v_2}{\mathrm{d}t^2} + \omega_0^2 v_2 = \omega_0^2 v_2 + 2\left(\gamma_0 - \gamma_2 v_2^2\right)\dfrac{\mathrm{d}v_2}{\mathrm{d}t} + \alpha_2\dfrac{\mathrm{d}v_1}{\mathrm{d}t} & \text{(6.8b)} \end{cases}$$

where ω_0 is the oscillation frequency, $\alpha_i = g_{mi}/(2C_i)$ for the i-th stage coupling factor. Other values are VDP parameters of the first stage

$$\delta_0 = \frac{\frac{1}{2}g_{m0} - R_1^{-1}}{2C_1}, \qquad \delta_2 = \frac{3K^2}{2C_1 8g_{m0}}, \tag{6.9}$$

and the second stage

$$\gamma_0 = \frac{\frac{1}{2}g_{m_0} - R_2^{-1}}{2C_2}, \qquad \gamma_2 = \frac{3K^2}{2C_2 8g_{m0}}. \tag{6.10}$$

For the sinusoidal regime, the solution of (6.8) is of the form

$$v_i = V_i \sin\left(\omega_0 t - \phi_i\right). \tag{6.11}$$

where V_i is the amplitude of the i-th stage and ϕ_i is the phase. Using the harmonic balance method [56], the amplitude and phase transient equations are

$$\begin{cases} \dfrac{dV_1}{dt} = \delta_0 V_1 - \dfrac{\delta_2 V_1^3}{4} - \dfrac{\alpha_1 V_2}{2}\cos\Delta\phi & (6.12a) \\ \dfrac{dV_2}{dt} = \gamma_0 V_2 - \dfrac{\gamma_2 V_2^3}{4} + \dfrac{\alpha_2 V_1}{2}\cos\Delta\phi & (6.12b) \\ \dfrac{d\phi_1}{dt} = \dfrac{\omega_0}{2} - \alpha_1 \dfrac{V_2}{2V_1}\sin\Delta\phi & (6.12c) \\ \dfrac{d\phi_2}{dt} = \dfrac{\omega_0}{2} - \alpha_2 \dfrac{V_1}{2V_2}\sin\Delta\phi. & (6.12d) \end{cases}$$

where $\Delta\phi = \phi_2 - \phi_1$ represents the outputs phase difference.

Simplifying the system (6.12) assuming no mismatches between the stages, i.e. $\alpha_1 = \alpha_2 = \alpha$, $\delta_0 = \gamma_0$, and $\delta_2 = \gamma_2$, we obtain

$$\begin{cases} \dfrac{dV_1}{dt} = \delta_0 V_1 - \dfrac{1}{4}\delta_2 V_1^3 - \dfrac{\alpha}{2} V_2 \cos\Delta\phi & (6.13a) \\ \dfrac{dV_2}{dt} = \delta_0 V_2 - \dfrac{1}{4}\delta_2 V_2^3 + \dfrac{\alpha}{2} V_1 \cos\Delta\phi. & (6.13b) \\ \dfrac{d\phi_1}{dt} = \dfrac{\omega_0}{2} - \alpha \dfrac{V_2}{2V_1}\sin\Delta\phi & (6.13c) \\ \dfrac{d\phi_2}{dt} = \dfrac{\omega_0}{2} - \alpha \dfrac{V_1}{2V_2}\sin\Delta\phi. & (6.13d) \end{cases}$$

To determine the equilibrium points we fist subtract (6.13c) from (6.13d) to obtain

$$\frac{d\Delta\phi}{dt} = \frac{d\phi_2}{dt} - \frac{d\phi_1}{dt} = -\frac{\alpha}{2}\left(\frac{V_1}{V_2} - \frac{V_2}{V_1}\right)\sin\Delta\phi. \tag{6.14}$$

Note that in steady-state $d\Delta\phi/dt = 0$. Thus, from (6.14), for the steady-state, we obtain

$$-\frac{\alpha}{2}\left(\frac{V_1}{V_2} - \frac{V_2}{V_1}\right)\sin\Delta\phi = 0. \tag{6.15}$$

We multiply both sides of (6.15) by V_1 and V_2, to avoid the indeterminate form $0/0$, resulting in

$$-\frac{\alpha}{2}\left(V_1^2 - V_2^2\right)\sin\Delta\phi = 0. \tag{6.16}$$

From (6.16) it is clear that equilibrium points exists for $V_1 = V_2$ and for $\Delta\phi = \pm\pi$. Applying these criteria to (6.13a) and (6.13b) we conclude that an equilibrium point, E_0, exists at $V_1 = V_2 = 0$. Moreover, note that the third term on the right-hand sides of both (6.13a) and (6.13b) have opposite signs. Hence, $\Delta\phi = \pm\pi/2$ and $V_1 = V_2$ also satisfies both equations. This leads us to the second equilibrium point: $E_1 = (V_{osc}, V_{osc}, \pi/2)$.

The equilibrium point E_0 has little interest because the oscillation amplitude is zero. We will derive the oscillation key parameters for the second equilibrium point, E_1. We assume equal output voltages, $V_1 = V_2 = V_{osc}$, and quadrature outputs $\Delta\phi = \pi/2$. From (6.13a), or from (6.13b), we obtain the oscillation amplitude:

$$V_{\text{osc}} = 2\sqrt{\frac{\delta_0}{\delta_2}} = \frac{8I_{\text{level}}}{\sqrt{3}g_{m0}}\sqrt{\frac{Rg_{m0}-2}{Rg_{m0}}}. \tag{6.17}$$

The oscillation frequency is obtained by adding (6.13c) and (6.13d):

$$\omega_0 = \alpha = \frac{g_m}{2C}. \tag{6.18}$$

6.2.5 Stability of the equilibrium points

To understand how the circuit reaches the steady-state we do the stability analysis. In the previous section we assume equal amplitudes and perfect quadrature since there are no mismatches between the stages. In this section we will prove that this assumption is correct.

The voltage of the $i-$th stage is given by (6.11). For $t = 0$ the voltage of the first stage is given by

$$v_1(0) = V_1 \sin(-\phi_i). \tag{6.19}$$

Note that the amplitude is not defined only by the initial conditions of the capacitance. Differentiating v_1 and dividing by ω we obtain

$$\frac{1}{\omega}\frac{\mathrm{d}v_1}{\mathrm{d}t}\bigg|_{t=0} = V_1 \cos(-\phi_i). \tag{6.20}$$

Note that the left-hand side of (6.20) is related to the current of the capacitance C. Thus, using $\omega = \alpha = g_m/(2C)$ in (6.20) we obtain

$$\frac{2}{g_m}C\frac{\mathrm{d}v_1}{\mathrm{d}t}\bigg|_{t=0} = \frac{i_c}{g_m/2} = V_1 \cos(-\phi_i). \tag{6.21}$$

The capacitance current, i_c, is related to the output current of the transconductance amplifier, i_1, plus the currents in the resistance, R, and in the negative resistance, R_N. To ease the problem, we assume that the negative resistance cancels R resulting

$$i_c \approx i_1 = (g_m/2)v_2. \tag{6.22}$$

Substituting (6.22) into (6.21) result in

$$v_2(0) = V_1 \cos(-\phi_i). \tag{6.23}$$

Combining (6.19) and (6.23), and solving with respect to the amplitude and phase we obtain

$$V_1 = \sqrt{v_1^2(0) + v_2^2(0)}, \tag{6.24}$$

and

$$\phi_1 = -\operatorname{atan}\left(\frac{v_1(0)}{v_2(0)}\right). \tag{6.25}$$

Similarly, for the second stage, we obtain

$$V_2 = \sqrt{v_1^2(0) + v_2^2(0)}, \tag{6.26}$$

and

$$\phi_2 = \operatorname{atan}\left(\frac{v_2(0)}{v_1(0)}\right). \tag{6.27}$$

From (6.24) and (6.26) we conclude that the amplitudes are equal, i.e. $V_1 = V_2 = V$. For the phase difference we combine (6.25) and (6.27) and use the mathematical identity $(\operatorname{atan}(x) + \operatorname{atan}(1/x) = \pi/2$ resulting

$$\Delta\phi = \phi_2 - \phi_1 = \operatorname{atan}\left(\frac{v_1(0)}{v_2(0)}\right) + \operatorname{atan}\left(\frac{v_2(0)}{v_1(0)}\right) = \frac{\pi}{2}. \tag{6.28}$$

Simplifying the system (6.13) by combining (6.13c) and (6.13d) and using $V_1 = V_2 = V$ and $\Delta\phi = \pi/2$, we obtain

$$\begin{cases} \dfrac{\mathrm{d}V}{\mathrm{d}t} = \delta_0 V - \dfrac{1}{4}\delta_2 V^3 & \text{(6.29a)} \\ \dfrac{\mathrm{d}\Delta\phi}{\mathrm{d}t} = 0. & \text{(6.29b)} \end{cases}$$

The system (6.29) is equivalent to the system obtained for the VDPO already solved in Chapter 2, Section 2.3.1. Thus, we conclude that the equilibrium point $E_0 = (0, 0, \Delta\phi)$ is unstable and the equilibrium point $E_1 = (V_{\text{osc}}, V_{\text{osc}}, \pi/2)$ is stable.

6.2.6 Oscillator with mismatches

Now we determine the impact of the components mismatched on the key parameters of the oscillator. We obtain first the steady-state solutions (equilibrium points) of the system (6.12). They are calculated by equating all derivatives to zero (i.e. $\mathrm{d}V_{o1}/\mathrm{d}t = \mathrm{d}V_{o2}/\mathrm{d}t = 0$ and $\mathrm{d}\phi_1/\mathrm{d}t = \mathrm{d}\phi_2/\mathrm{d}t = 0$). This gives

$$\begin{cases} \delta_0 - \dfrac{\delta_2 V_1^2}{4} - \dfrac{\alpha_1}{2}\dfrac{V_2}{V_1}\cos(\Delta\phi) = 0 & \text{(6.30a)} \\ \gamma_0 - \dfrac{\gamma_2 V_2^2}{4} + \dfrac{\alpha_2}{2}\dfrac{V_1}{V_2}\cos(\Delta\phi) = 0 & \text{(6.30b)} \\ \dfrac{\omega_0}{2} - \dfrac{\alpha_1}{2}\dfrac{V_2}{V_1}\sin(\Delta\phi) = 0 & \text{(6.30c)} \\ \dfrac{\omega_0}{2} - \dfrac{\alpha_2}{2}\dfrac{V_1}{V_2}\sin(\Delta\phi) = 0 & \text{(6.30d)} \end{cases}$$

We obtain equations (6.31a) and (6.31b) by adding and subtracting, respectively, (6.30a) and (6.30b). Similarly, equations (6.31c) and (6.31d) are obtained by subtracting and adding, respectively, (6.30c) and (6.30d):

$$\begin{cases} \delta_0+\gamma_0-\dfrac{\delta_2V_1^2+\gamma_2V_2^2}{4}=\dfrac{1}{4}\left(\alpha_1\dfrac{V_2}{V_1}-\alpha_2\dfrac{V_1}{V_2}\right)\cos(\Delta\phi) & (6.31a)\\ \delta_0-\gamma_0-\dfrac{\delta_2V_1^2-\gamma_2V_2^2}{4}=\dfrac{1}{4}\left(\alpha_1\dfrac{V_2}{V_1}+\alpha_2\dfrac{V_1}{V_2}\right)\cos(\Delta\phi) & (6.31b)\\ \left(\alpha_2\dfrac{V_1}{4V_2}-\alpha_1\dfrac{V_2}{4V_1}\right)\sin(-\Delta\phi)=0. & (6.31c)\\ \omega_0=\left(\alpha_1\dfrac{V_2}{4V_1}+\alpha_2\dfrac{V_1}{4V_2}\right)\sin(\Delta\phi). & (6.31d) \end{cases}$$

Assuming that the outputs are near quadrature, i.e. $\Delta\phi\approx\pm\pi/2$, and using the approximation $(\sin\Delta\phi\approx 1)$ one reduces (6.31c) to

$$\frac{1}{2}\left(\alpha_2\frac{V_1}{V_2}-\alpha_1\frac{V_2}{V_1}\right)=0, \tag{6.32}$$

This leads us to the conclusion that the relationship between amplitudes is given by

$$V_1=\sqrt{\frac{\alpha_1}{\alpha_2}}V_2=\sqrt{\frac{g_{m1}C_2}{g_{m2}C_1}}V_2. \tag{6.33}$$

A simplified equation for the oscillation frequency can be obtained substituting (6.33) into (6.31) and assuming again nearly quadrature outputs, i.e. $\Delta\phi\approx\pi/2$. This result in

$$\omega_0\approx\frac{1}{2}\sqrt{\alpha_1\alpha_2}=\frac{1}{2}\sqrt{\frac{g_{m1}g_{m2}}{C_1C_2}}, \tag{6.34}$$

Substituting $g_{m1}=g_m(1-\Delta g_m/(2g_m))$, $g_{m2}=g_m(1+\Delta g_m/(2g_m))$, $C_1=C(1-\Delta C/(2C))$, and $C_2=C(1+\Delta C/(2C))$ into the right-hand side of (6.34) gives

$$\omega_0\approx\frac{g_m}{2C}\sqrt{\frac{1-\left(\frac{\Delta g_m}{2g_m}\right)^2}{1-\left(\frac{\Delta C}{2C}\right)^2}}, \tag{6.35}$$

where $\Delta g_m=g_{m2}-g_{m1}$ and $\Delta C=C_2-C_1$. For small mismatches, $\left(\frac{\Delta g_m}{2g_m}\right)^2\ll 1$ and $\left(\frac{\Delta C}{2C}\right)^2\ll 1$, (6.35) becomes the well–known frequency equation:

$$\omega_0\approx\frac{g_m}{2C}. \tag{6.36}$$

To derive the amplitude mismatch we use the definition

$$\varepsilon_A=2\frac{V_2-V_1}{V_2+V_1}=2\frac{1-\sqrt{\frac{\alpha_1}{\alpha_2}}}{1+\sqrt{\frac{\alpha_1}{\alpha_2}}}. \tag{6.37}$$

If the coupling factors, α_i, in (6.37) are equal, it is clear that a perfect amplitude match can be obtained. Using in (6.37) the coupling factors $\alpha_i = g_{mi}/(2C_i)$ and the circuit parameters as function of the mismatches and rearranging the terms we obtain

$$\varepsilon_A = 2\frac{\sqrt{1+\frac{\Delta g_m}{2g_m}-\frac{\Delta C}{2C}-\frac{\Delta g_m}{2g_m}\frac{\Delta C}{2C}}-\sqrt{1-\frac{\Delta g_m}{2g_m}+\frac{\Delta C}{2C}-\frac{\Delta g_m}{2g_m}\frac{\Delta C}{2C}}}{\sqrt{1+\frac{\Delta g_m}{2g_m}-\frac{\Delta C}{2C}-\frac{\Delta g_m}{2g_m}\frac{\Delta C}{2C}}+\sqrt{1-\frac{\Delta g_m}{2g_m}+\frac{\Delta C}{2C}-\frac{\Delta g_m}{2g_m}\frac{\Delta C}{2C}}}. \tag{6.38}$$

If the mismatches are small the terms $\left(\frac{\Delta g_m}{2g_m}\frac{\Delta C}{2C}\right)$ in (6.38) can be neglected. Moreover, using the mathematical approximation $\left(\sqrt{1\pm x}\approx 1\pm x/2 \text{ for } |x|\ll 1\right)$ one find that

$$\varepsilon_A \approx \frac{1}{2}\left[\left(\frac{\Delta g_m}{g_m}\right)-\left(\frac{\Delta C}{C}\right)\right], \tag{6.39}$$

From (6.39), it is clear that the amplitude mismatch depends only on the transconductance and capacitance mismatches. The capacitance mismatches can be minimized by a careful layout, but cannot be fully eliminated. The transconductances mismatches can be controlled by adjusting the tail currents of the source–coupled pairs. Controlling each transconductance independently so that the transconductance mismatch be equal to the capacitance mismatch, results in a perfect amplitude matching, i.e. $\varepsilon_A = 0$.

The amplitude without mismatch is given by the well-known VDPO amplitude equation. It can be obtained from (6.30a) resulting in

$$V_{\text{osc}} = 2\sqrt{\frac{\delta_0}{\delta_2}} = \frac{4}{\sqrt{3}K}\sqrt{\frac{g_{m0}}{R}(Rg_{m0}-2)} = \frac{8I_{level}}{\sqrt{3}g_{m0}}\sqrt{\frac{Rg_{m0}-2}{Rg_{m0}}}. \tag{6.40}$$

where I_{level} is the tail current of the negative-resistance circuit. The amplitude of each stage is given by

$$V_1 = V_{\text{osc}}\left(1-\frac{1}{2}\varepsilon_A\right) = \frac{2I_{\text{level}}}{\sqrt{3}g_{m0}}\sqrt{\frac{Rg_{m0}-2}{Rg_{m0}}}\left[4-\left(\frac{\Delta g_m}{g_m}\right)+\left(\frac{\Delta C}{C}\right)\right]. \tag{6.41}$$

and

$$V_2 = V_{\text{osc}}\left(1+\frac{1}{2}\varepsilon_A\right) = \frac{2I_{\text{level}}}{3\sqrt{3}g_{m0}^2}\sqrt{\frac{Rg_{m0}-2}{Rg_{m0}}}\left[4+\left(\frac{\Delta g_m}{g_m}\right)-\left(\frac{\Delta C}{C}\right)\right]. \tag{6.42}$$

As will be shown next the amplitude match reduces the phase error.

To derive the phase-error, we divide (6.31d) by (6.31b). This gives us

$$\tan(\Delta\phi) = \frac{\omega_0}{(\delta_0-\gamma_0)-\frac{\delta_2V_1^2-\gamma_2V_2^2}{4}}. \tag{6.43}$$

To obtain from (6.43) the phase error, ε_ϕ, we relate the phase difference to the phase error as $\Delta\phi = \pi/2-\varepsilon_\phi$. Then, using the trigonometric identity $\tan\Delta\phi = \cot\varepsilon_\phi$ we obtain

$$\tan(\varepsilon_\phi) = \frac{1}{\cot\varepsilon_\phi} = \frac{4(\delta_0-\gamma_0)-\left(\delta_2V_1^2-\gamma_2V_2^2\right)}{4\omega_0}. \tag{6.44}$$

For small mismatches, $\varepsilon_\phi \ll \pi/2$, the Taylor series approximation gives

$$\varepsilon_\phi \approx \frac{4(\delta_0-\gamma_0)-(\delta_2 V_1^2-\gamma_2 V_2^2)}{4\omega_0}. \tag{6.45}$$

From the definition of VDP parameters, (6.9) and (6.10), it follows that

$$\delta_0-\gamma_0=\frac{g_{m0}R_1-2}{4R_1C_1}-\frac{g_{m0}R_2-2}{4R_2C_2} \tag{6.46}$$

Substituting $R_1=R(1-\Delta R/(2R))$, $R_2=R(1+\Delta R/(2R))$, $C_1=C(1-\Delta C/(2C))$, and $C_2=C(1+\Delta C/(2C))$ into (6.46) and rearranging the terms we obtain

$$\delta_0-\gamma_0=\frac{-2RC\left(\frac{\Delta R}{R}+\frac{\Delta C}{C}\right)+g_{m0}R^2C\left(\frac{\Delta C}{C}\right)}{4R^2C^2\left[1-\left(\frac{\Delta R}{2R}\right)^2\right]\left[1+\left(\frac{\Delta C}{2C}\right)^2\right]}. \tag{6.47}$$

where $\Delta R=R_2-R_1$ and $\Delta C=C_2-C_1$. Assuming small mismatches, equation (6.47) can be reduced to

$$\delta_0-\gamma_0\approx-\frac{2\left(\frac{\Delta R}{R}\right)-(g_{m0}R-2)\left(\frac{\Delta C}{C}\right)}{4RC}. \tag{6.48}$$

Now, substituting the VDP parameters, (6.9) and (6.10), in the second term of (6.48), $\delta_2V_1^2-\gamma_2V_2^2$, result in

$$\delta_2V_1^2-\gamma_2V_2^2=\frac{3K^2}{16g_{m0}}\left(\frac{V_1^2}{C_1}-\frac{V_2^2}{C_2}\right) \tag{6.49}$$

Using again $R_1=R(1-\Delta R/(2R))$, $R_2=R(1+\Delta R/(2R))$, $C_1=C(1-\Delta C/(2C))$, and $C_2=C(1+\Delta C/(2C))$ in (6.49) and rearranging the terms we obtain

$$\delta_2V_1^2-\gamma_2V_2^2=\frac{3K^2}{16g_{m0}}\frac{\left(V_1^2-V_2^2\right)+\left(\frac{\Delta C}{2C}\right)\left(V_1^2+V_2^2\right)}{C\left[1-\left(\frac{\Delta C}{2C}\right)^2\right]} \tag{6.50}$$

Now we substitute $V_1=V_{\rm osc}(1-\varepsilon_A/2)$ and $V_2=V_{\rm osc}(1+\varepsilon_A/2)$ into (6.50). Assuming $\left(\frac{\Delta C}{2C}\right)^2\ll 1$ the result is

$$\delta_2V_1^2-\gamma_2V_2^2\approx\frac{3K^2}{16g_{m0}C}V_{\rm osc}^2\left(\frac{\Delta C}{C}-2\varepsilon_A\right). \tag{6.51}$$

Further, substituting (6.39), and (6.40) into (6.51) gives us

$$\delta_2V_1^2-\gamma_2V_2^2\approx 2\frac{Rg_{m0}-2}{RC}\left[2\frac{\Delta C}{C}-\left(\frac{\Delta g_m}{g_m}\right)\right]. \tag{6.52}$$

Finally, substituting (6.36), (6.47), and (6.52) into (6.45) one obtains

$$\varepsilon_\phi\approx-\left[\left(\frac{\Delta R}{R}\right)+\left(\frac{\Delta C}{C}-\frac{\Delta g_m}{g_m}\right)\frac{(Rg_{m0}-2)}{2}\right]\frac{1}{Rg_m}. \tag{6.53}$$

Equation (6.53) gives an interesting insight: one can reduce the quadrature phase error by increasing the amplifier gain and, also, by equalizing the capacitance and the amplifiers

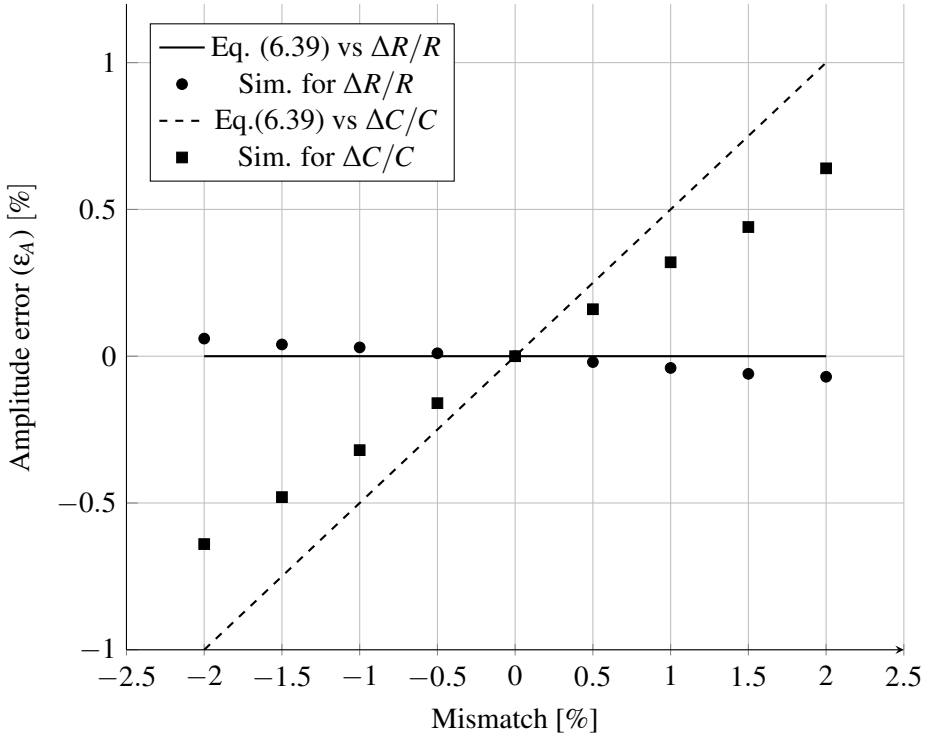

Figure 6.8: Impact of the resistance mismatches on the amplitude error.

transconductance mismatches. Moreover, if an imbalance between the capacitances and transconductances mismatches compensate the resistances mismatch, a zero phase-error is obtained. Note that the units in (6.53) are radians. To obtain the result in degrees, we multiply (6.53) by $180/\pi$. This gives

$$\varepsilon_\phi \approx -\frac{180}{\pi}\left[\left(\frac{\Delta R}{R}\right)+\left(\frac{\Delta C}{C}-\frac{\Delta g_m}{g_m}\right)\frac{(Rg_{m0}-2)}{2}\right]\frac{1}{Rg_m}. \tag{6.54}$$

6.3 Simulation results

The circuit shown in Fig. 6.2 was simulated using the parameters of 130 nm standard CMOS technology. The oscillation frequency is 2.4 GHz. The circuit parameters are $C_1 = C_2 = C$=77 fF, $R_1 = R_2 = R = 600\ \Omega$, (W/L)=115.2 µm/120 nm for transistors M_1, M_2, M_5, and M_6, (W/L)=14.4 µm/120 nm for M_3, M_4, M_7 and M_8, I_{level}= 0.8 mA, I=2 mA, and the supply voltage is 1.2 V. The voltage and current sources are assumed to be ideal.

To validate (6.39) we run several simulations with $\frac{\Delta C}{C} = 0$ and $\frac{\Delta g_m}{g_m} = 0$, and sweep the resistance mismatch ΔR from -2% to $+2\%$. The results show that indeed the resistance mismatches have only 0.1% as maximum contribution to the amplitude error (Fig. 6.8). Thus, the impact of the resistance mismatch on the amplitude error is negligible.

To validate the amplitude mismatch given by (6.39), several simulations were made varying the mismatches between the capacitances, C_1 and C_2. The results show that these mismatches have less

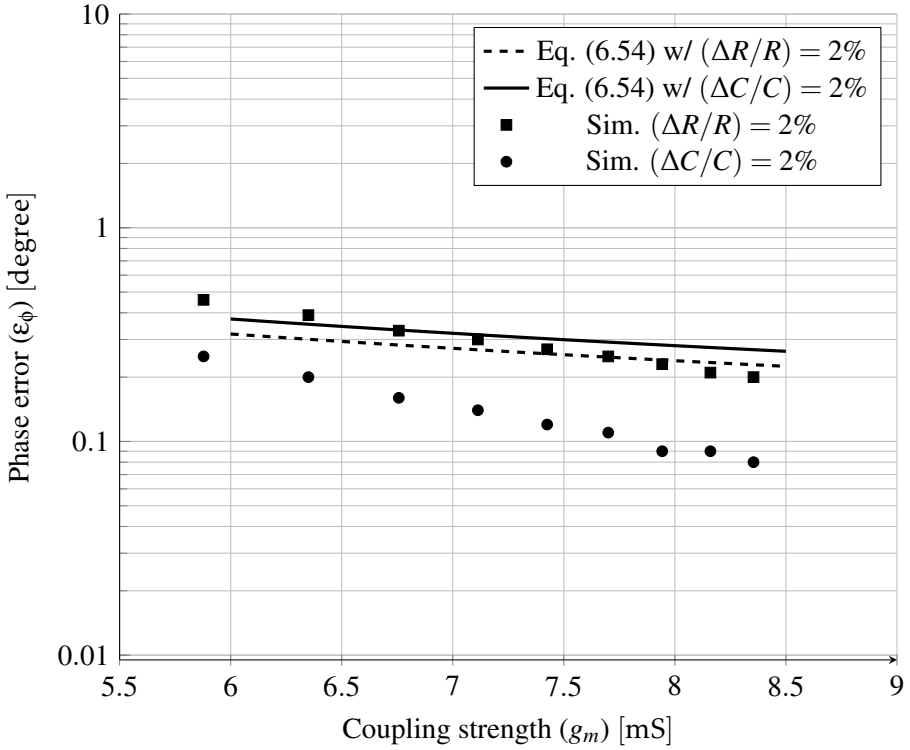

Figure 6.9: Phase error as function of transconductance.

impact on the quadrature error. However, they have a significant impact on the amplitude mismatch, as shown in Fig. 6.8. The deviation between simulation and analytical results are explained by the nonlinearities of the transistors capacitances and the parasitic capacitances.

The phase error (6.54) was also validated by simulation. First, we simulate the circuit with matched capacitances and a sweep of the resistance mismatches. The results show a small discrepancy between simulation data and the theory, as shown in Fig. 6.9. However, with the increase of the transconductance the phase error decreases. In the second simulation the resistance mismatch is zero and the capacitance mismatch is 2%. Again, the phase error decreases with the increase of the amplifiers transconductances, which is in line with the trend indicated by equation (6.54).

To determine the impact of the amplifier's gain, g_m, on the phase-error and phase-noise, the circuit was simulated with a constant component mismatch of 2% and increasing g_m. Two results are shown in Fig. 6.10 where the phase noise, at the offset of 10 MHz, is represented by white circles. The results show that the phase error is reduced when g_m increases, which is in agreement with the trend described by (6.54). To compensate the frequency shift, capacitor C was adjusted in each simulation to maintain the oscillation frequency close to 2.4 GHz.

To compare this oscillator with other works, we use the conventional figure-of-merit (FoM) [59]:

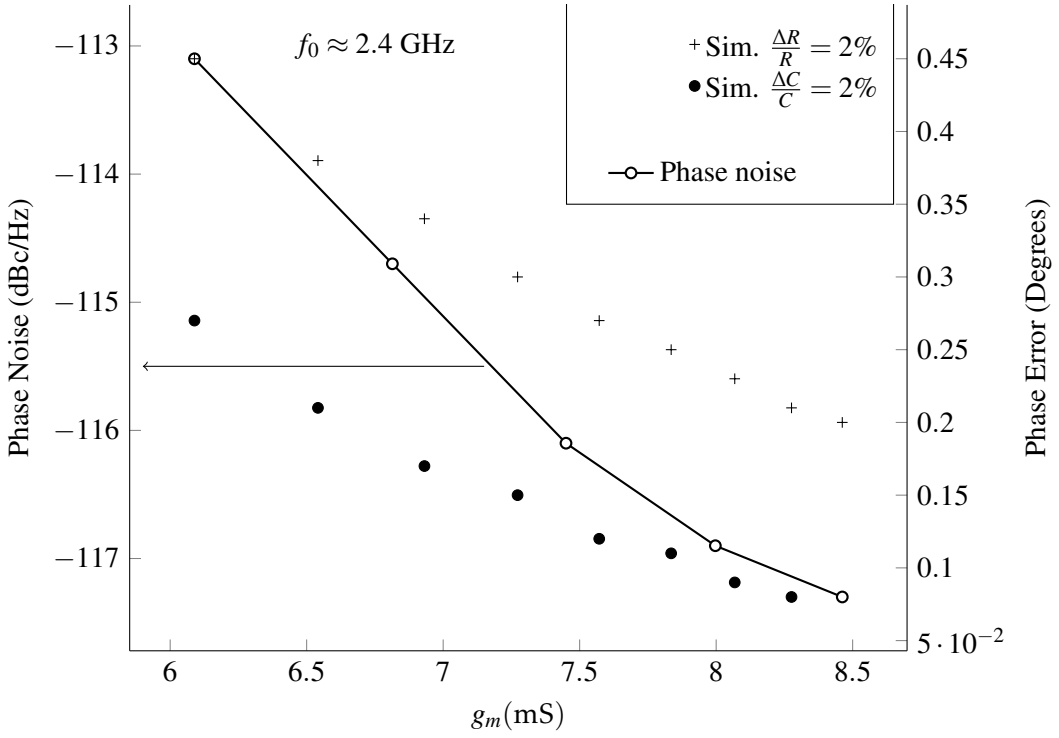

Figure 6.10: Phase noise and phase error as function of the gain [25].

Table 6.1: Comparison of state-of-the-art nearly sinusoidal $RC-$oscillators with a similar circuit topology.

Reference	f [GHz]	PN [dBc/Hz]	Δf [MHz]	P_{DC} [mW]	FoM	IQ	$\frac{f_{max}}{f_{min}}$
[64]	9.8	-94	2	75	-149.1	Yes	1.17
[65]	1.4	-117.3	10	9.6	-150.4	Yes	2.33
[66]	2.5	-95.4	1	2.8	-158.9	No	1.22
[67]	3.1	-110.3	10	7.7	-151.2	Yes	3.42
This work	2.4	-115	10	6.72	-153.2	Yes	5.47

$$\text{FoM} = \text{PN} + 10\log\left(\left(\frac{\Delta f}{f}\right)^2 \frac{P_{DC}}{P_{ref}}\right), \tag{6.55}$$

where PN is the phase noise, P_{DC} is the dissipated power in (mW), P_{ref} is the reference power of 1 mW, f is the oscillation frequency and Δf is the frequency offset.

Table 6.1 gives a comparison among the state-of-the-art of inductorless quadrature oscillators. A figure of merit (FoM) of -153.2 dBc/Hz is obtained for a power of 6.72 mW, which is the best performance for a QVCO with nearly sinusoidal output.

6.4 Conclusions

We presented the analysis of a low power and wide tuning range quadrature oscillator using the configuration with two integrators. The study is focused on the amplitude and phase error as functions of component mismatches. To minimize the impact of the mismatches on the quadrature error, the designer should increase the amplifiers transconductances. Increasing the transconductances also reduces the phase noise, unlike what happen in $LC-$oscillators which have a trade-off between the phase noise and phase error. The quadrature error can be minimized, and in some cases eliminated, by adjusting the transconductances to compensate the capacitance mismatch. However, to obtain outputs in perfect quadrature one must allow an amplitude error. Also, to limit the circuit mismatches, passive components can be replaced by their MOSFET counterparts, which due to the low process variations have less relative mismatches [68]. Furthermore, this approach allows the circuit to be trimmed.

An automatic compensation of the mismatches maybe performed by an auxiliary control circuit. This control circuit should do two independent adjustments. First, to minimize the amplitude mismatch, the current sources I_{level} should be adjusted based on the difference between the amplitudes of both stages. Then the resistances values can be adjusted based on the difference between the common-mode voltages of both outputs.

CHAPTER 7

CONCLUSIONS AND FUTURE RESEARCH

Contents

7.1 Conclusions

The objective of the study reported in this thesis was to investigate the impact of the components mismatches on the amplitude and phase errors of quadrature *RC*−oscillators working in the quasi-sinusoidal regime. Three quadrature oscillators were investigated: the active coupling *RC*−oscillator (in Chapter 4), the capacitive coupling *RC*−oscillator (in Chapter 5), and the two-integrator oscillator (Chapter 6). Quadrature oscillators are key blocks in modern receivers, e.g. the Low-IF and Zero-IF receivers. These receiver architectures allow the full integration of the receiver, which reduces the overall cost, but their performance is directly related to the image rejection ratio. The image rejection depends on the amplitude- and quadrature-errors of the QO. This study showed that amplitude- and quadrature-errors are directly related to components mismatches and inversely proportional to the coupling strength. Thus, for typical mismatches (around 1%) of standard 130 nm CMOS technology, it is possible to design a quadrature *RC*−oscillator with amplitude-error below 1% and quadrature-error below 1°.

Before the analysis of coupled oscillators, the model of a single *RC*−oscillator was reviewed. In the sinusoidal regime, the single *RC*−oscillator can be approximated by a series *RLC* circuit with a nonlinear current source. The circuit nonlinearities are similar to the nonlinear term of the VDPO. Thus, we used the VDPO as a model for the study of coupled oscillators. Simulation results showed that the theoretical model predicts well the oscillation amplitude. For the oscillation frequency, however, the simulation results showed that the oscillation frequency is 10% above the

value given by the theory. This difference can be explained by the approximations and by the effect of the channel-length modulation in the transistors drain currents (which was not accounted for in the model). These factors contribute to an effect similar to an increase of the transconductances of the transistors, leading to an increase of the oscillation frequency. The approximation of the single $RC-$oscillator by the VDPO was already used in other research works, but without relating the transistors operation modes with the VDP parameters.

Coupling of two oscillators consists of injecting a signal from one oscillator into the other. Hence, we study first the injection of a sinusoidal signal into a single $RC-$oscillator (injection locking). Afterwards, we substitute the external source by a second oscillator and derive the results for coupled oscillators. From the injection locking study, we conclude that an oscillator locks to the frequency of the injected signal within a limited band (locking range). The phase difference between the two signals and the oscillation amplitude are adjusted by the attenuation and phase imposed by the oscillator's resonant tank at the locked frequency. Moreover, the locking range is inversely proportional to the resonant tank quality factor and directly proportional to the ratio between the injected current and the oscillator's current amplitudes. Thus, oscillators with resonant tanks with a high-quality factor are more difficult to couple, and they have worse performance, than oscillators with resonant tanks with a low-quality factor. This is not a problem for coupling of $RC-$oscillators, since the maximum quality factor of these oscillators is one.

The study of the active and capacitive coupling showed that both are viable solutions to generate quadrature outputs. Both coupling methods showed similar results for the amplitude error and quadrature error. The error equations were derived with respect to the resistance and capacitance mismatches. It was found that the amplitude error is proportional to both mismatches and is inversely proportional to the coupling strength. The effects of the mismatches are independent and, therefore, are cumulative. In the capacitive coupling, the impact of the resistance mismatches is slightly different from that of the capacitance mismatches. It has a constant term (not dependent on the coupling strength) that sets the minimum value for the amplitude error. The coupling strength can be used to decrease the amplitude error. The phase error depends on the resistance and capacitance mismatches and is inversely proportional to the coupling strength. The impact of the resistance mismatches is slightly higher than that of the capacitance mismatches. Moreover, it was found that the phase error is proportional to the amplitude error. It was also found that the increase in the coupling strength has almost no impact on the phase noise.

The two-integrator oscillator has a working principle fundamentally different from that of coupled oscillators. Although being an $RC-$oscillator (inductorless), it is a single-loop oscillator with inherent quadrature outputs. For the two-integrator oscillator, the error equations were derived with respect to the resistance, capacitance, and transconductance mismatches. Similarly to the other two quadrature oscillators, the phase error is, directly, proportional to the resistance and capacitance mismatches and inversely proportional to the coupling strength. The transconductance mismatches, however, oppose the capacitive mismatches. Hence, if the transconductances are adjusted such that their mismatch compensates the resistance and capacitance mismatches, a perfect quadrature can be obtained. The amplitude error depends, mainly, on the transconductance and capacitance mismatches. However, these mismatches have an opposite impact on the amplitude error. The

transconductance increases the error and the capacitance mismatch decreases the error. Although, in theory, the amplitude error does not depend on the resistance mismatch, simulations showed that there is a slight relationship. The channel-length modulation effect explains this relationship. In the theory, the influence of the resistance mismatch is not predicted because the channel-length modulation was neglected. Note that the resistance mismatch has a tiny influence on the amplitude error and, therefore, to obtain outputs in perfect quadrature one must allow an amplitude error. Further, the simulation showed that the phase noise decreases with the increase of the coupling strength. Thus, contrary to what happen in coupled $LC-$oscillators, there is no trade-off between the phase noise and phase error.

7.2 Future research

- For the capacitive coupling oscillator, only the oscillation frequency equation was validated by measurement results. The amplitude- and phase-error theory was validated only by simulation. The validation of the theory by measurement of a prototype circuit is desirable.
- For the active coupling oscillator and the two-integrator oscillator, the oscillation frequency, amplitude- and phase-error equations were validated by simulation only. The validation of the theory by measurement of a prototype circuit is desirable.
- In the study of the two-integrator oscillator, it was found that the transconductance mismatch counterbalance the resistance and capacitance mismatches. In practice, this leads to the possibility of substantially reducing the quadrature error. An important topic of future research is to investigate the possibility to design a circuit to, automatically, compensate these mismatches. This control circuit should independently adjust the transconductances to compensate the resistance and capacitance mismatch. This is a challenging task since the compensation circuit also has its mismatches. A similar scheme can be used in the capacitive coupling because a relation was found between the phase error and the amplitude error. However, in this case, one should expect a slight reduction of the phase error.
- The theoretical analysis that was done assumed that the solution was sinusoidal, neglecting the harmonics generated by the nonlinearities of the circuit. Simulations showed that there are odd harmonics of the oscillation frequency. An extension of the study presented in this thesis is to determine the amplitude of these harmonics and their relationship to the circuit parameters. This might be used to minimizing the THD.
- A prototype circuit implemented in 130 nm standard CMOS was used to validate the equations. Verifying the validity of the theory presented in this thesis for a more recent technologies, is an important topic of future research.

APPENDIX A

THE MOSFET TRANSCONDUCTANCE WITH WEAK NONLINEARITY

Contents

The MOSFET transconductance for small signals is usually assumed to be constant with respect to the gate-source signal. However, for signals with moderate amplitude (hundreds of millivolts) this assumption is not valid.

Here we derive the MOSFET's signal dependent transconductance equations for the strong and weak inversion operation regions.

A.1 Strong inversion

For the considered technology the transistor is considered to be in strong inversion if $V_{GS} - V_T$ is higher than 100mV [56]. In this region the drain current is expressed as

$$i_D = \frac{k}{2}\frac{W}{L}(v_{GS} - V_T)^2, \tag{A.1}$$

Here k is a technology dependent parameter, W and L are the transistor dimensions, v_{GS} is the gate to source voltage and V_T is the threshold voltage of the transistor. Assume that v_{GS} is

$$v_{GS} = V_{GS} + v_{gs}, \tag{A.2}$$

where V_{GS} is the bias and v_{gs} is the incremental term.

The MOSFET's drain current can be represented by a Taylor expansion around the bias point, I_D, as

$$i_D = I_D + \frac{\partial i_D}{\partial v_{GS}} v_{gs} + \frac{1}{2}\frac{\partial^2 i_D}{\partial v_{GS}^2} v_{gs}^2 \tag{A.3}$$

Substituting (A.1) and (A.2) into (A.3), we obtain

$$\begin{aligned} i_D &= I_D + k\frac{W}{L}\left(V_{GS} - V_T\right) v_{gs} + \frac{1}{2}k\frac{W}{L}v_{gs}^2 \\ &= I_D + \underbrace{k\frac{W}{L}\left(V_{GS} - V_T\right)}_{g_{m0}} v_{gs} + \frac{1}{2}k\frac{W}{L}v_{gs}^2 \\ &= G_m\left(v_{gs}\right) v_{gs}, \end{aligned} \tag{A.4}$$

where G_m is the signal dependent tranconductance given by

$$G_m\left(v_{gs}\right) = g_{m0} + K v_{gs}. \tag{A.5}$$

with

$$K = \frac{1}{2}k\frac{W}{L} = \frac{g_{m0}^2}{4I_D}. \tag{A.6}$$

Equation (A.5) shows that the transistor transconductance is linearly dependent on v_{gs}.

The transconductance can also be written as a function of the small-signal drain current. From (A.5) follows that

$$i_d = g_{m0} v_{gs} + K v_{gs}^2 = g_{m0}\left(1 + \frac{K}{g_{m0}} v_{gs}\right) v_{gs}. \tag{A.7}$$

Assuming that $v_{gs} \approx \frac{i_d}{g_{m0}}$ and substituting it into (A.7), result in

$$i_d \approx g_{m0}\left(1 + K\frac{i_d}{g_{m0}^2}\right) v_{gs}, \tag{A.8}$$

This can be simplified to

$$i_d \approx \underbrace{g_{m0}\left(1 + \frac{1}{4}\frac{i_d}{I_D}\right)}_{g_m(i_d)} v_{gs}, \tag{A.9}$$

from which the signal dependent transconductance is obtained as

$$G_m(i_d) \approx g_{m0}(1 + K i_d), \tag{A.10}$$

where K is given by

$$K = \frac{1}{4I_D}. \tag{A.11}$$

A.2 Weak inversion

The transistor is in weak inversion if $V_{GS} - V_T$ is much lower than 100 mV [56]. In this region the MOSFET current-voltage relationship can be described by

$$i_D = I_{D0} \frac{W}{L} e^{\alpha(v_{GS} - V_T)}, \tag{A.12}$$

where the α is the exponential factor given by

$$\alpha = \frac{q}{nkT}. \tag{A.13}$$

Here q is the electron charge ($1.60217657 \times 10^{-19}$C), k is the Boltzmann's constant ($1.3806488 \times 10^{-23}$J K^{-1}) and T is the absolute temperature in degrees of Kelvin; I_{D0} is the drain current for $V_{GS} - V_T = 0$. Using the Taylor approximation in (A.3) the large-signal drain current (A.12) can be approximated as

$$i_D \approx I_D + I_D \alpha v_{gs} + \frac{1}{2} I_D \alpha^2 v_{gs}^2, \tag{A.14}$$

From (A.14) we obtain the equation for the transconductance with respect to v_{gs}

$$G_m(v_{gs}) \approx g_{m0}(1 + \alpha v_{gs}), \tag{A.15}$$

where g_{m0} is the transconductance that is given by

$$g_{m0} = \alpha I_D. \tag{A.16}$$

To obtain the transconductance with respect to the incremental current, i_d, we assume $v_{gs} \approx \frac{i_d}{g_{m0}}$. This result in

$$G_m(i_d) \approx g_{m0} \left(1 + \frac{\alpha}{g_{m0}} i_d\right) = g_{m0}(1 + K i_d),$$

where K is given by

$$K = \frac{1}{I_D}.$$

Thus for all cases it is possible to model the transistor's signal dependent transconductance as a linear function of the incremental drain current, i_d, or the gate-source voltage, v_{gs}, around the small-signal transconductance, g_{m0}.

If the transistor is working in a region between the strong and weak inversions, i.e. in moderate inversion, a model for which was proposed recently [57]; then for simplicity, one can use the strong inversion model considering, K, as a fitting parameter.

APPENDIX B

REDUCING VDP HOMOGENEOUS EQUATION TO THE FIRST ORDER

In this appendix we derive the solution for Van der Pol equation using the harmonic balance method [41]. The harmonic balance method consists of substituting a general form of the solution in the left- and right-hand side of the differential equation to obtain the solution which makes both sides equal. Lets rewrite the system dynamics equation of the Van der Pol oscillator in the form,

$$\frac{\mathrm{d}^2 v}{\mathrm{d}t^2} + \omega_0^2 v = 2\left(\delta_0 - \delta_2 v^2\right)\frac{\mathrm{d}v}{\mathrm{d}t}, \tag{B.1}$$

and assume a periodic solution of the form,

$$v(t) = a \cdot \sin(\omega t) - b \cdot \cos(\omega t) = A \sin(\omega t - \phi). \tag{B.2}$$

For the left-hand side of (B.1) we need the second derivative of the solution, $\frac{\mathrm{d}^2 v}{\mathrm{d}t^2}$, and the general form of the solution (B.2). For the right-hand side it is necessary the first derivative, $\frac{\mathrm{d}v}{\mathrm{d}t}$, and the product of the first derivative with the square of the general form, $v^2 \frac{\mathrm{d}v}{\mathrm{d}t}$.

The first derivative is

$$\frac{\mathrm{d}v}{\mathrm{d}t} = \left(\frac{\mathrm{d}a}{\mathrm{d}t} + b\omega\right)\sin(\omega t) + \left(-\frac{\mathrm{d}b}{\mathrm{d}t} + a\omega\right)\cos(\omega t), \tag{B.3}$$

and the second derivative is

$$\begin{aligned}\frac{\mathrm{d}^2 v}{\mathrm{d}t^2} = &\left(\frac{\mathrm{d}^2 a}{\mathrm{d}t^2} + 2\omega\frac{\mathrm{d}b}{\mathrm{d}t} - a\omega^2\right)\sin(\omega t) \\ &\left(-\frac{\mathrm{d}^2 b}{\mathrm{d}t^2} + 2\omega\frac{\mathrm{d}a}{\mathrm{d}t} + b\omega^2\right)\cos(\omega t).\end{aligned} \tag{B.4}$$

For the right-hand side we will need to derive the square of the solution, v^2, which is given by

$$\begin{aligned}v^2 &= a^2\cdot\sin^2(\omega t) - 2ab\cdot\sin(\omega t)cos(\omega t) + b^2\cdot\cos^2(\omega t) \\ &= \frac{a^2}{2} - \frac{a^2}{2}\cos(2\omega t) + \frac{b^2}{2} + \frac{b^2}{2}\cos(2\omega t) - ab\cdot\sin(2\omega t) \\ &= \frac{A^2}{2} + \frac{b^2-a^2}{2}\cos(2\omega t) - ab\cdot\sin(2\omega t)\end{aligned} \tag{B.5}$$

Substituting (B.2), (B.3), (B.4) and (B.5) into (B.1), assuming a slow variation of the amplitude $\frac{\mathrm{d}^2 a}{\mathrm{d}t^2} = \frac{\mathrm{d}^2 b}{\mathrm{d}t^2} \approx 0$, $\frac{\mathrm{d}a}{\mathrm{d}t} \ll b\omega_0$ and $\frac{\mathrm{d}b}{\mathrm{d}t} \ll a\omega_0$, yields

$$\begin{aligned}\left(2\omega\frac{\mathrm{d}b}{\mathrm{d}t} + a(\omega_0^2-\omega^2)\right)\sin(\omega t) + \left(2\omega\frac{\mathrm{d}a}{\mathrm{d}t} - b(\omega_0^2-\omega^2)\right)\cos(\omega t) = &\left(2\delta_0 - 2\delta_2\frac{A^2}{4}\right)b\omega\sin(\omega t) + \\ &\left(2\delta_0 - 2\delta_2\frac{A^2}{4}\right)a\omega\cos(\omega t) + \\ &\left(-\delta_2\frac{b^2-3a^2}{8}\right)b\omega\sin(3\omega t) + \\ &\left(-\delta_2\frac{b^2-3a^2}{8}\right)a\omega\cos(3\omega t).\end{aligned} \tag{B.6}$$

Neglecting the high-order terms, yields

$$\begin{cases}\dfrac{\mathrm{d}a}{\mathrm{d}t} = \dfrac{b(\omega_0^2-\omega^2) + 2a\omega\left(\delta_0 - \delta_2\frac{A^2}{4}\right)}{2\omega}, & \text{(B.7a)} \\ \dfrac{\mathrm{d}b}{\mathrm{d}t} = \dfrac{-a(\omega_0^2-\omega^2) + 2b\omega\left(\delta_0 - \delta_2\frac{A^2}{4}\right)}{2\omega}. & \text{(B.7b)}\end{cases}$$

Converting (B.7) to polar coordinates, where $A = \sqrt{a^2+b^2}$ and $\phi = \operatorname{atan}(b/a)$, results in

$$\begin{cases}\dfrac{\mathrm{d}A}{\mathrm{d}t} = \dfrac{1}{2A}\left(2a\dfrac{\mathrm{d}a}{\mathrm{d}t} + 2b\dfrac{\mathrm{d}b}{\mathrm{d}t}\right) = \delta_0 A - \delta_2\dfrac{A^3}{4}, & \text{(B.8a)} \\ \dfrac{\mathrm{d}\phi}{\mathrm{d}t} = \dfrac{1}{A^2}\left(a\dfrac{\mathrm{d}b}{\mathrm{d}t} - b\dfrac{\mathrm{d}a}{\mathrm{d}t}\right) = \dfrac{\omega^2-\omega_0^2}{2\omega}. & \text{(B.8b)}\end{cases}$$

From (B.8b) we can conclude that an oscillation frequency equal to the resonator frequency, $\omega = \omega_0$, is the only stable solution, which leads to the magnitude and phase derivatives to be

$$\begin{cases} \dfrac{\mathrm{d}A}{\mathrm{d}t} = \delta_0 A - \delta_2 \dfrac{A^3}{4}, & \text{(B.9a)} \\ \dfrac{\mathrm{d}\phi}{\mathrm{d}t} = 0. & \text{(B.9b)} \end{cases}$$

APPENDIX C

REDUCING VDP NONHOMOGENEOUS EQUATION TO THE FIRST-ORDER

In this appendix we derive the particular solution of the Van der Pol equation with a forcing term using the harmonic balance method [41]. The equation of the forced Van der Pol oscillator is

$$\frac{\mathrm{d}^2x}{\mathrm{d}t^2} - 2\left(\delta_0 - \delta_2 x^2\right)\frac{\mathrm{d}x}{\mathrm{d}t} + \omega_0^2 x = f(t), \tag{C.1}$$

where $f(t)$ is the forcing term. We assume that the forcing term is sinusoidal,

$$f(t) = F_a \sin(\omega_F t) - F_b \cos(\omega_F t) = F \sin(\omega_F t - \phi_F), \tag{C.2}$$

where F, ω_F and ϕ_F are, respectively, the amplitude, frequency and phase of the forcing signal. The solution x is a periodic solution of the form,

$$x(t) = a \cdot \sin(\omega t) - b \cdot \cos(\omega t) = A \sin(\omega t - \phi). \tag{C.3}$$

To solve it is necessary to linearize the differential equation (C.1). Hence, near the steady-state the second term of (C.1) can be neglected. The other terms of the left-hand side were already determined in Appendix B.

Substituting (C.3), (B.4) and (C.2) into (C.1) and assuming a slow variation of the amplitude (the second-order derivatives can be neglected $\frac{\mathrm{d}^2a}{\mathrm{d}t^2} = \frac{\mathrm{d}^2b}{\mathrm{d}t^2} \approx 0$, yields

$$\left(2\omega\frac{\mathrm{d}b}{\mathrm{d}t}+a(\omega_0^2-\omega^2)\right)\sin(\omega t)+\left(2\omega\frac{\mathrm{d}a}{\mathrm{d}t}-b(\omega_0^2-\omega^2)\right)\cos(\omega t)=F_a\sin(\omega_F t) - F_b\cos(\omega_F t). \tag{C.4}$$

To solve (C.4) we must express the $\sin\omega_F t$ and $\cos\omega_F t$ in terms of $\sin\omega t$ and $\cos\omega t$. Using trigonometric identities[1,2] we get

$$\cos(\omega_F t)=\cos(\Omega t)\cos(\omega t)-\sin(\Omega t)\sin(\omega t), \tag{C.5}$$

and

$$\sin(\omega_F t)=\sin(\Omega t)\cos(\omega t)+\cos(\Omega t)\sin(\omega t), \tag{C.6}$$

where $\Omega=\omega_F-\omega$. Substituting (C.5) and (C.6) into (C.4) we obtain

$$\left[2\omega\frac{\mathrm{d}b}{\mathrm{d}t}+a(\omega_0^2-\omega^2)\right]\sin(\omega t)+\left[2\omega\frac{\mathrm{d}a}{\mathrm{d}t}-b(\omega_0^2-\omega^2)\right]\cos(\omega t)=[F_a\sin(\Omega t)-F_b\cos(\Omega t)]\cos(\omega t) + [F_a\cos(\Omega t)+F_b\sin(\Omega t)]\sin(\omega t). \tag{C.7}$$

Separating the $\sin\omega t$ and $\cos\omega t$ terms we obtain the derivatives of the amplitudes

$$\begin{cases} \dfrac{\mathrm{d}a}{\mathrm{d}t}=\dfrac{b(\omega_0^2-\omega^2)+[F_a\sin(\Omega t)-F_b\cos(\Omega t)]}{2\omega}, & \text{(C.8a)}\\ \dfrac{\mathrm{d}b}{\mathrm{d}t}=\dfrac{-a(\omega_0^2-\omega^2)+[F_a\cos(\Omega t)+F_b\sin(\Omega t)]}{2\omega}. & \text{(C.8b)} \end{cases}$$

The system of equations Appendix C are considered to be in Cartesian coordinates, where a is the amplitude of the $\sin\omega t$ term and b the amplitude of $\cos\omega t$. Converting it to polar coordinates, with $A=\sqrt{a^2+b^2}$ and $\phi=\mathrm{atan}(b/a)$, results in

$$\begin{cases} \dfrac{\mathrm{d}A}{\mathrm{d}t}=\dfrac{\mathrm{d}\left[\sqrt{a^2+b^2}\right]}{\mathrm{d}t}=\dfrac{1}{2A}\left(2a\dfrac{\mathrm{d}a}{\mathrm{d}t}+2b\dfrac{\mathrm{d}b}{\mathrm{d}t}\right), & \text{(C.9a)}\\ \dfrac{\mathrm{d}\phi}{\mathrm{d}t}=\dfrac{\mathrm{d}\left[\mathrm{atan}\left(\frac{b}{a}\right)\right]}{\mathrm{d}t}=\dfrac{1}{A^2}\left(a\dfrac{\mathrm{d}b}{\mathrm{d}t}-b\dfrac{\mathrm{d}a}{\mathrm{d}t}\right). & \text{(C.9b)} \end{cases}$$

Substituting Appendix C into Appendix C results

$$\begin{cases} \dfrac{\mathrm{d}A}{\mathrm{d}t}=\dfrac{F}{2A\omega}\left[a\sin(\Omega t-\phi_F)+b\sin(\Omega t-\phi_F)\right], & \text{(C.10a)}\\ \dfrac{\mathrm{d}\phi}{\mathrm{d}t}=\dfrac{\omega^2-\omega_0^2}{2\omega}+\dfrac{F}{2A^2\omega}\left[a\cos(\Omega t-\phi_F)-b\sin(\Omega t-\phi_F)\right]. & \text{(C.10b)} \end{cases}$$

[1] $\cos(\alpha+\beta)=\cos\alpha\cos\beta-\sin\alpha\sin\beta$
[2] $\sin(\alpha+\beta)=\sin\alpha\cos\beta+\cos\alpha\sin\beta$

since $a = A\cos\phi$ and $b = A\sin\phi$, Appendix C become

$$\begin{cases} \dfrac{\mathrm{d}A}{\mathrm{d}t} = \dfrac{F}{2\omega}\sin(\Omega t - \Delta\phi), & \text{(C.11a)} \\ \dfrac{\mathrm{d}\phi}{\mathrm{d}t} = \dfrac{\omega^2 - \omega_0^2}{2\omega} + \dfrac{F}{2A\omega}\cos(\Omega t - \Delta\phi). & \text{(C.11b)} \end{cases}$$

where $\Delta\phi = \phi_F - \phi$ is the phase difference between the forcing signal and the oscillator output. From Appendix C we can conclude that the (C.1) can be reduce to a system of two first-order differential equations Appendix C from which we can obtain the particular solution. The equations in Appendix C are in fact phase shifted versions of the forcing signal attenuated by 2ω.

APPENDIX D

IMPACT OF THE MISMATCHES IN THE CAPACITIVE COUPLED OSCILLATOR

Contents

The dynamics of the capacitive coupled oscillator can be obtain from the following system of four differential equations of the first order:

$$\begin{cases} \dfrac{dI_{o1}}{dt} = \left(\delta_0 I_{o1} - \dfrac{1}{4}\delta_2 I_{o1}^3\right) + \dfrac{\alpha_{K1}}{2} I_{o2}\cos(\Delta\phi) & \text{(D.1a)} \\ \dfrac{dI_{o2}}{dt} = \left(\gamma_0 I_{o2} - \dfrac{1}{4}\gamma_2 I_{o2}^3\right) + \dfrac{\alpha_{K2}}{2} I_{o1}\cos(\Delta\phi) & \text{(D.1b)} \\ \dfrac{d\phi_1}{dt} = \dfrac{\omega^2 - \omega_{01}^2(1-\alpha_1)}{2\omega} + \dfrac{\alpha_{K1}}{2}\dfrac{I_{o1}}{I_{o2}}\sin(\Delta\phi) & \text{(D.1c)} \\ \dfrac{d\phi_2}{dt} = \dfrac{\omega^2 - \omega_{02}^2(1-\alpha_2)}{2\omega} - \dfrac{\alpha_{K2}}{2}\dfrac{I_{o2}}{I_{o1}}\sin(\Delta\phi). & \text{(D.1d)} \end{cases}$$

D.1 Oscillation frequency

We obtain the equation of the oscillation frequency from (D.1c) and (D.1d). Adding the two equations yields

$$\frac{d\phi_1}{dt} + \frac{d\phi_2}{dt} = \frac{2\omega^2 - \omega_{01}^2(1-\alpha_1) - \omega_{02}^2(1-\alpha_2)}{2\omega} + \frac{1}{2}\left(\alpha_{K1}\frac{I_{o2}}{I_{o1}} - \alpha_{K2}\frac{I_{o1}}{I_{o2}}\right)\sin(\Delta\phi). \qquad \text{(D.2)}$$

At steady-state $\frac{d\phi_1}{dt} = 0$ and $\frac{d\phi_2}{dt} = 0$ reducing (D.2) to

$$\frac{2\omega^2 - \left[\omega_{01}^2(1-\alpha_1) + \omega_{02}^2(1-\alpha_2)\right]}{2\omega} - (R_1\alpha_2 + R_2\alpha_1)\left(\frac{1}{L_1'}\frac{I_{o2}}{I_{o1}} + \frac{1}{L_2'}\frac{I_{o1}}{I_{o2}}\right)\sin(\Delta\phi) = 0. \quad \text{(D.3)}$$

Rearranging the terms in (D.3) we obtain the second-order polynomial

$$\omega^2 - R\omega\left[\alpha_2\left(1 - \frac{\Delta R}{2R}\right) + \alpha_1\left(1 + \frac{\Delta R}{2R}\right)\right]\left(\frac{1}{L_1'}\frac{I_{o2}}{I_{o1}} + \frac{1}{L_2'}\frac{I_{o1}}{I_{o2}}\right)\sin(\Delta\phi) - \frac{1}{2}\left[\frac{1}{L_1'C_1'} + \frac{1}{L_2'C_2'}\right] = 0. \quad \text{(D.4)}$$

Grouping the α_1 and α_2 parameters in the second term on the left-hand side of (D.4) we obtain

$$\omega^2 - R\omega\left[(\alpha_1+\alpha_2) + \left(\frac{\Delta R}{2R}\right)(\alpha_1-\alpha_2)\right]\left(\frac{1}{L_1'}\frac{I_{o2}}{I_{o1}} + \frac{1}{L_2'}\frac{I_{o1}}{I_{o2}}\right)\sin(\Delta\phi) - \frac{1}{2}\left[\frac{1}{L_1'C_1'} + \frac{1}{L_2'C_2'}\right] = 0,$$

and expanding α_1 and α_2 results in

$$\omega^2 - R\omega\left[2\alpha + \left(\frac{\Delta R}{2R}\right)\left(\frac{\Delta C}{C}\right)\alpha(1-\alpha)\right]\left(\frac{1}{L_1'}\frac{I_{o2}}{I_{o1}} + \frac{1}{L_2'}\frac{I_{o1}}{I_{o2}}\right)\sin(\Delta\phi) - \frac{1}{2}\frac{1}{LC}2(1-\alpha) \approx 0.$$

Assuming small mismatches (i.e. $\left(\frac{\Delta R}{R}\right) \approx 1\%$ and $\left(\frac{\Delta C}{C}\right) \approx 1\%$), $\left(\frac{\Delta R}{2R}\right)\left(\frac{\Delta C}{C}\right)(1-\alpha) \ll 2$ and we obtain

$$\omega^2 - 2R\alpha\omega\left(\frac{1}{L_1'}\frac{I_{o2}}{I_{o1}} + \frac{1}{L_2'}\frac{I_{o1}}{I_{o2}}\right)\sin(\Delta\phi) - \omega_0^2(1-\alpha) \approx 0.$$

Since $I_{o1} = I_{osc}\left(1 - \frac{\varepsilon_A}{2}\right)$ and $I_{o2} = I_{osc}\left(1 + \frac{\varepsilon_A}{2}\right)$ the square and the product of the amplitudes are approximate by $I_{o1}^2 \approx I_{osc}^2(1-\varepsilon_A)$, $I_{o2}^2 \approx I_{osc}^2(1+\varepsilon_A)$ and $I_{o1}I_{o2} \approx I_{osc}^2\left(1 - \frac{\varepsilon_A^2}{4}\right) \approx I_{osc}$. Finding a common denominator and substituting these approximations into Appendix D.1 we obtain

$$\omega^2 - 2R\alpha\omega\left[\frac{L_2' - L_1'}{L_1'L_2'}\varepsilon_A + \frac{L_1' + L_2'}{L_1'L_2'}\right]\sin(\Delta\phi) - \omega_0^2(1-\alpha) \approx 0.$$

Substituting L_1' and L_2' by their equations, we obtain

$$\omega^2 - \frac{2R\alpha}{L}\omega\left[\left(1 + \frac{\Delta R}{2R} - 1 + \frac{\Delta R}{2R}\right)\varepsilon_A + \left(1 + \frac{\Delta R}{2R} + 1 - \frac{\Delta R}{2R}\right)\right]\sin(\Delta\phi) - \omega_0^2(1-\alpha) \approx 0,$$

which clearly can be reduced to

$$\omega^2 - \frac{4R\alpha}{L}\omega\sin(\Delta\phi) - \omega_0^2(1-\alpha) \approx 0.$$

Note that $\frac{2R}{L} = \frac{\omega_0}{Q}$, where ω_0 is the average free running frequency and Q is the oscillator quality factor. Assuming that the oscillators synchronized and in quadrature we have two possibilities (i.e. $\Delta\phi \approx \frac{\pi}{2}$ and $\Delta\phi \approx -\frac{\pi}{2}$), we can substitute $\sin(\Delta\phi) \approx \pm 1$ resulting in

$$\begin{cases} \omega^2 - \dfrac{2\omega_0}{Q}\alpha\omega - \omega_0^2(1-\alpha) \approx 0, & \sin(\Delta\phi) \approx 1 \quad \text{(D.5a)} \\ \omega^2 + \dfrac{2\omega_0}{Q}\alpha\omega - \omega_0^2(1-\alpha) \approx 0. & \sin(\Delta\phi) \approx -1 \quad \text{(D.5b)} \end{cases}$$

From which results

$$\begin{cases} \omega = \dfrac{\omega_0}{Q}\alpha + \dfrac{1}{2}\sqrt{\dfrac{2^2\omega_0^2}{Q^2}\alpha^2 + 4\omega_0^2(1-\alpha)} & \text{(D.6a)} \\ \omega = \dfrac{\omega_0}{Q}\alpha - \dfrac{1}{2}\sqrt{\dfrac{2^2\omega_0^2}{Q^2}\alpha^2 + 4\omega_0^2(1-\alpha)} & \text{(D.6b)} \\ \omega = -\dfrac{\omega_0}{Q}\alpha + \dfrac{1}{2}\sqrt{\dfrac{2^2\omega_0^2}{Q^2}\alpha^2 + 4\omega_0^2(1-\alpha)} & \text{(D.6c)} \\ \omega = -\dfrac{\omega_0}{Q}\alpha - \dfrac{1}{2}\sqrt{\dfrac{2^2\omega_0^2}{Q^2}\alpha^2 + 4\omega_0^2(1-\alpha)} & \text{(D.6d)} \end{cases}$$

which can be simplified to

$$\begin{cases} \omega = \dfrac{\alpha}{Q}\omega_0 + \omega_0\sqrt{\dfrac{\alpha^2}{Q^2} + (1-\alpha)} & \text{(D.7a)} \\ \omega = \dfrac{\alpha}{Q}\omega_0 - \omega_0\sqrt{\dfrac{\alpha^2}{Q^2} + (1-\alpha)} & \text{(D.7b)} \\ \omega = -\dfrac{\alpha}{Q}\omega_0 + \omega_0\sqrt{\dfrac{\alpha^2}{Q^2} + (1-\alpha)} & \text{(D.7c)} \\ \omega = -\dfrac{\alpha}{Q}\omega_0 - \omega_0\sqrt{\dfrac{\alpha^2}{Q^2} + (1-\alpha)} & \text{(D.7d)} \end{cases}$$

The negative frequencies can be ruled out. Knowing the $\frac{4\alpha^2}{Q^2} \ll 1$ and that $\sqrt{1-x} \approx \left(1 - \frac{x}{2}\right)$ yields

$$\begin{cases} \omega \approx \omega_0\left(1 - \dfrac{\alpha}{2} + \dfrac{\alpha}{Q} + \dfrac{\alpha^2}{2Q^2}\right) & \text{(D.8a)} \\ \omega \approx \omega_0\left(1 - \dfrac{\alpha}{2} - \dfrac{\alpha}{Q} - \dfrac{\alpha^2}{2Q^2}\right) & \text{(D.8b)} \end{cases}$$

Simplifying results in

$$\begin{cases} \omega \approx \omega_0\left(1 + \dfrac{2 - Q + \alpha Q^{-1}}{2Q}\alpha\right) & \text{(D.9a)} \\ \omega \approx \omega_0\left(1 - \dfrac{2 + Q + \alpha Q^{-1}}{2Q}\alpha\right) & \text{(D.9b)} \end{cases}$$

D.2 Amplitude error

We obtain the amplitude error from (D.1c) and (D.1d). Subtracting (D.1c) by (D.1d) yields

$$\frac{\mathrm{d}\phi_2}{\mathrm{d}t}-\frac{\mathrm{d}\phi_1}{\mathrm{d}t}=\frac{\omega^2-\omega_{02}^2\left(1-\alpha_2\right)-\omega^2+\omega_{01}^2\left(1-\alpha_1\right)}{2\omega}-\frac{1}{2}\left(\alpha_{K2}\frac{I_{\mathrm{o}1}}{I_{\mathrm{o}2}}+\alpha_{K1}\frac{I_{\mathrm{o}2}}{I_{\mathrm{o}1}}\right)\sin\left(\Delta\phi\right). \quad \text{(D.10)}$$

At steady-state (D.10) reduces to

$$-\Delta\omega-\frac{1}{2}\left(\alpha_{K2}\frac{I_{\mathrm{o}1}}{I_{\mathrm{o}2}}+\alpha_{K1}\frac{I_{\mathrm{o}2}}{I_{\mathrm{o}1}}\right)\sin\left(\Delta\phi\right)=0. \quad \text{(D.11)}$$

where $\Delta\omega$ is the frequency mismatches given by

$$\Delta\omega=\frac{\omega_{02}^2\left(1-\alpha_2\right)-\omega_{01}^2\left(1-\alpha_1\right)}{2\omega}. \quad \text{(D.12)}$$

Substituting the free-running frequencies into (D.12) results in

$$\Delta\omega=\frac{1}{2\omega}\left(\frac{1}{L_2'C_2'}-\frac{1}{L_1'C_1'}\right). \quad \text{(D.13)}$$

The inductances are given by:

$$L_1'\approx 4R_1g_{m0}^{-1}\left(C_d+\frac{C_X}{2}\right)=4Rg_{m0}^{-1}\left(C_d+\frac{C_X}{2}\right)\left(1-\frac{\Delta R}{2R}\right)=L\left(1-\frac{\Delta R}{2R}\right); \quad \text{(D.14)}$$

$$L_2'\approx 4R_2g_{m0}^{-1}\left(C_d+\frac{C_X}{2}\right)=4Rg_{m0}^{-1}\left(C_d+\frac{C_X}{2}\right)\left(1+\frac{\Delta R}{2R}\right)=L\left(1+\frac{\Delta R}{2R}\right). \quad \text{(D.15)}$$

Note that L_1 and L_2 dependent only on the resistances mismatches $\frac{\Delta R}{2R}$ and are insensitive to the capacitances mismatches $\frac{\Delta C}{2C}$. Substituting the inductances into (D.12) results

$$\Delta\omega=\frac{1}{2\omega}\frac{1}{L}\left[\frac{1}{C_2'\left(1+\frac{\Delta R}{2R}\right)}-\frac{1}{C_1'\left(1-\frac{\Delta R}{2R}\right)}\right] \quad \text{(D.16)}$$

$$=\frac{1}{2\omega L}\left[\frac{C_1'\left(1-\frac{\Delta R}{2R}\right)-C_2'\left(1+\frac{\Delta R}{2R}\right)}{C_1'C_2'\left(1-\frac{\Delta R}{2R}\right)\left(1+\frac{\Delta R}{2R}\right)}\right] \quad \text{(D.17)}$$

$$=\frac{1}{2\omega L}\left[\frac{\left(C_1'-C_2'\right)-\frac{\Delta R}{2R}\left(C_1'+C_2'\right)}{C_1'C_2'\left(1-\frac{\Delta R^2}{4R^2}\right)}\right] \quad \text{(D.18)}$$

$$=\frac{1}{2\omega L}\left[\frac{C_1'-C_2'}{C_1'C_2'}-\left(\frac{\Delta R}{2R}\right)\frac{C_2'+C_1'}{C_1'C_2'}\right]. \quad \text{(D.19)}$$

$$\quad \text{(D.20)}$$

The capacitances are given by

$$C_1' = C\left(1-\frac{\Delta C}{2C}\right)+\frac{C_X}{2}; \qquad C_2' = C\left(1+\frac{\Delta C}{2C}\right)+\frac{C_X}{2}. \tag{D.21}$$

Substituting the capacitances equations into (D.20) results in

$$\begin{aligned}\Delta\omega &\approx \frac{1}{2\omega L}\left[\frac{C\left(1-\frac{\Delta C}{2C}\right)+\frac{C_X}{2}-C\left(1+\frac{\Delta C}{2C}\right)-\frac{C_X}{2}-\frac{\Delta R}{2R}\left[C\left(1+\frac{\Delta C}{2C}\right)+\frac{C_X}{2}+C\left(1-\frac{\Delta C}{2C}\right)+\frac{C_X}{2}\right]}{\left[C\left(1-\frac{\Delta C}{2C}+\frac{C_X}{2}\right)\right]\left[C\left(1+\frac{\Delta C}{2C}+\frac{C_X}{2}\right)\right]}\right]\\ &\approx \frac{1}{2\omega L}\left[\frac{-\left(\frac{\Delta C}{C}\right)C-\left(\frac{\Delta R}{2R}\right)(2C+C_X)}{\frac{1}{4}(2C+C_X)^2}\right].\end{aligned}$$

multiplying and dividing by C results in

$$\Delta\omega \approx \frac{-1}{2\omega LC}\left[\left(\frac{\Delta C}{C}\right)\frac{4C^2}{(2C+C_X)^2}+\left(\frac{\Delta R}{2R}\right)\frac{4C}{(2C+C_X)}\right]. \tag{D.22}$$

$$\approx -\frac{\omega_0^2(1-\alpha)}{2\omega}\left[\left(\frac{\Delta C}{C}\right)(1-\alpha)+\left(\frac{\Delta R}{R}\right)\right], \tag{D.23}$$

where $\alpha = \frac{C_X}{2C+C_X}$ is the coupling factor.

The second term on the left-hand side of (D.11) is:

$$-\frac{1}{2}\left(\alpha_{K2}\frac{I_{o1}}{I_{o2}}+\alpha_{K1}\frac{I_{o2}}{I_{o1}}\right)\sin\Delta\phi = 0, \tag{D.24}$$

where $\alpha_{K1} = -(R_2\alpha_1+R_1\alpha_2)\frac{2}{L_1'}$ and $\alpha_{K2} = (R_2\alpha_1+R_1\alpha_2)\frac{2}{L_2'}$. Expanding α_{K1} and α_{K2} gives

$$\alpha_{K1} = -\left[R\left(1+\frac{\Delta R}{2R}\right)\alpha_1+R\left(1-\frac{\Delta R}{2R}\right)\alpha_2\right]\frac{2}{L_1'} \tag{D.25}$$

$$= -\frac{2R}{L_1'}\left[(\alpha_1+\alpha_2)+\left(\frac{\Delta R}{2R}\right)(\alpha_1-\alpha_2)\right] \tag{D.26}$$

since the coupling factors are given by

$$\alpha_1 = \frac{C_X}{2C_1+C_X} = \frac{C_X}{2C\left(1-\frac{\Delta C}{2C}\right)+C_X}; \tag{D.27}$$

and

$$\alpha_2 = \frac{C_X}{2C_2+C_X} = \frac{C_X}{2C\left(1+\frac{\Delta C}{2C}\right)+C_X}. \tag{D.28}$$

Adding the coupling factors results

$$\alpha_1+\alpha_2 = \frac{C_X}{2C\left(1-\frac{\Delta C}{2C}\right)+C_X}+\frac{C_X}{2C\left(1+\frac{\Delta C}{2C}\right)+C_X} \tag{D.29}$$

$$= C_X\frac{2C\left(1+\frac{\Delta C}{2C}\right)+C_X+2C\left(1-\frac{\Delta C}{2C}\right)+C_X}{4C^2\left(1-\frac{\Delta C}{2C}+\frac{\Delta C}{2C}-\left(\frac{\Delta C}{2C}\right)^2\right)+2CC_X\left(1+\frac{\Delta C}{2C}\right)+2CC_X\left(1-\frac{\Delta C}{2C}\right)+C_X^2} \tag{D.30}$$

$$\approx C_X\frac{2(2C+C_X)}{(2C+C_X)^2} = 2\alpha. \tag{D.31}$$

Subtracting the coupling factors results

$$\alpha_1 - \alpha_2 = \frac{C_X}{2C\left(1-\frac{\Delta C}{2C}\right)+C_X} - \frac{C_X}{2C\left(1+\frac{\Delta C}{2C}\right)+C_X} \tag{D.32}$$

$$= C_X \frac{2C\left(1+\frac{\Delta C}{2C}\right)+C_X-2C\left(1-\frac{\Delta C}{2C}\right)-C_X}{4C^2\left(1-\frac{\Delta C}{2C}+\frac{\Delta C}{2C}-\left(\frac{\Delta C}{2C}\right)^2\right)+2CC_X\left(1+\frac{\Delta C}{2C}\right)+2CC_X\left(1-\frac{\Delta C}{2C}\right)+C_X^2} \tag{D.33}$$

$$\approx C_X \frac{2C\left(\frac{\Delta C}{C}\right)}{\left(2C+C_X\right)^2} = \left(\frac{\Delta C}{C}\right)\alpha(1-\alpha). \tag{D.34}$$

Substituting (D.31) and (D.34) into (D.26) results in

$$\alpha_{K1} \approx -\frac{2R}{L_1'}\left[2\alpha+\left(\frac{\Delta R}{2R}\right)\left(\frac{\Delta C}{C}\right)\alpha(1-\alpha)\right]. \tag{D.35}$$

Assuming small mismatches, i.e. $\frac{\Delta R}{R} \approx 1\%$ and $\frac{\Delta C}{C} \approx 1\%$, we can neglect the second term on the right-hand side of (D.35), which results in

$$\alpha_{K1} \approx -\frac{4R}{L_1'}\alpha. \tag{D.36}$$

Similarly the α_{K2} is

$$\alpha_{K2} \approx \frac{4R}{L_2'}\alpha. \tag{D.37}$$

Substituting (D.36) and (D.37) into (D.11) results in

$$\begin{aligned} -\Delta\omega - 2R\alpha\left(\frac{1}{L_2'}\frac{I_{o1}}{I_{o2}} - \frac{1}{L_1'}\frac{I_{o2}}{I_{o1}}\right)\sin\Delta\phi \approx 0, \\ -\Delta\omega - 2R\alpha\left(\frac{L_1'I_{o1}^2 - L_2'I_{o2}^2}{L_1'L_2'I_{o1}I_{o2}}\right)\sin\Delta\phi \approx 0. \end{aligned} \tag{D.38}$$

Since $I_{o1} = I_{osc}\left(1-\frac{\varepsilon_A}{2}\right)$ and $I_{o2} = I_{osc}\left(1+\frac{\varepsilon_A}{2}\right)$. Substituting theses into (D.38) results in

$$\begin{aligned} -\Delta\omega - 2R\alpha\left[\frac{L_1'I_{osc}^2\left(1-\varepsilon_A+\frac{\varepsilon_A^2}{4}\right) - L_2'I_{osc}^2\left(1+\varepsilon_A+\frac{\varepsilon_A^2}{4}\right)}{L_1'L_2'I_{osc}^2\left(1-\frac{\varepsilon_A}{2}\right)\left(1+\frac{\varepsilon_A}{2}\right)}\right]\sin\Delta\phi \approx 0, \\ -\Delta\omega - 2R\alpha\left[\frac{(L_1'-L_2') - (L_1'+L_2')\varepsilon_A}{L_1'L_2'\left(1-\frac{\varepsilon_A}{2}+\frac{\varepsilon_A}{2}-\frac{\varepsilon_A^2}{4}\right)}\right]\sin\Delta\phi \approx 0, \\ -\Delta\omega - 2R\alpha\left[\frac{L_1'-L_2'}{L_1'L_2'} - \frac{L_1'+L_2'}{L_1'L_2'}\varepsilon_A\right]\sin\Delta\phi \approx 0. \end{aligned} \tag{D.39}$$

Substituting the inductance equations into (D.39) results

$$-\Delta\omega - 2R\alpha\left[\frac{L\left(1-\frac{\Delta R}{2R}-1-\frac{\Delta R}{2R}\right)}{L^2\left(1-\frac{\Delta R}{2R}+\frac{\Delta R}{2R}-\left(\frac{\Delta R}{2R}\right)^2\right)}-\frac{L\left(1-\frac{\Delta R}{2R}+1+\frac{\Delta R}{2R}\right)}{L^2\left(1-\frac{\Delta R}{2R}+\frac{\Delta R}{2R}-\left(\frac{\Delta R}{2R}\right)^2\right)}\varepsilon_A\right]\sin\Delta\phi\approx 0.$$

$$-\Delta\omega+\frac{2R}{L}\alpha\left[\left(\frac{\Delta R}{R}\right)+2\varepsilon_A\right]\sin\Delta\phi\approx 0. \quad \text{(D.40)}$$

Substituting (D.23) into (D.40)

$$\frac{\omega_0^2(1-\alpha)}{2\omega}\left[\left(\frac{\Delta R}{R}\right)+\left(\frac{\Delta C}{C}\right)(1-\alpha)\right]\approx\mp\frac{2R\alpha}{L}\left[\frac{\Delta R}{R}+2\varepsilon_A\right]. \quad \text{(D.41)}$$

$$\omega_0^2(1-\alpha)\left[\left(\frac{\Delta R}{R}\right)+\left(\frac{\Delta C}{C}\right)(1-\alpha)\right]\approx\mp\frac{2\omega_0\omega\alpha}{Q}\left(\frac{\Delta R}{R}\right)\mp\frac{4\omega_0\omega\alpha}{Q}\varepsilon_A. \quad \text{(D.42)}$$

Note that $\omega\approx\omega_0\left(1+\frac{2-Q}{2Q}\alpha\right)$ for $\Delta\phi\approx\frac{\pi}{2}$, which yields

$$(1-\alpha)\left[\left(\frac{\Delta R}{R}\right)+\left(\frac{\Delta C}{C}\right)(1-\alpha)\right]\approx\mp\frac{2\left(1+\frac{2-Q}{2Q}\alpha\right)\alpha}{Q}\left(\frac{\Delta R}{R}\right)\mp\frac{4\left(1+\frac{2-Q}{2Q}\alpha\right)\alpha}{Q}\varepsilon_A. \quad \text{(D.43)}$$

Solving (D.43) with respect to ε_A we obtain

$$\varepsilon_A\approx-\left[\frac{(1-\alpha)Q}{4\left(1+\frac{2-Q}{2Q}\alpha\right)\alpha}+\frac{1}{2}\right]\left(\frac{\Delta R}{R}\right)-\left[\frac{(1-\alpha)^2Q}{4\left(1+\frac{2-Q}{2Q}\alpha\right)\alpha}\right]\left(\frac{\Delta C}{C}\right). \quad \text{(D.44)}$$

D.3 Phase error

We obtain the phase error from (D.1a) and (D.1b). Subtracting (D.1b) from (D.1a) yields

$$\frac{\mathrm{d}I_{o2}}{\mathrm{d}t}-\frac{\mathrm{d}I_{o1}}{\mathrm{d}t}=(\gamma_0-\delta_0)-\frac{1}{4}\left(\gamma_2I_{o2}^2-\delta_2I_{o1}^2\right)+\frac{1}{2}\left(\alpha_{K2}\frac{I_{o1}}{I_{o2}}-\alpha_{K1}\frac{I_{o2}}{I_{o1}}\right)\cos(\Delta\phi). \quad \text{(D.45)}$$

For steady-state (D.45) is reduce to

$$(\gamma_0-\delta_0)-\frac{1}{4}\left(\gamma_2I_{o2}^2-\delta_2I_{o1}^2\right)+\frac{1}{2}\left(\alpha_{K2}\frac{I_{o1}}{I_{o2}}-\alpha_{K1}\frac{I_{o2}}{I_{o1}}\right)\cos(\Delta\phi)=0. \quad \text{(D.46)}$$

Let us write the first term on the left-hand side of (D.46) as a function of the resistance and capacitances mismatches, $\frac{\Delta R}{R}$ and $\frac{\Delta C}{C}$, respectively. For this purpose, we substitute the parameters δ_0 and γ_0 by their equations as a function of the circuit elements:

$$(\gamma_0-\delta_0)=\frac{R_2\left(1-\frac{C_d}{C_2'}\right)-g_{m0}^{-1}}{L_2'}-\frac{R_1\left(1-\frac{C_d}{C_1'}\right)-g_{m0}^{-1}}{L_1'} \quad \text{(D.47)}$$

Further, substituting the resistances and inductance by the respective equations gives

$$(\gamma_0-\delta_0)=\frac{R\left(1+\frac{\Delta R}{2R}\right)\left(1-\frac{C_d}{C_2'}\right)-g_{m0}^{-1}}{L\left(1+\frac{\Delta R}{2R}\right)}-\frac{R\left(1-\frac{\Delta R}{2R}\right)\left(1-\frac{C_d}{C_1'}\right)-g_{m0}^{-1}}{L\left(1-\frac{\Delta R}{2R}\right)} \tag{D.48}$$

Moreover, assuming small mismatches $\left(\frac{\Delta R}{2R}\right)^2 \ll 1$, therefore, we can reduce both terms, on the right-hand side, to a common denominator which yields

$$(\gamma_0-\delta_0)\approx\frac{R\left(1-\frac{C_d}{C_2'}\right)-g_{m0}^{-1}\left(1-\frac{\Delta R}{2R}\right)-R\left(1-\frac{C_d}{C_1'}\right)+g_{m0}^{-1}\left(1+\frac{\Delta R}{2R}\right)}{L} \tag{D.49}$$

Rearranging the terms in (D.46) can further simplify to

$$(\gamma_0-\delta_0)\approx\frac{RC_d\left(\frac{1}{C_1'}-\frac{1}{C_2'}\right)+g_{m0}^{-1}\left(\frac{\Delta R}{R}\right)}{L} \tag{D.50}$$

$$\frac{1}{C_1'}-\frac{1}{C_2'}=\frac{C\left(1+\frac{\Delta C}{2C}\right)+\frac{C_X}{2}-C\left(1-\frac{\Delta C}{2C}\right)-\frac{C_X}{2}}{\left[C\left(1-\frac{\Delta C}{2C}\right)+\frac{C_X}{2}\right]\left[C\left(1+\frac{\Delta C}{2C}\right)+\frac{C_X}{2}\right]}$$

$$\frac{1}{C_1'}-\frac{1}{C_2'}=\frac{C\left(1+\frac{\Delta C}{2C}-1+\frac{\Delta C}{2C}\right)}{C^2\left(1-\left(\frac{\Delta C}{2C}\right)^2\right)+\frac{C_XC}{2}\left(1-\frac{\Delta c}{2c}+1+\frac{\Delta C}{2C}\right)+\frac{C_X^2}{4}}$$

Assuming $\left(\frac{\Delta C}{2C}\right)^2 \ll 1$ is reduced

$$\frac{1}{C_1'}-\frac{1}{C_2'}\approx\frac{C}{C^2+C_XC+\frac{C_X^2}{4}}\left(\frac{\Delta C}{C}\right)=\frac{1}{C}\left(\frac{\Delta C}{C}\right)(1-\alpha)^2. \tag{D.51}$$

$$\frac{1}{C_1'}+\frac{1}{C_2'}=\frac{C\left(1+\frac{\Delta C}{2C}\right)+\frac{C_X}{2}+C\left(1-\frac{\Delta C}{2C}\right)+\frac{C_X}{2}}{\left[C\left(1-\frac{\Delta C}{2C}\right)+\frac{C_X}{2}\right]\left[C\left(1+\frac{\Delta C}{2C}\right)+\frac{C_X}{2}\right]}$$

$$\frac{1}{C_1'}+\frac{1}{C_2'}=\frac{2C+C_X}{C^2\left(1-\left(\frac{\Delta C}{2C}\right)^2\right)+C_XC+\frac{C_X^2}{4}}$$

Assuming $\left(\frac{\Delta C}{2C}\right)^2 \ll 1$ is reduced

$$\frac{1}{C_1'}+\frac{1}{C_2'}\approx\frac{2}{C}(1-\alpha). \tag{D.52}$$

Substituting (D.51) into (D.50) results in

$$\begin{aligned}(\gamma_0-\delta_0)&\approx\frac{RC_d\left(\frac{\Delta C}{C}\right)(1-\alpha)^2+g_{m0}^{-1}C\left(\frac{\Delta R}{R}\right)}{LC}\\&\approx\omega_0^2(1-\alpha)\left[RC_d\left(\frac{\Delta C}{C}\right)(1-\alpha)+g_{m0}^{-1}C\left(\frac{\Delta R}{R}\right)\right].\end{aligned} \tag{D.53}$$

Let us now write the second term on the left-hand side of (D.46) as a function of the resistances and capacitances mismatches, $\frac{\Delta R}{R}$ and $\frac{\Delta C}{C}$, respectively. For this purpose, we substitute first the oscillators current amplitude given by : $I_{o1}=I_{osc}\left(1-\frac{\varepsilon_A}{2}\right)$ and $I_{o2}=I_{osc}\left(1+\frac{\varepsilon_A}{2}\right)$, resulting

$$\frac{1}{4}\left(\gamma_2 I_{o2}^2 - \delta_2 I_{o1}^2\right) = \frac{I_{osc}^2}{4}\left[\left(1+\varepsilon_A+\frac{\varepsilon_A^2}{4}\right)\gamma_2 - \left(1-\varepsilon_A+\frac{\varepsilon_A^2}{4}\right)\delta_2\right]$$
$$\approx \frac{I_{osc}^2}{4}\left[(\gamma_2-\delta_2)+(\gamma_2+\delta_2)\,\varepsilon_A\right] \tag{D.54}$$

Substituting the parameters δ_2 and γ_2 by their equations as a function of the circuit elements results in

$$\frac{1}{4}\left(\gamma_2 I_{o2}^2 - \delta_2 I_{o1}^2\right) \approx \frac{3K^2 I_{osc}^2}{4}\left[\left(\frac{R_2\left(1-\frac{C_d}{C_2'}\right)}{L_2'} - \frac{R_1\left(1-\frac{C_d}{C_1'}\right)}{L_1'}\right)\right.$$
$$\left. + \left(\frac{R_2\left(1-\frac{C_d}{C_2'}\right)}{L_2'} + \frac{R_1\left(1-\frac{C_d}{C_1'}\right)}{L_1'}\right)\varepsilon_A\right] \tag{D.55}$$

Since $K=\frac{3}{4I}$, $R_1 = R\left(1-\frac{\Delta R}{2R}\right)$, $R_2 = \left(1+\frac{\Delta R}{2R}\right)$, $L_1' = L\left(1-\frac{\Delta R}{2R}\right)$ and $L_2' = L\left(1+\frac{\Delta R}{2R}\right)$, the second term is reduced to

$$\frac{1}{4}\left(\gamma_2 I_{o2}^2 - \delta_2 I_{o1}^2\right) \approx \frac{3^3 I_{osc}^2 R}{4^3 I^2 L}\left[C_d\left(\frac{1}{C_1'}-\frac{1}{C_2'}\right)+\left(2-C_d\left(\frac{1}{C_1'}+\frac{1}{C_2'}\right)\right)\varepsilon_A\right] \tag{D.56}$$

Substituting (D.52) and (D.51) into (D.56) results

$$\frac{1}{4}\left(\gamma_2 I_{o2}^2 - \delta_2 I_{o1}^2\right) \approx \frac{3^3 I_{osc}^2 R}{4^3 I^2 LC}\left[C_d\left(\frac{\Delta C}{C}\right)(1-\alpha)^2 + 2\left(C - C_d(1-\alpha)\right)\varepsilon_A\right]. \tag{D.57}$$

Note that $I_{osc} \approx \frac{8I}{3}\sqrt{\frac{Rg_{m0}-\frac{C}{C-C_d}}{3Rg_{m0}}}$, which substituted into (D.57) reduces to

$$\frac{1}{4}\left(\gamma_2 I_{o2}^2 - \delta_2 I_{o1}^2\right) \approx \frac{Rg_{m0}-\frac{C}{C-C_d}}{Rg_{m0}}\omega_0^2 R\left[C_d\left(\frac{\Delta C}{C}\right)(1-\alpha)^2 + 2\left(C - C_d(1-\alpha)\right)\varepsilon_A\right]. \tag{D.58}$$

To conclude, let us now write the third term on the left-hand side of (D.46) as a function of the resistance and capacitances mismatches, $\frac{\Delta R}{R}$ and $\frac{\Delta C}{C}$, respectively. For this purpose, we substitute first the α_{K1} and α_{K2} by the circuit elements, resulting

$$\frac{1}{2}\left(\alpha_{K2}\frac{I_{o1}}{I_{o2}} - \alpha_{K1}\frac{I_{o2}}{I_{o1}}\right)\cos(\Delta\phi) = (R_2\alpha_1 + R_1\alpha_2)\left(\frac{1}{L_2'}\frac{I_{o1}}{I_{o2}} + \frac{1}{L_1'}\frac{I_{o2}}{I_{o1}}\right)\cos(\Delta\phi) = 0 \tag{D.59}$$

Multiplying both fractions by I_{o1} and I_{o2} respectively, results in $I_{o1}I_{o2}$ as common denominator:

$$\frac{1}{2}\left(\alpha_{K2}\frac{I_{o1}}{I_{o2}} - \alpha_{K1}\frac{I_{o2}}{I_{o1}}\right)\cos(\Delta\phi) = (R_2\alpha_1 + R_1\alpha_2)\left(\frac{1}{L_2'}\frac{I_{o1}^2}{I_{o2}I_{o1}} + \frac{1}{L_1'}\frac{I_{o2}^2}{I_{o1}I_{o2}}\right)\cos(\Delta\phi) = 0 \tag{D.60}$$

Substituting now the inductances and resistances: $L_1 = L\left(1-\frac{\Delta R}{2R}\right)$, $L_2' = L\left(1+\frac{\Delta R}{2R}\right)$, $R_1 = R\left(1-\frac{\Delta R}{2R}\right)$ and $R_2 = R\left(1+\frac{\Delta R}{2R}\right)$, results in

$$\frac{1}{2}\left(\alpha_{K2}\frac{I_{o1}}{I_{o2}}-\alpha_{K1}\frac{I_{o2}}{I_{o1}}\right)\cos(\Delta\phi)\approx \frac{R}{L}\left[(\alpha_1+\alpha_2)+\frac{\Delta R}{2R}(\alpha_1-\alpha_2)\right]\left(\frac{\left(I_{o1}^2+I_{o2}^2\right)+\frac{\Delta R}{2R}\left(I_{o2}^2-I_{o1}^2\right)}{I_{o2}I_{o1}}\right)\cos(\Delta\phi) \quad \text{(D.61)}$$

Further, substituting $I_{o1}^2 \approx I_{osc}^2(1-\varepsilon_A)$, $I_{o2}^2 \approx I_{osc}^2(1+\varepsilon_A)$ and $I_{o1}I_{o2} \approx I_{osc}^2$ into (D.61) results in

$$\frac{1}{2}\left(\alpha_{K2}\frac{I_{o1}}{I_{o2}}-\alpha_{K1}\frac{I_{o2}}{I_{o1}}\right)\cos(\Delta\phi)\approx \frac{R}{L}\left[(\alpha_1+\alpha_2)+\frac{\Delta R}{2R}(\alpha_1-\alpha_2)\right]\left(2+\frac{\Delta R}{2R}\varepsilon_A\right)\cos(\Delta\phi) \quad \text{(D.62)}$$

Note that if we assume small mismatches, the terms: $\frac{\Delta R}{2R}\varepsilon_A \ll 2$, $\frac{\Delta R}{2R}\frac{\Delta C}{2C}(1-\alpha) \ll 2$, $\alpha_1+\alpha_2 \approx 2\alpha$ and $\alpha_1-\alpha_2 \approx \alpha(1-\alpha)\left(\frac{\Delta C}{C}\right)$. Thus, (D.62) is reduced to

$$\frac{1}{2}\left(\alpha_{K2}\frac{I_{o1}}{I_{o2}}-\alpha_{K1}\frac{I_{o2}}{I_{o1}}\right)\cos(\Delta\phi) \approx 4RC\alpha\omega_0^2\cos(\Delta\phi) \quad \text{(D.63)}$$

Substituting (D.53), (D.58) and (D.63) into (D.46) and solved with respect to $\cos\Delta\phi$ we obtain

$$4RC\alpha\cos(\Delta\phi) = (1-\alpha)\left[RC_d\left(\frac{\Delta C}{C}\right)(1-\alpha)+g_{m0}^{-1}C\left(\frac{\Delta R}{R}\right)\right]+ -\frac{Rg_{m0}-\frac{C}{C-C_d}}{Rg_{m0}}\left[RC_d\left(\frac{\Delta C}{C}\right)(1-\alpha)^2+2R(C-C_d(1-\alpha))\varepsilon_A\right] \quad \text{(D.64)}$$

Rearranging the terms in (D.64), in order to group the $\frac{\Delta R}{R}$, $\frac{\Delta C}{C}$ and ε_A terms, results in

$$\cos(\Delta\phi) = \frac{(1-\alpha)^2}{\alpha}\frac{1}{4Rg_{m0}}\left[\frac{C_d}{(C-C_d)}\left(\frac{\Delta C}{C}\right)+\frac{1}{(1-\alpha)}\left(\frac{\Delta R}{R}\right) -2\left(Rg_{m0}-\frac{C}{C-C_d}\right)\left(\frac{1}{(1-\alpha)^2}-\frac{C_d}{C}\frac{1}{(1-\alpha)}\right)\varepsilon_A\right] \quad \text{(D.65)}$$

The phase difference is given by

$$\Delta\phi = \frac{\pi}{2}+\varepsilon_\phi, \quad \text{(D.66)}$$

where ε_ϕ is the phase error.

The cosine of the phase difference can be simplified to $\cos\Delta\phi = \sin\varepsilon_\phi$. Moreover, assuming that the phase error is small, (5.82) is approximated equal to the phase error

$$\varepsilon_\phi \approx \frac{(1-\alpha)^2}{\alpha}\frac{1}{4Rg_{m0}}\left[\frac{C_d}{C-C_d}\left(\frac{\Delta C}{C}\right)+\frac{1}{(1-\alpha)}\left(\frac{\Delta R}{R}\right)\right.$$
$$\left.-2\frac{Rg_{m0}-\frac{C}{C-C_d}}{(1-\alpha)^2}\left(1-\frac{C_d}{C}(1-\alpha)\right)\varepsilon_A\right] \quad \text{(D.67)}$$

For the specific case of $C = 2C_d$, the phase-error is reduced to

$$\varepsilon_\phi \approx \frac{(1-\alpha)^2}{\alpha}\frac{1}{4Rg_{m0}}\left[\left(\frac{\Delta C}{C}\right)+\frac{1}{(1-\alpha)}\left(\frac{\Delta R}{R}\right)-\frac{Rg_{m0}-2}{(1-\alpha)^2}(1+\alpha)\varepsilon_A\right]. \quad \text{(D.68)}$$

Note that the units of (D.68) are radians. To obtain the phase-error in degrees we multiply (D.68) by $\frac{180}{\pi}$:

$$\varepsilon_\phi \approx \frac{(1-\alpha)^2}{\alpha}\frac{45}{\pi Rg_{m0}}\left[\left(\frac{\Delta C}{C}\right)+\frac{1}{(1-\alpha)}\left(\frac{\Delta R}{R}\right)-\frac{Rg_{m0}-2}{(1-\alpha)^2}(1+\alpha)\varepsilon_A\right]. \quad \text{(D.69)}$$

REFERENCES

[1] P.-I. Mak, S.-P. U, and R. Martins, "Transceiver architecture selection: Review, state-of-the-art survey and case study", *IEEE Circuits Syst. Mag.* vol.7, no.2, pp. 6–25, 2007.

[2] L. Oliveira, J. Fernandes, et al., *Analysis and Design of Quadrature Oscillators*, Springer, 2008.

[3] B. Razavi, *RF microelectronics*, Prentice-Hall, 1998.

[4] A. Tarighat, R. Bagheri, and A. Sayed, "Compensation schemes and performance analysis of IQ imbalances in OFDM receivers", *IEEE Trans. Signal Process.* vol.53, no.8, pp. 3257–3268, August 2005.

[5] R. Adler, "A Study of Locking Phenomena in Oscillators", *Proceedings of the IRE*, vol.34, no.6, pp. 351–357, June 1946.

[6] S. Verma, H. Rategh, and T. Lee, "A unified model for injection-locked frequency dividers", *IEEE J. Solid-State Circuits*, vol.38, no.6, pp. 1015–1027, June 2003.

[7] R. Miller, "Fractional-Frequency Generators Utilizing Regenerative Modulation", *Proceedings of the IRE*, vol.27, no.7, pp. 446–457, July 1939.

[8] J. Lee and B. Razavi, "A 40-GHz frequency divider in 0.18-μm CMOS technology", *IEEE J. Solid-State Circuits*, vol.39, no.4, pp. 594–601, April 2004.

[9] L. B. Oliveira, A. Allam, et al., "Experimental Comparison of Phase-Noise in Cross-Coupled RC- and LC-oscillators", *Int. J. Circuit Theory Appl.* vol.38, no.7, pp. 681–688, September 2010.

[10] H. GHonoodi and H. M. Naimi, "A Phase and Amplitude Tunable Quadrature *LC* Oscillator: Analysis and Design", *IEEE Trans. Circuits Syst. I*, vol.58, no.4, pp. 677–689, April 2011.

[11] B. Razavi, "A study of phase noise in CMOS oscillators", *IEEE J. Solid-State Circuits*, vol.31, no.3, pp. 331–343, March 1996.

[12] Nam-Jin Oh, Sang-Gug Lee, and Jinho Ko, "A CMOS 868/915 MHz direct conversion. ZigBee single-chip radio", *IEEE Commun. Mag.* vol.43, no.12, pp. 100–109, December 2005.

[13] A. Rofougaran, J. Rael, M. Rofougaran, and A. Abidi, "A 900 MHz CMOS LC-oscillator with quadrature outputs", *IEEE Int. Solid-State Circuits Conf.* pp. 392–393, 1996.

[14] P. Andreani, "A low-phase-noise low-phase-error 1.8 GHz quadrature CMOS VCO", *IEEE Int. Solid-State Circuits Conf.* pp. 290–466, 2002.

[15] P. Andreani, A. Bonfanti, L. Romano, and C. Samori, "Analysis and design of a 1.8-GHz CMOS LC quadrature VCO", *IEEE J. Solid-State Circuits*, vol.37, no.12, pp. 1737–1747, December 2002.

[16] I. T. R. for Semiconductors. *Radio Frequency and Analog/Mixed-Signal Technologies for Wireless Communications*. June 2007. URL: http://www.itrs.net/links/2007_ITRS_CD/2007_Chapters/2007_Wireless.pdf.

[17] A. Willson, "Energy circulation quadrature LC-VCO", *IEEE Int. Symp. on Circuits and Systems*, p. 4, 2006.

[18] S. Gierkink, S. Levantino, et al., "A low-phase-noise 5-GHz CMOS quadrature VCO using superharmonic coupling", *IEEE J. Solid-State Circuits*, vol.38, no.7, pp. 1148–1154, July 2003.

[19] W. Li and K.-K. M. Cheng, "A CMOS Transformer-Based Current Reused SSBM and QVCO for UWB Application", *IEEE Trans. Microw. Theory Techn.* vol.61, no.6, pp. 2395–2401, June 2013.

[20] C. T. Fu and H. C. Luong, "A 0.8-V CMOS quadrature LC VCO using capacitive coupling", *IEEE Asia Solid-State Circuits Conf. (ASSCC'07)*, pp. 436–439, November 2007.

[21] L. B. Oliveira, I. M. Filanovsky, A. Allam, and J. R. Fernandes, "Synchronization of two LC-oscillators using capacitive coupling", *IEEE Int. Symp. Circuits and Systems (ISCAS'08)*, pp. 2322–2325, May 2008.

[22] J. Casaleiro, L. B. Oliveira, and I. Filanovsky, "Low-Power and Low-area CMOS Quadrature RC Oscillator with Capacitive Coupling", *IEEE Int. Symp. Circuits and Systems (ISCAS'12)*, pp. 1488–1491, May 2012.

[23] H. Tong, S. Cheng, et al., "An LC Quadrature VCO Using Capacitive Source Degeneration Coupling to Eliminate Bi-Modal Oscillation", *IEEE Trans. Circuits Syst. I*, vol.59, no.9, pp. 1871–1879, September 2012.

[24] J. Casaleiro, L. B. Oliveira, and I. M. Filanovsky, "A quadrature RC-oscillator with capacitive coupling", *INTEGRATION, the VLSI journal*, vol. (in press), September 2015.

[25] J. Casaleiro, L. B. Oliveira, and I. M. Filanovsky, "Amplitude and Quadrature Errors of Two-Integrator Oscillator", *Journal of Low Power Electronics (JOLPE)*, vol.11, pp. 340–348, 2015.

[26] J. Casaleiro, H. Lopes, L. B. Oliveira, and I. Filanovsky, "CMOS coupled multivibrators for WMTS applications", *Proc. 17th Int. Conf. Mixed Design Integrated Circuits and Systems (MIXDES'10)*, pp. 231–236, June 2010.

[27] J. Casaleiro, H. F. Lopes, L. B. Oliveira, and I. Filanovsky, "Analysis and Design of CMOS Coupled Multivibrators", *Int. J. Microelectronics and Computer Science*, vol.1, no.3, pp. 249–256, September 2010.

[28] J. Casaleiro, H. Lopes, et al., "A 1 mW low phase-noise relaxation oscillator", *IEEE Int. Symp. Circuits and Systems (ISCAS'11)*, pp. 1133–1136, May 2011.

[29] J. Casaleiro, L. B. Oliveira, and A. C. Pinto, "Van der Pol Approximation Applied to Wien Oscillators", *Procedia Technology-Conference on Electronics, Telecommunications and Computers*, vol.17, pp. 335–342, 2014.

[30] K. Kurokawa, *An Introduction to the Theory of Microwave Circuits*, Academic Press, 1969.

[31] L. Strauss, *Wave generation and shaping*, McGraw-Hill, 1970.

[32] "A low-noise, low-power VCO with automatic amplitude control for wireless applications", *IEEE J. Solid-State Circuits*, vol.34, no.6, pp. 761–771, June 1999.

[33] O. Casha, I. Grech, J. Micallef, and E. Gatt, "Design of a 1.2 V Low Phase Noise 1.6 GHz CMOS Buffered Quadrature Output VCO with Automatic Amplitude Control", *13th IEEE Int. Conf. on Electronics, Circuits and Systems*, pp. 192–195, December 2006.

[34] A. Zanchi, C. Samori, A. Lacaita, and S. Levantino, "Impact of AAC design on phase noise performance of VCOs", *IEEE Trans. Circuits Syst. II*, vol.48, no.6, pp. 537–547, June 2001.

[35] J. Rogers, D. Rahn, and C. Plett, "A study of digital and analog automatic-amplitude control circuitry for voltage-controlled oscillators", *IEEE J. Solid-State Circuits*, vol.38, no.2, pp. 352–356, February 2003.

[36] B. Linares-Barranco and T. Serrano-Gotarredona, "A loss control feedback loop for VCO stable amplitude tuning of RF integrated filters", *IEEE Int. Symp. on Circuits and Systems*, pp. 521–524, 2002.

[37] T. O'Dell, "Instability of an oscillator amplitude control system", *IEE Proc. Control Theory and Applications*, vol.151, no.2, pp. 194–197, March 2004.

[38] J. Osa and A. Carlosena, "MOSFET-C sinusoidal oscillator with variable frequency and amplitude", *IEEE Int. Symp. on Circuits and Systems*, pp. 725–728, 2000.

[39] I. M. Filanovsky and C. J. Verhoeven, "Sinusoidal and Relaxation Oscillations in Source-Coupled Multivibrators", *IEEE Trans. Circuits Syst. II*, vol.54, no.11, pp. 1009–1013, November 2007.

[40] I. Filanovsky and L. Oliveira, "Design of a MOS RLC-oscillator with specified total harmonic distortion", *IEEE 54th Int. Midwest Symp. on Circuits and Systems (MWSCAS)*, pp. 1–4, August 2011.

[41] D. W. Jordan and P. Smith, *Nonlinear Ordinary Differential Equations: An Introduction for Scientists and Engineers* (4th ed.), Oxford University Press, 2007.

[42] D. Leeson, "A simple model of feedback oscillator noise spectrum", *Proceedings of the IEEE*, vol.54, no.2, pp. 329–330, 1966.

[43] A. Hajimiri and T. Lee, "A general theory of phase noise in electrical oscillators", *IEEE J. Solid-State Circuits*, vol.33, no.2, pp. 179–194, February 1998.

[44] K. Clarke and D. Hess, *Communication circuits: analysis and design*, Addison-Wesley Pub. Co., 1971.

[45] J.-C. Nallatamby, M. Prigent, M. Camiade, and J. Obregon, "Extension of the Leeson formula to phase noise calculation in transistor oscillators with complex tanks", *IEEE Trans. Microw. Theory Techn.* vol.51, no.3, pp. 690–696, March 2003.

[46] R. W. Rhea. "Oscillator Design and Computer Simulation". in: Prentice-Hall, 1990, p. 47.

[47] M. Randall and T. Hock, "General oscillator characterization using linear open-loop S-parameters", *IEEE Trans. Microw. Theory Techn.* vol.49, no.6, pp. 1094–1100, June 2001.

[48] T. Ohira, "Rigorous Q-factor formulation for one- and two-port passive linear networks from an oscillator noise spectrum viewpoint", *IEEE Trans. Circuits Syst. II*, vol.52, no.12, pp. 846–850, December 2005.

[49] T. Ohira and K. Araki, "Active Q-Factor and Equilibrium Stability Formulation for Sinusoidal Oscillators", *IEEE Trans. Circuits Syst. II*, vol.54, no.9, pp. 810–814, September 2007.

[50] K. Kurokawa, "Injection locking of microwave solid-state oscillators", *Proceedings of the IEEE*, vol.61, no.10, pp. 1386–1410, 1973.

[51] L. Paciorek, "Injection locking of oscillators", *Proceedings of the IEEE*, vol.53, no.11, pp. 1723–1727, 1965.

[52] B. Razavi, "A study of injection locking and pulling in oscillators", *IEEE J. Solid-State Circuits*, vol.39, no.9, pp. 1415–1424, September 2004.

[53] A. Buonomo, A. Lo Schiavo, et al., "A CMOS Injection-Locked Frequency Divider Optimized for Divide-by-Two and Divide-by-Three Operation", *IEEE Trans. Circuits Syst. I*, vol.60, no.12, pp. 3126–3135, December 2013.

[54] L. Romano, S. Levantino, C. Samori, and A. L. Lacaita, "Multiphase LC oscillators", *IEEE Trans. Circuits Syst. I*, vol.53, no.7, pp. 1579–1588, July 2006.

[55] A. Buonomo and A. Lo Schiavo, "Analysis of emitter (source)-coupled multivibrators", *IEEE Trans. Circuits Syst. I*, vol.53, no.6, pp. 1193–1202, June 2006.

[56] D. A. Johns and K. Martin, *Analog Integrated Circuit Design* (2nd ed.), Wiley, 2011.

[57] I. M. Filanovsky, J. K. Järverhaara, and N. T. Tchamov. "On Moderate inversion/saturation". 2015.

[58] P. R. Gray, P. J. Hurst, S. H. Lewis, and R. G. Meyer, *Analysis and Design of Analog Integrated Circuits* (5th ed.), Wiley, 2009.

[59] J. .-. Plouchart, H. Ainspan, M. Soyuer, and A. Ruehli, "A fully-monolithic SiGe differential voltage-controlled oscillator for 5 GHz wireless applications", *IEEE Radio Frequency Integrated Circuits (RFIC) Symp. - Dig. Papers*, pp. 57–60, June 2000.

[60] L. B. Oliveira, J. R. Fernandes, et al., "Experimental Evaluation of Phase-Noise and Quadrature Error in a CMOS 2.4 GHz Relaxation Oscillator", *IEEE Int. Symp. Circuits and Systems (ISCAS'07)*, pp. 1461–1464, May 2007.

[61] L. Oliveira, J. Fernandes, I. Filanovsky, and C. J. M. Verhoeven, "Wideband two-integrator oscillator-mixer", *6th International Conference On ASIC (ASICON)*, pp. 642–645, 2005.

[62] J. van der Tang and D. Kasperkovitz, "A 0.9-2.2 GHz monolithic quadrature mixer oscillator for direct-conversion satellite receivers", *43rd IEEE Int. Solid-State Circuits Conf.* pp. 88–89, February 1997.

[63] J. Casaleiro, L. Oliveira, and I. Filanovsky, "Quadrature error of two-integrator oscillators", *IEEE 57th Int. Midwest Symp. on Circuits and Systems (MWSCAS)*, pp. 483–486, 2014.

[64] J. van der Tang, D. Kasperkovitz, and A. van Roermund, "A 9.8-11.5-GHz quadrature ring oscillator for optical receivers", *IEEE J. Solid-State Circuits*, vol.37, no.3, pp. 438–442, March 2002.

[65] E. Ortigueira, J. Fernandes, M. Silva, and L. Oliveira, "An ultra compact wideband combined LNA-oscillator-mixer for biomedical applications", *IEEE 55th Int. Midwest Symp. on Circuits and Systems (MWSCAS)*, pp. 162–165, August 2012.

[66] S. W. Park and E. Sanchez-Sinencio, "RF Oscillator Based on a Passive RC Bandpass Filter", *IEEE J. Solid-State Circuits*, vol.44, no.11, pp. 3092–3101, November 2009.

[67] J. F. Luís Oliveira Erik Snelling and M. Silva, "An Inductorless CMOS Quadrature Oscillator Continuously Tuneable from 3.1 to 10.6 GHz", *Int. J. Circuit Theory Appl.* vol.40, pp. 209–216, March 2012.

[68] Y. Cheng, "The influence and modeling of process variation and device mismatch for analog/rf circuit design", *Proc. of the Fourth IEEE Int. Caracas Conf. on Devices, Circuits and Systems*, April 2002.

Analysis and Design of Sinusoidal Quadrature RC-Oscillators

João Casaleiro

2015